AMMONIA CRACKING WITH HEAT TRANSFER IMPROVEMENT TECHNOLOGY

By

NAJLAA ALI HUSSEIN ALBOSHMINA

A thesis submitted in partial fulfilment of the requirements for the degree of

Doctor of Philosophy

in

Mechanical Engineering

(Power)

Cardiff University

School of Engineering

Cardiff, Wales / United Kingdom

2019

DECLARATION AND STATEMENTS

DECLARATION

This work has not been submitted in substance for any other degree or award at this or any other university or place of learning, nor is being submitted concurrently in candidature for any degree or other award.

Signed ……..…... (**Najlaa Alboshmina**) Date…….…….

STATEMENT 1

This thesis is being submitted in partial fulfilment of the requirements for the degree of Doctor of Philosophy (PhD).

Signed ……..…. (**Najlaa Alboshmina**) Date…….…….

STATEMENT 2

This thesis is the result of my own independent work/investigation, except where otherwise stated, and the thesis has not been edited by a third party beyond what is permitted by Cardiff University's Policy on the Use of Third Party Editors by Research Degree Students. Other sources are acknowledged by explicit references. The views expressed are my own.

Signed ……..… (**Najlaa Alboshmina**) Date…….…….

STATEMENT 3

I hereby give consent for my thesis, if accepted, to be available online in the University's Open Access repository and for inter-library loan, and for the title and summary to be made available to outside organisations.

Signed ……..…. (**Najlaa Alboshmina**) Date…….…….

ACKNOWLEDGEMENTS

First and foremost, I would like to praise and thank GOD for helping me to complete this thesis. I would like to give my biggest thanks for my country and a large number of heroes who have sacrificed their lives to protect IRAQ and keep it safe.

This thesis would never be possible without the support and guidance of various people at Cardiff University. My sincerest thanks begin with my PhD supervisors, Dr. Agustin Valera-Medina and Prof. Phil Bowen for giving me the opportunity to do my PhD under their supervision, thank you for all of the advice, recommendations, suggestions, patience in my inquiries, valuable feedback and for the constructive criticism which motivated me to do my best.

My great thanks also extended to all technicians of the laboratory and their help in offering me the facilities to complete my design and experiments. Special recognition to Mr Franck Lacan from Additive Manufacturing Laboratories for his help to manufacture my new design using 3D Printer technique. I sincerely appreciate the help of the technical team of the Mechanical Engineering Workshop especially Mr Malcom Seaborne, Mr Andrew Rankmore and Mr Paul Malpas whose technical knowledge contributed to the successful completion of this work.

I would like to extend my thanks to the Iraqi Government for sponsoring my PhD study, and many thanks for the staff of the Iraqi cultural attaché in London for their help during my stay in the UK. My deepest thanks, love and gratitude for all of my family, parents, brothers, sisters and friends who have had never let me feel alone over these years, thanks for your calls and incredible messages.

Extraordinary thanks should be given to my steadfast husband, my superhero, Ali Alsaegh, for his enduring love, for believing in me and sharing my wish to reach the goal of completing this task, thanks for your constant care and kindness in the most difficult days and thanks for being my GPS on the road trip of my life. My deepest thanks for my lovely kids Nawar and Hussein, who inspired me with their patience and love, even as they bore my permanent activity. I could not have done this without you all and my journey from Iraq to Cardiff would have remained simply a dream.

ABSTRACT

In recent decades, ammonia has been used as a means of hydrogen storage that, because it is easily dissociated, can be used as a sustainable fuel for, e.g., power generation. Ammonia as a fuel, offers significant advantages in comparison to hydrogen in terms of cost and convenience, its higher density and its easier storage and distribution.

However, due to its noticeably low flame speed, green ammonia is very difficult to use directly in conventional internal combustion engines and gas turbines (GTs). However, a limited number of studies have suggested that ammonia combustion can achieve acceptable levels of efficiency if the ammonia is partially cracked into hydrogen and nitrogen, so that the fuel is a mix of ammonia and hydrogen.

This thesis reports the design, build and testing of a novel cracker system that employs energy from the combustion process to pre-crack ammonia. A unique geometry has been tested and shown to provide the energy required for the cracking process, and simultaneously establish recirculation regions that improve flame stabilisation. The project has also achieved reduced NO_x emission levels by injecting a small percentage of the fuel mix into the region upstream of the cracker and downstream of the burner.

Numerical and experimental results demonstrate that a particular configuration, i.e. a hemispherically tipped bluff body, located in the centre of a swirl combustor can enhance flame retention (i.e. better blowoff resistance), generate larger recirculation zones for increased residence time, and the anchoring structures holding the cracker in place can be used to disperse unburned ammonia for NO_x control purposes. Thus, it is concluded that the system presented here is viable for use with ammonia as a fuel, and it is expected that the system will mitigate NO_x emissions whilst enabling the efficient combustion of ammonia-based blends.

TABLE OF CONTENTS

FIGURES INDEX

TABLES INDEX

Nomenclature

Alphabetic Symbols

A	Area	[m^2]
A_i	Pre-exponential factor	[-]
a_{stoi}	Moles of air for stoichiometry	[mol]
a	Coefficients of products in NH_3 /H_2/Air chemical reaction	[-]
b	Coefficients of products in NH_3 /H_2/Air chemical reaction	[-]
Cp	Specific heat	[kJ/kg.K]
d	Inner diameter	[mm]
D	Mass diffusion	[m^2/s]
D_h	Swirler hub diameter	[mm]
D_s	Swirler diameter	[mm]
E_i	Activation energy of the reaction	[cal/mol]
F	Corrective factor	[-]
f	Mixture fraction	[-]
G_θ	Axial flux of tangential momentum	[kg.m/s]
G_x	Axial momentum flux	[kg.m/s]
h	Heat transfer coefficient	[W/m^2.K]
h_k	Specific enthalpy of the kth specie	[J/kg]
h_{fi}	Forward rate constant of the ith reaction	[mol/L·s]
H	Height of the bluff body	[mm]
k	Kinetic energy of turbulent fluctuations per unit mass	[-]
k_f	Thermal conductivity of the fluid	[W/m.K]
$\dot{m}$	Mass flow rate	[Kg/s]
Nu	Nusselt number	[-]
P	The static pressure	[N/m^2]
Pr	Prandtl number	[-]
q	Heat transfer rate	[W]
q	Heat flux as a source term	[W/m^2]
r	The radial coordinate	[m]
r_e	Characteristic radius	[m]
R_c	Universal gas constant	[kJ/kmol K]
Re	Reynolds number	[-]
S_M	Body Force	[kg/m^2 s^2]
S_N	Swirl number	[-]
T	Temperature	[K]
t	Time	[s]
U	Overall heat transfer coefficient	[W/m^2K]
u	Velocity components in x direction	[m/s]
V	Reactor volume	[m^3]
V_k	Ordinary diffusion velocity	[mol/m^2/s]
$\vec{V}$	Velocity vector	[m/s]
v	Velocity components in y direction	[m/s]
W	Width of the bluff body	[mm]

W_k	Thermal diffusion velocity	[K/m^2 /s]
$\bar{W}$	Mean molecular weight of the mixture	[kg/mol]
w	Velocity components in z direction	[m/s]
x	Coefficients of reactants in NH_3/H_2/ Air chemical reaction	[-]
X	Volumetric fraction of ammonia/hydrogen that is injected in the post-combustion section	[-]
Y_k	Mass fraction of the kth species	[-]
y	Coefficients of reactants in NH_3/H_2/ Air chemical reaction	[-]
Z_i	The elemental mass fraction of the element i	[-]

Greek symbols

α	Thermal diffusivity	[m^2/s]
β_i	Temperature exponent of the ith reaction	[-]
ΔT	Temperatur difference	[K]
η	Efficiency	[-]
∅	Fuel/air equivalence ratio	[-]
ϕ	Dissipation function	[-]
ε	Viscous dissipation rate of turbulent kinetic energy	[m^2/s^3]
λ	Viscosity coefficient	[m^2/s]
Γ	Exchange coefficient of diffusion circulation	[m^2/s]
μ	Dynamic viscosity	[kg/m/s]
ρ	Density	[kg/m^3]
τ	Viscous stress	[N/m^2]
τ_{ij}	Viscous stress component acts in the j-direction on a surface normal to i direction	[N/m^2]
θ	Vane angle	[deg]
$\dot{\omega}_k$	Net rate of production the kth species	[mol/m^3/s]

Superscripts

av	Average
c	Cold fluid
e	Exit condition
f	Fuel, fluid
h	Hot fluid
i	Inlet condition
i,j,k	refer to the three directions of a Cartesian coordinate system
m	Mean temperature
o	oxidizer
ox	oxidizer stream inlet

ABBRIVATION LIST

AFR	Air/ Fuel ratio
atm	A unit of Atmospheric Pressure
CFD	Computational Fluid Dynamics
CR	Compression Ratio
CRN	Chemical Reactor Network
CRZ	Central Recirculation Zone
DNS	Direct Numerical Solution
FDM	Finite Difference Method
FEM	Finite Element Method
FVM	Finite Volume Method
GT	Gas Turbine
HHV	High Heating Value
HMFR	High Momentum Flow Region
ICEs	Internal Combustion Engines
IRZ	Internal Recirculation Zone
LES	Large Eddy Simulation
LHV	Lower Heating Value
LMTD	Log-Mean Temperature Difference Corrective Factor
NH_3	Ammonia
NO_x	Nitrogen Oxides
ORZ	Outer Recirculation Zone
PDF	Probability Density Function
PFR	Plug Flow Reactors
PIV	Particle Image Velocimetry
PSR	Perfectly Stirred Reactors
PVC	Precessing Vortex Core
RANS	Reynolds-Averaged Navier-Stokes
RZs	Recirculation Zones
SCR	Selective Catalytic Reduction
SI	Spark Ignition Engine
SL	Shear Layer

CHAPTER 1
INTRODUCTION

"We can create a more sustainable, cleaner and safer world by making wiser energy choices."

Robert Alan Silverstein

1.1 Motivation and Overview

One of the most significant of current research discussions concerns the increase in air pollution, with acid rain and global warming, due to greenhouse gases; issues which are considered injurious to public health. These problems could be exacerbated by the increasing demand for fuels for transportation, power generation and local consumption. At present, the transportation and power generation sectors depend primarily on petroleum-based fuels which are made up of a chain of hydrocarbons that when burned produce not only energy but CO and CO_2, among other products. Both CO and CO_2 are considered primary sources of air pollution with harmful effects on human health and the environment. In consequence of the release of greenhouse gases and global warming effects polar animals, for example, will exist only in zoos, and it will become very difficult to live in the hottest regions such as the Middle East, or low lying land as in the Maldives and Bangladesh which are likely to be submerged by rising sea levels. Therefore, the search for alternatives to fossil fuels has extended in all directions. In recent decades, many researchers from China, Europe, Japan, the Middle East, USA and UK have been looking for alternative fuels amongst, which is ammonia. Ammonia (NH_3) has been recently used as a chemical hydrogen storage compound that can be easily dissociated and used as a sustainable fuel for gas turbine power generation and can supply the power for hydrogen fuel cells [1].

The principal problem with the use of ammonia as an engine fuel is the slow flame speed of ammonia/air mixtures. Also, ammonia can also be difficult to ignite, and has a long ignition delay, a high auto-ignition temperature and narrow flammability limits. The challenge of ammonia is to achieve complete combustion at the right time, so that

efficient engine operation can be realised without the emission of large quantities of ammonia in the exhaust.

However, while the properties of ammonia as a fuel are still not fully understood, there is a strong demand to have systems capable of using ammonia efficiently as a reliable source of deliverable energy while unravelling the fundamentals of its combustion [2]. This work has focused on offering new insight into these challenges.

1.2 Ammonia as a Fuel

In comparison to hydrogen, ammonia offers significant advantages in cost and suitability as a fuel. This is due to its higher density, relative ease of storage and distribution, and accessibility [3]. Ammonia dissociates into its constituents hydrogen and nitrogen according to the reaction [3] :

$$2NH_3 \leftrightarrow N_2 + 3H_2 \tag{1.1}$$

In the early twentieth century, German chemists, Fritz Haber in 1918 and Carl Bosch in 1931, were each awarded the Nobel Prize for chemistry. Haber found a means of producing ammonia from hydrogen and nitrogen, and Bosch developed it into an industrial process making ammonia in large quantities by high-pressure catalytic reactions of nitrogen (from the air) with hydrogen. This is typically done at pressures of 200 bar and temperatures of 773 K in the presence of an iron oxide catalyst. The Haber-Bosch process remains the basis for modern ammonia production, although many improvements have been made over the years [4].

Natural ammonia originates from decaying organic matter, man-made ammonia can be obtained from all kinds of fossil fuels as feedstock (natural gas, petroleum, coal, naphtha, etc.), with water and air as primary materials, and from waste heat (e.g., nuclear) or heat obtained from any renewable energy source (solar, wind, hydro, geothermal, etc.) [5, 6]. Therefore, ammonia is fully recyclable because it can be made from substances (water and hydrogen) which are naturally available almost everywhere and its combustion products are ecologically neutral, being mainly water and nitrogen with no carbon content. As mentioned above, hydrogen can be obtained from ammonia by thermal cracking or chemical decomposition. Several other recent studies [7–10] analysed the potential of ammonia as fuel and concluded that, although

it can act as a poison when improperly handed, NH_3 represents an attractive fuel due to the following features:

- ✓ It is safer than various fuels and hydrogen with respect to its flammability and explosive nature (i.e. slower relative reactivity and diffusivity) [8].

- ✓ It has a relatively high octane number and so could be a good fuel for internal combustion engines (ICE) and gas turbines [9].

- ✓ It can be cracked into hydrogen and nitrogen thermally. There are some studies that have used only about ~12.7 % of its lower heating value (LHV of ammonia =18.6 $MJkg^{-1}$) to produce hydrogen for fuel-cells [10].

1.2.1 Ammonia as a Fuel Pathway

Figure (1-1) shows the pathway from production to utilization of ammonia. The figure shows ammonia as capable of use in most energy applications: gas turbines, compression ignition and spark ignition internal combustion, heat generation, fuel cell, etc. [11].

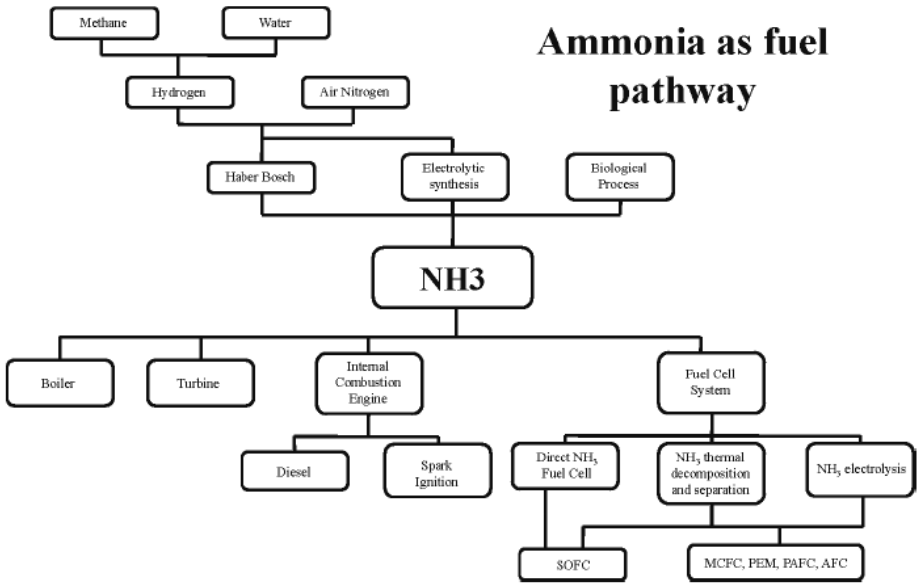

Figure 1- 1: Ammonia as fuel pathway [11].

1.2.2 Properties of Ammonia

Ammonia is a colourless gas with a piercing smell. The boiling point of pure ammonia is 239.72 K, and its freezing point is 195.44 K, with an auto-ignition temperature of 924 K under atmospheric conditions. It has a high heat of vaporisation (23.3 kJ/ mole at its boiling point) with and relatively high octane number ~ 130 and can be handled as a liquid in thermally insulated containers in the laboratory. The shape of the ammonia molecule is a trigonal pyramid with three hydrogen atoms and an unshared pair of electrons attached to the nitrogen atom. The combustion of ammonia produces nitrogen gas and water, with a stoichiometric air-to-fuel ratio of 6.06 by weight [12]. The properties of ammonia are shown in the Table (1-1) [12],

Table 1- 1: Properties of ammonia [12]

Molecular mass	17.0312 kg/mol
Molecular volume (at 273 K, 1 bar)	22.081 mol^{-1}
Gas constant (R)	0.48818 kJ/kg K
Liquid density (at 273 K, 1 bar)	0.6386 g cm^{-3}
Gas density (at 273 K, 1 bar)	0.7714 gl^{-1}
Liquid density (at 239.72 K, 1 bar)	0.682 g cm^{-3}
Gas density (at 239.72 K, 1 bar)	0.888 gl^{-1}
Critical pressure	112.8 bar
Critical temperature	405 K
Critical density	0.235 gcm^{-3}
Critical volume	4.225 cm^3 g^{-1}
Critical compressibility	0.242
Critical thermal conductivity	0.522 kJ K^{-1} h^{-1} m^{-1}
Critical viscosity	23.90 × 10^{-3} mPa s
Melting point (triple point)	195.44 K
Heat of fusion (at 1 bar)	332.3 kJ kg^{-1}
Vapor pressure (triple point)	0.06077 bar
Boiling point (at 1 bar)	239.72 K
Heat of vaporization (at 1 bar)	1.37 MJ kg^{-1}
Standard enthalpy of formation (gas at 298 K)	−46.22 kJ mol^{-1}
Standard entropy (gas at 298K, 1 bar)	192.731 J mol^{-1} K^{-1}
Free enthalpy of formation (gas at 298 K, 1 bar)	−16.391 kJ mol^{-1}
Net heating value (LHV)	18.577 MJ kg^{-1}
Gross heating value (HHV)	22.543 MJ kg^{-1}
Electrical conductivity (at 238 K), very pure	1×10^{-11} $\Omega^{-1}cm^{-1}$
Electrical conductivity (at 238 K), commercial	3×10^{-5} $\Omega^{-1}cm^{-1}$
Ignition temperature according to DIN 51794	924 K
Explosive limits:	
NH_3/O_2 mixture at 293 K, 1 bar	5–79 vol% NH_3
NH_3/air mixture at 293 K, 1 bar	16–27 vol% NH_3
NH_3/air mixture at 393 K, 1 bar	15.5–28 vol% NH_3

1.2.3 Ammonia Storage, Cost and Transportation Aspects

The issue of energy storage is a significant challenge for portable fuel cells. It seems that only hydrogen-based fuel provide the efficiency of energy conversion that would justify the change of technology required in the field of vehicle propulsion [5]. In such a situation, ammonia is being considered as a potential hydrogen carrier to solve the problem of onboard storage. Although NH_3 is not a pure hydrogen compound, it is easily stored in a liquid state requiring a pressure of about 10 bar at ambient temperatures (288 K) [13].

Zamfirescu and Dincer [5] compared ammonia with conventional fuels (gasoline, liquefied petroleum gas [LPG], compressed natural gas [CNG], methanol and hydrogen). They listed the fuel and the type of storage as shown in Table (1-2) from the point of energy storage density per unit mass or volume, and the cost per unit of storage tank volume. They found that the ease of storing ammonia in a liquid state gives it an advantage in energy density per unit volume, being about three times as effective as pure hydrogen. This table is evidence of the economic and ecological value of NH_3 as a fuel.

Table 1- 2: Comparison of ammonia with other fuels including hydrogen [5]

Fuel/storage	P [bar]	ρ Density [kg/m^3]	HHV [MJ/kg]	Energy density [GJ/m^3]	Specific volumetric cost [$/m^3]	Specific energetic cost [$GJ^{-1}]
Gasoline, C_8H_{18}/liquid	1	736	46.7	34.4	1000	29.1
CNG,CH_4/integrated storage	250	188	42.5	10.4	226	28.2
LPG, C_3H_8/pressurized tank	14	388	48.9	19	548	28.8
Methanol, CH_3OH/liquid	1	786	14.3	11.2	421	37.5
Hydrogen, H_2/metal hydrides	14	25	142	3.6	100	28.2
Ammonia, NH_3/pressurized tank	10	603	22.5	13.6	181	13.3
Ammonia, NH_3/metal amines	1	610	17.1	10.4	183	17.5

Moreover, as mentioned by Klerke, et al.[14], ammonia can be easily transported via pipelines, railway cars, auto-cisterns and ships, and delivered to the points of consumption where it can be used as a fuel, chemical, fertiliser, refrigerant, etc.

1.2.4 Ammonia Safety

Exposure to high concentrations of ammonia may cause severe body burns or injuries. In extreme cases, such exposure may also cause blindness, lung damage, heart attack, or death. Despite these safety concerns ammonia is classed as an inhalation hazard not a poison. Nevertheless, safety must be an important consideration in the design, testing, and use of all ammonia-based hydrogen generators [15].

Regarding chemical safety, ammonia poses a low risk of ignition in the presence of sparks or open flames and is classified as a non-flammable liquid. Its potential for fire and explosion is much lower than other gases and it can be made to be as safe as is necessary [16].

Ammonia is considered safer than other fuels due to the following properties:

- ✓ If ammonia escapes to the atmosphere, it dissipates rapidly because its density is less than that of air.

- ✓ It is self-alarming: due to its pungent aroma any leakage can be detected by its smell in concentrations as low as 5 ppm [5].

- ✓ It has a narrow flammability range and, therefore, it is generally considered non-flammable, presenting no explosion danger when appropriately transported.

Therefore, one alternative to the use of ammonia is to employ it as a fuel in systems such as gas turbines, which presents its own challenges.

1.3 Gas Turbines for Power Generation

A gas turbine is a machine that converts the chemical energy of a fuel into usable power. Gas turbines may be used for an assortment of applications and these fall within two basic categories: (a) for the provision of thrust as is the case with a gas turbine aircraft engine; (b) for rotation of a shaft to drive machinery such as a pump, compressor or generator [17]. The most common machine for generating electricity is the gas turbine [17].

The gas turbine, also called a combustion turbine, is a type of continuous combustion ICE. All gas turbines comprise three major sections, see Figure (1-2) [18]: an upstream rotating gas compressor; followed by a combustion chamber or combustors, then a downstream turbine on the same shaft. Gas turbines for power generation can utilise a range of gaseous and liquid fuels such as natural gas, oil and even low calorific value fuels [17].

In a gas turbine, the air is drawn into the intake by a compressor which is connected to the main shaft. Air pressure and temperature increase as the air passes through the compressor stage. The air then leaves the compressor and passes through a diffuser which converts the kinetic energy to pressure. Next the air passes into the combustor. The fuel, pressurised by fuel pumps, is injected into the combustion chamber where it mixes with incoming primary air to form a combustible mixture which is then ignited.

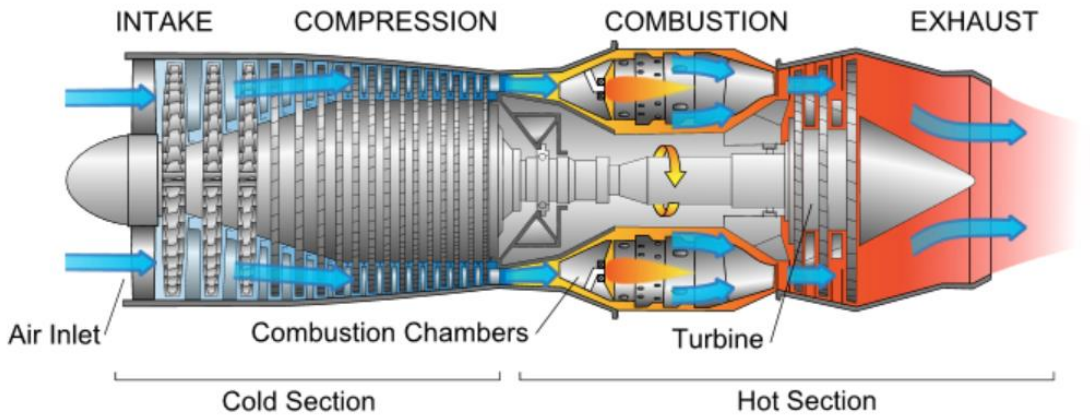

Figure 1- 2: Gas turbine schematic [18].

In general, GT combustion chambers can be classified according to the design of the GT, the purpose for which the GT will be used and the space available for the combustion system [17]. The fuel-air mixture is injecting inside the combustion chamber by the burner nozzle. Inside the combustion chambers, the heat of combustion increases the gas temperature and volume, increasing the velocity of the flow. After leaving the combustors, the hot gases enter the nozzle guide vanes which direct the flow onto the turbine blades, causing the turbine discs to rotate. The output power of the turbine powers the compressor, and the remaining power is used to drive a shaft or electricity generator.

1.3.1 Gas Turbine Combustion Technologies

The two main GT combustion injection systems are the non-premixed diffusion flame and swirl lean premixed combustion. In non-premixed or diffusive combustion systems, fuel and oxidant (usually air) enter separately into the reaction zone and the fuel-air mixing process, and combustion both happen at the same time in the primary combustion zone. In general, this combustion system has been very flexible and used with many types of fuel with a wide range of fuel concentrations. The rich primary combustion of non-premixed flame produces a very high flame temperature as the fuel-air mixture that is combusting is near stoichiometric. A major drawback of diffusion flames is the generation of high levels of NOx emissions due to elevated burning temperature. On the other hand, the diffusion flame can give stable and efficient combustion, wide operating envelopes and good flashback resistance [17]. Generally, the primary zone plays a vital role in holding the flame seated on the burner for both swirl and non-swirl flow. It ensures the complete combustion of the fuel-air mixture by enabling sufficient time, flow turbulence and the required temperature for the combustion process to complete [19].

Today, most GTs operate with lean pre-mixed staged flames with the intention of producing only low levels of emissions, this is because in lean burn systems the combustion takes place at a relatively low temperature. GT combustors which utilise this system have four main features: a fuel/air injection unit, stability device, pre-mixed zone and flame stabilisation zone. In this system, fuel and air are fully mixed before the primary zone to produce a homogeneous lean mixture which passes to the reaction zone where the combustion process takes place [20].

Compared with diffusion flame combustion, lean combustion has low levels of NOx emissions. However, there are drawbacks to this system, flame stability problems, the potential for flashback, and the need for careful combustion settings [19, 20]. In order to cope with these problems, hydrodynamic mechanisms have been employed over the years to increase flame stability whilst anchoring the flame and recirculating species for higher combustion efficiency. One of the most deployed methods is the use of swirling flows.

1.3.2 Swirl Flow Mechanism

A swirling flow is defined as one undergoing simultaneous axial and vortex motion. It results from a spiralling motion, a swirl (tangential) velocity component being imparted to the flow by the use of swirl vanes, axial-plus tangential entry swirl generators or by direct tangential entry of fuel and air into the chamber [21]. Swirl stabilised combustion is widely used in GT combustors. Experimental studies [22] show that the swirl has a substantial effect on the flow field, flame stability, combustion intensity, and the size of the flame. Swirling flows create internal flow recirculation zones in the GT combustion chamber which entrain a portion of the hot combustion products. These recirculation zones not only act as a heat reservoir but also play an active role in improving the mixing and blowoff limits. This reduces both combustor size and unwanted emissions [23].

Swirling flows depend on the aerodynamically formed central recirculation zone (CRZ) which recirculates heat and active chemical species to the root of the flame and creates low-velocity regions so that the flame speed can match the local velocity of the unburned mixture [22, 23]. Vortex breakdown phenomena represent a crucial factor in the formation of the CRZ and determine its size and strength. The phenomenon, the CRZ, is initiated due to the formation of flow stagnation points when swirling flow meets a sudden expansion of the cross-sectional area, see Figure (1-3) [24].

A high centrifugal force and tangential velocity gradient result in a radial pressure gradient with a low-pressure region observable along the central axis near the burner exit. The tangential velocity decays as the flow expands and pressure is recovered, creating a negative pressure gradient along the central axis. Consequently, the flow will stagnate at a certain point downstream of the expansion, resulting in the formation of a reverse flow region. This region is characterised by rapid changes in the flow pattern accompanied by a reduction in the velocity of the approaching flow known as the CRZ [23]. The flow structure of a typical GT swirl injector is shown in Figure (1-3) [24].

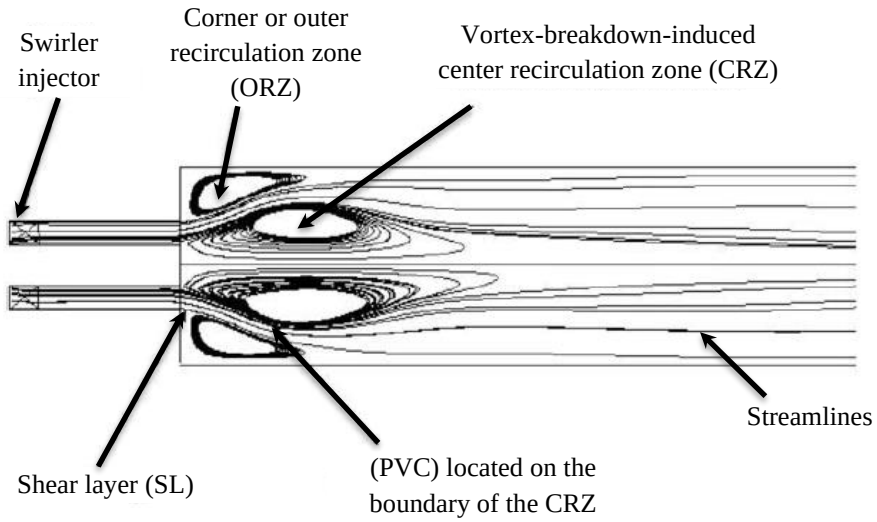

Figure 1- 3: Flow structures of a typical confined swirl burner. Reproduced from [24].

The flow field presents three salient features: a vortex breakdown-induced centre recirculation zone (CRZ) downstream of the injector, a precessing vortex layer (PVC) surrounding the CRZ, and shear layers originating from the outer edge of the inlet annulus. It is established that in swirl flow, a PVC cannot be formed without a CRZ first occurring. These structures significantly affect the stability of the burner in both positive and negative ways.

The PVC develops when a central vortex core starts to precess, at a well-defined frequency, around the axis of symmetry. This phenomenon is usually linked to vortex breakdown and the associated recirculation zone in high Reynolds number flows. The displacement of the vortex core from the axis of symmetry squeezes the flow field on one side against the chamber wall and causes a considerable increase in the tangential velocity in the squeezed flow region due to the conservation of angular momentum. The presence of a PVC also helps explain the occurrence of instantaneous negative azimuthal velocity in the region near the centerline of the chamber [25].

The recirculation zones incorporate a variety of flow features, for example, sudden expansion, bluff bodies and combinations of domes and swirls. As axial distance from the nozzle increases, the flow increases in the tangential and radial directions. the tangential velocity profile of the swirl flow, and together with the effect of a bluff body creates a reduction in velocity and an area of low or even negative pressure along the

central axis of the burner [22]. The decay of tangential velocity with distance along the central axis causes a corresponding decay in the radial distribution of the centrifugal pressure gradient with distance along the central axis. The resulting low or negative pressure creates a force sufficiently strong to push fluid back toward the nozzle, creating a recirculation zone around the central axis of the burner, the CRZ.

In addition, as a result of the sudden expansion in the combustor cross-sectional area, an outer recirculation zone (ORZ) will appear, located between the corners of the combustion chamber and annular jet or the high momentum flow region (HMFR). The ORZ, is sometimes referred to as the external or corner recirculation zone. Shear layers located between the internal recirculation zones (IRZ) and the high momentum flow region can be highly distorted [22,24,26]. The ORZ appears in swirling flow in addition to the effective CRZ. Unlike the CRZ the ORZ is not essential for flame stability, however, like the CRZ, the ORZ also re-circulates hot unburned gases into the reactant mixture [27].

Since the PVC is located at the boundary of CRZ, confinement has considerable effects on the flow field, such as increasing the frequency of PVC. This could also lead to the secondary radial structures. The formation of a secondary PVC is undesirable as it will be become a mechanism of instability [23]. The external eddies are well known to be toroidal in nature and to increase with a sudden expansion. These eddies can be eliminated by using a quarl at the burner exit. Another set of eddies is observed between the shear flow and CRZ and shows the initial separation of 3D coherent structures. These 3D coherent structures are formed as a consequence of the CRZ undergoing division and the creation of a secondary recirculation zone, the so-called CRZ_2.

Figure (1-4) shows the two CRZs. The conditions under which CRZ_2 can form, under confined the zone is highly asymmetric and rotates with the same frequency as the high momentum crescent shaped velocity region with the rapid pressure decay conditions. This result confirms the importance of pressure variations in the development and shape of the inner structures in such types of flow. The system showed strong second and third harmonics. There is also evidence that CRZ_1 and CRZ_2 reach a height where they merge. Overall CRZ_1 and CRZ_2 increased the extent of recirculation, as shown in Figure (1-4) [23, 28, 29].

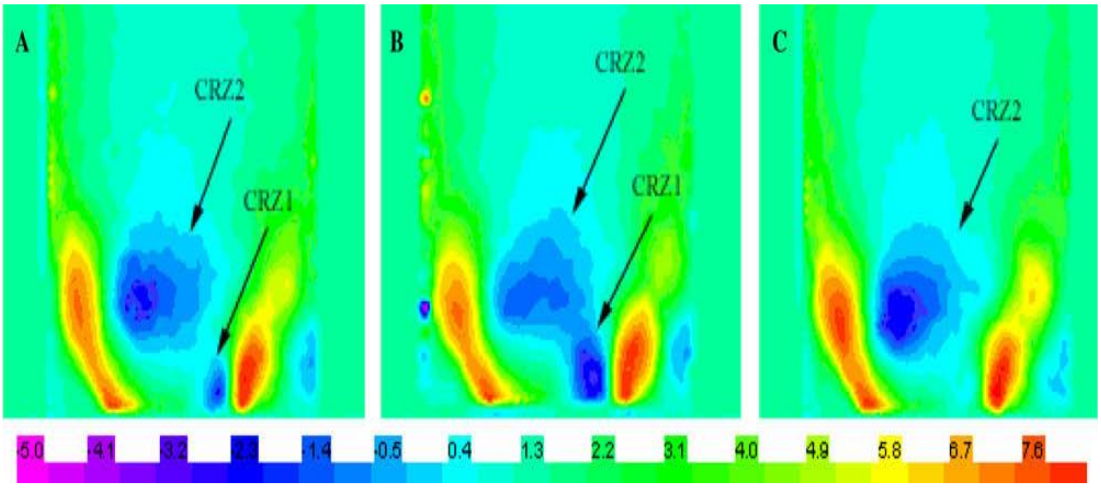

Figure 1- 4: Central recirculation zones [29].

1.4 Role of Ammonia in Gas Turbine Power Generation

In this study, ammonia is proposed as a novel alternative fuel source for gas turbine use. Ammonia has recently started to receive attention as an alternative renewable fuel for the energy consumption requirements over the world due to concern these new fuels, and new systems are a response to the demand for more efficient, more cost-effective, and less polluting systems [30]. To justify the potential role of ammonia fuel blends for gas turbine power generation, a number of concerns related to the benefits and challenges of ammonia use in gas turbine need to be answered. These are summarised in the following sections.

1.4.1 Advantages of Ammonia Use

According to the data compiled by Pfromm [31], estimated ammonia production world-wide exceeded 174 million metric tonnes in 2017. Over 85% of ammonia was for agricultural use as fertiliser. Ammonia cost about $600 per tonne in 2016, with a minimum price of $500 per tonne since 2008.

The large volume of production, and relatively low cost as compared with hydrogen, gives ammonia a solid advantage as a sustainable fuel for ICEs and gas turbines. Other advantages are [32–39]:

- ✓ Anhydrous liquid ammonia stores more energy per unit volume than liquid hydrogen.

- ✓ Technology for storage, utilization and transportation of ammonia is well established and widely available.

- ✓ Hydrogen produced from ammonia can be used in gas turbine applications that are the least costly and with low emissions.

- ✓ The physical properties of ammonia mimic those of liquid propane, and it can be stored under moderate pressure.

- ✓ Using ammonia as a fuel in power plants does not generate CO_2 emission during combustion.

- ✓ To dissociate ammonia into nitrogen and hydrogen gases, only 12.7% of the energy stored in the ammonia is needed.

- ✓ Pure ammonia has an energy density of 13.6 GJ/m^3, which is higher than methanol (11.2 GJ/m^3).

- ✓ Ammonia's strong odour makes leak detection simple, reducing some of the storage risks.

- ✓ It has a potential solvent characterization for post-combustion capture of the pollutants in flue gases such as NO_x.

- ✓ Ammonia has a high hydrogen content and is relatively easy to handle as a liquid.

1.4.2 Challenges of Ammonia Combustion

For cost-effective power generation applications, it is necessary to reduce the temperature and cost of ammonia dissociation. Also, special consideration must be given to the health and safety of site personnel and any nearby human habitation, and

environmental factors, when using ammonia for combustion. Thus, ammonia combustion must overcome many challenges before it can be fully implemented.

The combustion of ammonia under normal conditions forms nitrogen oxides (NO_x), which are mainly nitric oxide (NO) and nitrogen dioxide (NO_2). Nitrogen oxides are known to be radiatively and chemically active gases and make a significant contribution to the greenhouse effect; NO_x is also the main component of acid rain [40].

Ammonia is corrosive to some materials such as copper, nickel, and plastics which is a technical challenge to its implementation. Another challenge to using ammonia as a fuel is that it is difficult to ignite due to its high auto-ignition temperature (T ~ 924 K) as compared to other fuels (gasoline, 713 K; diesel, 498 K) [41]. For combustion of pure ammonia in a compression-ignition engines there are narrow ignition limits: 16–25% by volume in air is required. Also, the power output using ammonia in spark-ignition engines is about 20% less than for conventional gasoline. Ammonia has a high latent heat, low energy content, and a low boiling point [41], so the combustion of ammonia in engines can be achieved only with appropriate combustion strategies.

A number of different approaches have been followed to enable the use of ammonia as a flexible fuel in gas turbines [2, 42]. However, the use of pure liquid ammonia in gas turbine combustors with stable, efficient combustion has presented a series of challenges including low flame temperatures and slow kinetics. Balestri et al. [43] concluded that ammonia could be burned in combustors in the vapour phase, but there is a need to develop systems capable of vaporising ammonia or cracking the molecules, to increase flame speed and burning ratios. Valera-Medina et al. [2, 42]. suggested different injection strategies and a low swirl number to optimise gas turbine power generation, but these strategies still need further enhancement.

More details about the combustion of ammonia in gas turbines for power generation will be found in Chapter Two.

1.5 Ammonia Cracking Methodologies

The expression “cracking” is used to describe any cleavage of complex molecules under the effect of catalysts, solvents or heat that process these more complex molecules into simpler molecules. There are several methods of cracking depending

on the temperature, pressure and presence of catalytic materials. Several studies [44 – 46] have demonstrated that to use ammonia as a fuel, in most applications the ammonia needs to be doped with hydrogen, which can be obtained from cracking the ammonia molecule. That way, faster flame speeds can be obtained for use in large power applications. Usually, ammonia is cracked via thermal or catalytic cracking.

1.5.1 Thermal Methods

Thermal cracking results in the fragmentation of one large molecule into several smaller components using an extremely high temperature, which makes the entropy ($\Delta S°$) larger than the enthalpy ($\Delta H°$) in the Gibbs free energy equation:

$$\Delta G° = \Delta H° - T\Delta S° \tag{1.2}$$

1.5.1.1 Thermal Cracking

Thermal cracking can occur at both high or low pressures. High-pressure thermal cracking operates at absolute pressures of about 70 bar, and it is used to dissociate heavy fractions to produce light fractions. The actual reaction is known as homolytic fission which is the basis for the economically viable production of polymers. The earliest thermal cracking process was invented by Russian engineer Vladimir Shulkhov in 1891 [47].

Hacker and Kordesch [12] found that the complete decomposition of ammonia occurs at approximately 703 K at atmospheric pressure. Grannell et al. [45] developed a thermal cracking process in 2011 for ammonia flame cracker systems in order to decompose ammonia into hydrogen and nitrogen, using heat derived from combustion of a portion of the ammonia used. It was found that ammonia begins to decompose in a silicon carbide tube when the wall temperature reaches about 1573 K.

1.5.1.2 Steam Cracking

Steam cracker units are facilities in which a feedstock is thermally cracked through the use of steam in a bank of pyrolysis furnaces to produce lighter fractions. The products obtained depend on the composition of the feedstock, the fuel to steam ratio, the cracking temperature and furnace residence time [48].

In steam cracking, gaseous or liquid fuel is diluted with steam and heated in a furnace without the presence of oxygen. The temperature of the reaction is very high, around 1123 K, but the reaction is only allowed to take place very briefly.

1.5.2 Catalytic Methods

Catalytic cracking includes the presence of catalysts such as iridium nickel, platinum and silica-aluminium which promote a heterolysis breakage of bonds yielding pairs of ions of opposite charges [46]. Hydrogen from ammonia dissociation could be used to construct a hydrogen generating plant to eliminate the problem of hydrogen storage [12].

1.5.2.1 Fluid Catalytic Cracking

Fluid catalytic cracking is commonly used in petroleum refineries and is more efficient than traditional thermal cracking. The first fluid catalytic cracking method was used about 1942 based on a low activity alumina catalyst [49]. Alumina-catalysed cracking systems are still in use in high school and university laboratories in experiments concerning alkanes and alkenes. In newer designs, cracking takes place over a short-contact time using a very active zeolite-based catalyst in a vertical or upward-sloped pipe called the "riser" [50].

1.5.2.2 Hydrocracking

The hydrocracking process is a catalytic cracking which occurs by adding hydrogen gas to the ammonia. The products of the hydrocracking process depend on the reaction conditions (temperature, pressure, catalyst activity), under a wide range of very high pressures (70-140 bar) and fairly high temperatures (673 K – 1073 K), in the presence of hydrogen and a special catalyst [47].

Thus, in order to support the efforts of decarbonizing in the power generation sector, it is highly important to develop cracking systems by using thermal methodologies that enable the utilisation of hydrogen to achieve the maximum possible efficiency in addition to as low as possible NO_x emissions.

More details about ammonia cracking can be found in Chapter Two.

1.6 Summary

Although several studies have examined the potential efficiency of a hydrogen operated engine that utilizes on-board decomposition of ammonia, there are still several points of concern regarding development of a highly reliable and cost-effective technology before full commercialisation can be achieved. Studies have suggested that it could be possible to use catalysts or thermal crackers to decompose ammonia, resulting in a mixture of ammonia with additional hydrogen for ignition enhancement purposes, to improve the overall efficiency of a power engine. Thus, there is a need for new cracking methodologies to change the composition of the combusting mixture to achieve better flame stability, increase the efficiency of the engine, reduce NOx emissions and provide excellent power loading for the use of the chemical agents in gas turbines.

1.7 Aim and Objectives

The aim of this research is to develop an ammonia fuelled, highly efficient, ultra-low emission gas turbine combustor for large scale power generation.

The objectives of this study are to;

- ✓ Gather information of all relevant ammonia cracking technologies and using their advances work on a novel concept that can be employed on gas turbine combustors.

- ✓ Develop a new system to crack ammonia in an efficient way to enhance the combustibility of the ammonia by producing hydrogen which is added to the ammonia to provide a fuel that is a mix of hydrogen-ammonia.

- ✓ Numerical modelling will be used to decide the shape and dimensions of the final cracking system, which will be then manufactured and experimentally tested.

- ✓ Determine the efficiency of the process when used with gas turbine combustion systems using ammonia.

- ✓ Evaluate the best NH_3/H_2 blends for highest combustion efficiency.

- ✓ Assess different post-combustion recirculation zones to evaluate the impact of bluff body configuration.

- ✓ Study the effect of post-combustion injection of different amounts of ammonia/hydrogen blends downstream of the primary flame zone as a means of reducing NOx emissions.

- ✓ Study the effects of residence time in order to reduce NO_x emission when employing a pre-combustion cracking system.

- ✓ Present new ideas for improvement that can be assessed in follow up projects.

1.8 Thesis Structure

This thesis is divided into eight chapters, as follows:

- ❖ **Chapter 1:** An introduction that describes the use of ammonia as a fuel for gas turbine power generation. It presents the properties of ammonia, its storage, safety aspects, advantages and challenges. In addition, the basic principles of gas turbines with general aspects of combustion technologies are introduced. Also, the chapter covers the basics of cracking methodologies.

- ❖ **Chapter 2:** A review of work using ammonia as an alternative fuel for ICEs and fuel cells, ammonia combustion related to gas turbine applications, its distribution, global presence and most relevant technology to crack ammonia.

- ❖ **Chapter 3:** CFD modelling, Manufacture of the new design under the best-case study, setup of the cracking system and Chemical kinetics models.

- ❖ **Chapter 4:** Numerical results from the model of the proposed design of a new cracking, flame stabilisation system, and relative advantages of various configurations to thermally cracked ammonia in gas turbines.

- **Chapter 5:** Experimental evaluation of the cracking system on combustion and flow characteristics.

- **Chapter 6:** Numerical analyses to evaluate the best ammonia and hydrogen blends for combustion in gas turbines, and how NOx emissions could be reduced when employing ammonia cracking.

- **Chapter 7:** Discussions of results from all chapters.

- **Chapter 8:** Conclusions and recommendation for future work.

CHAPTER 2
LITERATURE REVIEW

"To raise new questions, new possibilities, to regard old problems from a new angle, requires creative imagination and marks a real advance in science."

Albert Einstein, scientist (1879-1955)

2.1 Ammonia as Fuel for Power Generation

As stated previously there is still a substantial lack of information concerning the use of nitrogen-based fuels to supply energy needs, despite alternative fuels to coal, oil and gas being discussed widely. Therefore, fuels such as ammonia need accelerated development to be of use in power generation devices in the foreseeable future.

2.1.1 Ammonia in Fuel Cells

In the past years, ammonia attracted much attention as a valuable fuel source for fuel cells which could use ammonia directly, or the hydrogen generated by cracking ammonia using catalysts or promoter systems [51, 52].

Fuel cells are static energy conversion devices that convert the chemical reaction of fuels directly into electrical energy with heat and water. Fuel cells are classified according to the choice of electrolyte and fuel, with five different major types of fuel cells as follow [53]:

1. Proton exchange membrane fuel cell (PEMFC)
2. Alkaline fuel cell (AFC)
3. Phosphoric acid fuel cell (PAFC)
4. Molten carbonate fuel cell (MCFC)
5. Solid oxide fuel cell (SOFC)

Fuel cell systems use ammonia in many applications and range in size from sub-kilowatt, small power devices such as power traffic signals and battery replacement, to multi-megawatt stationary power generation and vehicular transport. The

characteristics and operating temperatures, materials and efficiencies of major commercial fuel cells have been summarised by Giddey et al. [54], see Table (2-1).

Table 2- 1: The characteristics and technology status of major commercial fuel cells [54].

Fuel cell type	T_{op}, K	Fuel and purity	Electric efficiency (thermal), %	Module size available	Applications
PEMFC	298-353	H_2 (>99.99)	40−48 (35−40)	0.5−200 kW	T, S
PAFC	473-493	H_2 (>99.99)	40−45 (35−40)	100−460 kW	S
MCFC	923	H_2, CO, CH_4	45−55 (30−40)	300 kW−3 MW	S
SOFC	873-1273	H_2, CO, CH_4	50−55 (30−40)	1−250 kW	S
S: stationary. T: transport.					

Low-temperature PEMFCs are the only fuel cell options for portable devices. AFCs are the most convenient for the direct use of ammonia [55]. Direct ammonia high-temperature SOFCs are not suitable for use in transport applications due to their slow start-up, but are good candidates for small-scale energy production, i.e. when used as auxiliary power units for lorries, coaches, planes or ships [56]. Afif et al. [56] have reported that an ammonia-fed SOFC was the most promising energy source for next-generation fuel cell technology. Furthermore, Afif et al. [56] concluded that for alkaline membrane fuel cells the power density is low due to the low catalytic activity of the electrode materials at low operating temperatures. It is difficult to identify good anode and cathode catalysts; and, the crossover of ammonia through the polymeric membrane electrolyte may reduce the open circuit voltage and efficiency. Additionally, the oxidation of diffused ammonia at the cathode may generate toxic NO. Ammonia cracking systems are suitable for use with AFCs and SOFCs due to their tolerance of un-reacted ammonia at medium temperatures (~923 K).

Meanwhile, both PEMFCs and PAFCs can be used at higher system operating temperatures (e.g. 1223 K) although there are concerns about possible effects on durability where levels of unreacted ammonia are deficient [37].

2.1.1.1 Proton Exchange Membrane Fuel Cell (PEMFC)

Ammonia has been proposed for its use in PEFCs; however, because of the low temperature of PEMFC operation, ammonia must be decomposed externally at higher temperatures to provide the hydrogen required for the fuel cell. If the conversion of ammonia to hydrogen is not 100%, there will be a trace of ammonia in the hydrogen

feed, which would be a serious problem as ammonia has been shown to act as a poison to the membranes used in PEMFCs.

The electrochemical reactions in a direct ammonia fuel cell that uses a proton conducting electrolyte comprise three main sections, anode, cathode and electrolyte as shown in the following equations [57]:

$$\begin{cases} 2NH_3 + heat \rightarrow 3H_2 + N_2 \\ 3H_2 \rightarrow 6H^+ + 6e \end{cases} \quad \begin{matrix}\text{Anode} \\ (Fuel\ side)\end{matrix} \quad (2.1)$$

$$\begin{cases} {}^3/_2\, O_2 + 6e \rightarrow 3O^{2-} \\ 6H^+ + 3O^{2-} \rightarrow 3H_2O + heat \end{cases} \quad \begin{matrix}\text{Cathode} \\ (Air\ side)\end{matrix} \quad (2.2)$$

$$2NH_{3+}\, {}^3/_2\, O_2 \rightarrow N_2 + 3H_2O \quad Overall \quad (2.3)$$

At the anode, the ammonia is catalytically decomposed to N_2 + H_2 at a high temperature and low pressure. Removal of hydrogen from the anode drives the decomposition reaction to completion, see Equation (2.1). The oxygen, mostly from ambient air, is fed into the cathode to provide the chemical force driving the fuel cell, providing the heat of reaction for the decomposition of the ammonia, see Equation (2.2). The overall reactions of an ammonia PEMFC system requires inputs of ammonia and oxygen, with nitrogen, water, electric power and heat as outputs. Exemplary methods and apparatus for decomposition of ammonia to obtain pure hydrogen for use with fuel cells and other application have been documented and patented by Chellappa and Powell [58]. The apparatus uses a thermo-catalytic hydrogen generation reactor which includes a reaction chamber containing a catalyst-coated substrate, and a combustion chamber also containing a catalyst coated substrate. The hydrogen generation device operates at a relatively low temperature, preferably from about 823 K to about 923 K to crack 99.9% of the ammonia.

Recent developments in the use of PEMFC systems have led to considerable interest by the US military in fuel cell technology [59]. These systems require an improved hydrogen storage capacity for the ammonia. Thus, the US Army Communications-Electronics Research, Development, and Engineering Center has tested several low-to-mid power range (0 –100 W) reactors. They developed a reactor which they called

an ammonia hydride hydrogen generator composed of three main components: a rechargeable ammonia canister, a LiAlH4 reactor bed, and an ammonia getter. Experimental and analytic results suggest that the ammonia hydride hydrogen generator system is suitable as a low power (5 W) supply, providing higher energy density up to 480 Wh/kg while operating over long periods, in excess of 50 h, at both ambient and near freezing temperatures.

2.1.1.2 Solid Oxide Fuel Cell (SOFC)

Ammonia is problematic when used with PEMFCs because both membrane conductivity, and the activity of the catalysts are affected negatively by trace amounts of ammonia in the fuel feed. PEMFC require either a 100% conversion of ammonia to hydrogen, which cannot always be guaranteed, or total removal of the ammonia from the feed which is rarely practical. Thus, several studies have investigated the use of ammonia with the SOFC.

A novel concept was developed and successfully employed by Wojcik et al. [60], to use the massive quantities of ammonia available in the form of biogas to fuel an SOFC, and to compare the performance with respect to hydrogen. Various electrode/catalyst combinations were tested with a silver anode coupled to an in-situ iron catalyst. Ammonia could be directly inputted into the SOFC without any pre-treatment and gave a performance similar to that obtained from an equivalent supply of pure hydrogen.

In 2008, Ni and co-workers [61, 62] developed a new vehicular automotive unit, using ammonia-based fuel cells. They found that energy produced by proton-conducting electrolytes (SOFC–H+) have superior efficiencies to ion conducting electrolytes (SOFC –O). This was confirmed in 2011 by Ni [63] when he investigated the conjugate heat and mass transfer, as well as the chemical/electrochemical reactions in a SOFC running on ammonia, by combining a 2-D Computation Fluid Dynamics (CFD) model with electro-chemical and chemical models to study the performance of an NH_3-fueled SOFC. He found that an increase in inlet gas velocity decreased the SOFC performance slightly, but did not affect the temperature field.

Cinti et al [11]. reported experimental tests to evaluate the feasibility of NH_3 being fed directly to a 50 cm^2 single cell SOFC. This was to compare the performance of the cell with pure ammonia with an equivalent mixture of ammonia, nitrogen, and hydrogen.

The results obtained at temperatures below 1073 K showed that the cracking reaction takes place in the cell active area due to presence of the nickel catalyst, with the efficiency of the fuel cell increasing by up to 30% with a power density of 300 mW/cm^2, depending on the Lower Heating Value (LHV) of the blend used. Similar work, also carried out by Cinti et al. [64], demonstrated that an ammonia fuelled SOFC is more efficient than an equivalent hydrogen cell and could provide electrical efficiencies of up to 50%. The performance of SOFCs with nickel-based materials and zirconia, fuelled with H_2 or NH_3 has been investigated by Molouk et al.[65]. The results demonstrated that the power generated from ammonia was at the same level as that obtained using hydrogen.

2.1.1.3 Alkaline Fuel Cell (AFC)

AFCs using ammonia have US patent applications going back to 2003 [66]. Here, the method to obtain a mixture of hydrogen and nitrogen from ammonia is based on the catalytic dissociation of gaseous ammonia in a cracker at about 773 K to 1023 K. The dissociation unit as shown in Figure (2-1) consists primarily of a catalyst bed containing aluminium oxide pellets. The active catalyst is a metal; nickel, ruthenium, and/or platinum. The ammonia cracker supplies the hydrogen and nitrogen to a fuel cell and channels a portion of the hydrogen produced to provide heat for further decomposition. This process may comprise vaporising liquid anhydrous ammonia to produce gaseous ammonia, hydrogen and nitrogen mixtures which may then be supplied to the AFC.

Recently, Hejze et al. [67] reported that small amounts of ammonia could be tolerated in the feed gas to AFCs, with no noticeable adverse effects. This was in contrast to acid PEMFCs. This was demonstrated experimentally when a platinum catalyst was used at both anode and cathode. A mixture of hydrogen, nitrogen and ammonia was fed to a single cell on the anode side, and synthetic air on the cathode side. The electrolyte was forced to circulate between the fuel cell and the storage tank by a small stream of nitrogen. It was found that because of the simplicity of the conversion reaction and the absence of carbon monoxide and carbon dioxide, hydrogen produced by the cracking of ammonia was an ideal fuel supply for AFCs.

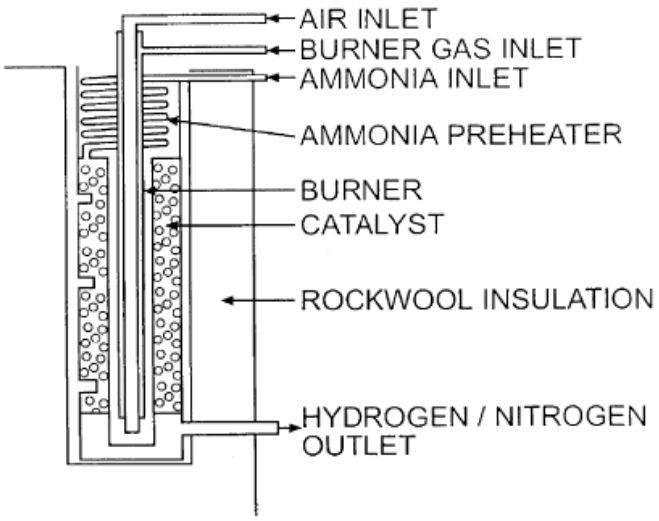

Figure 2- 1: The dissociation unit [66]

The efficiency of alkaline ammonia -fed fuel cells for off-grid power applications have been assessed by Cox and Treyer [36]. An unfamiliar type of AFC powered by decomposition of ammonia is being developed and compared with a diesel generator. The cracking reaction takes place over a platinum group metal based catalyst, supported on aluminium oxide. The cracker reaction chamber is manufactured from 74% nickel, 26% chromium with a stainless-steel shell. Here combustion of the ammonia and hydrogen in the anode off-gases provides heat for the endothermic cracking reaction. This assessment compared the environmental and economic performance of the two systems using life cycle assessment (LCA) and the levelised cost of electricity. The results show that the source of the ammonia (biomass, reforming, partial oxidation or electricity) dominates the LCA, and could result in a 23% lower lifetime climate change impact than a diesel generator system when using biomass as the source. Renewable ammonia production pathways significantly improved environmental performance. Unfortunately, the cost of the electricity produced was 14% more than that produced by the diesel engine.

A group from Apollo Energy Systems [68] designed an AFC system with circulating electrolyte for vehicles on intermittent duties and small units for uninterruptable hybrid power supplies. They developed a low-cost ammonia cracker with a cracking efficiency that provided better than 99.99% conversion, using an Ni-Ru – catalyst. They found that 1 kW of ammonia plus heat produced 1.15 kW hydrogen, and 80 litres of ammonia produced 60 kW of electrical power for Silver Volt electric cars (modified

General Motors automobiles) providing a 240 mile driving range which, for the time (2007), was good. Gobesfeld [69] also studied the conversion of the chemical energy of ammonia to electric energy for use in commercial fuel cell electric vehicles. He developed a polymer electrolyte alkaline fuel cell as a viable power source for electric vehicles such as the Toyota Mirai. His findings highlight the advantages of liquid ammonia as a fuel over compressed hydrogen gas including a straightforward and cheaper fuel infrastructure; significantly higher energy density which meant system dimensions could be favourably reduced.

2.1.2 Application of Ammonia for Internal Combustion Engines

Internal combustion engines (ICEs) are one of the most widely used and more cost-effective energy conversion systems for producing power. Previously, relatively few studies have investigated the use of ammonia as a fuel in ICEs, either in spark ignition (SI) engines or diesel engines. While it is well known that hydrogen can be effectively stored using ammonia, ammonia is still underdeveloped as a fuel due to its disadvantages. Some properties of ammonia and other transportation fuels presented by Kong et al. [70] are reproduced in Table (2-2).

Table 2- 2: Comparison of ammonia with other transportation fuels [70].

Fuel	Molecule	Boiling Point K	$(Air/Fuel)_s$	Latent Heat (kJ/kg)	Energy Content (MJ/kg-fuel)	Energy Content (MJ/kg-stoichiometric mixture)
Methanol	CH_3OH	337	6.435	1203	20.0	2.6900
Ethanol	C_2H_5OH	351	8.953	850	26.9	2.7027
Gasoline	C_7H_{17}	---	15.291	310	44.0	2.5781
Diesel	$C_{14.4}$ $H_{24.9}$	---	14.322	230	42.4	2.7660
Ammonia	NH_3	239	6.046	1371	18.6	2.6414

However, due to low flame velocity and higher ignition temperatures of ammonia 924K against 713 K for gasoline and only 498 K for diesel. There are several technical issues which need more research before ammonia can be used as fuel for ICEs [70]. However, more recently ammonia has been recognised by many researchers as a possible fuel for use in ICEs by mixing with other fuels (gasoline, diesel, methanol,

kerosene, etc.) as combustion promoters [71], or by decomposing ammonia partially by cracking into H_2 and N_2 in order to better initiate the combustion process [72].

In 1967, Pearsall and Garabedian [73] investigated the use of ammonia over a broad range of loads in a pilot injected diesel engine. They found that the engine could run efficiently if the load was controlled by variation of intake pressure using throttling and turbocharging, while the ammonia/air equivalence ratio was held constant. However, this engine was found to suffer retrogression of combustion quality and an increasing ignition delay with decreasing intake pressures, $\leq$ 0.5 bar, at loads corresponding to the throttled operation. Literature surveys by Aliasghar [74] and Hollinger [75] give similar recommendations for the use of high compression ratios, > 20:1, and gaseous ammonia induction with the intake air at a constant equivalence ratio to improve the combustion of ammonia.

The use of ammonia as a fuel for mobile applications has been investigated by Woo et al. at the Korea Institute of Energy Research [76]. They developed a methodology to ignite ammonia-air mixtures and complete combustion without any use of conventional fuels. In this study, both a compression ignition and a SI engine used ammonia as the primary fuel.

2.1.2.1 Compression-Ignition Engine

Emissions and combustion characteristics of a compression-ignition engine using mixtures of ammonia and dimethyl ether (DME) were investigated experimentally in [77, 78]. Ammonia was injected directly into the manifold providing a premixed air-ammonia-diesel mixture for ignition. Operation was attempted with up to 95% ammonia and 5% diesel. Engine torque increase suddenly once vapour ammonia was inducted. It was found that with direct injection, exhaust ammonia emissions are much lower than in other approaches and that output power could be increased by adding greater quantities of ammonia [78]. Diesel fuel was replaced by ammonia in the previous dual-fuel operation for the same power output as mentioned in [77]. As would be expected, NO_x emissions decreased with decreasing levels of ammonia, and cracking efficiencies reached 60% due to a lower combustion temperature.

Iowa State University [79, 80] has also investigated the effect of fuel mixture composition using NH_3 and DME blends on engine performance and exhaust

emissions of a diesel engine using a modified direct injection strategy. Combustion characteristics such as combustion duration, cycle-to-cycle variation, and exhaust emissions including CO, HC, soot, NO_x, and NH_3 emissions were analysed with different blends (100% DME, 20%NH_3-80%DME, 40%NH_3-60%DME and 60%NH_3-40%DME). The results showed that increased ammonia caused longer ignition delays and limited the engine load due to its higher autoignition temperature and lower flame speed. Also, the inclusion of ammonia in the fuel mixture decreased combustion temperature, resulting in higher CO and HC emissions. However, soot emissions remained extremely low, and exhaust ammonia emissions are a few hundred ppm under most of the conditions tested, however NO_x emissions increased due to the formation of fuel NO_x.

According to Ryu et al. [81], when a blend of 40%DME–60%NH_3 was used, there were significant cycle-to-cycle variations and the engine performance decreased as ammonia concentration in the fuel mixture increased. Thus modification of the engine is required to achieve better combustion and higher engine loads when using higher ammonia concentrations. Such a modification was achieved by increasing the injection pressure to 200 bar using Bosch fuel injectors [82].

2.1.2.2 Spark-Ignition Engine

In the past, few studies investigated the use of ammonia as a fuel in SI engines. However, recently, when there were genuine concerns that oil reserves were limited, and that pollution problems related to CO_2 emissions being a serious threat to health, the search for an alternative to fossil fuels led to a number studies on this subject [83]. Recent studies have confirmed that a SI engine cannot, generally, give an acceptable performance when fuelled only by ammonia, requiring the ammonia be blended with other fuels to provide a good power response [83].

Since 2008, Grannell et al. [83, 84] have researched the possibility of using an ammonia-gasoline mix in a dual-fuelled SI engine [83]. They investigated the operating characteristics of a stoichiometric, ammonia-gasoline dual-fuelled SI engine using a single cylinder, variable compression ratio, supercharged Cooperative Fuel Research engine at various ratios of gasoline to ammonia. They concluded that most of the gasoline burned by SI engines could be replaced by ammonia, provided the indicated mean effective pressure is higher or equal to 4 bar. The compression ratio

has only a weak effect on the combustion promoter requirement at the rough limit. They found a decrease in the thermal efficiency and of the proportion of ammonia that can be used for compression ratios, CR > 10:1. However, they suggested that an improved combustion chamber geometry should yield a slightly higher optimal compression ratio for efficiency, and for the knock and rough limit crossovers; a ratio of near 12:1 was suggested for both.

Furthermore, Grannell et al. [84], measured the engine-out and post-catalyst emissions of ammonia, carbon monoxide, hydrocarbons, nitric oxide and nitrous oxide from the engine. They found that an ordinary three-way catalytic converter can be used to successfully remove these emissions, but that lean operation must be avoided completely. The clean-up region has been found to occur between stoichiometric and 0.2% rich fuel conditions. The engine-out exhaust emissions reflected the proportion of ammonia in the intake fuel mixture when the engine was operating satisfactorily from the standpoint of combustion stability and overall thermal efficiency. The effect of lean and rich operation on post-catalyst NH_3, NO, and N_2O emissions becomes stronger when ammonia is used and for that reason, it was suggested that the inclusion of a post-catalyst oxygen sensor is necessary with ammonia.

Due to ammonia's low flame speed and high resistance to auto-ignition, it needs to be mixed with other fuels as combustion promoters to make it a viable fuel in SI engines. This has been confirmed by other dual-fuel studies in IC engines using ammonia and various doping agents [85]. It was confirmed that it is necessary to add an accelerant such as hydrogen (which has the advantage of being carbon-free) to the air-ammonia mixture to improve ignition and to increase combustion velocity and provide a wide flammability range.

Recent studies [86], have demonstrated the possibility of using a SI engine with a mixture of ammonia and hydrogen, where ammonia was the fuel, and the hydrogen was a combustion promoter, supplied by an on-board catalytic reactor. Hydrogen from cracked ammonia is kept at its working temperature by heat from the engine exhaust gases. The process was highly beneficial when compared to pure ammonia injection. On the other hand, it led to higher combustion temperatures and, consequently, higher NO_x emissions. Regarding emissions, research has investigated the mechanisms of NO formation in ammonia- hydrogen fuelled SI engines [87]. They investigated the

unburned ammonia in the exhaust, and it was found that the amount of emissions ranges from 10-25 ppm which is above the allowable range. However, it was revealing that addition of excess ammonia will eliminate all NO_x emissions with a SCR catalyst treatment.

More recent studies [88, 89] have suggested that in order to reduce NO_x, a selective catalytic reduction (SCR) system is needed. The value of the SCR is that ammonia can be used. Although the SCR reaction is exothermic, it would not have an adverse effect on the ammonia desorption processes. Using SCR to reduce NO_x emissions to N_2 and water would not require significant amounts of ammonia, see Equation (2.4):

$$4NH_{3+}4NO + O_2 \rightarrow 4N_2 + 6H_2O \quad (2.4)$$

However, the main challenge to using SCR on a vehicle is how to avoid major ammonia slip under varying load conditions.

2.1.3 Ammonia in Gas Turbines

One of the most significant trends in current studies is the potential combustion of ammonia in gas turbine combustors. Gas turbines can be divided into three general types according to their power generation: a) heavy duty gas turbines which produce power from 30 to 500 MW, b) lightweight gas turbines which are derived from aircraft engines and produce less than 60 MW, and c) micro-gas turbines which distribute less than 5 MW of power. In principle, gas turbines can be up to 60% efficient with steam co-generation, produce low levels of emissions (NO_x < 10 ppm), have low maintenance costs and multi-fuel capacity [90]. Ammonia has attracted attention as a potential fuel for industrial gas turbines and has been proposed as a candidate for helping move towards a low carbon economy, due to its lower cost per unit of stored energy and high volumetric energy density [91]. However, understanding ammonia combustion stability and emissions are still the main challenges for its use in gas turbines.

The past fifty years have seen increasingly rapid advances in the burning of ammonia in gas turbines [92, 93]. In 1964, the U. S. Army Engineer Research and Development Laboratories [92], published a report demonstrating that ammonia combustion showed the same features as conventional hydrocarbon fuels, but with a significant reduction in the range of flammability. A single-can gas turbine engine with a size range of up

to 200 kW was used with two different ammonia combustion systems. One system was comparable to that for a conventional hydrocarbon, while the second used a catalytic aid to reduce the combustor volume and increase the fuel reaction rate. One of the more significant findings from this study was that at the same turbine temperatures the power extracted from ammonia burning increases from 10-20% with fuel consumption 2.25 times greater than hydrocarbons fuels by weight.

The above finding is consistent with another report study by D. T. Pratt from the University of California in 1967 [93], who investigated gaseous ammonia-fired gas turbine combustors both theoretically and experimentally. His analyses demonstrated that the final size the chosen combustor is chemically rate limited almost equally by turbulent diffusion and mixing at high pressures. Thus, it was concluded that the fundamental problem with using gaseous ammonia as a turbine fuel is the relatively slow chemical reaction between ammonia and air. However, reducing air flow and Reynolds number to allow sufficient residence time for the reaction to progress, leads to decreased combustion efficiency. The solution proposed for this problem was to use a smaller fuel nozzle orifice to create a stronger fuel jet in the primary zone, this could be achieved by cracking the ammonia or using of an additive to achieve the needed optimisation.

However, there are only a few studies in the literature that deal with ammonia as a fuel for a gas turbine, this is due to most of this research being classified as a commercially confidential by companies which are looking for green energy sources. Nevertheless, there have been some studies in the literature reporting gas turbines using ammonia in complex flows. These include reports by SPG Advancing Propulsion and Energy [90, 94] Cardiff University in collaboration with Siemens from the United Kingdom [42, 95] Fukushima Renewable Energy Institute, in collaboration with the National Institute of Advanced Industrial Science and Technology and Tohoku University from Japan [96–99]

Karabeyoglu and Evans [90, 94] have pointed out that higher ammonia mass flow rates are required to generate the same work output, or more, at the same or lower outlet temperature. They also confirmed that using ammonia would lead to a reduction of NO_x emissions. There are, however, some technical challenges to the use of pure ammonia in a turbojet combustor, including unstable combustion with liquid NH_3, low

flame temperatures and the slow kinetics of NH_3 combustion. To solve these problems they suggested cracking the ammonia into hydrogen and nitrogen to help flame stability. Another option is to use ammonia in the vapour phase which will burn more readily in turbojet combustors. This requires a heat exchanger to vaporise the ammonia and produce H_2 to increase the reaction rate. Thus, partially cracking of ammonia should give better efficiency, greater flame stability, lower NO_x values, and improved power loading. SPG has asserted the need for a good cracking system to allow stabilisation of the flame, this could be achieved using a pre-burner to ensure splitting the molecules under extremely fuel-rich mixture conditions as shown in Figure (2-2). This finding highlights that ammonia has the possibility of becoming a green alternative fuel for the near future.

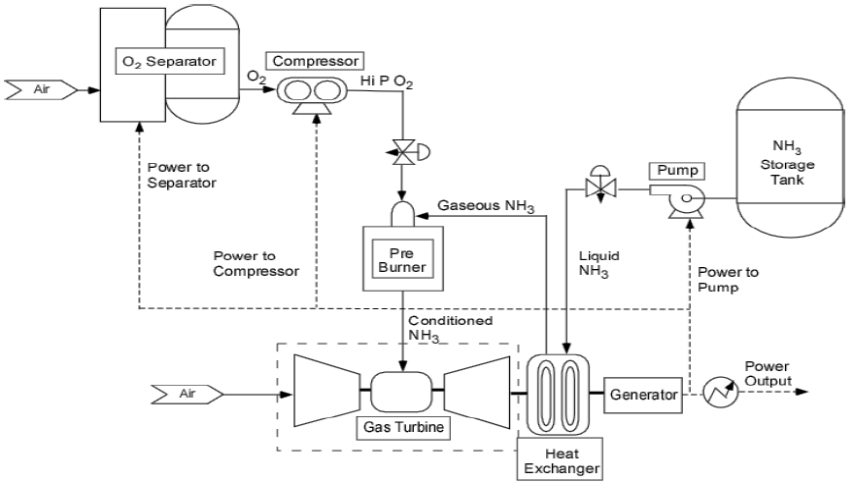

Figure 2- 2: Ammonia plant for power generation. [94]

One of the most significant current studies is the potential combustion of ammonia in gas turbine combustors. Valera-Medina et al. [42, 95] presented a series of numerical and experimental studies using a generic swirl burner that was fuelled by a variety of ammonia, hydrogen and methane blends. It was concluded that a fully premixed injection strategy is not appropriate for optimising ammonia combustion and it was observed that a stratified injection methodology needed to be developed to decrease emissions by encouraging the production of reactive species to produce water while reacting with NO_x. i.e., a new hydrogen injection strategy was required to ensure stable combustion, as simple premixing eventually led to flashback. Also, reducing the swirl

number to allow more time for the ammonia to fully react in the combustion chamber was recommended. Initial results have revealed a reduction in NO_x and CO emissions at high equivalence ratios > 1.10.

Recently, researchers from Japan have also shown an interest in micro-gas turbines firing ammonia blends, to test the potential of ammonia as a fuel. Iki at al., developed a 50 kW class micro-gas turbine using a mix of ammonia and kerosene as fuel [96–99]. This gas turbine was made by Toyota Turbine and Systems Inc. The standard combustor was replaced by a prototype bi-fuel combustor with diffusion combustion for to its flame stability. The results revealed that as the proportion of ammonia in the supply rose from 10%, to 30% and to 38%, the corresponding output power reduced from 25 kW, to 21 kW and then to 17 kW. However, the concentration of NO_x in the exhaust gas for ammonia/ kerosene combustion exceeded 600 ppm in this particular micro-gas turbine. Adding ammonia gas to the NO_x removal equipment could reduce NO_x emissions by employing SCR methods, which led to emissions below 10 ppm.

Kurata et al. [99] claimed to be the first to successfully use of ammonia-air combustion for power generation using a 50 kW class micro-gas-turbine system. They found that without any additives or pre-cracked ammonia, they successfully produced electric power of 44.4 kW at a rotational speed of 80,000 rpm and combustion efficiencies of the combustor ranging from 89% to 96% for higher-power generation operation. The higher power limits were due to the high temperature of the fuel, and the lower power limit was due to unburnt ammonia and NO_x emissions. Both emissions of NO and unburnt ammonia depended on the combustor inlet temperature. To achieve low NO_x concentrations in this micro-gas turbine, it was suggested burning large quantities of ammonia fuel to produce both rich and lean fuel mixtures in the primary combustion zone, and unburnt ammonia is expected to react with NO through selective non-catalytic reduction.

Analytic studies have also supported the use of ammonia in gas turbines. The effect of ammonia fuel fraction on the exergetic performance of a Turbec T100 micro-gas turbine was investigated by Ayaz et al. [100]. This gas turbine consisted of a centrifugal compressor, radial turbine, single can combustor, exhaust gas heat exchanger, recuperator and generator. Three different fuels were used to operate the gas turbine: (i) 100% CH_4, (ii) 10% CH_4 - 90% NH_3 and (iii) 20% CH_4 - 80% NH_3.

The micro-gas turbine was modelled with EPSILON software, and the results found that a 20% ammonia fraction is more environmentally friendly than a 10% ammonia fraction. It was found that control of the ammonia fraction was essential to sustain the exergy efficiency of the micro-gas turbine.

2.2 Ammonia Cracking

The concept of using ammonia as a hydrogen carrier is not new, and hydrogen can be produced from ammonia decomposition, or "cracking" to use as a fuel in various ways. Ammonia cracking is typically conducted at elevated pressures, temperatures and/or in the presence of a catalyst in order to ensure an efficient cracking process. Most of the available literature is devoted to catalytic cracking of ammonia with few articles addressing thermal decomposition. Catalytic cracking of ammonia into hydrogen is about 98-99% efficient at temperatures < 698 K. At temperatures > 773 K, ammonia starts cracking thermally without needing a catalyst. In practice, the rate of ammonia conversion depends on temperature, pressure and catalysts used [7].

2.2.1 Catalyst Cracking

Recent studies on catalytic ammonia decomposition have focused more on man-made ammonia. The kinetics of ammonia decomposition has been studied using metals, including; Cr, Co, Cu, Fe, Ir, Ni, Pd, Pt, Rh, Ru, Se, and Te, see Ganley et al. [46] ; or alloys of aluminum oxide with nickel, ruthenium and platinum [66], and alloys of iron with other metal oxides including Al, Ce, Si, Sr, and Zr [66]. Ganley et al. [101] demonstrated significant improvements in a structured aluminium-anodized alumina micro-reactor for decomposing ammonia to nitrogen and hydrogen at moderate temperatures. Adjustments to the geometry of the microreactor's features, use of a rubidium precursor, and application of a catalyst promoter were each shown to affect the reactor performance. The reactor converts 99% of ammonia at 873 K into the equivalent of 60 W of hydrogen. This would be sufficient hydrogen production for a number of applications such as fuel cell, internal combustion engine and gas turbine applications.

Different supporting structures have also been investigated to increase decomposition, and maintain the effective area of the catalyst under reaction conditions. Yin et al. [102, 103] investigated the use of more expensive elements including Pd, Pt, Rh and

Ru, as the active component in ammonia decomposition. It was shown that Ru, when supported on carbon nanotubes (CNTs), achieved an ammonia conversion level of about 84.65%, with a H_2 formation rate of 28.35 mmol/min gcat. The results were evaluated under ambient pressure and a temperature of 773 K. After the CNTs were modified with KOH, the ammonia cracking reached 99.74%, and H_2 formation rate was 47.88 mmol/min gcat. According to these results, Ru was the most active catalyst, CNTs were the most effective support, and KOH the best promoter. A later study by Wang et al. [104] investigated the effects of promoter cations and the amount of potassium on the structure of a Ru/CNT catalyst. They found that when Ru/CNT is treated with potassium nitrate, potassium hydroxide or potassium carbonate, the rate of ammonia cracking and the rate of hydrogen evolution significantly improved.

Different carbon powder pre-treatment solutions and catalyst deposition conditions were evaluated by Huang et al. [105] using Ru or Cs-Ru as the catalyst. The hydrogen generation rate was measured for different catalyst compositions, for ammonia inlet flow rates, decomposition temperatures, degree of catalyst packing, and the ratio of Cs to Ru. A maximum ammonia conversion rate of 90%, and hydrogen generation rate of 29.8 mmol/min g_{cat} were obtained at 673 K.

Due to the high cost of the ruthenium catalyst, some researchers started to seek a cheaper catalyst. Plana et al. [106] suggested alternative catalytsts such as layers of well-dispersed Ni on mesoporous γ-alumina. This catalyst is low cost, stable and exhibits high activity, achieving complete conversion of pure NH_3 at a temperatures of 880 K making this catalyst a promising candidate for in-situ H_2 generation from ammonia to feed fuel cells in vehicles or industry. Di-Carlo and his team [107, 108] studied a numerical simulation of ammonia cracking reactions over Ni/Al_2O_3 and Ru/Al_2O_3 catalysts. The results showed that to obtain satisfactory ammonia decomposition with Ni/Al_2O_3 and Ru/Al_2O_3 catalyst, the system must operate at a temperature of at least 823 K.

Increasing the reactor pressure seems to make the dissociation conditions worse but a pressure considerably higher than 1 bar is needed to counteract they partial pressure of hydrogen and get good permeation through the membranes. These conditions are reached around 10 bar. A different situation was observed when studying the Ru/Al_2O_3 catalyst experimentally at three different temperatures (673 , 723 and 773 K) and three

different operating pressures (1 bar, 5 bar and 10 bar). It was found that the dissociation was always higher than 99% at 1 bar, while at 5 bar it varied from 96% at 673 K to 99% at 773 K . At 10 bar chemical equilibrium was reached at 723 K and 773 K with dissociations equal to 95.5% and 97.2% respectively. At 673 K a dissociation close to the chemical equilibrium (92%) was observed. The efficiency of ammonia decomposition was estimated by the following expression:

$$\eta = \frac{\dot{m}_{NH3_{in}} - \dot{m}_{NH3_{out}}}{\dot{m}_{NH3_{in}}} \% \quad (2.5)$$

Gobina et al. [109] investigated the application of a catalytic membrane process for the elimination of dilute concentrations of NH_3 contained in coal-derived gas streams. The results demonstrated the superiority of such a composite membrane reactor system over other methods, and ammonia destruction of 100% was achieved even at a relatively low upstream pressures of 5 bar. Another model presented by Abashar [110] showed that an integrated catalytic membrane reactor is an attractive application for the removal of toxic ammonia traces from coal gasification streams. The results showed a fundamental improvement in the reactor performance regarding high levels of conversion, low temperatures and reduced mass of the catalyst used.

Papapolymerou and Bontozoglou [111] studied the unimolecular decomposition of ammonia at temperatures from 500 K to 1900 K. They used polycrystalline wires and foils of Pd and Ir as catalysts. They found that the decomposition rate of ammonia to N is fastest on Ir by several orders of magnitude when compared with other metals, becoming flux limited above 750 K. A series of fine powders of Fe–MOx catalyst, where M represent different metal components (M = Ce, Al, Si, Sr, and Zr) was investigated by Itoh et al. [112]. They found that ammonia decomposition over Fe–(Ce, Zr)O_2 was highest because the additive (Ce, Zr)O_2 solution worked as a solid acid to enhance ammonia adsorption and reaction probability of Fe components at relatively low temperatures. A CeO_2 promotor was also used by Zheng et al.[113] to enhance the catalytic activity and stability of Ni/Al_2O_3 catalysts for ammonia decomposition to CO_x-free hydrogen, with 98.3% NH_3 conversion and 32.9 mmol/min g_{cat} H_2 formation rate at 823 K. As a portable fuel cell power supply, Sørensen et al. [114] and Wang et al. [115] developed a miniature ammonia cracker produced by the catalytic decomposition of ammonia at low temperature in micro-fabricated reactors

with high efficiency CO_x-free hydrogen conversion. Wang et al. [115] found the ammonia conversion was better than > 99.9 % at 873 K during a 300-hour test.

Minak et al.[116] patented an invention for the treatment of vapours containing ammonia and from 5% to 40% by volume hydrogen sulfide, such as can arise in a coking plant or from crude oil. The vapours are initially are fed into a cracking furnace operating at a temperature of between 1273 K to 1473 K. This will produce a process gas which is fed through an ammonia-cracking catalyst that could be nickel, iron and/or nickel/iron, resulting in a hydrogen/nitrogen mixture. Another patent submitted in 1998 by Busson et al. [117] concerns a process and apparatus for cracking ammonia present in a fluid containing hydrogen sulphide. They introduced the fluid into a reactor comprising a suitable catalyst, and a catalytic cracking effluent is recovered. The reaction zone temperature is between 1273 K and 1673 K. The reactor comprised at minimum of one heating and one catalyst chamber in which the ammonia can be cracked without cracking the hydrogen sulphide.

MCM-41, SBA-15 and fumed SiO_2, as catalyst support for Ni and Ru have been used by Li et al. [118] to generate CO_x-free H_2 from ammonia. It was shown that the Ru catalysts were more active than the corresponding Ni catalysts. In 2014, a new class of catalysts for ammonia decomposition not based on the commonly used transition or noble metals was reported by David et al. [119]. Sodium amide ($NaNH_2$) and sodium metal (Na) were used as catalysts via their stoichiometric decomposition. The decomposition efficiency of ammonia was 99.2% at 800 K at the flow rates used.

Zhang et al. [120] investigated a series of synthesising nano-sized Ni/Al_2O_3 and $Ni/La–Al_2O_3$ catalysts loaded on various supports, such as active carbon, Al_2O_3, CNTs, MgO and SiO_2 which showed a performance comparable with present Ru catalysts The results demonstrated that the Lanthanum-promoted Ni catalysts were an interesting alternative to the noble metal-based systems for the application to NH_3 decomposition. In another study, Liu et al. [121] evaluated Ni/SBA-15 nano-sized catalysts to produce CO_x-free hydrogen. These catalysts exhibited higher performance than other nickel-based catalysts, and also some supported Ru catalysts, with ammonia conversion greater than 96% at temperature 873 K. Furthermore, the Ni/SBA-15 catalyst is very stable due to the strong interactions between nickel grains and the SBA-

15 support during the catalytic evaluation operation. An ammonia cracking device which includes an ammonia cracking catalyst has been presented by Hikazudani [122]. The cracking of the ammonia to produce hydrogen was by means of an ammonia-oxidation as shown in Figure (2-3) with a catalyst supporting ruthenium, rhodium, nickel, and/or iron.

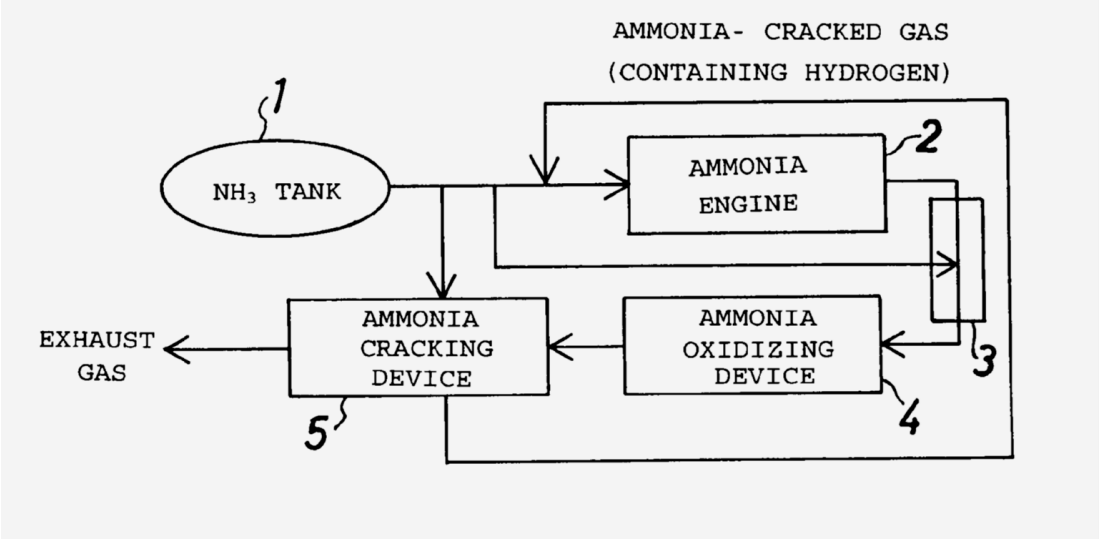

Figure 2- 3: Ammonia engine device. [122]

They found that 100% of ammonia cracking occurs at 600 K and above. These inventors found that ammonia produces heat when it undergoes an oxidation reaction with oxygen as expressed by Equation (2.6):

$$NH_3 + \frac{3}{4}O_2 \rightarrow \frac{1}{2}N_2 + \frac{3}{2}H_2O \quad (2.6)$$

In a follow-up study, Nagaoka et al. [123] considered the use of an acidic RuO_2/γ-Al_2O_3 catalyst on ammonia and oxygen at room temperature. This process can produce hydrogen, nitrogen and water vapour; the process does not require any external energy source or use of any complicated procedure. Because adsorption of ammonia onto the catalyst is exothermic, this study demonstrated the concept of catalysts self-heating by adsorption of reactant molecules, which is a novel strategy for the cold-start process of hydrogen production from ammonia and other reactions.

The performances of various catalysts for ammonia cracking, reviewed in this section, are summarised in Table (2-3).

Table 2- 3: Summary of ammonia decomposition catalysts performance reported.

Catalyst /Support	Temp. (K)	Conv. Eff. (%)	Ref.
aluminium-anodized	873	99.00	[101]
Ru/ CNT	773	84.65	[103]
Ru/ CNT treated with KOH	773	99.74	[103]
Ru/ Cs	673	90.00	[105]
Ru/ Al_2O_3 at (1 bar)	673	99.00	[108]
Ru/ Al_2O_3 at (5 bar)	673	96.00	[108]
Ru/ Al_2O_3 at (5 bar)	773	99.00	[108]
Ru/ Al_2O_3 at (10 bar)	673	92.00	[108]
Ru/ Al_2O_3 at (10 bar)	723	95.50	[108]
Ru/ Al_2O_3 at (10 bar)	773	97.20	[108]
Ni/ Al_2O_3	823	98.30	[113]
Ni-CeO_2 / Al_2O_3	873	99.90	[115]
Na/ $NaNH_2$	800	99.20	[119]
Ni/ SBA-15	873	96.00	[121]

2.2.2 Thermal Cracking

The first serious attempt at thermal cracking of ammonia was in 1933 when the United States patent office published details of Burke's "Apparatus for decomposing ammonia" [124]. Liquid ammonia was heated in tubes to produce gaseous ammonia which was heated further in a second chamber where it flowed in heated tubes over a suitable catalyist. Burke claimed his invention gave 90% decomposition of ammonia at temperatures between 823 K and 923 K. A patent by Normand, registered in 1978, provides a method for generating hydrogen and nitrogen by cracking gaseous ammonia and cleaning and recycling a previously generated atmosphere that had already been used [44].

In a subsequent patent, Graville reported a method of combusting waste gas containing at least 50% by volume of ammonia by adding an oxygen-air mix, see Figure (2-4) [125] Both cracking and combustion take place in the combustion zone, and the process is sufficiently intense for Graville [125] to claim "no ammonia remains". For complete combustion, the oxygen supplied had to be between 75% to 98% of the total stoichiometric requirement of all the combustible fluids. Controlling the combustion conditions allows the formation of NO_x to be minimised.

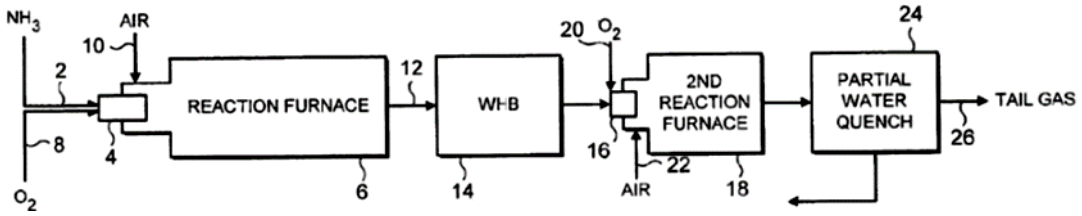

Figure 2- 4: Destruction of waste gas [125].

A process for the "production of hydrogen by autothermic decomposition of ammonia" to produce high purity hydrogen was patented by Goetsch et al. [126]. This invention used the hydrogen produced to supply a fuel cell. The inventors found that the ammonia decomposition reaction could be made autothermic, not needing heat to be added from any outside source. Auto-thermal operation takes place when an exothermic reaction can continue to drive itself as well as any coupled endothermic reactions. This is achieved by burning a proportion of the hydrogen produced in the same reaction zone in which ammonia decomposition is taking place. This autothermal reformation of ammonia still required catalyst bed technology.

Arana et al. have designed a micro-electro-mechanical system (MEMS) with suspended-tube chemical reactors that addresses the critical issues of thermal management in portable fuel cell systems [127]. They reported the first demonstration of combustion and ammonia cracking simultaneously at high temperature in a MEMS device without electrical power input. Thermal characterization revealed that the reactor could be operated up to about 1173 K, and that intrinsic heat loss (conduction in the solid) is very low. Based on experimental results, these losses are estimated to be less than 0.1 W at 1073 K. Other losses (conduction and natural convection through the ambient air, and radiation) can be substantially reduced by proper packaging. The paper also presents results from catalytic, auto-thermal butane combustion, and ammonia cracking in the reactor.

Grannell et al. [128] presented a conference paper related to the decomposition of ammonia into a hydrogen gas mixture. A method of decomposing a portion of a mixture of anhydrous ammonia is initiated within a conduit. The hydrogen produced mixes with the gas mixture and the released heat is used to complete the combustion reaction. A mixture of gaseous products which includes non-combusted hydrogen gas

results from the reaction, and are expelled from the outlet of the conduit, and may be used for other purposes. It was found that the theoretical performance limit of this ammonia flame cracker with zero losses, based on the LHV, gave a product containing about 52% H_2 by volume, with a NH_3 – H_2 thermal conversion efficiency of 97.3%. Full cracking occurred at an equivalence ratio of 6.66.

Engbaek [129] designed an ammonia cracker for hydrogen generation for PEMFC power applications. Ammonia decomposition methods depending on hydramine catalyst beds which deliver ammonia to the cracker by using a counter-current flow heat exchanger were also assessed. He found that 83% ammonia cracked to hydrogen with 800 ppm of NH_3 concentration at the output, with 92% conversion efficiency with emissions of nitrogen and water.

According to a US patent by Page et al. [130], an ammonia thermal cracker including a combustion chamber was used as a hydrogen fuel source for alkaline membrane fuel cells. The cracker produced about 75% H_2 and 25% N_2 with about 1 ppm to 20 000 ppm of residual ammonia concentrations. In 2011, another patent related to energy efficient generation of hydrogen from ammonia for fuel cells was recorded by Dabasish et al. [131]. This invention is based on the use of solid ammonia stored in metal ammine salts such as, $Ca(NH_3)_8Cl_2$ or $Sr(NH_3)_8Cl_2$) in a friendly way. The power generation utilises waste heat from the cracker to release ammonia from the stored material. A high reaction temperature (823 to 1023 K) is required to achieve the maximum conversion of ammonia according to the endothermic reaction Equation (2.7):

$$NH_3 \rightarrow 1.5\,H_2 + 0.5N_2 \quad ,\Delta H_{298} = 46\ KJ/mol_{NH_3} \tag{2.7}$$

This heat can be used usefully either by aiding the combustion of fuels or electrical heating. However, electrical heating is not only expensive, but is unavailable during start-up if the system does not contain a battery. Therefore, it is preferred that this heat will be provided by the combustion of an appropriate fuel, preferably ammonia or hydrogen as in the invention of Grannell and Gillespie [45]. which relates to cracking ammonia into a hydrogen gas mixture. This method of ammonia decomposition includes a flow of premixed, ammonia-rich gaseous mixture of anhydrous ammonia and air into a conduit. The products of the gaseous mixture along with uncombusted hydrogen resulting from the reaction may then be used for other purposes.

The total ammonia /air reaction is described by the following equation:

$$0.79N_2+0.21O_2+0.28\emptyset\ NH_3\rightarrow 0.42H_2O+(0.93+0.14(\emptyset-1)X)N_2 +0.42X(\emptyset-1)H_2+0.28(\emptyset-1)(1-X)NH_3 \quad (2.8)$$

Where

$\emptyset$: ammonia/air equivalence ratio, and $\emptyset > 1$.

X: decomposition yield of the un-combusted ammonia, and $0 \geq X \geq 1$

An efficient way to crack ammonia was invented by Brandenburg [132]. A resonant cavity was divided into two compartments separated by a dielectric diaphragm. Ammonia gas was injected into one of the compartments, as shown in Figure (2-5). A microwave antenna emits electromagnetic energy into the other compartment. The level and frequency of the signal is such that a plasma discharge is generated, see Figure (2-5). The plasma discharge is an effective means of breaking down anhydrous ammonia which crosses the membrane and leaves the cavity by means of an outport.

The outer walls of the microwave device should be constructed from any metal that is a good conductor of electricity. A stainless steel or nickel metal would be preferred for the internal surface coating to prevent chemical corrosion during ammonia cracking. Little heat escapes from the system and, it was claimed the plasma cracker could crack one litre/s of ammonia with a power consumption of 2 kW. The hydrogen produced could be stored for later use or combusted in a fuel cell producing 12 kW of power at a high efficiency of about 80%.

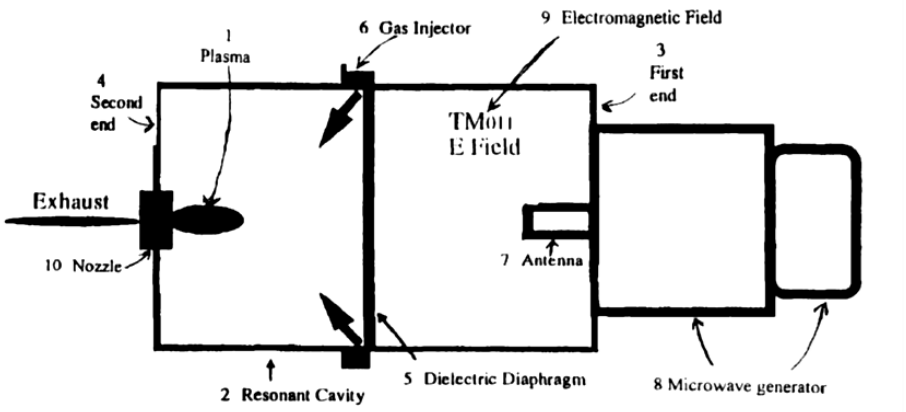

Figure 2- 5: Plasma reactor for cracking ammonia and hydrogen-rich gases to hydrogen [132].

2.3 Ammonia Fuel Combustion

Since the early 1960s, extensive studies have been performed to investigate the combustion of ammonia, both experimentally and numerically. There have been many investigations of rich, lean and stoichiometric ammonia flames under various pressures and different conditions [92]. In general, the primary interest of these studies was to understand the function of hydrogen and ammonia in the formation and consumption of nitrogen oxides. Other researchers stopped working on the topic because of ammonia's very low combustion efficiency until, the end of the 1980's when several studies on the chemistry of the atmospheric pollutant, N-C-O-H, revealed various thermal NO and prompted NO mechanisms. Serious studies on ammonia as a hydrogen-energy carrier gained attention and many ammonia fuel associations have been established across the world since the 2000 to study ammonia combustion by deepening the understanding of reaction models and the knowledge of the flame characteristics of various blends.

Pratt and Starkman [133] studied a non-catalytic, gas-phase combustion reaction between ammonia and air in an adiabatic well-stirred reactor. They concluded that the overall reaction rate for ammonia-air combustion could be well represented by the Arrhenius equation. They found that the interaction with the reactor wall plays a vital role in the kinetic mechanism for slow reactions, but not for fast reactions. Thus, additional studies on the kinetics of ammonia combustion were required.

In the early 1980s, Dasch and Blint [134] investigated both experimentally and theoretically the significant properties of lean to stoichiometric ammonia-oxygen-nitrogen atmospheric pressure flames, to identify the reactions and conditions that control the conversion of the nitrogen contained in ammonia to NO or N_2. The ammonia flames ranged over an equivalence ratio of $\emptyset$ = 0.5-1.1, the flame speeds varied between 25-130 cm/s and temperatures were in the range 2000 K-2700 K. They concluded that the conversion of the nitrogen from NH_3 to N_2 is mainly dependent on the NH_2 + NO reactions, because the ratio of the products of this reaction influence the flame speed.

Both experimental and modelling investigations of ammonia chemistry in post-combustion gases that were below flame temperatures, were reported by Grcar et al. [135]. The results of the experiments were considered in terms of a simplified mixing

reactor, plug-flow, and 2-D direct numerical simulation. It was shown that the final products the process were sensitive to mixing of the post-combustion gases. Ammonia oxidation at low temperatures occurred in a premixed reaction zone, but at sufficiently high temperatures, a non-premixed reaction zone that produces significantly less NO than the equivalent premixed system might be developed.

In general, prior studies show that the main contributor to NO_x formation in ammonia flames is fuel-bound nitrogen rather than thermal NO_x production by atmospheric nitrogen [136]. Therefore, a comprehensive understanding of ammonia combustion chemistry and detailed analysis of NO_x formation pathways is required for accurate prediction of emissions due to fuel-bound nitrogen.

2.3.1 Reaction Mechanism Models for Ammonia Combustion

Several chemical kinetic models have been developed and implemented to analyse ammonia oxidation and NO_x formation reactions. Relevant experimental and modelling studies on ammonia combustion at low pressure (0.04 bar) were performed by Tian et al. [137]. They studied the flame structure of 11 premixed $NH_3/CH_4/O_2/Ar$ flames at stoichiometric equivalence ratios using tuneable synchrotron vacuum ultraviolet photo-ionisation coupled with molecular-beam mass spectrometry. This study considered both the role of the conversion reactions of NO with NH_2, and analysed flow rate sensitivity to determine the main reaction pathways of CH_4 and NH_3 oxidation and their mutual interaction. Recently, Tain's mechanism [137] has been used widely over a wide range of conditions.

Skreiberg et al. [138] established a detailed chemical kinetic model using the SENKIN and CHEMKIN codes for ammonia oxidation in the presence of hydrogen, carbon monoxide, and methane. Stoichiometries range from slightly lean to very fuel rich conditions, temperatures from room temperature to 1330 K, and NO levels from 0 to 2500 ppm. In this mechanism several reactions were characterised more accurately, and its use was suggested for assessing the possible reduction of NO during combustion of gases derived from biomass. It is also suggested as being useful for assessing NO formed by the combustion of the products of coal gasification. The results were summarised as: high temperatures promote the reaction path $NH_3 \rightarrow NH_2 \rightarrow NH \rightarrow N_2$, and at lower temperatures the sequence $NH_3 \rightarrow NH_2 \rightarrow N_2$ is significant. Konnov [139] has developed mechanism for simulating hydrocarbon/NH_3 and H_2/NH_3

oxidation reactions. This mechanism has proved a good performance predictor of NO_x emissions in several ammonia combustion studies [140–142].

In specific studies, comparison of results predicted by the Konnov reaction mechanism and experimental data have been performed to avoid inaccurate and possibly misleading predictions [141, 142]. Duynslaegher et al. [141] have studied the structure of an ammonia-oxygen-hydrogen-argon premixed flat flame by using molecular beam mass spectrometry and confirmed that the Konnov mechanisms and experimental results were 'in agreement' but that using the Konnov mechanisms tended to overvalue the mole fractions of the radical NH_2 while underrating those of N_2O. Duynslaegher et al. [142] improved Konnov's ammonia combustion mechanism model by investigating the ammonia flame at low pressures and for various fuel mixtures, stoichiometries, and combustion conditions. The reduced mechanism contains 80 elementary reactions and 19 chemical species and allows for a better understanding of all the nitrogen oxides formation pathways. However, the results of this reduced mechanism are unable to produce reliable predictions for flame speed and NO_x emission for very lean or very rich conditions. Therefore, obtaining a reaction mechanism valid over a wide range of conditions remains an important factor in obtaining reliable numerical simulations.

There is a large volume of published studies describing ammonia oxidation and NO_x formation/removal in flames during oxy-fuel combustion in a flow reactor [143, 144] or shock tube [145–149] or by using laser-induced / saturated fluorescence [150, 151]. Mendiara and Glarborg [143] measured the effects of a high CO_2 concentration on ammonia chemistry during methane oxidation in a flow reactor. The experimental work was demonstrated under atmospheric pressure conditions and for the various stoichiometric ratios of the fuel, from rich to lean and a temperature range 873–1773 K. The kinetics of the model were based on the Tian mechanism [137]. Through pathway analysis it was identified that the formation of NO is related mostly to HNO which is primarily sourced from NH_2 + O. Also, the direct reactions between N-radicals and CO_2 are responsible for the effect of high CO_2 concentrations on ammonia conversion.

The effect of enhancing the oxygen content of the air for combustion of ammonia-air blends was investigated numerically by Li et al. [144]. They investigated possible

improvements in NH_3 combustion by increasing the oxygen from 21% to 30% with emphasis on flame speed and temperature, and ignition. The rate of production of N-related intermediate species such as NH_2, NH, N, and HNO is significantly increased because of the higher rate of the reactions attacked by H, O, and OH, as the O_2 content is increased. The results of this study indicate that increasing the O_2 content in the combustion air has a positive affect on the ammonia laminar burning velocity and adiabatic flame temperature. Therefore, this technique is likely to be favoured for improving NH_3 combustion, although it needs to be carefully considered due to the increase amount of OH, H and O radicals that promote HNO.

A number of significant studies have investigated the combustion mechanisms containing an ammonia-sub mechanism to characterise NH_3/H_2/air mixtures at a wide range of pressure, temperature and equivalence ratio [145–149]. These studies revealed that the low-temperature ignition delay times measured in shock tubes (below 1000 K) could not be well-predicted. The results indicated that equivalence ratio variations have no effect on delay times, but an increase of pressure prompts a strong decrease in delay times. Therefore, in order to extend the validity of these mechanisms, they should be tested by comparing the modelled and the experimental results obtained from, e.g., burners and flow or jet stirred reactors. Mathieu and Petersen [149] studied the oxidation of ammonia for a wide range of conditions under high temperatures (1560–2455 K), pressures of 1.4, 11, and 30 bar, and for equivalence ratios of 0.5, 1.0, and 2.0. The established chemical mechanisms were compared to several models available in the literature which had proved accurate in predicting ignition delay times of ammonia oxidation under conditions relevant to many industrial applications.

Recently, Li et al. used laser-saturated fluorescence and probe sampling to study ammonia-doped methane/air flames on a perforated plate burner at atmospheric pressure [150]. NO concentrations in the post-flame zone were measured. It was concluded that the results obtained for ammonia conversion in rich flames disagreed with some earlier experiments. It was hypothesised that the differences could be due to the lack of a proper protective coating inside the ammonia storage cylinders used by previous researchers. This hypothesis also indicated that the experimental results of NO_x formation were accurately reproduced by flame models using the ammonia conversion mechanism developed by Skreiberg et al.[138] and Konnov [139] both in lean and in rich flames.

Laser-based diagnostics has also been used to investigate the structure of premixed ammonia- air flames on a porous-plug burner at atmospheric pressure for lean, stoichiometric and rich mixtures [151]. The radical concentration profiles of NH, OH, and NO in the reaction and post-flame zones showed a good match between the proposed kinetic model and the experimental results in terms of temperature and flame front position at all equivalence ratios, except for NO concentration in the rich flame. It was concluded that this model should be extended to other combustion systems, such as ignition and flame propagation, and be tested by further experimentation.

There are chemical models developed initially for hydrocarbon fuels which can usefully be applied to ammonia combustion studies. For example, the GRI Mech 3.0 software [152] was developed for, and is widely used to model the combustion of natural gas. It includes the mechanisms related to the formation of NO_x and re-burn chemistry. These mechanisms have also been used by Zieba et al. [153] with satisfactory results. Zieba et al. researched the interaction of the ammonia molecule with methane for flameless oxidation technology. The necessary radicals for ammonia conversion are generated from hydrogen oxidation. The results showed that at lean conditions in the presence of natural gas, ammonia reacts slowly leading to high NO_x emissions, while the complete decomposition reaction of ammonia was reached very rapidly in the fuel-rich region of the jet.

Shmakov et al. [154] demonstrated experimentally the progression of the hydrogen flames' chemistry when doped with NO and ammonia, using molecular-beam mass-spectrometry. They compared the experimental results with the results from a numerical simulation using premix codes from CHEMKIN-II. They then presented a comprehensive study of different groups who have performed the analysis using different molecules in lean ($\emptyset$ =0.47), near-stoichiometric ($\emptyset$ =1.1) and rich ($\emptyset$ =2) hydrogen blends with O_2 and N_2. Their findings showed that laminar burning velocity increased exponentially as the hydrogen fraction in the blend was increased. The flame structure showed a good agreement at lean and near stoichiometric blends, while in the rich flames a significant discrepancy was observed between simulated and measured profiles of NO concentration.

Despite an extensive number of studies, more work is required to validate the reaction mechanism model of ammonia combustion over a broader range of conditions, a need demonstrated by some recent studies.

2.3.2 Ammonia/Hydrogen Combustion

Recently, researchers have published several studies describing the influence of blended hydrogen on ammonia combustion. Kumar and Meyer [155], for example, performed a comparison study between experimental and modelling of laminar flame speeds for premixed H_2/NH_3 combustion. This work was undertaken at atmospheric ambient conditions with a jet flame configuration. The NH_3 fraction within the fuel was varied in step increases of deliverable energy, up to a maximum of 80%, for equivalence ratios between 0.5 and 1.1. Computational models used were CHEMKIN-PRO, and GRI-Mech 3.0 [152] with the Tian [137], and Konnov [139] reaction mechanisms. The Tian and Konnov mechanisms were shown to produce better agreement with experimental results than the GRI-Mech 3.0, revealing that the production of the OH radical is a key performance variable in modelling laminar ammonia decomposition.

Several studies [156–158] have supported the argument that ammonia could be an effective green additive for improving the safety of hydrogen, but with the challenges of the relatively slow chemical reaction rate of NH_3-air blends, and fuel bond NO_x emissions. The group from Sungkyunkwan University published work using a co-flow non-premixed flame configuration to characterise the stability limits and emission profiles of blended H_2/NH_3 flames. This work was performed under atmospheric ambient conditions and compared to modelled data produced using the commercially available CFD code FLUENT 6.3. The results showed that the ammonia addition significantly reduced the stability limits of the non-premixed flames. Also, the FLUENT model suggests NH_3 is consumed further upstream nearer the burner than H_2, as a result of the relative diffusivities of each fraction [157]. Nozari and Karabeyoglu [158] developed a reduced chemical mechanism for the combustion of ammonia/hydrogen based on the Konnov mechanism [139]. It was concluded that the total NO_x formation of ammonia-doped flames would noticeably decrease by operating under fuel rich conditions and reduced to minimum values near an equivalence ratio of 1.2, as shown in Figure (2-6). They obtained these results by

comparing the performance of the reduced mechanism with the full mechanism and experimental data. These revealing the ability to predict the combustion characteristics in a wide range of fuel conditions.

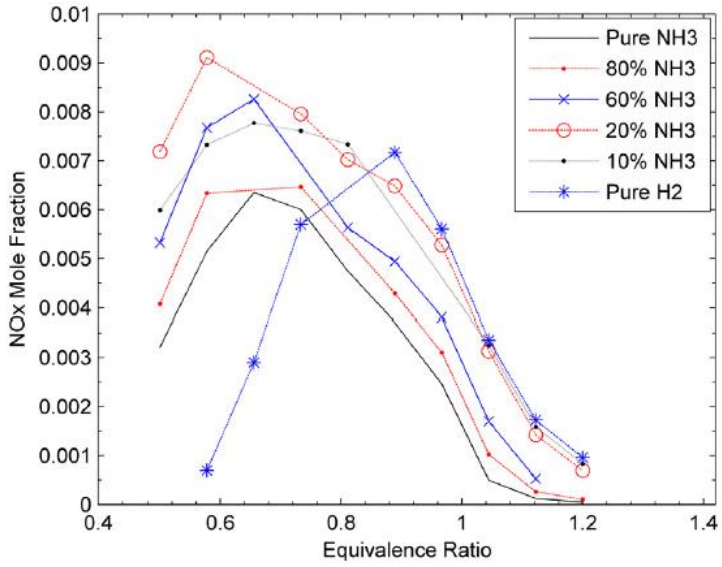

Figure 2- 6: Total NOx mole fraction as function of equivalence ratio, P = 17 bar, T = 673 K [158].

Hayakawa et al. [159] raised several concerns about hydrogen enhanced ammonia flames at high pressures (up to 5 bar). They suggested that the addition of hydrogen would improve the ammonia reaction and the swirling flow in real gas turbine combustors would increase flame stability. It was demonstrated that the laminar burning velocity of the ammonia/hydrogen/air premixed flame increased exponentially with the increase in the hydrogen ratio and decreases as the initial mixture pressure increases.

Xiao and Valera-Medina [160] from Cardiff University compared twelve different chemical kinetic models of ammonia/hydrogen blends over a wide range of conditions found in industry. All the models were tested regarding flame speed, NO_x emissions and ignition delay against experimental data. Results show that the Mathieu mechanism had the best agreement with the experimental data within the given range of different initial NH_3 concentrations in the NH_3/H_2 fuel mixtures, equivalence ratios and pressures. In addition, this mechanism gives the best prediction of laminar flame

speed under fuel rich condition (Ø >1.20) with an average relative error of 1.38%, and the maximum flame speed is achieved around an equivalence ratio of 1.1.

The same group from Cardiff University developed an improved Mathieu mechanism in terms of NO_x emission calculations to validate premixed combustion characteristics of ammonia and hydrogen fuel blends for gas turbine applications [161]. The results of the numerical simulation using 2-D large-eddy simulation (LES) indicated that the mechanism developed offers considerably higher efficiency, hence utilization, for future 3-D CFD analysis under gas turbine combustion conditions [162]. Kobayashi [163] also studied the flow structure of the swirling ammonia flames in a mono-fuelled micro-gas turbine using 3-D numerical analysis of LES, under rich conditions. He concluded that controlling equivalence ratios is an effective way for NO emission reduction.

2.4 Emissions of Ammonia Combustion

As highlighted by most of the studies mentioned above, the principal exhaust emissions produced when burning ammonia are unburned ammonia and nitrogen oxides (NO_x) unless the process involves some mixture of carbon-based fuels such as methane, gasoline or diesel, in which cases CO_2 emissions must be considered. NO_x emissions, nitrogen monoxide (NO), nitrogen dioxide (NO_2) and nitrous oxide (N_2O) are responsible for urban smog and some forms of acid precipitation. Nitrogen monoxide (NO) is formed in ammonia flames by two main paths: thermal NO, which is produced by oxidation of nitrogen in the air and requires a sufficiently large temperature and time to form, NO as described by the Zeldovich mechanism , and fuel NO produced by the following reaction [164]:

$$NH_i + OX \rightarrow NO + H_iX \tag{2.9}$$

Where *OX* is an oxygenated species and NH_i a radical.

There have been several studies in the literature reporting that NO_x emissions can be successfully controlled and reduced. One of the most common methods is to use a SCR system [87, 98], [165–168]. SCR requires ammonia or urea to be injected into the exhaust downstream of the combustion process before a catalyst; the ammonia reacts with NO in the presence of the catalyst to form molecular nitrogen and water. These SCR catalysts are manufactured from various ceramic materials used as carriers.

However, poor durability of catalyst and low NO_x reduction (10-40%) in the actual exhaust gases remain a problem. Hence, alternative homogenous gas-phase selective non-catalytic reduction technology using NH_3/urea has been investigated by Nam and Gibbs [169] for diesel NO_x reduction. This technology, which originally referred to a thermal $DeNO_x$ process, depends on injecting nitrogen-based species directly into the downstream hot exhaust gases of diesel engines in the presence of excess oxygen in order to reduce NO_x concentrations without the need for a catalyst. Both techniques offer lower system cost due to the reduction of additional equipment needed to reduce the emission. Also, they give a better fuel economy but require a reductant to be stored on board the vehicle.

Some recent studies [170] have demonstrated that homogeneous charge compression ignition technology may provide 40-50% efficiency for compression ratios > 40:1. NO_x emissions are minimized by partial decomposition of ammonia, after that, the hydrogen is separated from the nitrogen and fed to the cylinder as almost pure hydrogen to improve the combustion, Figure (2-7). Similarly, a partial cracking of ammonia as described by Nozari et al. [171] showed high efficiency when burning premixed ammonia /hydrogen/ air flames using silicon-carbide as a porous media with a large operational range. The results indicated that NO_x concentrations as low as 35 ppm under rich conditions can be achieved.

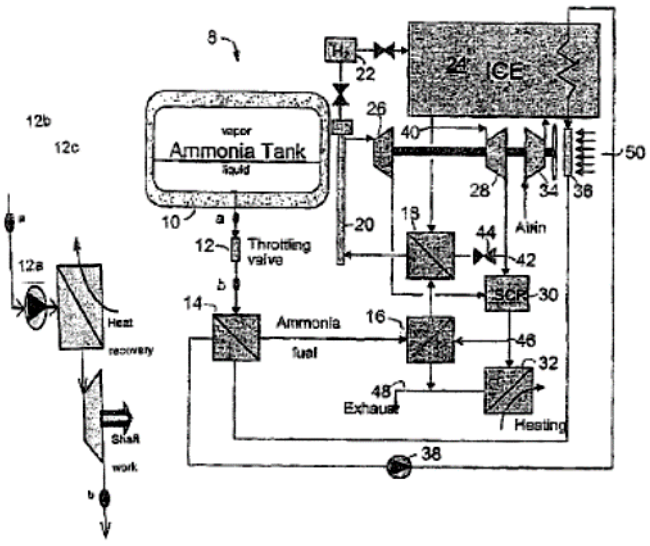

Figure 2- 7: Apparatus for using ammonia as a sustainable fuel, refrigerant and NO reduction agent [170]

Hayakawa et al. claim that little attention has been paid to the study of the characteristics of ammonia/air flames using spherical vessel methods, especially at high pressures [172]. The results, so obtained revealed that flame velocity decreased with increasing pressure, and the maximum flame speed occurred at $\emptyset$ =1.1 for all initial mixtures and pressure conditions. Lee et al. [173] raised the same concerns regarding laminar premixed ammonia/hydrogen/ air flames to determine the burning velocities, and NO_x and N_2O emissions. They suggested hydrogen as a promising additive for enhancing flame sensitivity to stretch with low NO_x and N_2O emissions under fuel-rich conditions. Lee et al. [174], also examined the effect of ammonia substitution on ammonia/hydrogen/air flames both experimentally and computationally, and found similar results to those obtained by [173].

Li et al. [156] performed an in-depth study of various blends of hydrogen and ammonia in order to experimentally observe the emissions produced by these carbon free fuels at different equivalence ratios. It was conclusively shown that the burning velocity of ammonia improved with increased numbers of hydrogen atoms in the flame. Fuel-NO_x plays the major role, and thermal-NO_x a minor role in H_2/NH_3-air combustion. The results showed that suitable combinations of H_2/NH_3 as a fuel gas could enhance combustion performance with moderate NO_x emission.

Valera-Medina et al. [2] indicated that using strong swirling flows with both CH_4/NH_3 and H_2/NH_3 blends could reduce NO_x emissions. Ammonia swirl-stabilized flames with hydrogen and methane has been investigated by Meyer et al. [175] in a 40 kW burner with swirl-plate stabilizers, accessible flame, an easily movable fuel nozzle, laser diagnostics and a self-sustaining heat exchanger. It was found that the use of a flame holder gave a more uniform temperature with a reduction in NO_x emissions, see Figure (2-8), and hence increased combustion efficiency.

Woo et al. [176], experimentally investigated the production characteristics of NO_x in co-flow non-premixed CH_4 jet flames at different concentrations of oxygen/hydrogen/ammonia which were also analysed using 1-D and 2-D numerical simulations. The numerical simulations were carried out using the detailed chemical kinetics contained in GRI Mech 3.0. The results showed that NO_x emissions increased for both relatively low and high oxygen ratios in the oxidizers. On the other hand, NO_x emissions actually decreased between the two ranges of the oxygen ratio, a

phenomenon that appears to be due to a reduction in reaction rates at the same time as the ammonia accelerated production of NO in the internal layers, while playing the role of a NO_x inhibitor in the external layers. However, as previously stated, this chemical reaction model showed a lower performance when analysing ammonia-based fuels.

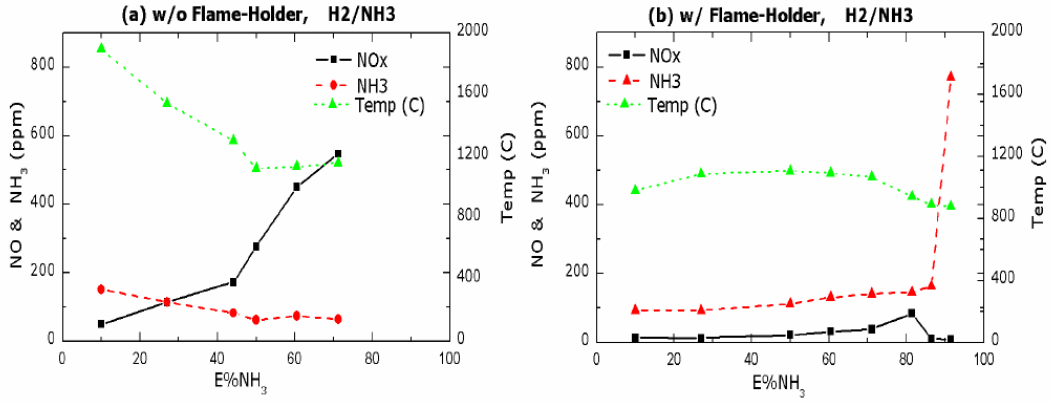

Figure 2- 8: Comparison for NOx and NH_3 and flame temperature in H_2/NH_3/air mixture, Tair = 573 K & Ø =0.95, Heat rate ~ 15 KW (a) without flame holder (b) with flame holder [175].

Xiao et al. [177] performed a 1-D numerical analysis of ammonia/methane combustion in gas turbines using Chemical Reactor Network theory. They compared in detail four different mechanisms (Tian, Teresa AA and Konnov) with the experimental work to identify their accuracy in representing reaction kinetics under real gas turbine combustor conditions. The results suggested that the Tian mechanism was best suited to determine the effects of pressure and temperature on NO_x production. Results also indicated that a slightly fuel-rich combustion and pressure can achieve a considerable decrease in NO_x emissions.

A non-staged model combustor (PSR-PFR) was well presented by Rutar and Malte [178]. Li et al. [179] modelled the characteristics of NO_x formation in a NH_3/CH_4 fired combustor using perfectly stirred reactors (PSR) and plug flow reactors (PFR) with the Tian mechanism. It was found that lower NO_x emissions were achievable in simple two-stage combustion for a fuel-rich Ø =1.5) condition with 40% NH_3. Further reduction of NO_x in the post-combustion zone under fuel-rich conditions can be

achieved through the NH_i and N_2O pathways, and by an increase in residence time in the post-combustion zone, see Figure (2-9).

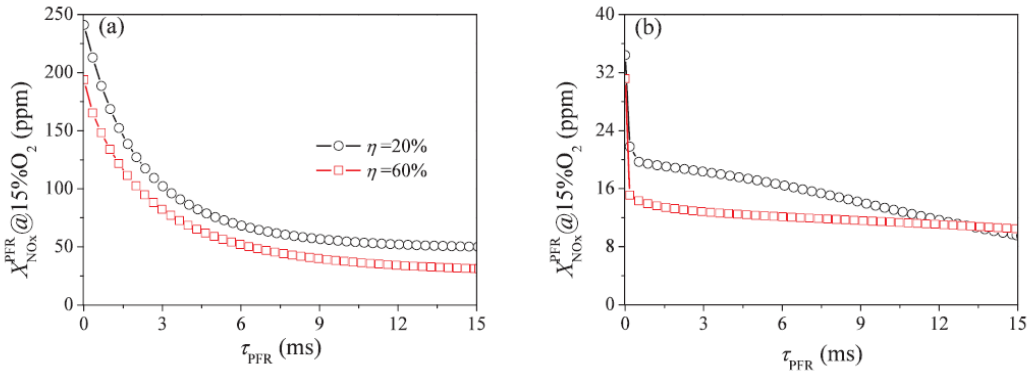

Figure 2- 9: The evolution of NOx with residence time in the plug flow reactor of the primary stage with a) Ø=1.2 and b) Ø =1.5. [179]

Somarathne et al. [180] carried out a numerical study of the emission characteristics of turbulent premixed NH_3/air flames in a gas turbine at high pressure using large eddy simulation and the finite rate chemistry technique by using an OpenFOAM code without and with injection of secondary air. The study found that under rich flame conditions the NO and unburnt NH_3 emissions were reduced at high pressure and the third body reaction of OH+H+M ↔H_2O+M also played a significant role on the reduction of OH and, therefore, NO concentration. Also, the results found under rich flame condition the unburnt ammonia in the primary combustion zone paved the way for NO generation again in the secondary combustion zone.

2.5 Summary

A literature review of topics related to the use of ammonia as an alternative fuel for power generation, either directly or after cracking, has been carried out in this chapter. The chapter also summarises ammonia combustion related technologies to gas turbine applications, especially the reaction mechanisms used to analyse ammonia oxidation and NO_x formation reactions and how to reduce the emissions from the combustion of ammonia.

It could be noticed that there are several noteworthy patents available, relevant to the use of ammonia as a fuel for in a number of applications. These patents were taken out

by individuals and/or commercial enterprises to protect their intellectual and property rights for using ammonia as a green fuel for near future. These patents are summarized in Table (2-4).

Table 2- 4: Patents summary

Ref.	Classification			Sub- Classification				Purpose
	Catalyst	Heat Transfer	Plasma	Material	Process	Design	Fuel Delivery	
[66]	X			X	X		X	Cracking
[116]	X				X			Usage
[117]	X				X			Cracking
[122]	X					X		Cracking
[124]		X				X		Cracking
[44]		X			X			Cracking
[125]		X			X			NO_x Reduction
[126]		X		X			X	Cracking
[130]		X		X			X	Fuel cell
[131]		X		X		X		Fuel cell
[45]		X			X	X		Cracking
[132]			X		X			Cracking
[58]	X			X		X		Fuel cell
[71]		X		X			X	I.C.E
[72]	X			X	X			I.C.E & Fuel cell
[165]	X			X			X	NOx Reduction
[166]	X					X		NOx Reduction
[170]		X				X	X	NOx Reduction

Furthermore, it can be concluded that:

- Ammonia has the advantage of being widely produced globally with an existing transport and storage infrastructure, which is a significant advantage over hydrogen. It has been shown to be a cost-effective competitor to hydrogen storage. The energy cost of ammonia is less than hydrogen. In addition, the power life cycle cost is lower than either methanol or hydrogen.

- In diesel applications, the use of direct injection of liquid diesel and gaseous ammonia into the engine cylinder needs to use high injection pressure to overcome the in-cylinder pressure as ammonia will liquefy in the injection line. In engines, the direct injection of liquid ammonia into the cylinder will be very challenging. However, the direct injection of gaseous ammonia could be

achieved in gasoline engines by using the narrow injection window before the cylinder pressure rises.

- Relatively low flow rates are not suitable for gas turbine application. However, it was found that there does not exist a reaction model capable of accurately capturing the great variety of ammonia burning conditions. There remains considerable progress to be made before a generalised model can be proposed and implemented, particularly at specific conditions where low NO_x is measured.

- Currently, each combustion condition has presented different degrees of reaction, making critical the development of explanatory mechanisms for specific conditions and fuel blends. Promising results have revealed a reduction in NO_x and CO emissions at high equivalence ratios $\geq$ 1.10 and that the maximum flame speed is achieved around an equivalence ratio of 1.1.

- Although a high temperature of 873 K or more is required for ammonia thermal decomposition, the contact decomposition using a catalyst can be performed at a reaction temperature of between 673 K and 873 K.

- An optimum catalyst for ammonia decomposition is ruthenium (Ru) or Ru/Al_2O_3, but they are costly, and Ni-based hydrogen-producing catalysts are preferred but require longer contact time for achieving the same conversion efficiency as Ru- based catalysts.

- Among all catalysts reported, potassium promoted CNTs supporting ruthenium catalysts appear to be the most promising candidates due to their high ammonia conversion rates at lower temperatures. Considering the high costs of noble metals and their preparations, a low cost but highly active catalyst is needed for the practical conversion of ammonia under industrial conditions.

- The ammonia decomposition reaction can be performed by using a general gas-solid phase contact reaction apparatus using a conversion resistance

material such as stainless steel, nickel steel, nickel, nickel-copper or nickel-chromium alloy or the like.

- Ammonia cracking is needed to obtain good power loading, flame stability, low NOx emissions and increase efficiency. The thermal cracking method has been considered the best due to increased efficiency of the decomposition process while reducing the cost by eliminating the need for exotic materials. However, to the best of the author's knowledge, there is no report available that uses thermal cracking methods without the need for a catalyst. Therefore, this study will focus on the possibility of using a thermal method to crack ammonia and ensure if this method will meet the energy sector requirements i.e. fuel sustainability, decarbonization of the energy sector, increasing efficiency and decreasing emissions.

CHAPTER 3

The Numerical and Experimental Methodologies

"All ideas in science were born in the dramatic conflict between reality and our attempt to understand it."

Albert Einstein, scientist (1879-1955)

3.1 Introduction

This chapter presents the numerical methodology used to assess the design of a new system to crack ammonia into hydrogen, nitrogen and ammonia. This helped ensure the cracked blend had the appropriate properties to burn in a GT combustion system. The chapter also describes the experimental equipment and measuring techniques used to evaluate the cracking system.

3.2 Numerical Methodology

In recent years, there has been a dramatic increase in the use of computational fluid dynamics (CFD) to predict flow characteristics, both internal and external. The development of, relative to only a decade ago, super-powered computers means high quality, efficient CFD software of proven accuracy is now available to provide accurate predictions at affordable computational cost [181]. Thus, CFD is now commonly used in the design of industrial processes and analysis of systems which include fluid dynamics, heat transfer, and chemical reactions. The technique has expanded to a wide range of industrial and non-industrial applications such as power plant combustion processes, internal combustion engines, gas turbines, diffusers, aerodynamics of aircraft and vehicles, hydrodynamics of ships, electrical and electronic engineering, chemical process engineering, and more [181].

In this investigation the CFD code ANSY16 was utilised. This software package is comprised of many routines, three of which have been used in this study. The first was used for geometric modelling; the second was for mesh generation; the last was used to model fluid mechanics, heat transfer, chemical reactions and combustion calculations.

FLUENT is a programme that uses the mesh generated by ANSY16, and applies the governing equations of fluid dynamics [182]. From these laws the conservation of mass-energy and force momentum equations are derived [183]. These equations vary depending on the properties of the particular flow in question; additional equations often need to be solved for flows, including turbulent flows such as those investigated in this work, i.e. heat transfer and species transport. These equations are replaced by the equivalent numerical descriptions that are solved by a finite volume method, to give solutions for the flow, i.e. define the required parameters at discrete locations within the flow field [182].

All types of CFD contain three elements: (a) a pre-processor, (b) a solver, and (c) a post-processor [184, 185].

3.2.1 Pre-Processor

The pre-processing consists of the input of a flow problem to a CFD programme by conversion of the input into a suitable form for use by the solver. This includes the following steps [186, 187]:

- Definition of the computational domain, modelling goals, specific results and the degree of accuracy required from the CFD model.
- Selection of a suitable type of grid topology.
- Choice the physical model and chemical phenomena equations and the conditions of the flows, i.e. laminar or turbulent, steady or unsteady.
- Specification of suitable conditions at cell boundaries which coincide with the domain boundary.

3.2.2 Solver

The basis of the numerical methods used by the solver depend on successfully performing the following steps:

- Approximation of the unknown flow variables using simple functions.
- Manipulation of the mathematical substitution of the approximations into the governing flow equations.
- Solving the algebraic equations.

The numerical solver in CFD uses three types of method: a) finite difference, b) finite element, and c) finite volume. The main differences between the three methods are associated with how the flow variables are approximated and with the discretisation processes.

The finite difference method describes the unknown Φ of the flow problem using point samples at the nodes of a grid of coordinate lines [185]. Finite differences approximate derivatives of Φ in terms of the point samples at each grid point and its immediate neighbours. The most common method is the truncated Taylor series expansion [185]. The derivatives that appear in the governing equations are replaced by finite differences, yielding an algebraic equation for the value of Φ at each grid point.

The finite element method uses simple piecewise functions, linear or quadratic, on elements to describe the local variations of the unknown flow variable, Φ [184]. The most versatile of the discretisation techniques used in CFD is the finite volume method (FVM). The first step in the FVM is to divide the domain into a number of control volumes or cells where the variable of interest is located at the centroids of the control volumes. The next step is to integrate the differential form of the governing equations over each control volume [187]. The variation of the given variable between cell centroids is then described by interpolating profiles between the cell centroids. The subsequent equation is called the discretised or discretisation equation and expresses the conservation of the variable within a control volume. The most impressive feature of the FVM is that the resulting solution satisfies the conservation equations of such quantities as mass, momentum, energy and species. These features are satisfied not only for the control volume but also for the entire computational domain [185].

3.2.3 Post-Processor

Recently, considerable development has taken place regarding the post-processing field. This is largely due to the increasing popularity of engineering workstations, and many packages are now equipped with versatile data visualisation tools [181].

More recent facilities include animation for dynamic display of results. In addition to graphics, all codes produce good alphanumeric outputs and have data export facilities for further manipulation of the code.

3.3 Governing Equations

The molecular structure of fluids shows no resistance to external shear forces. Therefore, every single action creates a motion of the fluid, and it is assumed that all fluids obey the laws of motion [188–190] that;

- The mass of fluid is conserved.
- The rate of change of momentum is equal to the sum of the forces acting on a fluid particle (Newton's second law).
- The rate of energy change is equal to the sum of the rate of heat addition and the rate of work done on a fluid particle (first law of thermodynamics).

Thus, conservation of mass, momentum and scalars (energy, species etc.) should be sustained for a control volume [191].

3.3.1 Mass Conservation Equation

The mass balance for a fluid element (continuity equation) states that the rate of increase of mass in a fluid element equals to the net rate of mass flow into the fluid element.

The continuity equation can be express as [181]:

$$\frac{\partial \rho}{\partial t} + \frac{\partial (\rho u)}{\partial x} + \frac{\partial (\rho v)}{\partial y} + \frac{\partial (\rho w)}{\partial z} = 0 \tag{3.1}$$

Alternatively, in vector notation:

$$\frac{\partial \rho}{\partial t} + div\left(\rho \vec{V}\right) = 0 \tag{3.2}$$

Where,

ρ = fluid density.

t = time.

u, v, w = velocity components in x, y and z respectively.

$\vec{V}$ = velocity vector.

Equation 3.2 is for unsteady, three-dimensional mass conservation or continuity and is used with compressible fluids. The first term of the equation is the rate of change of

density (mass per unit volume); the second term describes the net flow of mass out of the element across its boundaries, and is called the convective term [184, 185].

3.3.2 Momentum Equation

From Newton's second law, two types of forces can be distinguished:

1. Surface forces (pressure and viscosity), and

2. Body forces (gravity, centrifugal, Coriolis, and electromagnetic).

Applying these to a fluid passing through an infinitesimal, fixed control volume yields the following equations [181],

• The x-component of the momentum equation:

$$\rho \frac{Du}{Dt} = \frac{\partial(-P+\tau_{xx})}{\partial x} + \frac{\partial \tau_{yx}}{\partial y} + \frac{\partial \tau_{zx}}{\partial z} + S_{Mx} \tag{3.3}$$

• The y-component of the momentum equation:

$$\rho \frac{Dv}{Dt} = \frac{\partial \tau_{xy}}{\partial x} + \frac{\partial(-P+\tau_{yy})}{\partial y} + \frac{\partial \tau_{zy}}{\partial z} + S_{My} \tag{3.4}$$

• The z-component of the momentum equation:

$$\rho \frac{Dw}{Dt} = \frac{\partial \tau_{xz}}{\partial x} + \frac{\partial \tau_{yz}}{\partial y} + \frac{\partial(-P+\tau_{zz})}{\partial z} + S_{Mz} \tag{3.5}$$

Where

P= static pressure.

τ_{ij} = viscous stress component acts in the j-direction on the surface normal to i-direction.

S_{Mi} = gravitational body force in i-direction.

The sign associated with the pressure is opposite to that associated with the normal viscous stress because the usual sign convention takes tensile stress to be the positive normal stress so that the pressure, which is by definition a compressive normal stress, has a minus sign.

The effects of surface stresses are accounted explicitly; the source terms $S_{Mx}, S_{My}\ and\ S_{Mz}$ in equations (3.3 to 3.5) include contributions due to body forces only. As a result, the body force due to gravity, for example, would be expressed by $S_{Mx} = 0$, $S_{My} = 0$ and $S_{Mz} = -\rho g$.

In a Newtonian fluid, the viscous stresses are proportional to the rates of deformation. The three-dimensional form of Newton's law of viscosity for compressible flow involves two constants of proportionality: the dynamic viscosity, μ to relate stresses to linear deformations, and the viscosity λ to relate stresses to the volumetric deformation. The viscous stress components are related to $\mu\ and\ \lambda$. Substituting the values of viscous stress in the momentum equations yields the equations called Navier-Stokes equations [181].

$$\rho \frac{Du}{Dt} = -\frac{\partial p}{\partial x} + div(\mu\ grad\ u) + S_{Mx} \tag{3.6}$$

$$\rho \frac{Dv}{Dt} = -\frac{\partial p}{\partial y} + div(\mu\ grad\ v) + S_{My} \tag{3.7}$$

$$\rho \frac{Dw}{Dt} = -\frac{\partial p}{\partial z} + div(\mu\ grad\ w) + S_{Mz} \tag{3.8}$$

3.3.3 Energy Equation

The energy equation is derived from the first law of thermodynamics, which states that the rate of change in energy of a fluid particle is equal to the rate of heat added to the fluid particle plus the rate of work done on the particle. The rate of change in energy of a fluid particle per unit volume is given by $\rho \frac{DE}{Dt}$.

The total rate of work done on a fluid particle by a surface force can be expressed as [184, 185].

$$\rho \frac{DE}{Dt} = -div\left(P\vec{V}\right) + \left[\frac{\partial(u\tau_{xx})}{\partial x} + \frac{\partial(u\tau_{yx})}{\partial y} + \frac{\partial(u\tau_{zx})}{\partial z} + \frac{\partial(v\tau_{xy})}{\partial x} + \frac{\partial(v\tau_{yy})}{\partial y} + \frac{\partial(v\tau_{zy})}{\partial z} + \frac{\partial(w\tau_{xz})}{\partial x} + \frac{\partial(w\tau_{yz})}{\partial y} + \frac{\partial(w\tau_{zz})}{\partial z}\right] \tag{3.9}$$

If any source of energy exists with S_E energy per unit volume per unit time, the energy equation becomes:

$$\rho\frac{DE}{Dt} = -div\left(P\vec{V}\right) + \left[\frac{\partial(u\tau_{xx})}{\partial x} + \frac{\partial(u\tau_{yx})}{\partial y} + \frac{\partial(u\tau_{zx})}{\partial z} + \frac{\partial(v\tau_{xy})}{\partial x} + \frac{\partial(v\tau_{yy})}{\partial y} + \frac{\partial(v\tau_{zy})}{\partial z} + \frac{\partial(w\tau_{xz})}{\partial x} + \frac{\partial(w\tau_{yz})}{\partial y} + \frac{\partial(w\tau_{zz})}{\partial z}\right] + div(K\ grad\ T) + S_E \quad (3.10)$$

Equation (3.10) could be written in vector form as follow:

$$\frac{\partial(\rho E)}{\partial t} + div\left(\rho E\vec{V}\right) = 0 = -div\left(P\vec{V}\right) + \Phi + div(K\ grad\ T) + S_E \quad (3.11)$$

Φ: Dissipation function represent the long stress term.

The dissipation function is non-negative since it contains only squared terms and represents a source of internal energy due to the work done deforming the fluid particle. This work is extracted from the mechanical power, which causes the deformation and converts it into internal energy or heat [181].

3.3.4 General Transport Equation

It is clear that there are considerable commonalities between the various equations, and the conservative form of all fluid flow equations can be written as:

$$\frac{\partial(\rho\Phi)}{\partial t} + div\left(\rho\Phi\vec{V}\right) = div(\Gamma\ grad\ \Phi) + S_\Phi \quad (3.12)$$

Equation 3.12 is the so-called transport equation of property, Φ. It highlights various transport processes: the rate of change term and the convective term on the left-hand side and the diffusive term (Γ being the diffusion coefficient) and source term, respectively, on the right-hand side [181].

3.4 Turbulence Modelling

Turbulence is that state of fluid motion characterised by random and chaotic three-dimensional vorticity, and it usually dominates all other flow phenomena, causing increased energy dissipation, heat transfer, mixing and drag. Turbulence is not truly chaotic, since turbulent flows are both time- and space-dependent [192] and most researchers now believe the solutions of the fluid mechanical equations could be determined uniquely by their boundary and initial conditions. However, as with non-linear dynamical systems, the deterministic solutions of the non-linear fluid mechanics equations exhibit behaviour that appears to be random. These solutions are called turbulent, and because of the chaotic appearance and apparently random behaviour of

turbulence, we will need statistical techniques for most of our study of turbulence [192].

Turbulent flows are characterised by fluctuating velocity fields. These fluctuations mix transported quantities such as momentum, energy, and species concentration, and cause the transported quantities to fluctuate as well. Since these fluctuations can be of a small scale and high frequency, it is too computationally expensive to simulate them directly in practical engineering calculations. Instead, the instantaneous (exact) governing equations can be time-averaged, ensemble-averaged, or otherwise manipulated to remove the resolution of small scales, resulting in a modified set of equations that are computationally less expensive to solve. However, turbulence variables and turbulence models are needed to determine these variables in terms of known quantities [184]. The choice of turbulence model will depend on considerations such as the physical properties of the flow, established practice for solving a specific class of problem, the level of accuracy required, the available computational resources, and the amount of time available for the simulation. Thus, to achieve good designs, an engineer using CFD needs to be aware of the presence of turbulence. Models used in this study will be explained under this title.

Conventionally, three principal strategies have been used to model turbulent combustion flow with good adaptivity: Direct Numerical Simulation (DNS), Reynolds-Averaged Navier-Stokes (RANS) and Large Eddy Simulation (LES). As can be seen in Figure (3-1); DNS can be used to compute the whole range of fluctuation for the flow, LES can compute the problem-based part of the flow and model homogeneous eddies, while Reynolds Averaged Navier-Stokes (RANS) models the full range of turbulence (assuming isotropy).

The more modelling exists in the solution, the less computational power is needed. Thus, RANS-based solutions need very little computational resources compared to DNS. The resources required for LES depends on selection of cut-off wavelength. In other word, the fewer the eddies resolved, the more computation power is needed. Either way, the computational power needed for LES is between that needed for RANS and DNS. For academic studies, RANS is the best method since, LES is almost expensive in terms of computing tools and time needs as compared to the classical

RANS approach [193]. Therefore, this work employed RANS for the study of novel techniques for the efficient burning of ammonia blends.

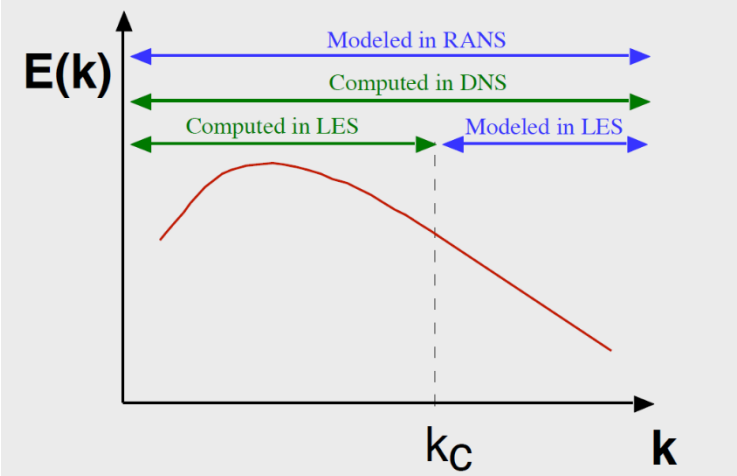

Figure 3- 1: Energy spectrum and cut off wavelength [193]

3.4.1 Reynolds Averaged Navier-Stokes Simulations (RANS)

This method was created because of the computational power required for DNS. Instead of treating Navier-Stokes equations directly and obtaining solutions after years of number crunching, engineers have chosen a way of obtaining mean values and reaching a solution much more quickly. This method requires a split between average and fluctuating values. This is called Reynolds Averaging, where mean values of the flow and fluctuations can be treated separately. The continuity equation written in terms of Reynolds Averaging is:

$$\frac{\partial \bar{\rho}}{\partial t} + \frac{\partial}{\partial x_i}(\overline{\rho u_1}) = \frac{\partial \bar{\rho}}{\partial t} + \frac{\partial}{\partial x_i}\left(\bar{\rho}\,\overline{u_1} + \overline{\rho \acute{u}_1}\right) = 0 \tag{3.13}$$

By constant density assumption, the equation can be simplified as:

$$\acute{\rho} = 0\ ,\ \rho = \bar{\rho}$$

$$\frac{\partial \rho}{\partial t} + \frac{\partial(\rho\overline{u_1})}{\partial x_i} = 0 \tag{3.14}$$

And the corresponding momentum equation is:

$$\frac{\partial(\rho\overline{u_1})}{\partial t} + \frac{\partial}{\partial x_j}\left(\rho\,\overline{u_1}\,\overline{u_J} + \rho\overline{\acute{u}_1\acute{u}_J}\right) = -\frac{\partial \bar{P}}{\partial x_i} + \frac{\partial \overline{\tau_{iJ}}}{\partial x_j} \tag{3.15}$$

Where the $\overline{\tau_{iJ}}$ are the mean viscous stress tensor components.

3.4.2 Standard k-epsilon Turbulence Model

Models such as k-epsilon, or $K-\varepsilon$ were first introduced by Jones and Launder in 1972 [194]. The idea of the model is to describe the turbulent viscosity by the production and destruction equations of turbulence. Empiric relationships are constructed by the help of experimental data. For $K-\varepsilon$ models, turbulent viscosity is defined as:

$$\mu_t = \bar{\rho} C_\mu \frac{K^2}{\varepsilon} \tag{3.16}$$

$K\ and\ \varepsilon$ are described by the closure of two balance equations:

$$\frac{\partial}{\partial t}(\bar{\rho}K) + \frac{\partial}{\partial x_i}(\bar{\rho}\widetilde{u_i}K) = \frac{\partial}{\partial x_i}\left[\left(\mu + \frac{\mu_t}{\sigma_k}\right)\frac{\partial K}{\partial x_i}\right] + P_K - \bar{\rho}\varepsilon \tag{3.17}$$

$$\frac{\partial}{\partial t}(\bar{\rho}\varepsilon) + \frac{\partial}{\partial x_i}(\bar{\rho}\widetilde{u_i}\varepsilon) = \frac{\partial}{\partial x_i}\left[\left(\mu + \frac{\mu_t}{\sigma_\varepsilon}\right)\frac{\partial \varepsilon}{\partial x_i}\right] + C_{\varepsilon 1}\frac{\varepsilon}{K}P_K - C_{\varepsilon 2}\bar{\rho}\frac{\varepsilon^2}{K} \tag{3.18}$$

The source term P_K is given by:

$$P_K = -\bar{\rho}\widetilde{u_i''u_j''}\frac{\partial \widetilde{u_i}}{\partial x_j} \tag{3.19}$$

The standard model constants have the default values and they are listed in Table 3-1. Since these default constants are derived from experimental data for fundamental turbulent flows including frequently encountered shear flows like boundary layers, mixing layers and jets as well as for decaying isotropic grid turbulence. The standard k- ε model is relatively accurate for a wide range of wall-bounded and free shear flows. However, improvements will be made when other types of flows are considered, e.g. swirling flows [195].

Table 3- 1: Constant values used in standard k - ε turbulence model [195].

C_μ	0.09
$C_{\varepsilon 1}$	1.44
$C_{\varepsilon 2}$	1.92
σ_K	1.0
σ_ε	1.3

3.5 Combustion Modelling

Combustion requires that the fuel and oxidiser are mixed at a molecular level. This usually depends on turbulent mixing. During combustion, a fuel reacts with the oxidant, which is normally air, to release heat and form products of combustion. These products are not a result of one reaction but invariably a sequence of chemical reactions. For instance, more than 1000 elementary reactions are involved in the combustion process of methane (CH_4), one of the simplest hydrocarbon fuels. In addition, the flow equations and transport equations for the mass fraction m_j of each species j, must be solved. The species equations can be written using the general transport equation [181]:

$$\frac{\partial(\rho m_j)}{\partial t} + div\left(\rho m_j \vec{V}\right) = div\left(\Gamma_j \, grad \, m_j\right) + S_j \tag{3.20}$$

The volumetric rate of generation (or destruction) of species due to chemical reactions appears as the source (or sink) term S_j in each transport equations. In a simple chemical reaction system, infinitely fast chemical reactions are assumed, and the intermediate reactions are ignored. The transport equations for the fuel and oxygen mass fraction may be written as:

$$\frac{\partial(\rho m_f)}{\partial t} + div\left(\rho m_f \vec{V}\right) = div\left(\Gamma_f \, grad \, m_f\right) + S_f \tag{3.21}$$

$$\frac{\partial(\rho m_o)}{\partial t} + div\left(\rho m_o \vec{V}\right) = div(\Gamma_o \, grad \, m_o) + S_o \tag{3.22}$$

Under the assumption of equal diffusivities $\Gamma_f = \Gamma_o = \Gamma$, the species equations can be reduced to a single equation for the mixture fraction, f:

$$f = \frac{Z_i - Z_{i,ox}}{Z_{i,fuel} - Z_{i,ox}} \tag{3.23}$$

Where Z_i is the elemental mass fraction for element i. The subscript "ox" denotes the value at the oxidizer stream inlet and the subscript $fuel$, denotes the value at the fuel stream inlet. The reaction source terms in the species equations cancel, and thus f, is a conserved quantity. Whilst the assumption of equal diffusivities is problematic for laminar flows, it is generally acceptable for turbulent flows where turbulent convection is much a greater factor than molecular diffusion [182].

3.5.1 Non-Premixed Combustion Modelling

Turbulent non-premixed flames are common in engineering applications, e.g. industrial burners and diesel internal-combustion engines, it is also favoured for GT combustion systems used in an aeronautical applications [196].

In non-premixed combustion, the time needed for turbulent mixing is longer than the time needed for combustion reactions to occur. However, the non-premixed mixture in GT combustors shows greater flame stability in operation than other types of mixtures. This was found experimentally and confirmed using CFD simulation [197].

Fuel and oxidiser do not mix before the combustion zone; they enter the combustion chamber separately. However, they both mix and burn during the combustion process. The flame is called a diffusion flame, and its response depends critically on preferential diffusion processes which are generally characterised by the Lewis number, L_e, defined as:

$$L_e = \frac{\alpha}{D} \tag{3.24}$$

Where α is the thermal diffusivity and D is the mass diffusion governed by Fick's law. When $L_e = 1$, the combustion process is said to be diffusionally neutral and adiabatic as total energy conservation is maintained. When $L_e < 1$, the mass transport exceeds heat loss resulting in an increase in combustion intensity. When $L_e > 1$, the heat loss exceeds mass transport and the combustion intensity decreases accordingly.

Modelling of non-premixed combustion has been specially developed for the simulation of turbulent diffusion flames with prompt chemistry. For such systems, the method offers many benefits over other formulations, i.e. eddy dissipation. The non-premixed model enables prediction of intermediate species, dissociation effects, and rigorous turbulence chemistry coupling. The method is computationally efficient in that it does not require the solution of a large number of species transport equations. When the underlying assumptions are valid, the non-premixed approach is preferred over the eddy-dissipation formulation [196]. Therefore, this was the method employed for the calculations in this research.

3.6 Heat Transfer Modelling

Heat transfer is considered to be the basic process of all process industries. During heat transfer, one fluid at higher temperature transfers its energy in the form of heat to another fluid at a lower temperature. Fluids can transfer heat by: conduction, convection and radiation. Radiation is not a common mode of heat transfer in process industries but plays a vital role in heat transfer in combustion furnaces [198].

The conduction heat transfer could be calculated from Fourier's law of heat conduction equation as follows:

$$q_x = -kA\frac{\partial T}{\partial x} \tag{3.25}$$

Convection heat transfer from a surface is described by the following equations:

$$q = hA\left(T_{surface} - T_{free\ stream}\right), \text{ for exterior flows} \tag{3.26}$$

$$q = hA\left(T_{surface} - T_{fluid\ bulk}\right), \text{ for flow in channels} \tag{3.27}$$

Where,

q: Heat transfer rate (W)

A: Area (m^2)

k: Thermal conductivity (W/m.K)

h: Heat transfer coefficient (W/m^2 K)

Conduction and convection are the most common modes of heat transfer ecountered in the process industries in, for example, heat exchangers which transfer heat between two or more fluids. Shell-and-tube heat exchangers are widely used in industry due to their low cost, ease of cleaning, simplicity of structure and because they have the highest log-mean temperature difference, correction factor. Generally, they are cylindrical in shape and contain a bundle of tubes, usually finned, through which one of the fluids runs [198] .

For this study, different shell and tube heat exchangers were considered for pre-heating the ammonia, with the ammonia passed through the bundle of tubes. Then the pre-heated ammonia was passed through passages within the bluff body to crack the

ammonia, and the products obtained from cracking the ammonia would be used later as a primary fuel. The hot exhaust gases from the combustor were used on the shell side for heat exchanger. In the simulation of heat transfer in the bluff body, constant wall temperature was assumed.

ANSYS FLUENT allows the operator to include heat transfer within the fluid and/or solid regions in the model. For simulating conjugate heat transfer, the heat exchanger was discretized into a fluid and a solid domain in order to have better control over the number of nodes. In this pressure-based simulation, the absolute velocity formation and steady state were selected for the solver option. For the model option, the energy equation was chosen, and the viscous model was set as a standard $K-\varepsilon$ with a standard wall function.

In ANSYS FLUENT, the heat exchanger core is treated as a fluid zone with momentum and heat transfer. Pressure loss is modelled as a momentum sink in the momentum equation, and heat transfer is modelled as a heat source in the energy equation [182].

The governing equations of the flow are modified according to the conditions being simulated. Since the problem is assumed to be steady, time dependent parameters are dropped from the continuity, energy and Navier-Stokes momentum equations. The resulting equations are:

- Conservation of mass:

$$div\left(\rho\vec{V}\right)=0 \tag{3.28}$$

- The x-component of the momentum equation:

$$div\left(\rho u\vec{V}\right)=-\frac{\partial P}{\partial x}+\frac{\partial \tau_{xx}}{\partial x}+\frac{\partial \tau_{yx}}{\partial y}+\frac{\partial \tau_{zx}}{\partial z} \tag{3.29}$$

- The y-component of the momentum equation:

$$div\left(\rho v\vec{V}\right)=-\frac{\partial P}{\partial y}+\frac{\partial \tau_{xy}}{\partial x}+\frac{\partial \tau_{yy}}{\partial y}+\frac{\partial \tau_{zy}}{\partial z}+\rho g \tag{3.30}$$

- The z-component of the momentum equation:

$$div\left(\rho w\vec{V}\right)=-\frac{\partial P}{\partial z}+\frac{\partial \tau_{xz}}{\partial x}+\frac{\partial \tau_{yz}}{\partial y}+\frac{\partial z}{\partial z} \tag{3.31}$$

- Energy equation:

$$div\left(\rho E\vec{V}\right) = -div\left(P\vec{V}\right) + div(K\ grad\ T) + q + \Phi \quad (3.32)$$

Where, Φ is the dissipation function that can be calculated from the following equation:

$$\Phi = \mu\left[2\left[\left(\frac{\partial u}{\partial x}\right)^2 + \left(\frac{\partial v}{\partial y}\right)^2 + \left(\frac{\partial w}{\partial z}\right)^2\right] + \left(\frac{\partial u}{\partial y} + \frac{\partial v}{\partial x}\right)^2 + \left(\frac{\partial u}{\partial z} + \frac{\partial w}{\partial x}\right)^2 + \left(\frac{\partial v}{\partial z} + \frac{\partial w}{\partial y}\right)^2 + \right.$$
$$\left. +\lambda\left(grad\ \vec{V}\right)^2\right] \quad (3.33)$$

3.7 Chemical Kinetics Modelling

Based on the fundamental reaction theory, in order to describe a reaction system as complex as combustion, a chemical kinetic mechanism has been developed, which describes all the reactions present in the combustion process by a compilation of all the species, elementary reactions and reaction rate parameters involved [199, 200].

In order to characterise the proposed combustion system, Chemical Kinetic models were employed to determine the performance of the currently designed systems to reduce NO_x and increase ammonia combustion via cracking technologies, thus setting up the first precedent to the integrated use of this technology for gas turbine applications.

Many practical combustors, such as internal combustion engines, rely on premixed flame propagation, and burner-stabilized laminar premixed flames are often used to study chemical kinetics in a combustion environment. Thus, the ability to model chemical kinetics and transport processes in such flames is critical to interpreting flame experiments and to understanding the combustion process [201]. Such flames are effectively 1D, and can be made very steady, thus facilitating detailed experimental measurements of temperature and species profiles. Also, the laminar flame speed is often used to characterize the combustion of various fuel-oxidizer combinations [201].

Burner-stabilized, laminar, premixed flames with known mass flow rates have often been used for analysing species profiles in flames. However, since the chemistry depends strongly on temperature, it is essential to know the temperatures accurately to draw accurate conclusions about the chemical kinetics. The freely propagating

adiabatic flame was considered in this study. For cases where the heat losses are known to be negligible, the temperatures can be computed from the energy conservation equation. Flame speed depends, in part, on the transport of heat, and predicting the temperature distribution is an integral part of the flame speed calculation [201][202].

The equations governing steady, isobaric, quasi-one-dimensional flame propagation may be written as [201]:

- Continuity:

$$\dot{m} = \rho u A \tag{3.34}$$

- Energy:

$$\dot{m}\frac{dT}{dx} - \frac{1}{Cp}\frac{d}{dx}\lambda A\frac{dT}{dx} + \frac{A}{Cp}\sum_{k=1}^{K}\rho Y_k V_k Cp_k\frac{dT}{dx} + \frac{A}{Cp}\sum_{k=1}^{K}\dot{\omega}_k h_k W_k = 0 \tag{3.35}$$

- Species:

$$\dot{m}\frac{dY_k}{dx} + \frac{d}{dx}(\rho A Y_k V_k) - A\,\dot{\omega}_k W_k = 0 \quad (k = 1, \ldots\ldots\ldots K) \tag{3.36}$$

- Equation of State:

$$\rho = \frac{P\bar{W}}{R_c T} \tag{3.37}$$

In these equations *x* denotes the spatial coordinate; $\dot{m}$ is the mass flow rate (which is independent of *x*); *T* the temperature; Y_k the mass fraction of the *k*th species; *p* the pressure; *u* the velocity of the fluid mixture; ρ the mass density; W_k the molecular weight of the *k*th species; $\bar{W}$ the mean molecular weight of the mixture; R_c the universal gas constant; λ the thermal conductivity of the mixture; Cp the constant-pressure heat capacity of the mixture; Cp_k the constant pressure heat capacity of the *k*th species; $\dot{\omega}_k$ the molar rate of production by chemical reaction of the *k*th species per unit volume; h_k the specific enthalpy of the *k*th species; V_k the diffusion velocity of the *k*th species; and *A* is the cross-sectional area of the stream tube encompassing the flame normalised by the burner area.

The net chemical production rate $\dot{\omega}_k$ of each species results from a competition between all the chemical reactions involving that species. We presume that each

reaction proceeds according to the law of mass action and the forward rate coefficients are in the form of a modified Arrhenius equation [201],

$$k_{fi} = A_i \, T^{\beta_i} exp\left(\frac{-E_i}{RT}\right) \tag{3.38}$$

Where k_{fi} is the forward rate constant of the *i*th reaction, A_i is the pre-exponential factor, E_i is the activation energy of the reaction and β_i is the temperature exponent of the *i*th reaction. The details of the chemical reaction equations and the thermochemical properties are found in the user's manuals for CHEMKIN-III, a program designed to evaluate these expressions [203]. As demonstrated in previous combustion studies where detailed chemical kinetic mechanisms were used to describe the transformation of reactants into products at the molecular level through a huge number of elementary steps [200]. For instance, Mathieu's mechanism [149] is a well-established reaction model for ammonia combustion chemistry for use with practical applications such as the control of NO_x formation or for NO_x removal processes.

3.8 Experimental Methodology

This section describes the 3D printing technology used to manufacture the cracking system (due to its complex shape), the measurement techniques, and instrumentation used in the experimental study.

3.8.1 Bluff Body: Conceptual Design and its Manufacture

This section begins by describing the process for designing and manufacturing the most complex part of the rig, the cracking system - a bluff body surrounding by an axial vane, as shown in Figure 3-2. A 3D model of the cracking system was designed using CAD software (Solid Works). Figure 3-2 shows the final design of the bluff body, ready for manufacture. The evolution of nanocomposite materials combined with 3D printing have made possible the rapid prototyping of complex designs. Here a 3D printing process cast nanocomposite materials in a mould cavity.

This technique ensures high-quality build and is suitable for all qualified metals including titanium and aluminium. It is widely used to produce heat exchangers, injection moulding inserts with conformal cooling channels, lightweight aerospace components, and customised dental and medical implants [204].

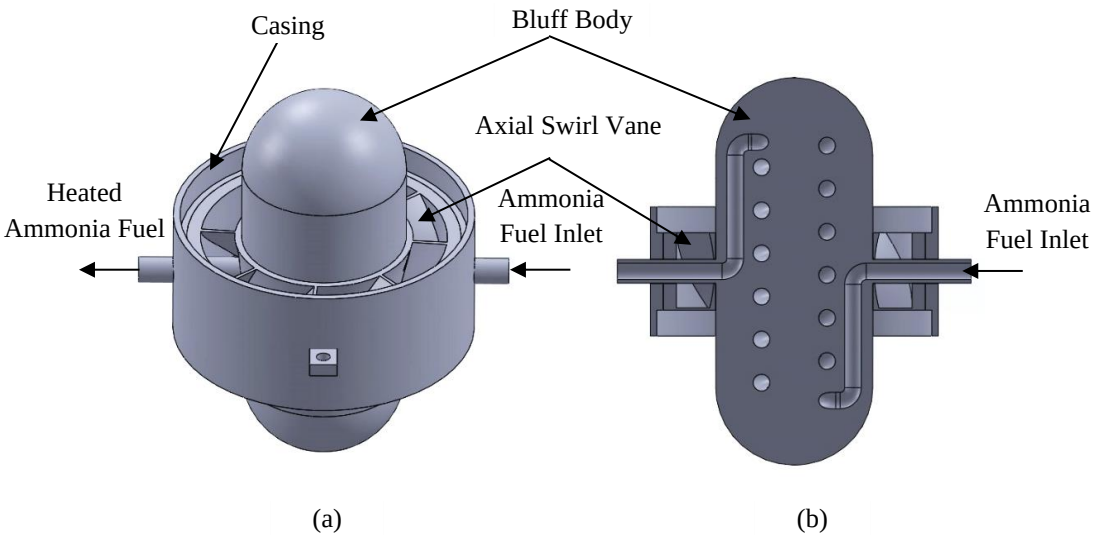

Figure 3- 2: (a) Cracking system, (b) Section view showing tubular passage through which the Ammonia flowed while being heated

3.8.1.1 Renishaw's AM250 Laser Melting System

The Renishaw AM250 Laser Melting System provides the designer with tremendous freedom to create components with free-form and intricate features, saving time and money. Here the laser melting system, Figure (3-3), was used to build the final bluff body design directly from the digital CAD files using powder bed fusion technology with stainless-steel as the powder.

Figure 3- 3: Renishaw's AM250 laser melting system.

Renishaw's AM250 laser melting system includes, see Figure (3-4):

1. A dedicated Optical Control Software (OCS) module controlled the optical functions of the AM250: laser focus and beam steering, ensuring precision of the product.

2. A gas knife lens window protection system which emits a flow of gas to form a barrier to emissions accumulating on the window, thus maximising laser efficiency throughout the process and maintaining accuracy.

3. A high capacity filtration system which helps maintain a clean environment, enabling larger builds to proceed with minimal user intervention.

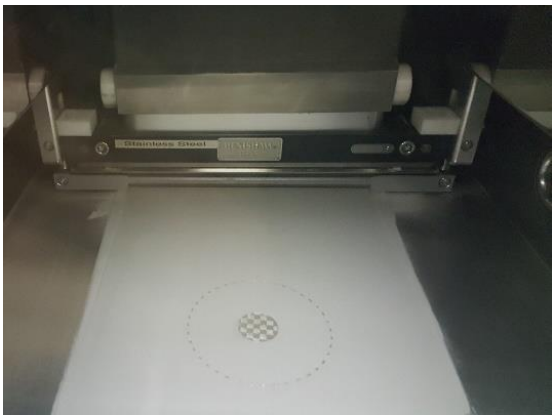

Figure 3- 4: AM250 build chamber.

The 3D Printer builds the design, layer by layer directly from the CAD 3D data file, Figure (3-5) a. The final bluff body at the end of the printing process is shown in Figure (3-5) b. The bluff body after post-processing to remove sacrificial supports added to the design to enable a successful build is shown in Figure (3-5) c and d. Finishing machines such as Lathe (Turning) machine and Wire Cutter machine have been used to remove these sacrificial supports.

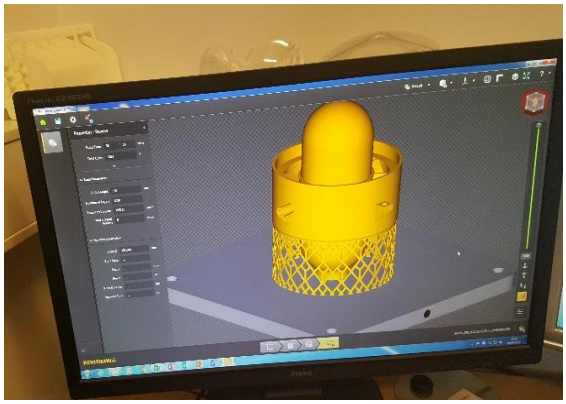

(a)

(b)

(c)

(d)

Figure 3- 5: (a) CAD 3D data file of bluff body cracking system, (b) Cracking system after printing process, (c and d) Final bluff body post-processing.

3.8.2 Rig Setup

A 20-kW generic swirl burner was used to investigate flame characteristics and other combustion features by using different fuels (methane and/or ammonia). At the top is a swirler to provide a swirling flow for anchoring purposes. This component was previously designed at Cardiff School of Engineering, Figure (3-6) [205].

Figure 3- 6: A Picture of the manufactured Combustor before setup [205].

Swirling flows in a non-premixed combustor is characterized by its swirl number (S), which is defined as the ratio of the axial flux of the tangential momentum to the axial momentum flux, and a characteristic radius [206], see Equation 3.39:

$$S = \frac{G_\theta}{G_x . r_e} \tag{3.39}$$

In this study, the swirler was made up of four tangential inlets distributed symmetrically with a swirl number of 1.05 [206]. The fuel exits into the flame zone through a nozzle with internal diameter 28 mm and length 30 mm, see Figure (3-7).

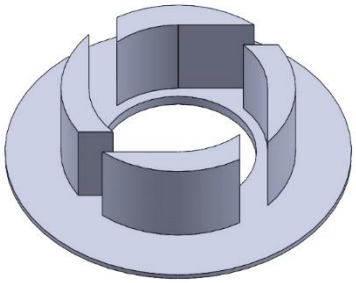

Figure 3- 7 : Swirl vane with swirl number 1.05.

The swirl nozzle projects the reactant mixture into the flame zone. The flame is confined within three quartz tubes; a bottom tube (84 mm internal diameter, 100 mm long), a middle tube (100 mm diameter, 90 mm long) joined together by a stainless-steel cylindrical ring 10 mm long, see Figure 3-8. The middle tube is connected with a third quartz tube (100 mm diameter and 200 mm long) through the designed bluff body. This ring allows for the increase in tube diameter while injecting a mix of

ammonia and hydrogen to enable further reduction of NOx emissions, as will be explained later in Chapter 6.

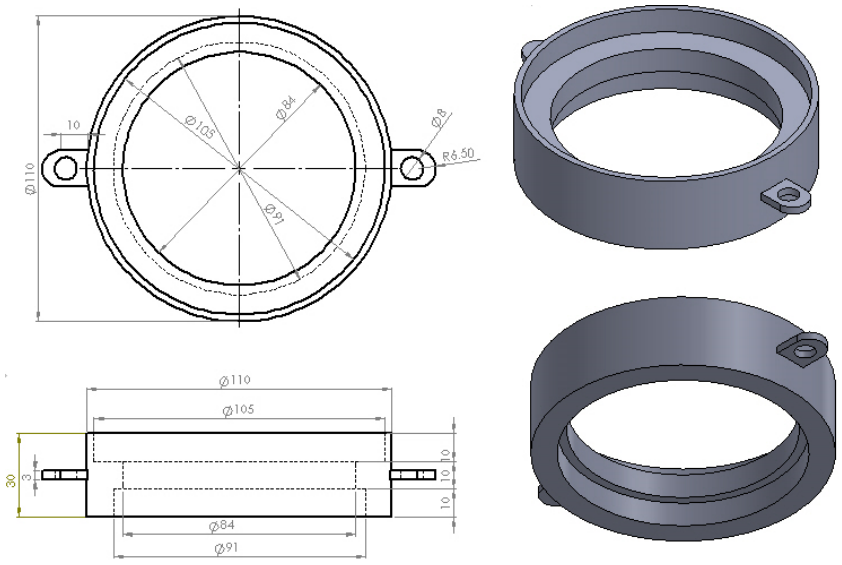

Figure 3- 8: CAD drawing of the connected ring between bottom confinement and the middle confinement tube.

A low-pressure gauge of PGI series with lower mount was used where vacuum is required, the gauge used are dry case stainless steel with bottom entry and safety pattern glass window [207]. To protect the system and the researchers, to prevent build-up of pressure due to any possible blockage in the bluff body a pressure relief valve was fitted upstream of the cracker, see Figure 3-9 [208]. This valve was designed for low pressure applications, up to 20.6 bar. The nominal pressure range of the valve used in the system was 0.7-15.5 bar, when set at 3 bar.

Figure 3-10 shows the final setup of the ammonia cracking system rig. Methane (CH_4) and/or ammonia (NH_3) would be supplied by fuel lines fed from external cylinders, located in a gas cage next to the lab. The diffusive mode of injection was used. The flame was ignited using a methane pilot. The two thermocouples were used to determine the temperature differences of the fuel which is passed through the bluff body to determine the performance of this new design of thermal cracking system.

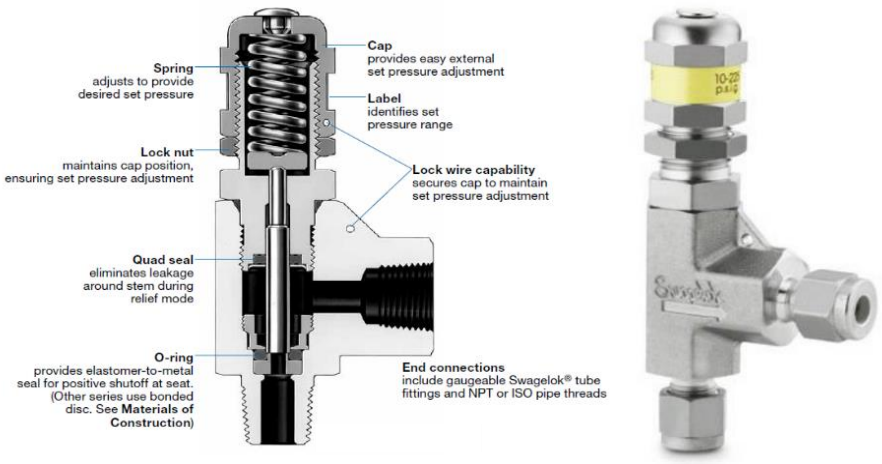

Figure 3- 9: RL3S4 series relief valve.

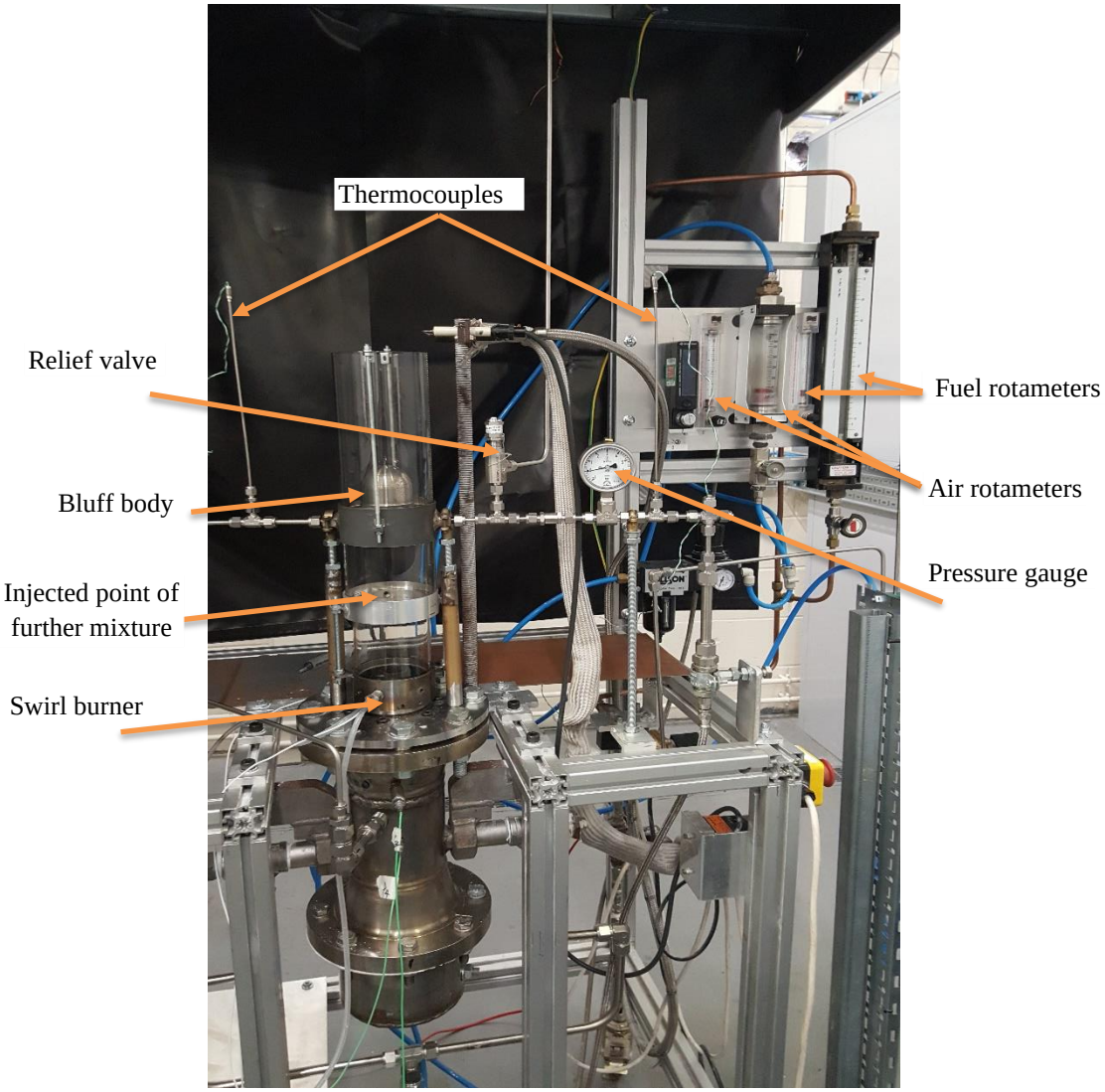

Figure 3- 10: The set-up of the experimental rig.

3.8.3 Measurement Techniques and Instrumentation

3.8.3.1 Flame Shape Measurement

A digital camera, a 24.2-megapixel Nikon DSLR camera model D7200 with 18-105mm VR Nikon lens was used to measured flame shape kinematics for different fuel ratios. The ISO range of 100–25600 make it a good choice to capture a photograph no matter the light strength. The most important feature of this camera was the shutter speed (1/8000-30 s) with 6 fps continuous shooting which is essential to capture the unsteady flow behaviour of the flame.

3.8.3.2 Heat Transfer Measurement

An Omega data acquisition system was used to determine the efficiency of the thermal cracking system. It did this by measuring the temperature difference between inlet and outlet of the fuel flowing through the spiral passage inside the bluff body.

The OM-DAQ-USB-2401 Omega data acquisition system is a thermocouple/voltage input data acquisition module. All configurable options (including individual channel input type and range) are software programmable. All input channels can be measured sequentially at about 1 ms per channel. A total of 1000 samples per second can be taken, divided across all active channels [209].

The Omega data logger provided thermocouple (TC) measurements and automatically converts voltage readings into compensated-linearized temperature readings. The DAQ system can make thermocouple and volts measurements concurrently as shown in Figure (3-4).

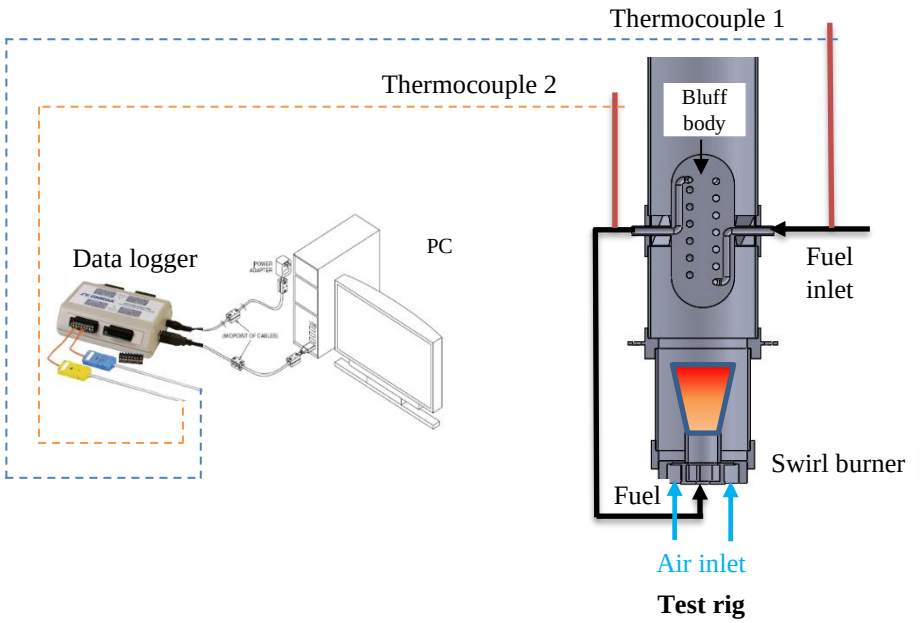

Figure 3- 11: Schematic of Omega data acquisition system in place.

3.8.3.3 Particle Image Velocimetry

The Particle Image Velocimetry (PIV) system was used to determine the behaviour of the flow field in the second recirculation zone, located under the bluff body. The PIV setup required positioning various components in specific positions relative to one another. The rig was positioned in the centre of the laboratory, leaving space for optical tables on the right, left and front of the rig.

A Stroboscope BVS-II Wotan and line converter were mounted so the desired plane was illuminated. This was done by standing the stroboscope line converter on a Perspex sheet using metal legs placed in holes along the top of the line converter to illuminate the chosen plane [210].

The focal point of the line sheet was set by adjusting the cylindrical lens. This was done by turning the stroboscope on, select the internal trigger by pressing 'Trigger'. This caused the stroboscope to fire. While the scope was firing the cylindrical lens was adjusted, so the centre of the inspection area received a narrow fine sheet of light. This set up is visually depicted in Figure 3-12.

Figure 3- 12: Image processing stroboscope.

A fog machine ProSound800 [211] was employed to trace the flow, see Figure 3-13. To set up this fog machine, the feeder tube with filter deep was placed inside the full fog fluid container. Only high-quality water-based fog fluid was used. When the fog machine is plugged to the electric socket, the red LED on the remote controller would be lighted up. When the fog machine has reached operating temperature, the green LED lights up indicating that the fog machine becomes workable and it is ready for emission by passing the button.

Figure 3- 13: The fog machine ProSound800 parts.

A Baumer-GAPI Viewer camera was used with this system and it was must be mounted perpendicular to the light sheet in all directions [212]. It should be placed on the tripod and align it perpendicular to the light sheet at a required distance from the light plane, so that it would capture the desired inspection window within the flow. The lens of the camera needed to be manually focused. This was done by placing the calibration plate below the stroboscope, so it sat where the light sheet would be projected. After the camera had been checked as positioned correctly, it was interfaced with the computer.

The frame rate, sequence length, exposure and gain of the camera should be set before data acquisition. The exposure and gain are the most important and should be adjusted to give a reasonably dark image with bright spots where smoke was passing through the burner. An over bright image can be dimmed by reducing the intensity of the stroboscope.

Descriptions of all the parameters are found below:

a) Frame Rate – the frame rate is the speed that the camera will capture images. This particular camera can capture at up to 30 frames per second (30 Hz, this is the default setting) but can be set to slower values depending on the flow rate of the fluid.

b) Sequence Length – this is the number of frames that will be taken in one cycle; the default is 10 but can be adjusted up to 150 frames giving 5 seconds of continuous capture.

c) Exposure – affects the brightness of the image and can also affect the capture rate if too high an exposure is used. For this application, a maximum exposure of 3000 was sufficient even in the darkest of environments.

d) Gain – amplifies the difference between dark background and the bright parts, it can be used to produce a brighter picture for shorter exposure times allowing the camera to run at its full frame rate. If the image is dark, it is better to increase the gain up to its maximum rather than extending the exposure time, which would limit capture time.

Suggested settings can be found in Table 3-2.

Table 3- 2: Suggested parameters for different lighting conditions.

Parameter	Bright conditions	Medium Conditions	Dark Conditions
Exposure	1000	2000	3000
Gain	1.5	2	2.7

The last step before data acquisition was calibrating the camera. This was done by placing the calibration plate within the flow where the light sheet was present (as described earlier for camera focusing). Then after activating the fog machine to obtain an idea of the flow lines under the bluff body, the camera began taking images. When the stroboscope ceased to flash this signified the end of that capture sequence. The series of images was then placed in the specified directory.

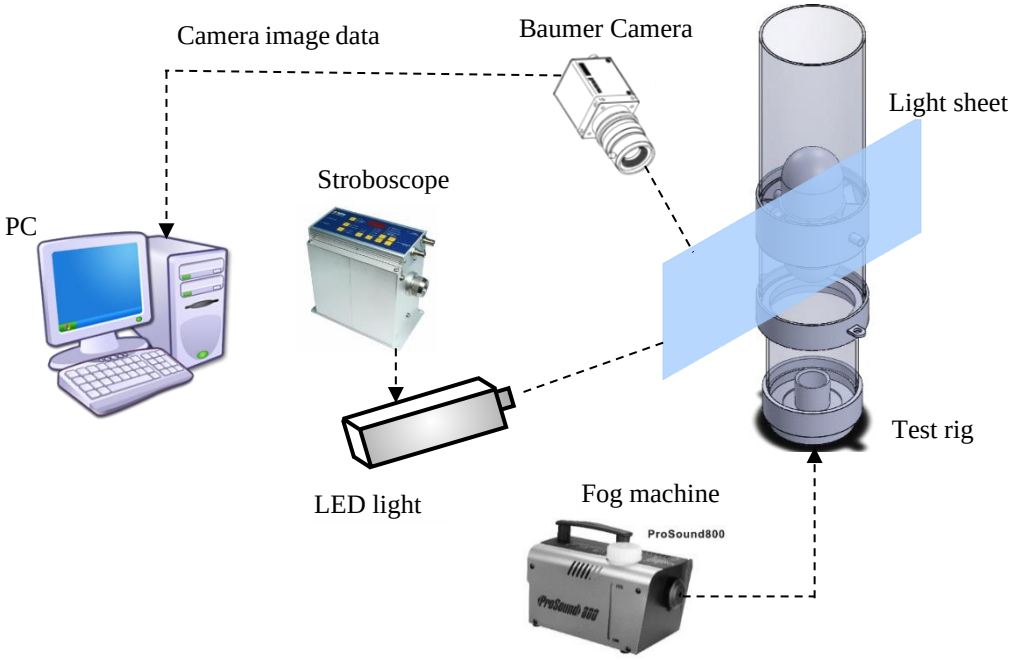

Figure 3- 14: Isometric view of PIV apparatus

3.9 Summary

This chapter has described the experimental apparatus, CFD methodology, and manufacture of a new cracking system, all to be used to test the proposal that the bluff body system described here can be used to dissociate ammonia so that it can be used as a sustainable fuel for GTs.

Firstly, the relevance of CFD techniques and turbulence models to this work was presented. CFD is described as an important tool in the analysis and design of systems involving fluid flow, heat transfer and combustion, as in GTs. ANSYS 16 FLUENT was used to analyse both the combustion and heat transfer regimes in order to produce

a model that could be tested experimentally. The non-premixed combustion model was used, using the finite volume method. The CFD work was based on the RANS turbulent combustion flow model, using the standard k- ε model because it is considered accurate for a wide range of wall-bounded and free shear flows. Also, the modelling of the chemical kinetics of laminar burner-stabilised flames, and freely propagating flames, was done using steady, 1D studies to describe the combustion of various fuels.

Secondly, experimental techniques including the use of a 3D printer to manufacture the complex shape required for the bluff body cracking system have been described. In addition, the equipment used in the experiments was described. A 20 kW swirl combustor was used for experimental investigations and the flow field was analysed under confined conditions using quartz cylinders. Particle Image Velocimetry (PIV) was used to specify the swirling behaviour of the flow field in the recirculation zone upstream the bluff body. A Baumer camera was used to visualise the flows. An Omega data acquisition system was used to record measurements made.

Methane was used as the baseline fuel and the diffusive mode of injection will be used. The flame was ignited using a methane pilot. The main areas of interest will be flame stability limit, the efficiency of the cracking system and the effect of the shape of the swirl flow field on the second recirculation zone. The heat transfer efficiency of the cracking system will be predicted by measuring the temperature differences between the inlet and outlet fuel through the bluff body which was designed to crack the ammonia through spiral passages.

CHAPTER 4

Numerical Predictions for an Ammonia Cracking System

"The science of today is the technology of tomorrow."

Edward Teller

4.1 Introduction

It is possible to construct a hydrogen generating system using thermal cracking of ammonia to supply the fuel, hence eliminating the problems of hydrogen storage and transport. In this study, the proposed system will use high temperature exhaust gases from gas turbines to thermally crack ammonia to produce hydrogen: the resulting hydrogen-ammonia mixture to be used as a fuel for a modern gas turbine. The proposed ammonia cracker should have a high cracking efficiency, be of an acceptable mass and volume to be included as an auxiliary component of the combustion hardware of the gas turbine. In this study, both numerical and experimental programmes have been carried out to enhance the design of a thermal cracking system using ammonia as a working fluid.

Computational fluid dynamics (CFD) simulation can be an effective means of demonstrating new concepts or a new design before a system is constructed. CFD is structured around numerical algorithms that can used to solve problems in fluid dynamics, and provide the solvers with user-friendly access by the application of input parameters, thus allowing the results to be examined in depth [185]. The level of accuracy of CFD methods has significantly improved the design process over the past decade. Employing CFD as a tool in the design process leads to far fewer prototypes being required during the development process of any system, and less prototype testing will diminish the cost of new developments.

This chapter will discuss the pre-steps of constructing the proposed thermal cracker at the Additive Manufacturing Laboratories in the School of Engineering of Cardiff University. The CFD simulation of the combustion process will be followed by numerical heat transfer analysis of the suggested design. Added to the current system

is a novel device that uses a bluff body to thermally pre-crack ammonia. A diagram of the conceptual design is provided in Figure (4-1). Numerical modelling was used to decide the shape and dimensions of the system, which was then manufactured and experimentally tested, see Chapters 3 and 5 for further details. In the following subsections, the numerical predictions will be presented in a logical sequence.

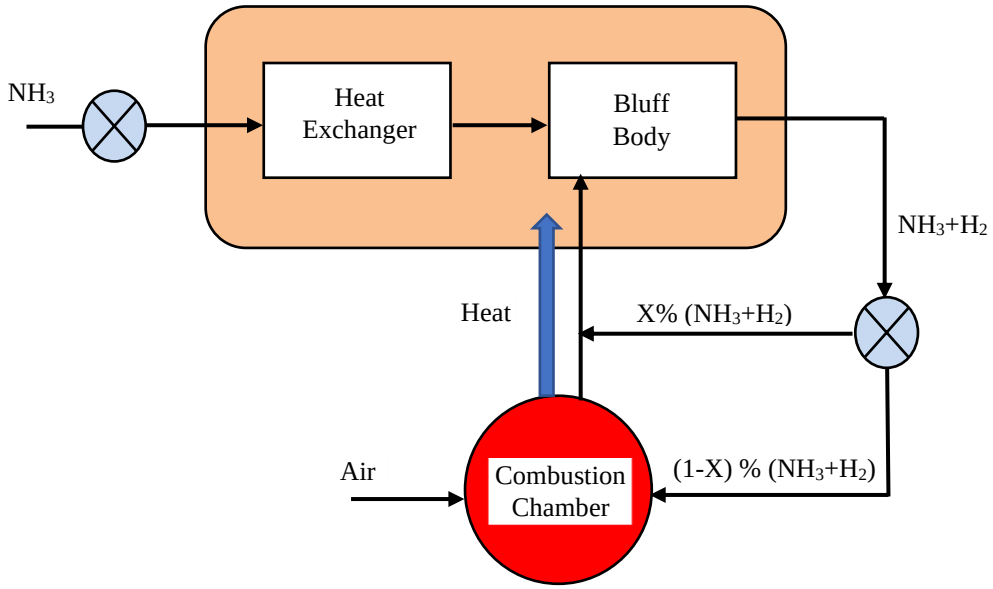

Figure 4- 1: Conceptual diagram of the proposed system.

4.2 Combustion Simulation

4.2.1 CFD Pre-Processor and Models Used

One of the design issues in a gas turbine combustion chamber is stabilizing the flame. Non-premixed swirling flames are used in some designated aero combustors because of their advantages regarding flame stabilization [197]. However, swirling flows are very complicated and hard to simulate, even without the combustion reaction. Consequently, in these numerical trials a diffusion non-premixed burner will be considered.

A 3D model of the cracking system was designed using CAD software (Solid Works).

4.2.1.1 Design of the Burner

This section introduces a non-premixed, no-swirling jet burner which was designed using CAD software (Solid Works), see Figure (4-2). This burner is similar in design

to the Sydney burner [213], which has shown itself to be conductive to turbulent flame modelling [214]. The burner consists of six fuel injectors with an inner diameter of 4 mm spaced equally on a ring of diameter 56 mm. Primary air is supplied through an annulus with inner and outer diameters 76 and 84 mm, respectively. The secondary air is supplied through four injectors of inner diameter 7 mm spaced equally on a ring of diameter 29 mm. Non-premixed 100% methane enters the burner through the six injectors while the air enters the combustion chamber through the primary annulus and secondary injectors.

The size, number, and spacing between the injectors and annulus were chosen to produce uniform flow rates of flame products across the burner exit plane. This design for the burner was adopted at this stage of the study because it provided an adequate source of heat to start the simulation trails and later to choose the best-case study for further investigation.

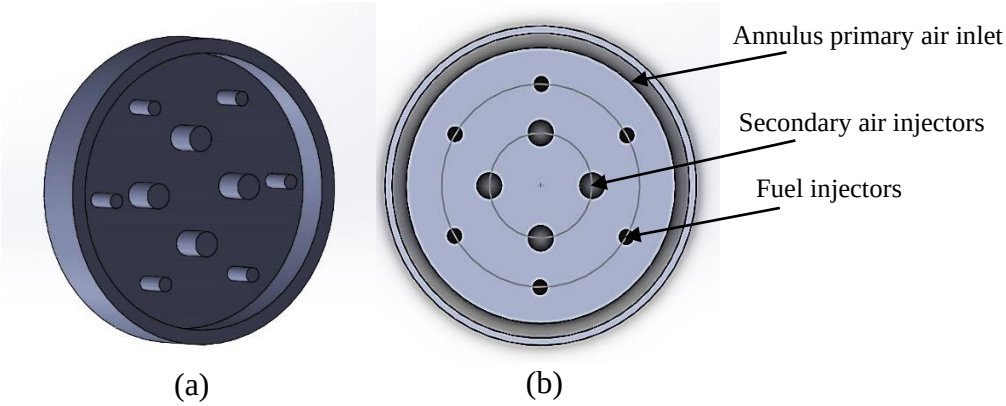

Figure 4-2: (a) Physical domain; (b) Schematic diagram of the burner

This design provides stable ignition and minimises the aerodynamic and thermal effects on the main flame [213].

4.2.1.2 Design of the Combustor

A circular quartz tube of total length 400 mm was placed vertically at the burner outlet to form the combustor's outer wall (precise details could be found in Chapter Three). The reason for using a quartz tube is that it can resist high temperatures of up to 1370 K whilst providing visual access to the flame. The combustor's inner diameter

was 84 mm which suddenly increased to 100 mm to provide adequate space to place a bluff body inside, in the centre, see Figure (4-3).

A bluff body will create a region of a wake or turbulence in the flow behind it. Thus, this aerodynamic wake of the bluff body is necessary in order to separated flow over a substantial part of its surface and provide a vortex which makes the flow fully turbulent [215]. A bluff body was attached to the combustion chamber casing by a new designed of an axial swirl vane, further details will be mentioned later in this chapter.

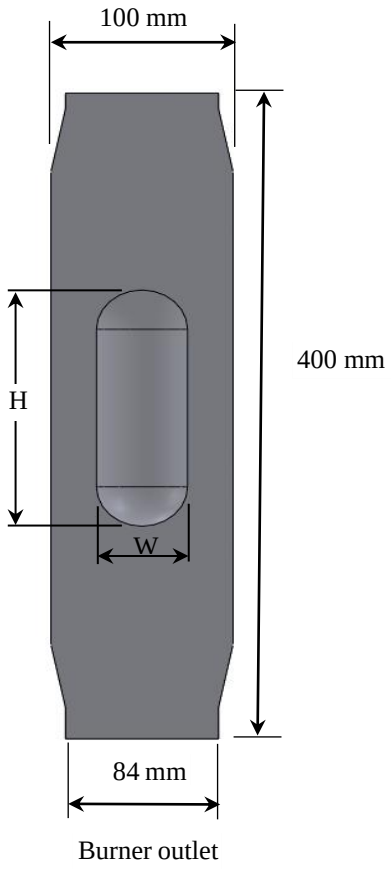

Figure 4-3: Dimensions of the first combustor design.

4.2.1.3 Effect of a Bluff Body's Shape and Position on Burner Efficiency

Various bluff body geometries (shape, size and position) were examined to attempt to enhance the heat transfer rate and the ammonia cracking process. Twelve different geometries were investigated, with the end of the bluff body facing the burner having, in turn, a circular, triangular and parabolic profile. The details of the geometries of the 12 cases are shown below in Figure (4-4), refer also to Figure (4-5).

Case 1: Bluff body at 125 mm from inlet, H=150 mm, Circular

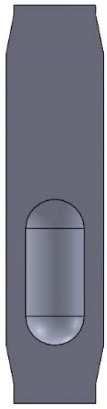

Case 2: Bluff body at 60 mm from inlet, H=150 mm, Circular

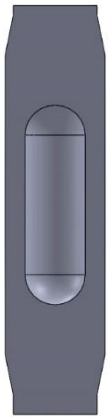

Case 3: Bluff body at 100 mm from inlet, H=200 mm, Circular

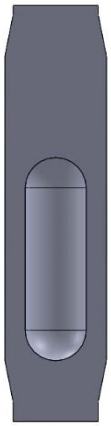

Case 4: Bluff body at 60 mm from inlet, H=200 mm, Circular

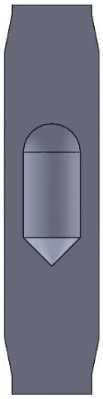

Case 5: Bluff body at 125 mm from inlet, H=150 mm, Triangular

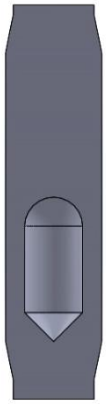

Case 6: Bluff body at 60 mm from inlet, H=150 mm, Triangular

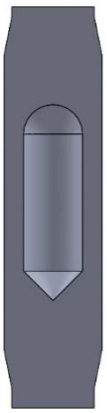

Case 7: Bluff body at 100 mm from inlet, H=200 mm, Triangular

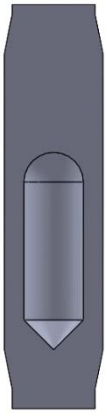

Case 8: Bluff body at 60 mm from inlet, H=200 mm, Triangular

Case 9: Bluff body at 125 mm from inlet, H=150 mm, Parabolic

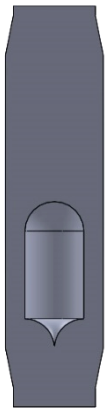

Case 10: Bluff body at 60 mm from inlet, H=150 mm, Parabolic

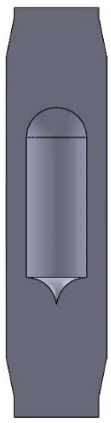

Case 11: Bluff body at 100 mm from inlet, H=200 mm, Parabolic

Case 12: Bluff body at 60 mm from inlet, H=200 mm, Parabolic

Figure 4- 4: Geometry of the various bluff bodies. In all cases the bluff body was on the centre line of the combustor and its width was W = 60 mm and H is length of bluff body.

4.2.2 Modelling of the Combusting Flow

A confined non-premixed burner (10 kW) was modelled using the geometry described above. For the simulation, ANSYS Fluent 16 solver was used to solve the governing equations for the turbulent non-premixed combustion flame. The flow model considered was based on a 3-D, steady state and turbulence closure model for Reynolds-Averaged-Navier-Stokes (RANS) simulation. The probability density function (PDF) model was used to predict the primary properties of the mixture and to illustrate the interaction between chemical reaction and turbulence [216, 217].

The RANS turbulence model used the k-epsilon simulation which has the advantage that it is easy to use (requiring initial and boundary conditions only) with a well-established structure that produces excellent result for turbulent flows. The thermo-physical properties of the reactants were calculated at ambient conditions (atmospheric pressure and temperature).

4.2.2.1 The Combustor Model

The first step of the CFD simulation was to prepare the model to analyse the fluid flows, the flow domains were split into smaller subdomains made up of geometric primitives such as tetrahedral cells. The governing equations were then solved inside each of the subdomains. A better mesh quality (smaller cells) gives a more accurate solution, so a good quality mesh is desirable in those regions where the flow field is more complicated. A high-quality mesh increases the accuracy of the CFD solution and improves convergence beyond what a poorer quality mesh could provide.

The combustor model considered in this research was first simulated for different bluff body configurations. This model consists of three parts: a) a non-premixed burner, b) a bluff body, and c) a combustion chamber, see Figure (4-5).

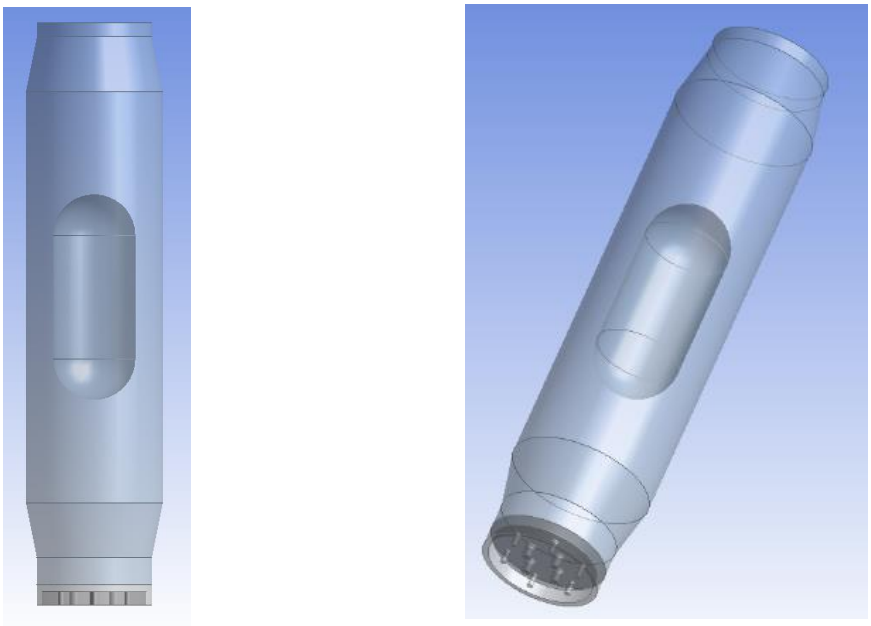

(a) Side view (b) Isometric view

Figure 4-5: Side and isometric views of the CFD model.

4.2.2.2 Mesh Construction

The independency mesh analysis was used to select the suitable mesh size and calibrate the results. A fine tetrahedron unstructured cell element type was used. Each cell is used to define nodes where fluid properties are calculated. The solution is iterated at each node based on the values obtained from the neighbouring nodes. Thus, a higher number of elements results in a higher number of nodes and ultimately more calculations required, i.e. higher computation costs. A mesh independency analysis must be performed so that the variation in the mesh does not affect the quality of the results and allows a reduction in computational time.

Three levels of tetrahedral unstructured meshes were created as shown in Figure (4-6). The three cases were tested using the boundary condition assumptions discussed in the immediately following Section 4.2.2.3. The time step was changed from 1e-1 to 1e-5, from one mesh to the next to test for better convergence. Figure (4-6) shows each of the meshes with different node densities: (a) mesh size=1e-3 mm, (b) mesh size=1.5e-3 and (c) mesh size=2e-3.

The first mesh illustrated, Figure (4-6) a, is the finest, giving the highest number of elements generated, requiring a longer computational time, with a single run requiring nearly ten days. However, the solution was not stable for some viscous models. The number of cells was reduced from $22x10^6$ to $6.5x10^6$, but this also required too long a time for a converged solution. The final mesh, see Figure (4-6) c contained $2.9x10^6$ elements and gave a satisfactorily accurate solution while taking only two days for the solution to converge with an accuracy similar to that for the 6.5 million cell mesh. The list of meshes is given in Table 4-1.

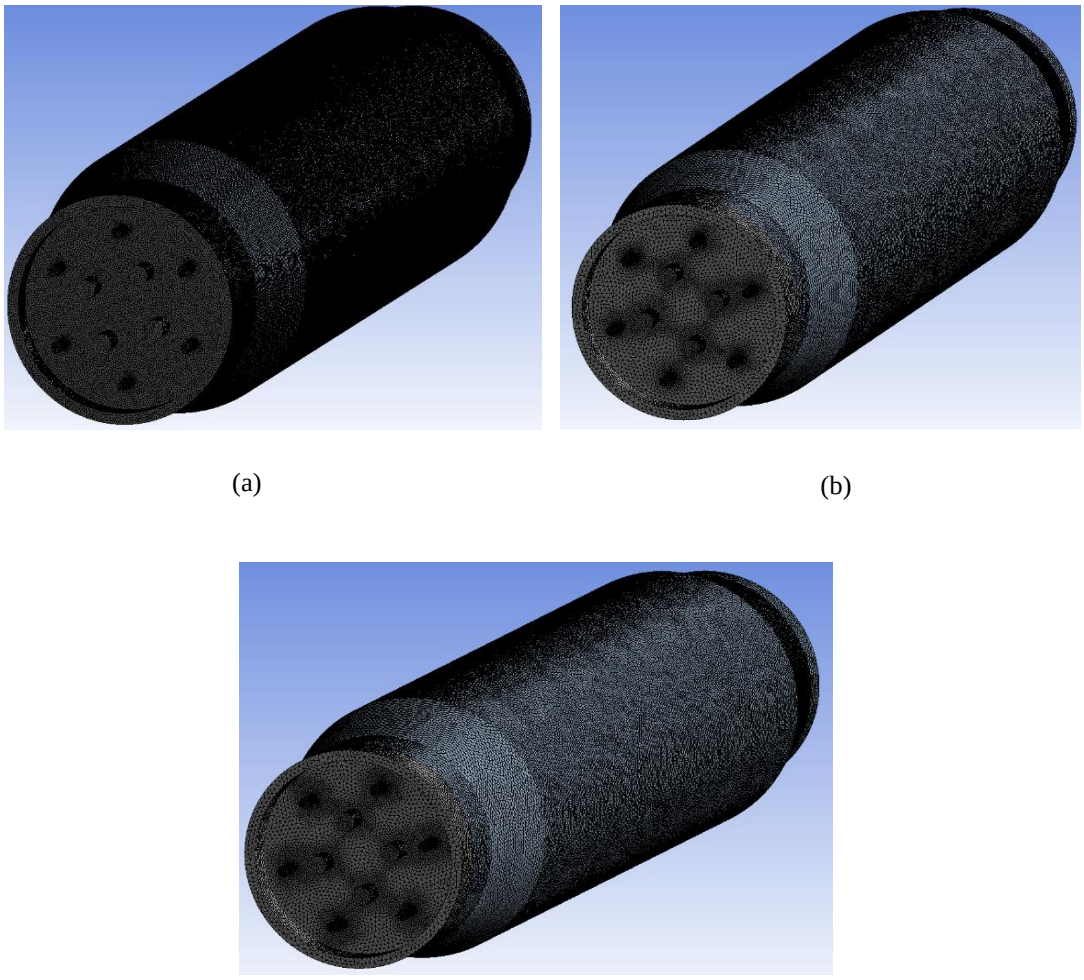

(a) (b)

(c)

Figure 4-6: Three levels of combustor mesh generation, see Table 4-1

Table 4- 1: List of meshes.

Mesh Number	Mesh density	Number of Nodes	Number of Elements
a	Fine quality	3,830,582	22,195,923
b	Medium quality	1,124,523	6,521,983
c	Coarse quality	523,742	2,933,450

4.2.2.3 Combustion Simulations and Boundary Conditions

After mesh independency was obtained, the combustion model was used to simulate the flow using 100% methane under non-premixed condition. This model is available in ANSYS Fluent 16 and default parameters for this model can be found in [182]. Solver options for the combustion model can be seen in Table (4-2). All the CFD analyses were conducted using an output power of 10 kW at 0.2 g/s flowrate of fuel. The energy transport equation was solved to account for heat losses or gains within the system, since a non-adiabatic and non-premixed combustion model was considered. When using the non-premixed combustion model, a PDF table should be created. This table contains information on the thermo-chemistry of the fuel mixture and its interaction with the turbulence. ANSYS Fluent code interpolates the PDF table during when solving for non-premixed combustion. The inlet diffusion option was chosen in this study to enable the mixture fraction to diffuse through the inlets and outlets of the domain.

Table 4- 2: Solver options for a combustion model.

Solver	Pressure-based
Turbulence Model	Standard k-epsilon
Wall Function	Standard
Combustion Species Model	Non-Premixed Combustion/ PDF Option (Inlet Diffusion)
Pressure-Velocity Coupling	SIMPLE
Spatial Discretization	Second Order Upwind

4.2.2.3.1 Theoretical Calculation

It was assumed that the fuel (CH_4) burned completely and produced carbon dioxide (CO_2) and water (H_2O), and the air consisted of 79% nitrogen (N_2) and 21% oxygen (O_2), by volume.

The reaction equation was:

$$CH_4 + 2O_2 + 7.52N_2 \rightarrow CO_2 + 2H_2O + 7.52N_2 \quad (4.1)$$

It was also assumed that the equivalence ratio ∅=1,

Power=10 kW,

Number of fuel injectors =6,

Number of air injectors =4,

The lower heating value of methane, LHV=50 (MJ/Kg), [218]

Fuel and air rates were calculated as:

$$\dot{m}_{fuel\ total} = \frac{Power}{LHV}\ (kg/s) \quad (4.2)$$

$$\dot{m}_{fuel\ per\ injectors} = \frac{\dot{m}_{fuel\ total}}{number\ of\ fuel\ injectors}\ (kg/s) \quad (4.3)$$

$$\dot{m}_{air\ total} = \frac{\dot{m}_{fuel\ total}}{(F/A)_{stoichometry}}\ (kg/s) \quad (4.4)$$

The fraction of the total air mass flow rate passing through the annulus primary inlet was equal to 0.75 of the air total mass flow rate. The rest went through the secondary injectors as follows:

$$\dot{m}_{primary\ air} = \dot{m}_{air\ total} * 0.75\ (kg/s) \quad (4.5)$$

$$\dot{m}_{secondary\ air\ injectors} = \frac{\dot{m}_{air\ total} * 0.25}{number\ of\ air\ injectors}\ (kg/s) \quad (4.6)$$

4.2.3 Results

A selection of static temperatures, turbulent intensities, velocity magnitude contours and axial velocity vectors obtained from CFD simulations are shown in Figures (4-8 - 4-11). In addition, comparison criteria considered for the selection of the best mesh (Figure (4-6) c) were based on axial velocity contours and turbulence intensities located in the five planes: P1, P2, P3, P4 and P5 downstream of the burner throat. Figure 4-7 shows these five planes.

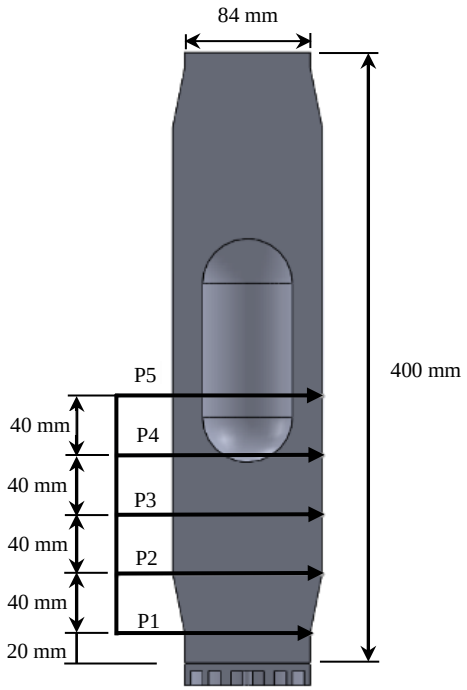

Figure 4-7: Combustor comparison planes.

Figure (4-8) shows that, as the fuel was injected, mixed and reacted with the air it followed the primary and secondary flow paths in the reaction zone, so the flame did not run along the centreline (i.e., the flame was in a circle sited above the fuel injectors symmetrical around the centre line of the combustor). Accordingly, most of the combusting gases went into the flame zone resulting in a temperature rise in this volume [214]. However, the off-centre flame had an acceptably efficiency for the present cases.

It can be seen in Figure (4-8) that the major portion of the hot combustion gas flowed to the reaction zone and made this volume a relatively uniformly hot region, while the area near the walls remained relatively cold. Also, the configuration of the bluff body had a significant effect on the topology of the flame. In all cases a stable flame was generated when the bluff body was placed at the centre of the combustion chamber. However, when the bluff body was positioned near the burner, the flame tended to become unstable when using a “sharp cornered" bluff body, triangular or parabolic cross-section. The bluff body with circular cross-section was best able to maintain a stable flame.

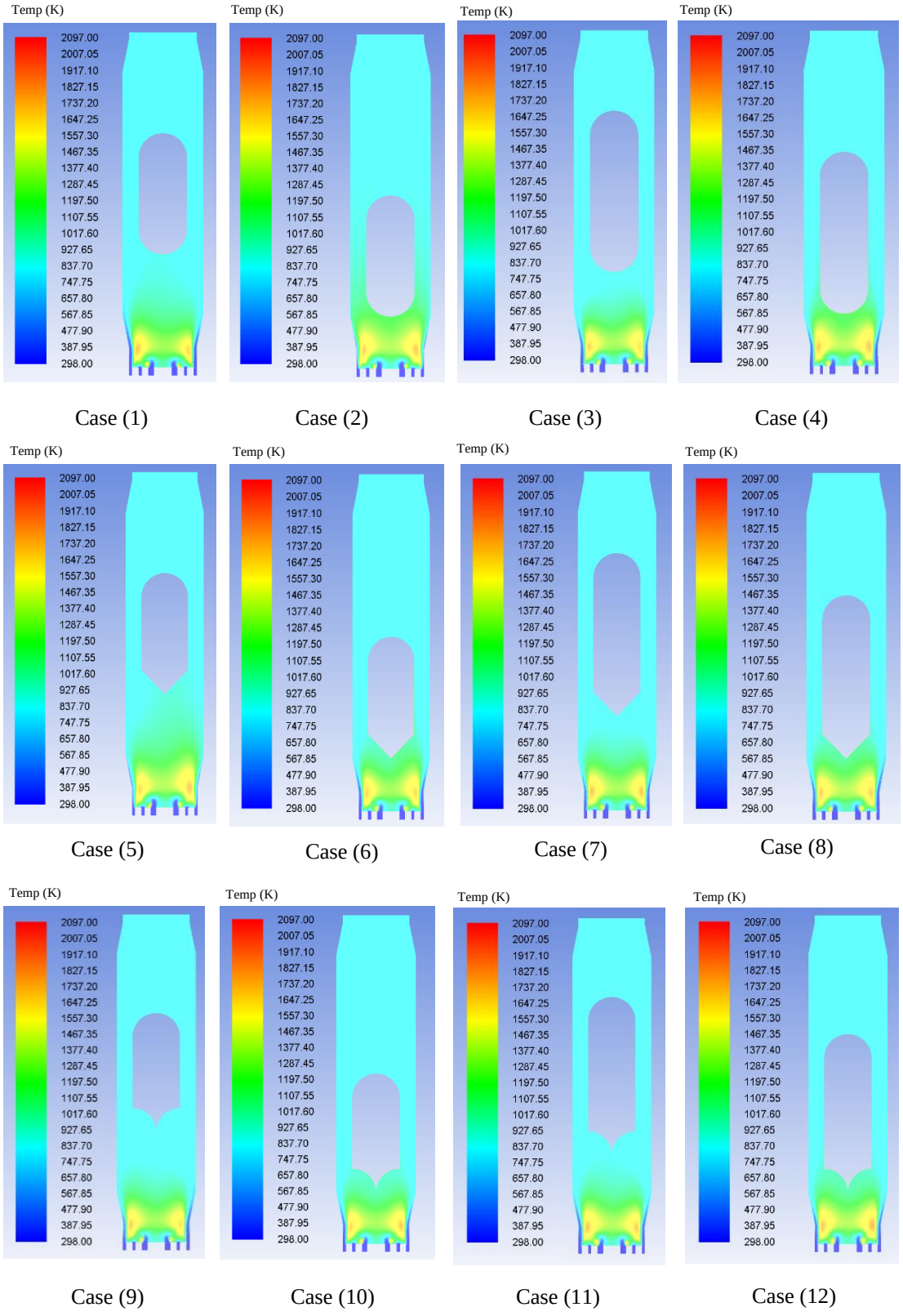

Figure 4-8: Contours of static temperature (K) for 12 Cases.

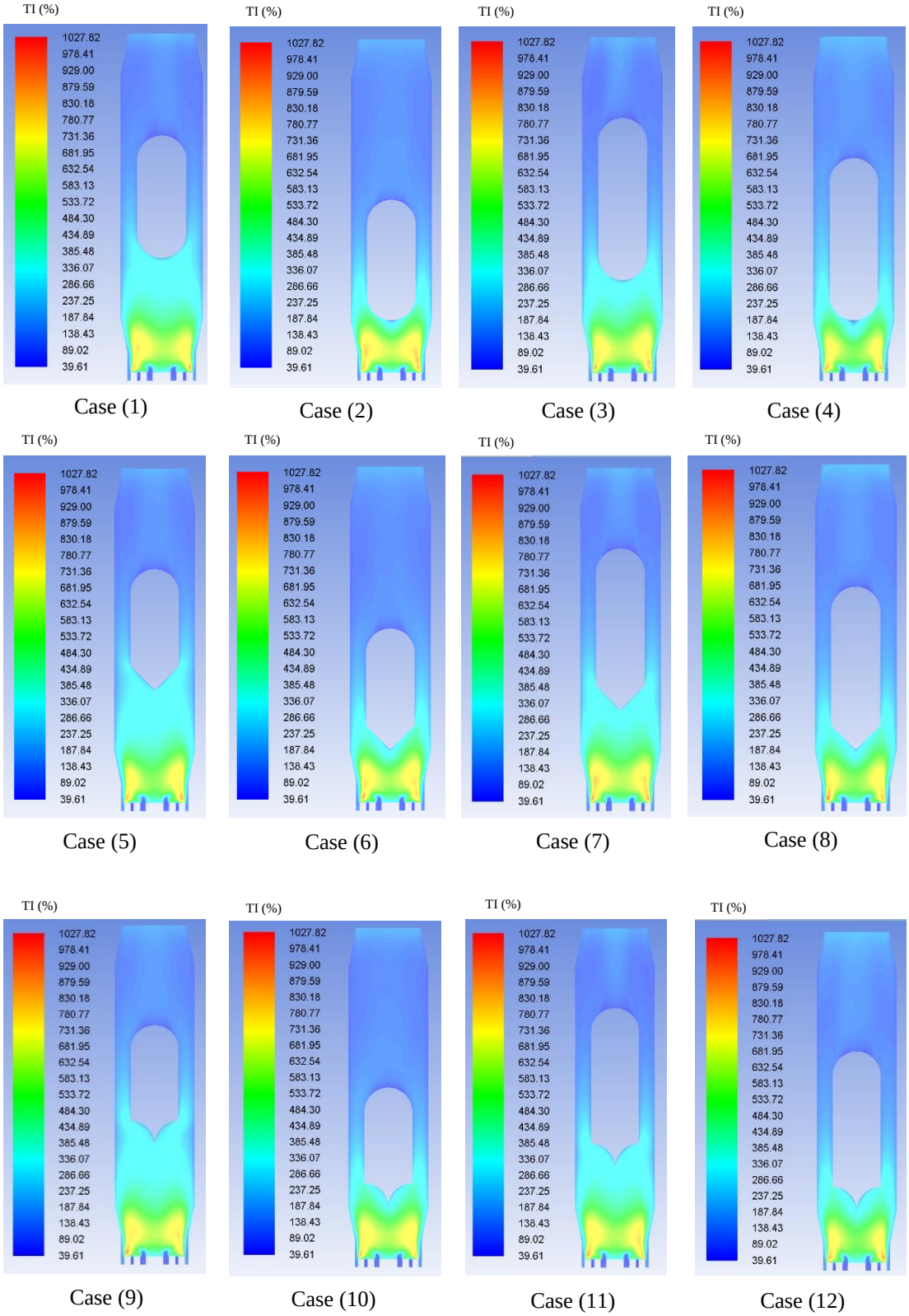

Figure 4-9: Contours of turbulent intensity (%) for 12 Cases.

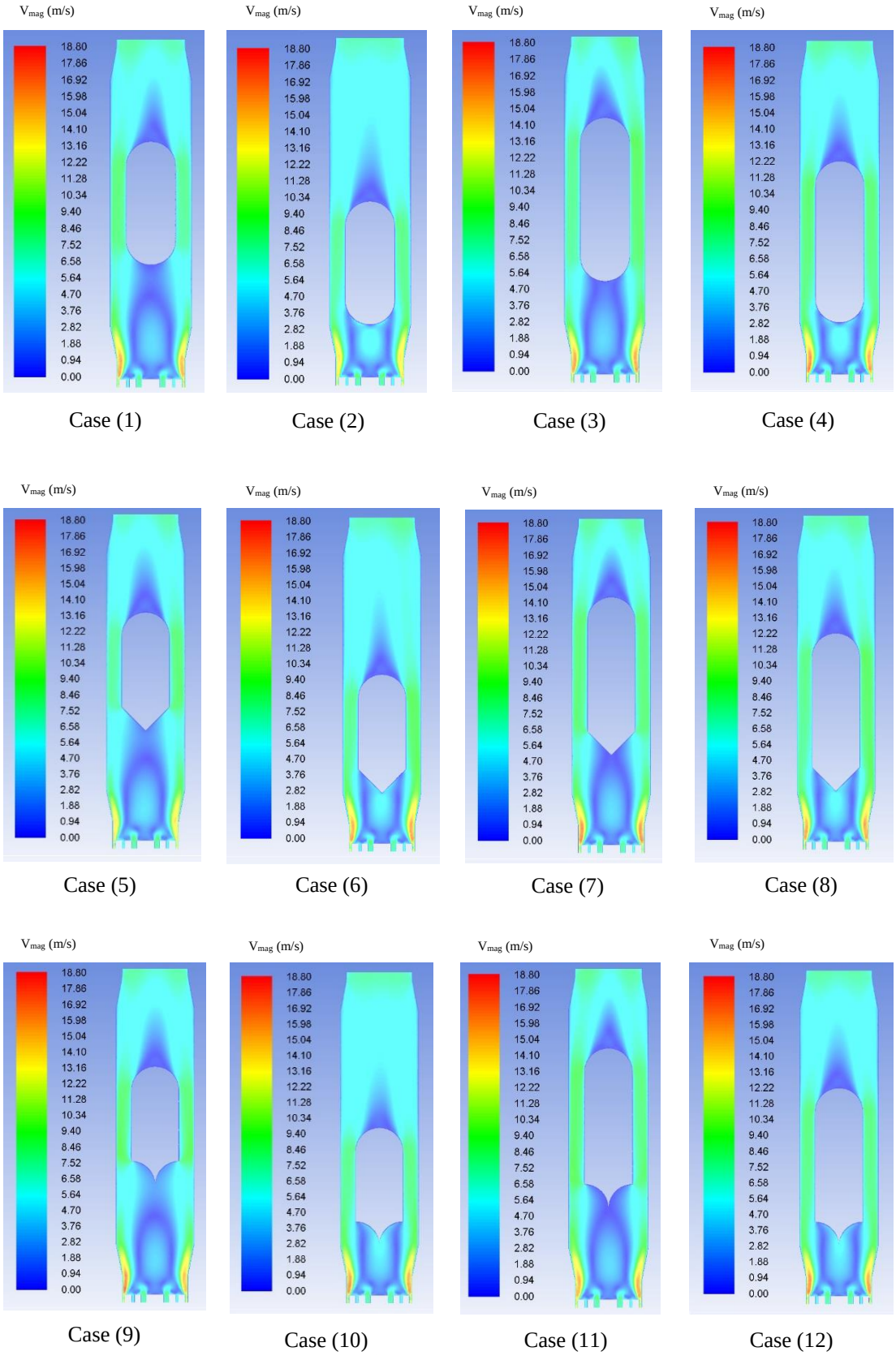

Figure 4-10: Contours of velocity magnitude (m/s) for 12 Cases.

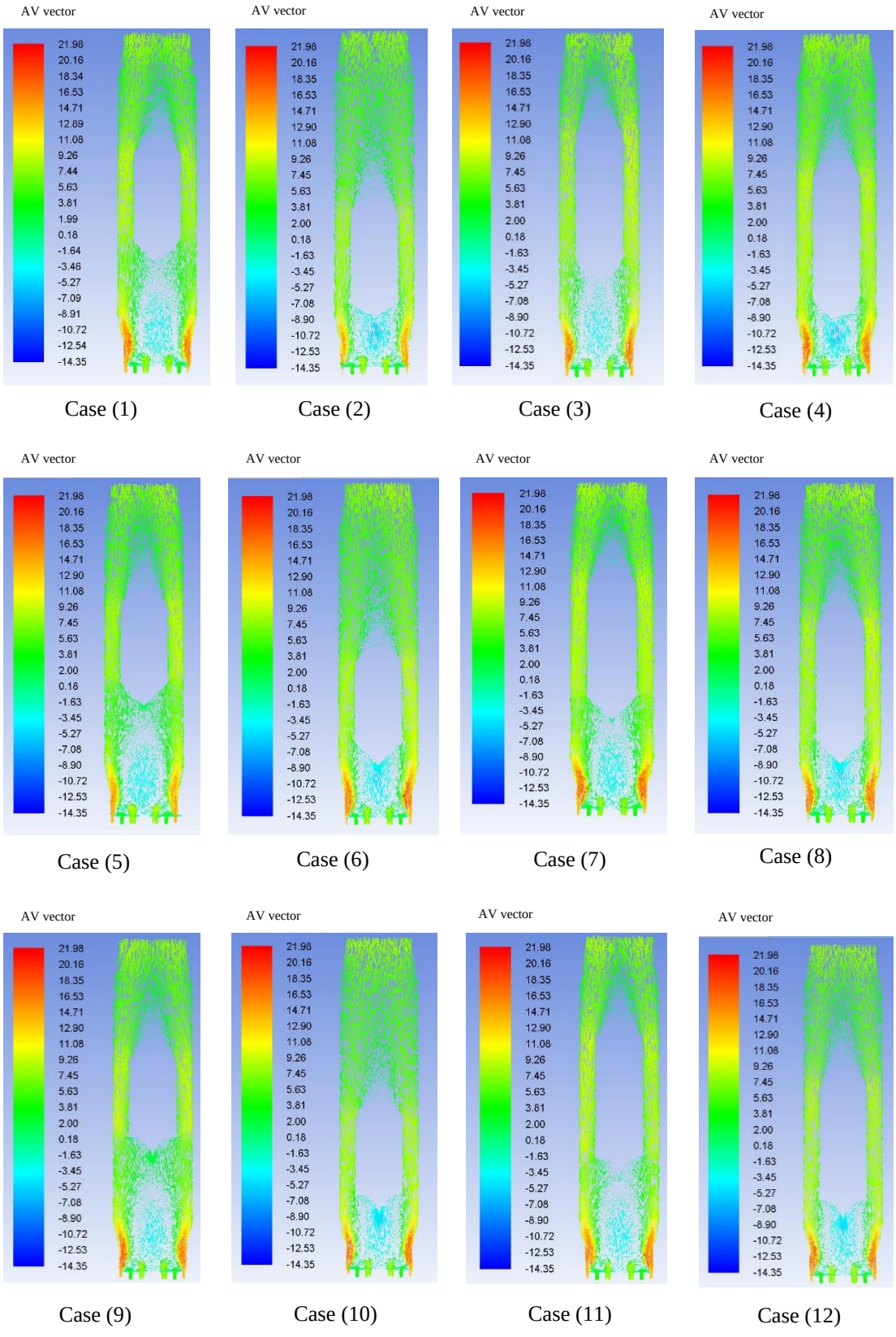

Figure 4-11: Contours of axial velocity vectors for 12 Cases.

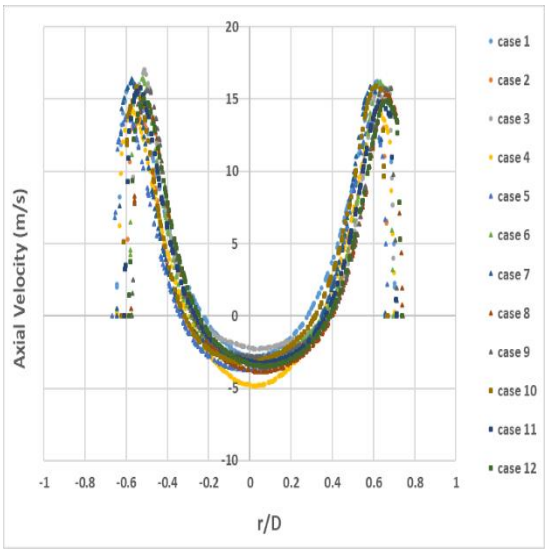

P1

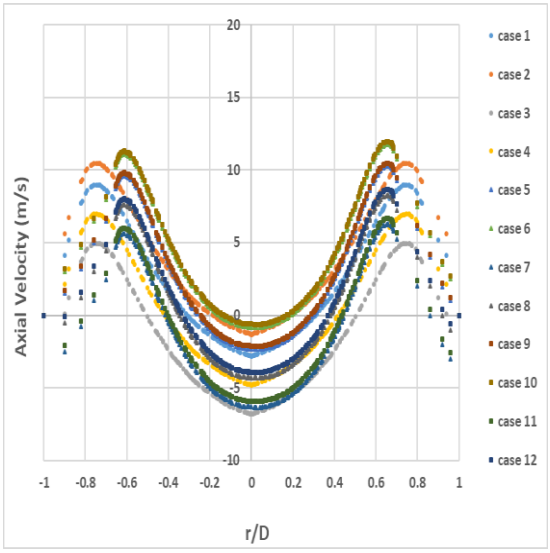

P2

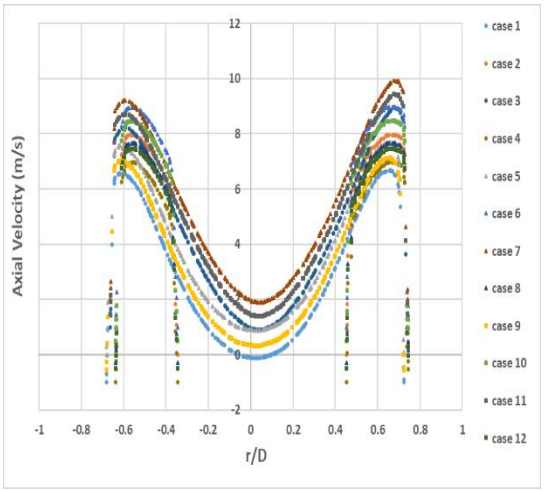

P3

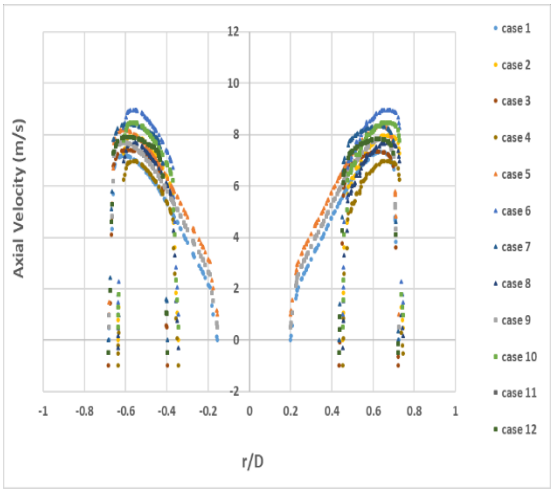

P4

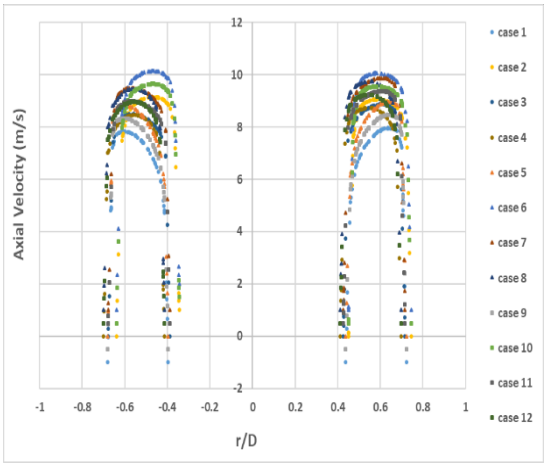

P5

Figure 4-12: Comparison of axial velocity (m/s) for 12 cases at the five planes: P1, P2, P3, P4 and P5.

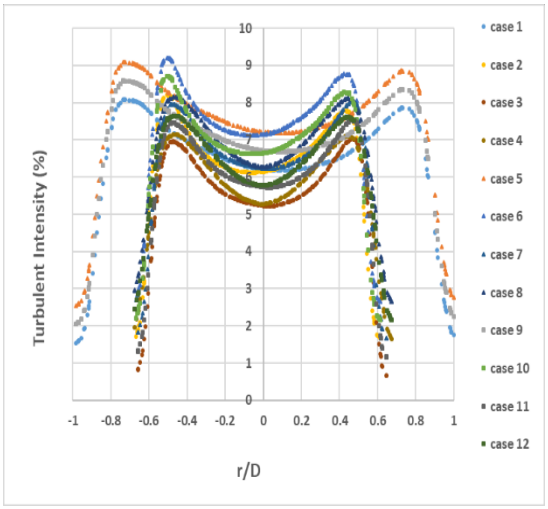

P1

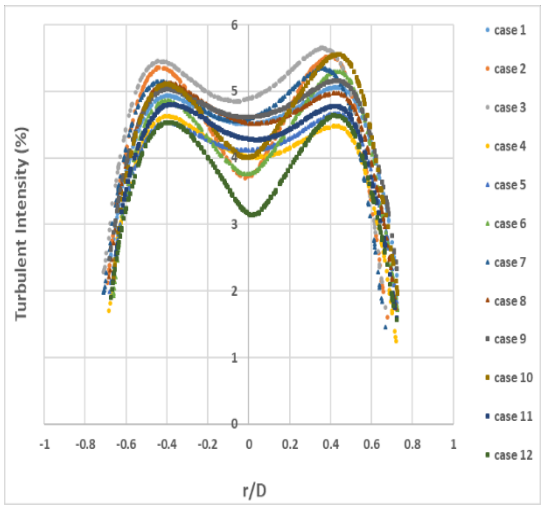

P2

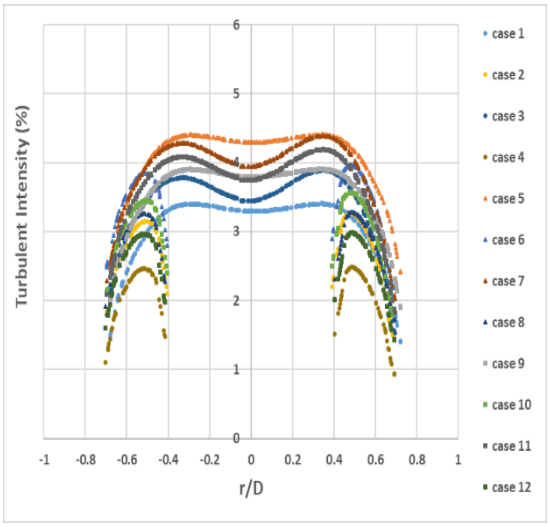

P3

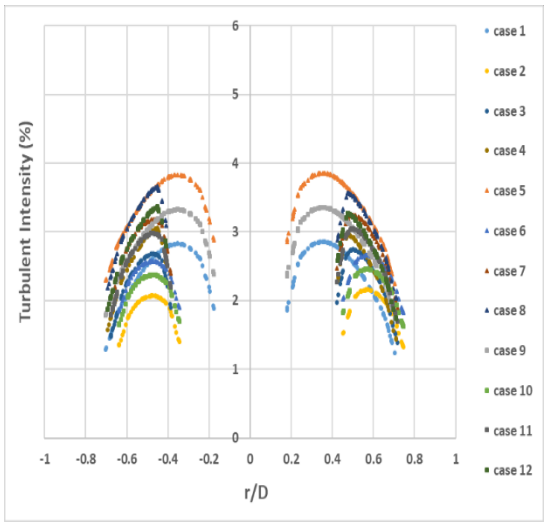

P4

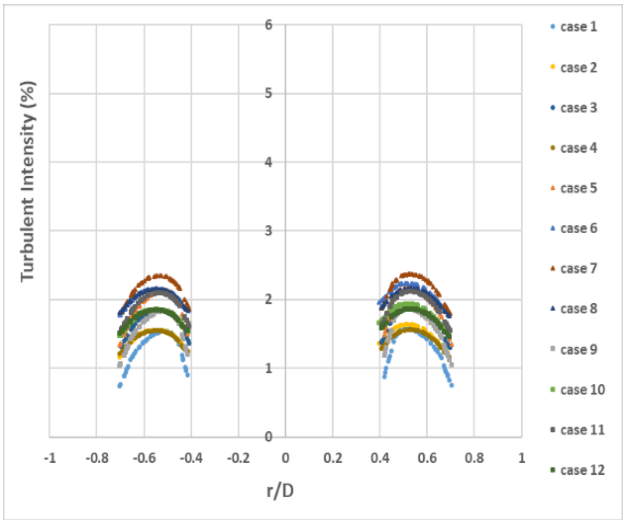

P5

Figure 4-13: Comparison of turbulent intensity (%) for 12 cases at the five planes: P1, P2, P3, P4 and P5.

Figure (4-9) clearly shows the turbulent intensities inside the combustion zone for different positions and shapes of the bluff body. In turbulent jet flames, an important source of turbulence is caused by turbulence shear layers. An increase in turbulence intensity was observed when the bluff body was located at the centre of the combustor with an increase in displacement and stretching of the reaction zone. The volume of the reaction zone increased due to the higher interaction between turbulent eddies and the reaction zone inside the combustor which led to a faster reaction time for the fuel/air blend [219]. However, moving the bluff body to the mid-point along the length of the combustor increased turbulence intensity, and the sharp cornered bluff bodies reduced turbulence intensity compared to the circular cross-section bluff body by increasing the volume of the central recirculation zone.

Figure (4-10) presents velocity magnitudes and it is clear that the deflection of the streamlines behind all the bluff bodies is almost identical. For a comparison of velocity vectors downstream of the bluff bodies, Figure (4-11) shows two features: the flow oriented downstream of the bluff body, and wall-bounded vortices formed in the bottom corner of the combustor. Due to the geometry of the bluff bodies and the inlet flow conditions, the flows moved around the bluff bodies and toward the wall. This motion made the streamlines larger when the bluff bodies were located away from the injectors towards the middle of the combustor with a smaller corner vortex, which helped flame stability. Moving the bluff body further downstream, the streamlines became thinner, and the flow gradually transitioned to the fully-developed condition.

When comparing the axial velocity profiles of all cases in the five planes (Figure 4-12), maximum velocities were measured where the shearing flow, i.e. the high momentum flow region (HMFR), was located. The point at which the flow diverged negatively, where $r/D < 0.4$, indicated that the HMFR was becoming slimmer and stronger. This was because of the greater negativity of the reactivity of the blend, and the squeezing of the shearing flow. The maximum velocity in the profile was observed where $r/D = 0.6$, while the lowest velocities were obtained at the centre of the system.

From Figure (4-13), it can be seen that the highest turbulent intensity occurred in the region of the outer shear layer ($r/D = 0.6$). There are qualitative similarities between the plots for each of P1 to P5, but there are quantitative differences between the twelve case studies. The smallest values of turbulent intensity occur on the centreline. The

vortex core was not, in fact, stable which resulted in higher values for the turbulence intensity.

Case (1), where the bluff body was at the mid-point of the combustor, was 150 mm in length, and was positioned 125 mm from the inlet, was found to be the design which gave the most homogeneous flame profile which provide an efficient temperature to heat the bluff body which in turn used to crack the ammonia passing through it. The cracked ammonia could be a source of fuel for the burner.

4.2.4 Modification for the Best Case

After choosing Case 1, as the best for our purposes, some modifications were made to enhance the flow characteristics inside the combustor and give better mixing of gases at the outlet. An axial swirl vane was added, and also used to hold the bluff body, see Figure (4-14). In addition, the diameter of the bottom of the combustor was reduced from 100 mm to 84 mm to increase homogeneity by further mixing of the flue gases with secondary air see Figure (4-15).

4.2.4.1 CFD Simulation for Enhancement the Flow Inside the Combustor

An axial swirl vane was designed to support the bluff body and to enhance the flow distribution and heat transfer, as shown in Figure (4-14). It consisted of eight straight swirl vanes, each with a thickness of 1.5 mm. The swirl vanes were fixed at an angle of 40° from the axial centreline. The outer diameter of the swirl vane was D_s = 96 mm, while the swirl vane hub diameter was D_h = 64 mm. The geometrical swirl number (S_{N_v}) is based on the following equation [17]:

$$S_{N_v} = \frac{2}{3}\left[\frac{1-\left(\frac{D_h}{D_s}\right)^3}{1-\left(\frac{D_h}{D_s}\right)^2}\right]\tan\theta \qquad (4.7)$$

Where θ is the vane angle orientation from the centreline axis could be varied between 30^o and 60^o.

Vane thickness, t_v = 0.7 – 1.5 mm

Number of vanes, N_v =8 –16

$S_{N_v} > 0.6$

$\frac{D_h}{D_s} > 0.5$

The swirl number was calculated at 0.7, which was sufficient to recirculate the flow.

Figure 4-14: An axial Swirl supporting vane.

Figure (4-15) represents the physical model and the grid distribution for the modified case study which consisted of 2,843,872 elements.

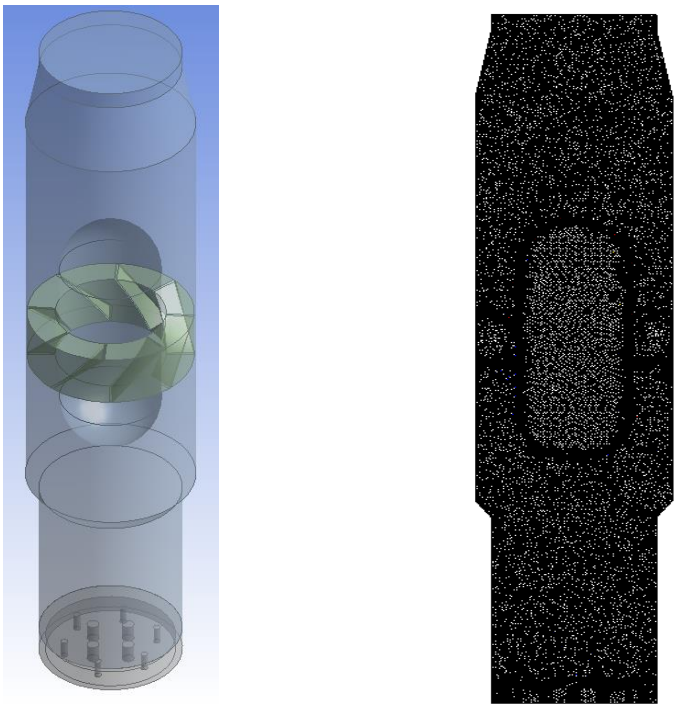

(a) (b)

Figure 4-15: (a) Physical Domain, (b) Grid Generation.

The purpose of the axial swirl vanes was to generate turbulent kinetic energy inside the combustion chamber, around the bluff body. High flow velocity and turbulent kinetic energy would accelerate the diffusion and mixing of the flue gases and guide the products to the exit. Figure (4-16) presents the results for the best case which is represented by Case 1 with swirl vanes added. This arrangement was the one chosen. It depended on the next CFD simulation of the heat exchanger where the exhaust gas properties were taken as an inlet boundary condition to the heat exchanger as the ammonia was passed through it.

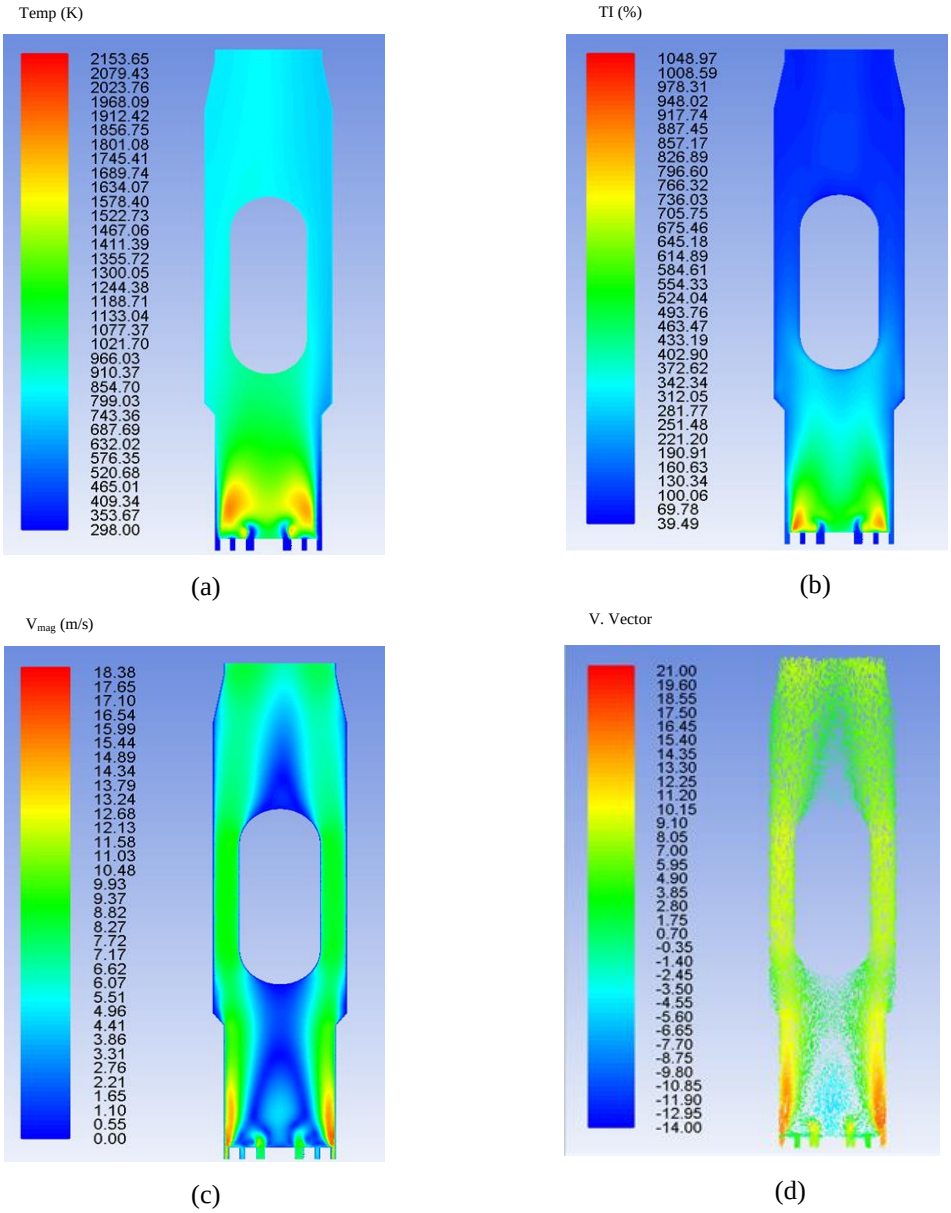

Figure 4-16: Results for the best (modified) case, (a) Contours of static temperature (K), (b) Contours of turbulent intensity (%), (c) Contours of velocity magnitude (m/s) and (d) Velocity vector coloured by Y velocity (m/s).

For the purpose of comparison with Case 1, Figure (4-16) a, shows the static temperature profiles generated when using an axial swirl vane holder, which also held the bluff body in place. The static temperature was compared for the five planes, P1 to P5, see Figure 4-17. For all planes, the addition of the swirl vanes modified flow patterns to produce better behaviour of the flame with higher temperatures.

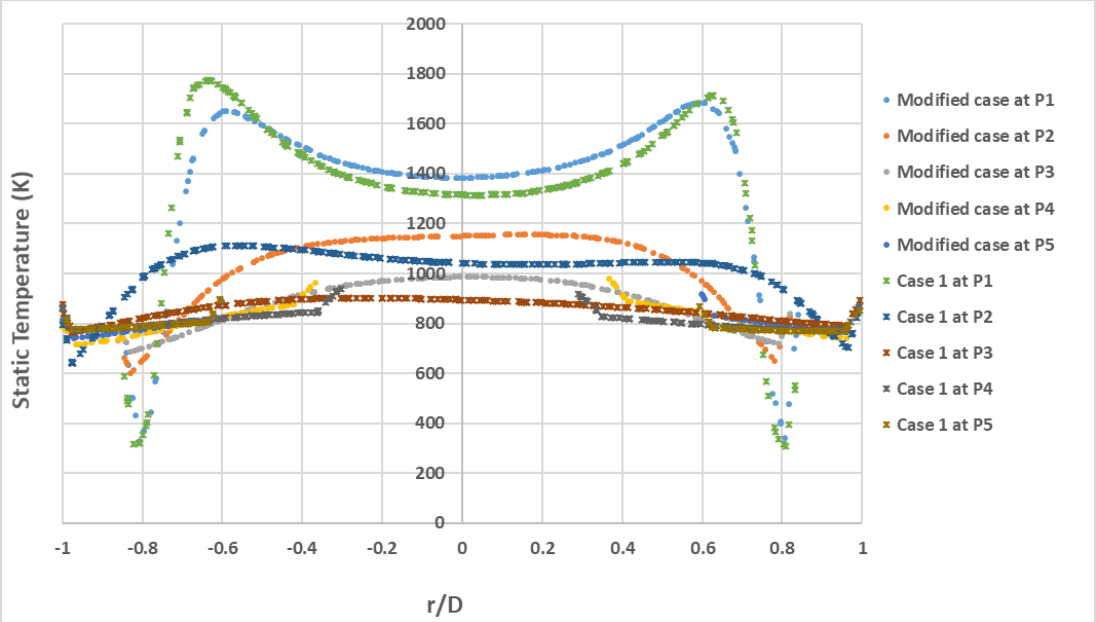

Figure 4-17: Comparison of static temperature between Case 1 and Modified case to include swirl vanes at five different planes; P1, P2, P3, P4 and P5.

The presence of the axial vanes reduced the velocities before and after the bluff body zone, compared with no axial vanes (Case 1), reducing the velocity of the high momentum flow region, and enhancing the effect of combustor geometry on flame topology. A reduction in size of the recirculation zones upstream and downstream of the bluff body were observed when the vanes were added, see Figure 4-18 (b). This was as expected, due to the effect of the breakdown happening downstream of the axial vanes which reduced the rate of expansion of the flow upstream of the vanes. There is also the effect of the difference in the diameter confining the primary zone that affects the size and the strength of the swirl flow, i.e. the CRZ and the shear layer thickness.

Consequently, it may be said that the use of axial swirl vanes can increase the performance of a burner and reduce emissions, due to enhanced mixing of gas products at the outlet. As a result, the exhaust gas properties predicted from the simulation study of the modified case will depend on later to the heat exchanger CFD simulation.

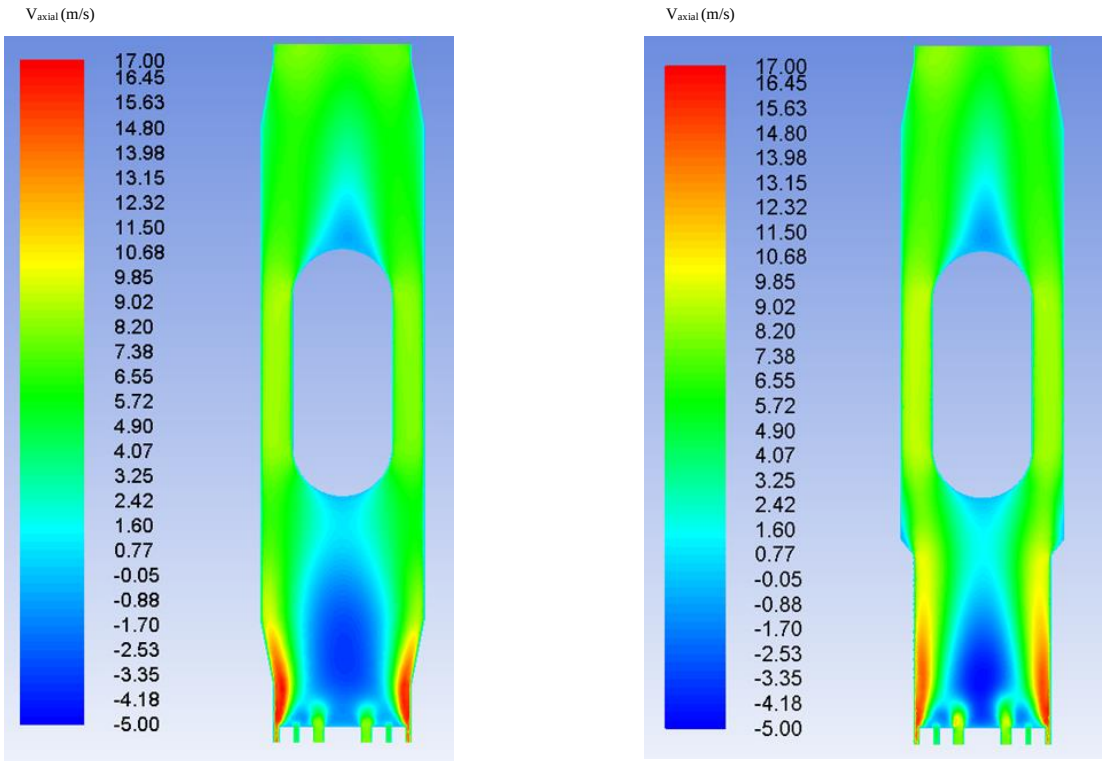

(b) Case 1

(a) Modified Case

Figure 4-18: Comparison of the recirculation zone size before and after the bluff body region between Case 1 and Modified case to include swirl vanes.

4.3 Heat Exchanger Simulation

For this particular study, different shell and tube heat exchangers were considered for pre-heating the ammonia. Then the pre-heated ammonia passed through different passages inside the bluff body to crack the ammonia, which would later be used as a primary fuel. The bundle of tubes is used for the ammonia and the hot exhaust gases from Case 1 with swirl vanes, and these are all on the shell side.

The heat exchanger model in the present study was also meshed using a design modeller in ANSYS Fluent 16. The entire geometry was divided into three domains, a

cold fluid domain inside the bundle of tubes (ammonia vapour), a hot fluid shell (exhaust gases, CO_2) and a solid domain for the steel tube wall.

For simulating the conjugate heat transfer phenomenon, the heat exchanger was discretized into a fluid and a solid domain in order to have better solution control over the number of nodes.

The analysis of this new heat exchanger was simplified through some reasonable and realistic assumptions:

1. The heat transfer processes are steady state and the flow is turbulent.
2. Kinetic and potential energy changes are negligible.
3. The specific heat of a fluid (exhaust gases and ammonia) is constant.
4. The outer surface of the heat exchanger is perfectly insulated; hence the heat loss to the environment can be ignored.
5. The tube wall temperature is kept constant.
6. The thermal properties of the shell side fluid are constant.

In this pressure based simulation, the absolute velocity formation and steady state were selected for the solver option. In the model option, the energy equation was chosen, and the viscous model was set as standard (k- epsilon 2nd equation) with a standard wall function.

Three case studies of shell and tube with cross flow were designed and simulated. This procedure allowed us to predict the temperature of the outlet ammonia which is passed through the pipe before entering again inside the chosen modified bluff body. The specification of the three case studies and mesh construction are illustrated in Figures (4-19 to 4-21). Shell diameter 80 mm, tube diameter 6.35 mm (= ¼ in) and a simplified model with shell length 140 mm, shell side fluid (exhaust gases) and tube side fluid ammonia, were selected.

Case I consisted of three tube passes, Case II consisted of five tube passes and Case III had a spiral tube shape.

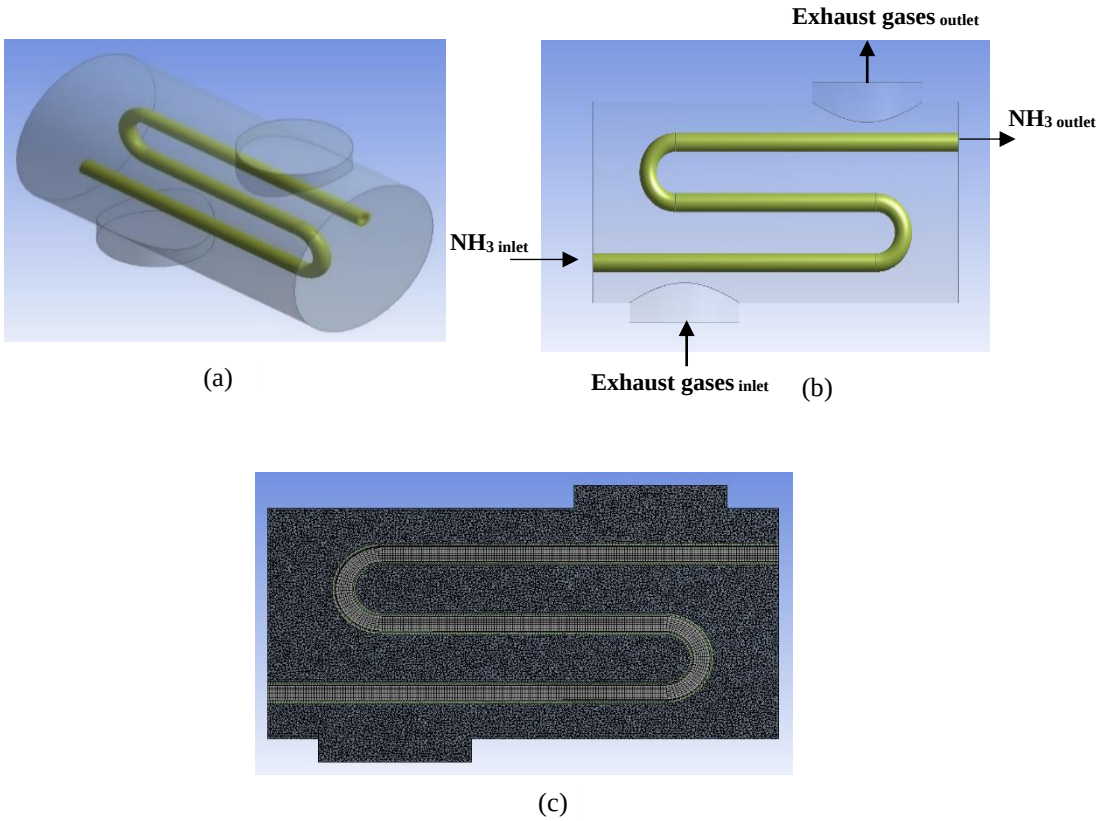

Figure 4-19: (a) Physical domain, (b) Schematic diagram of heat exchanger; (c) Grid generation for Case I.

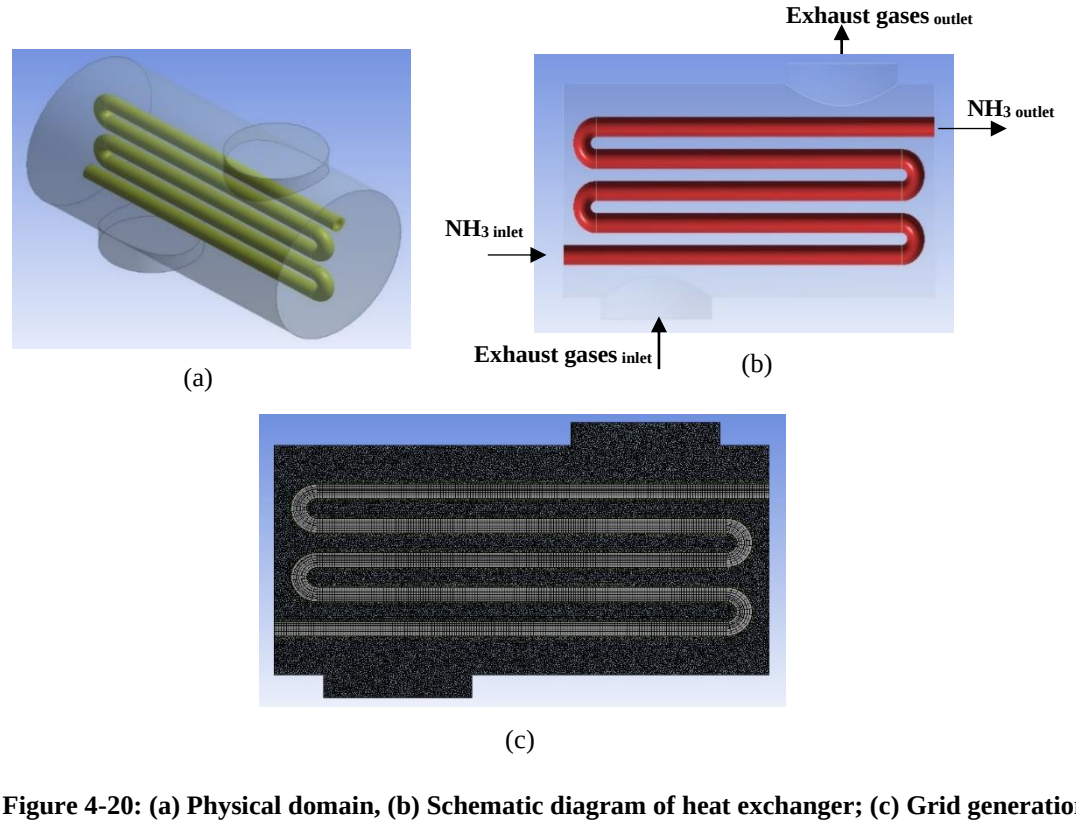

Figure 4-20: (a) Physical domain, (b) Schematic diagram of heat exchanger; (c) Grid generation for Case II.

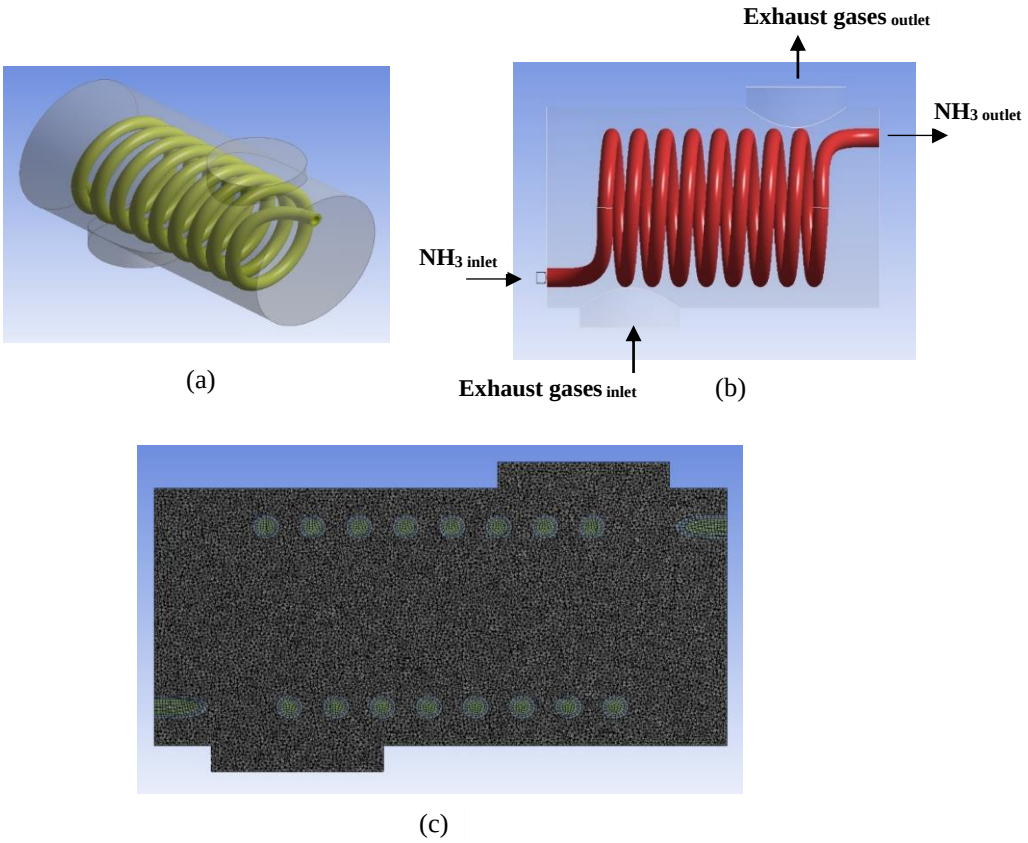

Figure 4-21: (a) Physical domain, (b) Schematic diagram of heat exchanger; (c) Grid generation for case III.

The list of meshes is given in Table 4-3.

Table 4- 3: Mesh generation specification.

Case study	Number of Nodes	Number of Elements
1	757,470	4,439,787
2	808,709	4,297,449
3	875,989	4,026,927

4.3.1 Heat Transfer Aspects

Based on the above assumptions, it follows at once from the first law of thermodynamics that the rate of heat transfer from the cold fluid is equal to the rate of heat transfer to the hot fluid [220].

The heat transfer rate to the cold fluid (ammonia) is given as

$$q_c = m_c Cp_c \Delta T_c \tag{4.8}$$

while the heat transfer rate to the hot fluid (exhaust gases) is given as

$$q_h = m_h Cp_h \Delta T_h \tag{4.9}$$

Where,

the m = mass flow rate and is calculated by Equation (4.10):

$$m = \rho v A \tag{4.10}$$

The value of the LMTD for parallel and counter-flow streams is calculated from:

$$\Delta T_m = \frac{\Delta T_1 - \Delta T_2}{\ln(\Delta T_1 / \Delta T_2)} \tag{4.11}$$

It is suitable to use an average effective temperature difference (ΔT_m) for the entire heat exchanger [221]:

$$q = UA\Delta T_m \tag{4.12}$$

Where

q = Heat transfer rate (W)

A = Heat transfer area (m^2)

U = Overall heat transfer coefficient (W/m^2 K)

ΔT_m= average temperature differences (K)

$LMTD$ = Logarithmic mean temperature difference (K)

$$\Delta T_m = LMTD, \quad (for\ one\ tube\ pass) \tag{4.13}$$

$$\Delta T_m = F(LMTD), \quad (for\ a\ more\ than\ one\ tube\ pass) \tag{4.14}$$

$$F = 1, \ (for\ parallel\ flow)$$

The heat transfer coefficient (h) could be calculated by using the following equation:

$$h = \frac{Nu\, K_f}{d} \tag{4.15}$$

Where

$$Nu = 0.023\ (Re)^{0.8}(Pr)^{n} \tag{4.16}$$

n = 0.4 for heating

n =0.3 for cooling

$$Re = \frac{\rho v_f d}{\mu} \tag{4.17}$$

$$Pr = \frac{\mu\, C_p}{K_f} \tag{4.18}$$

Where,

v_f is the fluid velocity inside the tube,

d is the equivalent (hydraulic) diameter,

K_f is the fluid thermal conductivity,

Where the thermo-physical properties for the hot exhaust gases and the cold ammonia are presented in Table 4-4.

Table 4- 4: Thermo-physical properties for the working fluids of the heat exchanger.

Material properties		
Material Properties	Ammonia	Exhaust Gases (CO_2)
Density (kg/m^3)	0.6894	1.7878
Conductivity (W/m$^-$K)	0.0247	0.0145
Specific heat capacity (kJ/kg$^-$K)	2.158	0.84037
Viscosity (kg/m-s)	1.015 e^{-5}	1.37 e^{-5}

4.3.2 Heat Exchanger Boundary Conditions

The boundary conditions for all case studies of the shell and tube heat exchanger were defined as required by the model. The inlet temperatures and velocities for the hot gases entering the heat exchanger were defined from the outlet exhaust gases from the previous combustion modelling in the final modified case study. The inlet conditions for the cold ammonia were set at atmospheric pressure and temperature. The boundary conditions can be seen in Table 4-5. The solution methods and the solution control options are listed in Table 4-6.

Table 4- 5: Boundary Conditions.

Inlet Conditions		
Boundary Condition	Ammonia	Exhaust Gases (CO_2)
Velocity inlet (m/s)	1.0	7.2
Temperature (K)	288	830

Table 4- 6: Discretization scheme followed.

Solution Methods	
Scheme	Simple
Gradient	Least square cell based
Pressure	Second order
Momentum	Second order upwind
Turbulent Kinetic	Second order upwind
Solution Control	
Pressure	0.3 Pascal
Density	1 kg/m^3
Body forces	1 ($kg/m^2\ s^2$)
Momentum	0.7 (kg-m/s)
Turbulent Kinetic energy	0.8 (m^2/s^2)

In cell zone conditions the ammonia was in the vapour phase, CO_2 was selected for the hot fluid and steel was the material of the tube wall. The mesh interfaces included the conduction and convection associated with the intermediate solid wall. The details of the interfaces for all three case studies are shown in Figures (4-22) to (4-24).

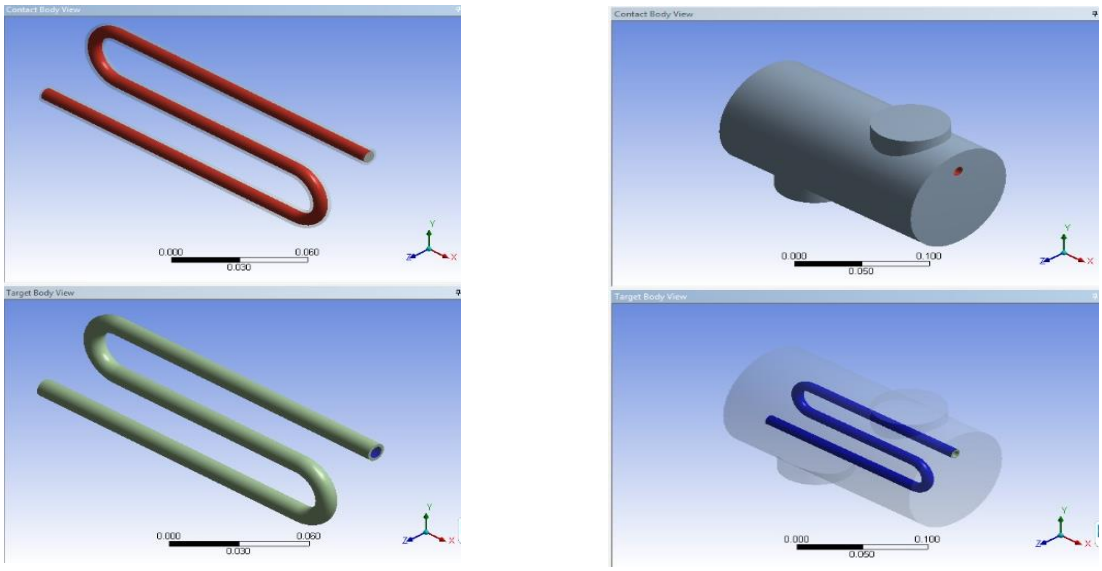

(a) (b)

Figure 4-22: Mesh interfaces for Case I, (a) Interface between tube wall (steel) and fluid domain inside the tube (NH3) and (b) Interface between tube wall (steel) and the shell (CO2.

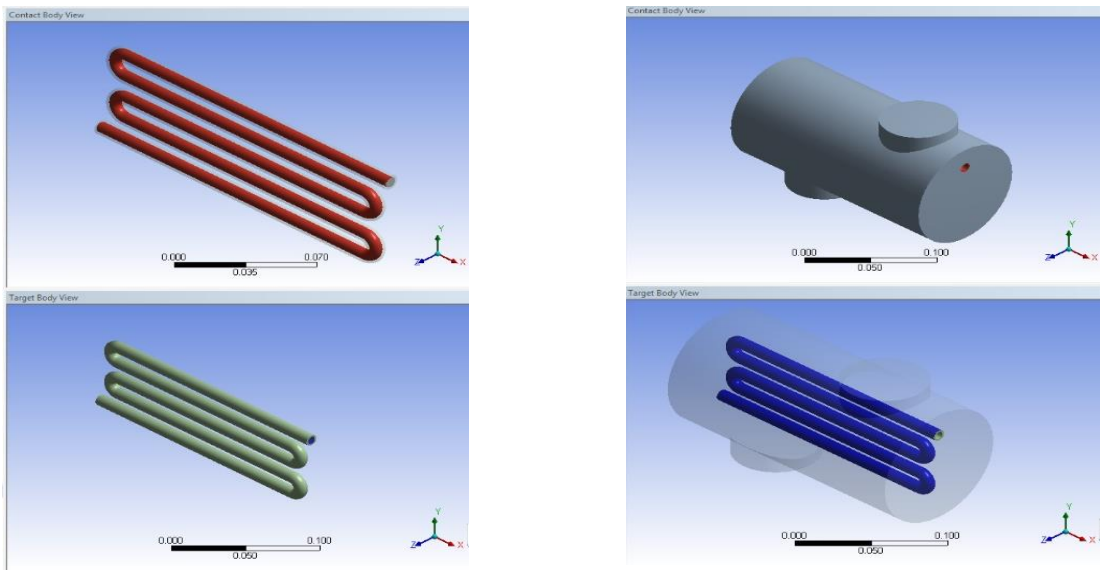

(a) (b)

Figure 4-23: Mesh interfaces for Case II, (a) Interface between tube wall (steel) and fluid domain inside the tube (NH3) and (b) Interface between tube wall (steel) and the shell (CO2).

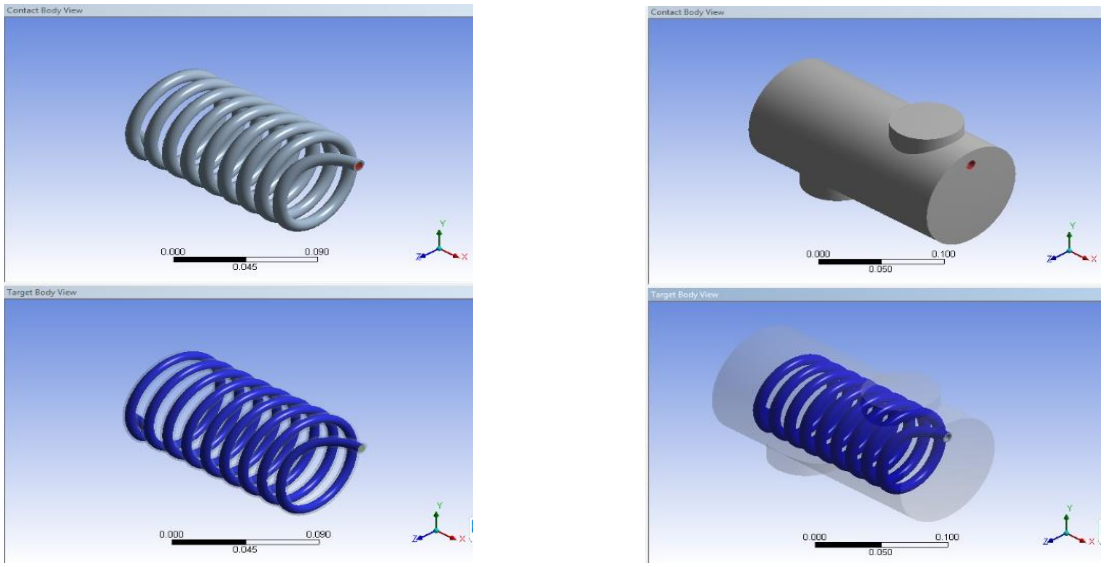

(a) (b)

Figure 4-24: Mesh interfaces for Case III, (a) Interface between tube wall (steel) and fluid domain inside the tube (NH3) and (b) Interface between tube wall (steel) and the shell (CO2).

4.3.3 Heat Exchanger Results

The simulation was set for 10,000 iterations. The convergence criteria for continuity, X-velocity, Y-velocity, Z-velocity and k-epsilon should be less than 10^{-4}, and for energy should be less than 10^{-6}. If these values all behave in a a satisfactory manner, then the solution will converge.

The temperature, turbulent intensity, static pressure, velocity vector and velocity distribution along the heat exchanger can be seen through the side view on the plane of symmetry for each case study. The contour plots in Figures 4-25 to 4-27 show useful results which give an idea of the heat transfer distribution along the flow for the three case studies.

It can be seen that there is a drop in temperature at the shell outlet, this is for several reasons, mainly the cross-flow at the inlet. Besides, the temperature difference between the shell side and the tube side is much higher. It was observed that the fluid near the inlet for the hot gases in the shell lost temperature much more than the fluid at the outer edge, due to its sudden exposure to the cold fluid, ammonia, in the inlet tube. The fluid temperature inside the tubes rose gradually along the length of the heat exchanger. This could be noted in all profiles. At the shell outlet, the inner fluid tended

to mix with the external fluid, and this caused some smoothing of the temperature profile.

The velocity profile also denotes that the outer fluid of the shell was moving at higher velocity than the inner fluid. The velocity reached its maximum value at the outlet of the shell and gradually dropped to zero near the tube wall. It can be seen that the velocity profile at the shell inlet was not consistent due to crossflow and high-pressure gradients. It could also be concluded that not much vorticity was produced in the mean flow field where the majority of the hot gases was flowing through the tube passages.

From the CFD results, we could predict the temperature of the ammonia outlet for all three cases. The values were: Case I, T_{NH3} =725 K, for both cases II and III $T_{NH3} \approx 801$ K. These values were used as a boundary condition to the next simulation for the final design of the bluff body.

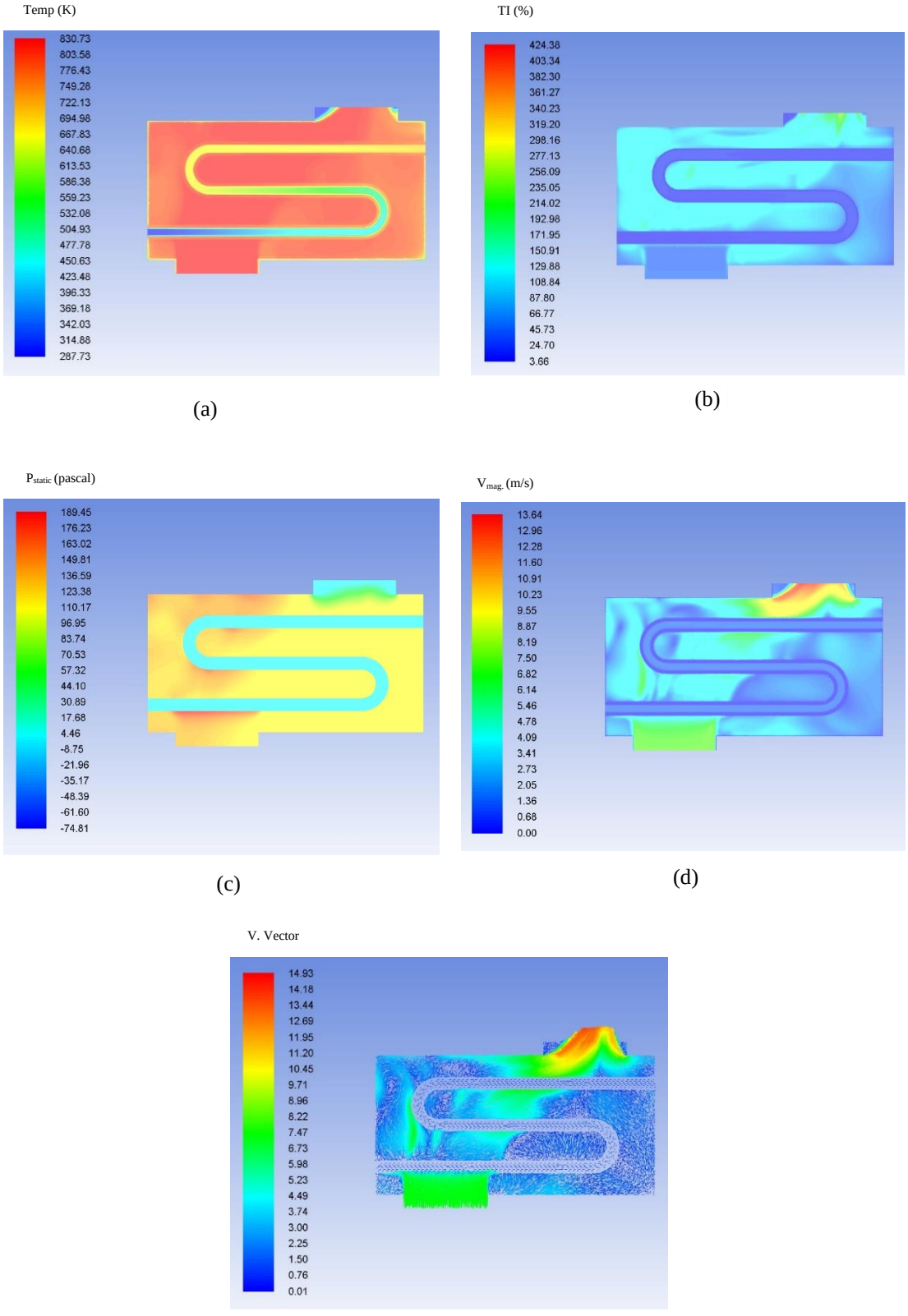

Figure 4- 25: Results for Case I of heat exchanger, (a) Contours of static temperature (K), (b) Contours of turbulent intensity (%), (c) Contour of static pressure (pascal) (d) Contours of velocity magnitude (m/s) and (e) Velocity vector coloured according to velocity magnitude (m/s).

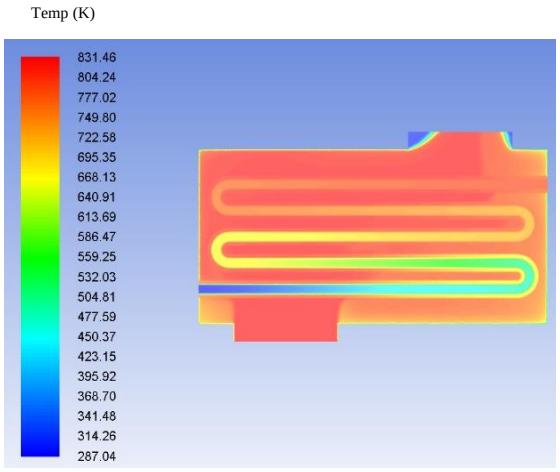

(a)

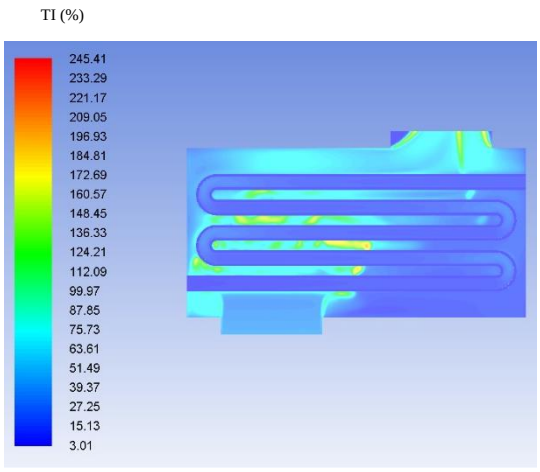

(b)

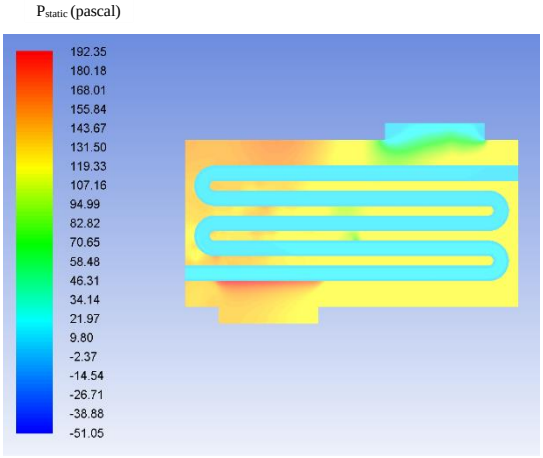

(c)

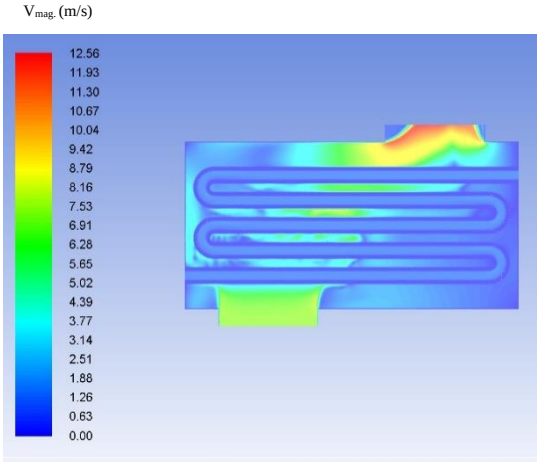

(d)

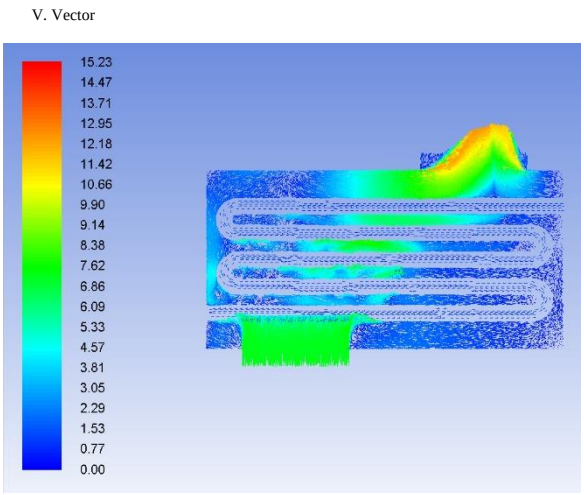

(e)

Figure 4-26: Results for Case II of heat exchanger, (a) Contours of static temperature (K), (b) Contours of turbulent intensity (%), (c) Contour of static pressure (pascal) (d) Contours of velocity magnitude (m/s) and (e) Velocity vector coloured according to velocity magnitude (m/s).

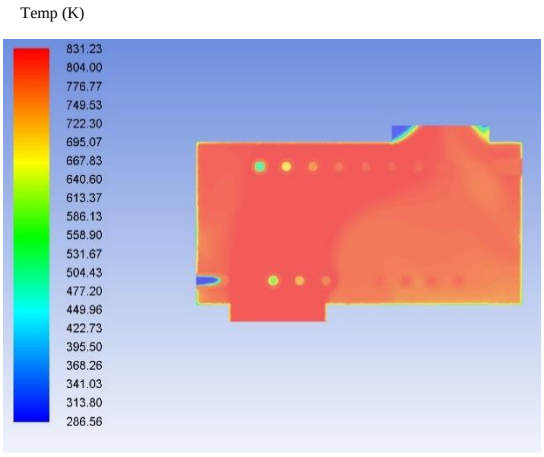

(a)

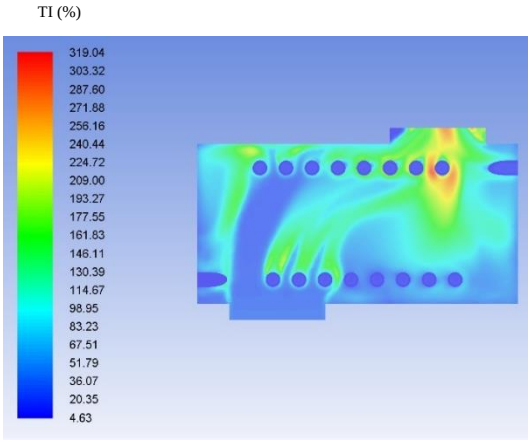

(b)

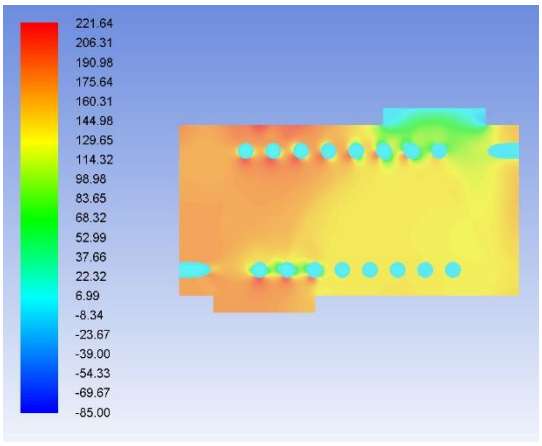

(c)

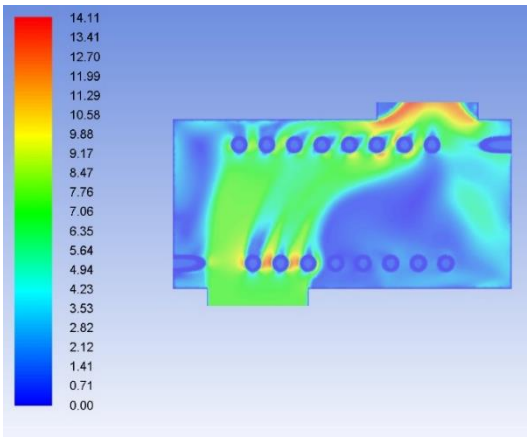

(d)

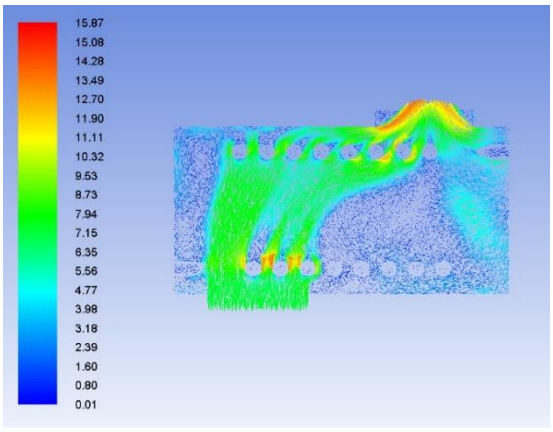

(e)

Figure 4-27: Results for Case III of heat exchanger, (a) Contours of static temperature (K), (b) Contours of turbulent intensity (%), (c) Contour of static pressure (pascal) (d) Contours of velocity magnitude (m/s) and (e) Velocity vector coloured according to velocity magnitude (m/s).

4.4 Final Bluff Body Simulation

The final bluff body design had to be based on a profile that allowed high temperature for ammonia cracking. Thus, from previous analyses (i.e. shape, improved heat exchange, flow patterns, feasibility for manufacturing purposes, etc.) and the following considerations, a final design was conceptualised. The ammonia temperature had to be low enough to cool the bluff body and, at the same time, reach a suitable temperature to start the cracking process after passing through the bluff body. According to many researchers, the temperature of ammonia should be above 873 K to start thermal cracking [44, 124].

A very fine mesh of size (=1e^{-3}) was imposed on the bluff body. Tube passages through the bluff body were added in order to pass ammonia into the bluff body. Constant temperature distribution was specified for the bluff body wall; this was calculated from the modified case study as illustrated in Figure (4-28).

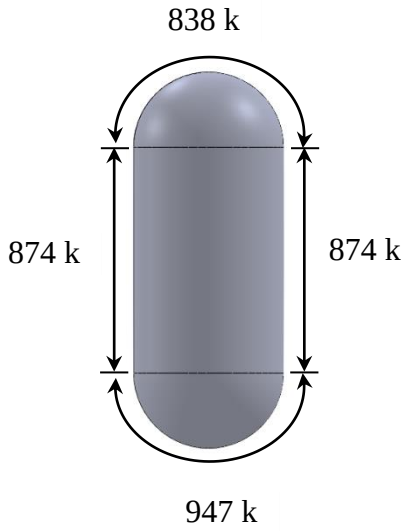

Figure 4-28: Temperature distribution around the bluff body from previous simulations.

The average temperature of the bluff body may be calculated from CFD results as follows:

$$T_{av.} = \frac{838+2(874)+947}{4} = 884\ k$$

Both the outlet temperatures of the ammonia, 725 K and 801 K obtained from the heat exchanger simulation were tested here as the input boundary condition for the three different shapes of pipe inside the bluff body.

Figure (4-29) represents the physical model and the grid distribution for the three case studies, while Figure (4-30) indicates the temperature distribution of the preheated ammonia through the bluff body at two levels of input temperature for each case. The value of the input and output temperatures of the ammonia are listed in Table 4-7.

Table 4-7: Input and outlet ammonia temperatures, flow through the bluff body.

Case study	Input Temperature (K)	Output Temperature (K)
1	725	792
	801	838
2	725	831.5
	801	855.5
3	725	872
	801	880

It may be seen from the static temperature values presented in Table 4-7 that the outlet temperature of ammonia for Cases 1 and 2 is lower than the temperature required to crack ammonia (> 873 K). For Case 3, however, the required temperature for ammonia cracking was obtained.

Some changes were made to the final system to reduce the cost of installation, for example, using a previously characterized swirl burner which is available at Cardiff University [205], instead of using a diffusive non-premixed burner.

The final new system to crack the ammonia is shown in Figure (4-31). This system is ready to be manufactured as final rig to test its efficiency.

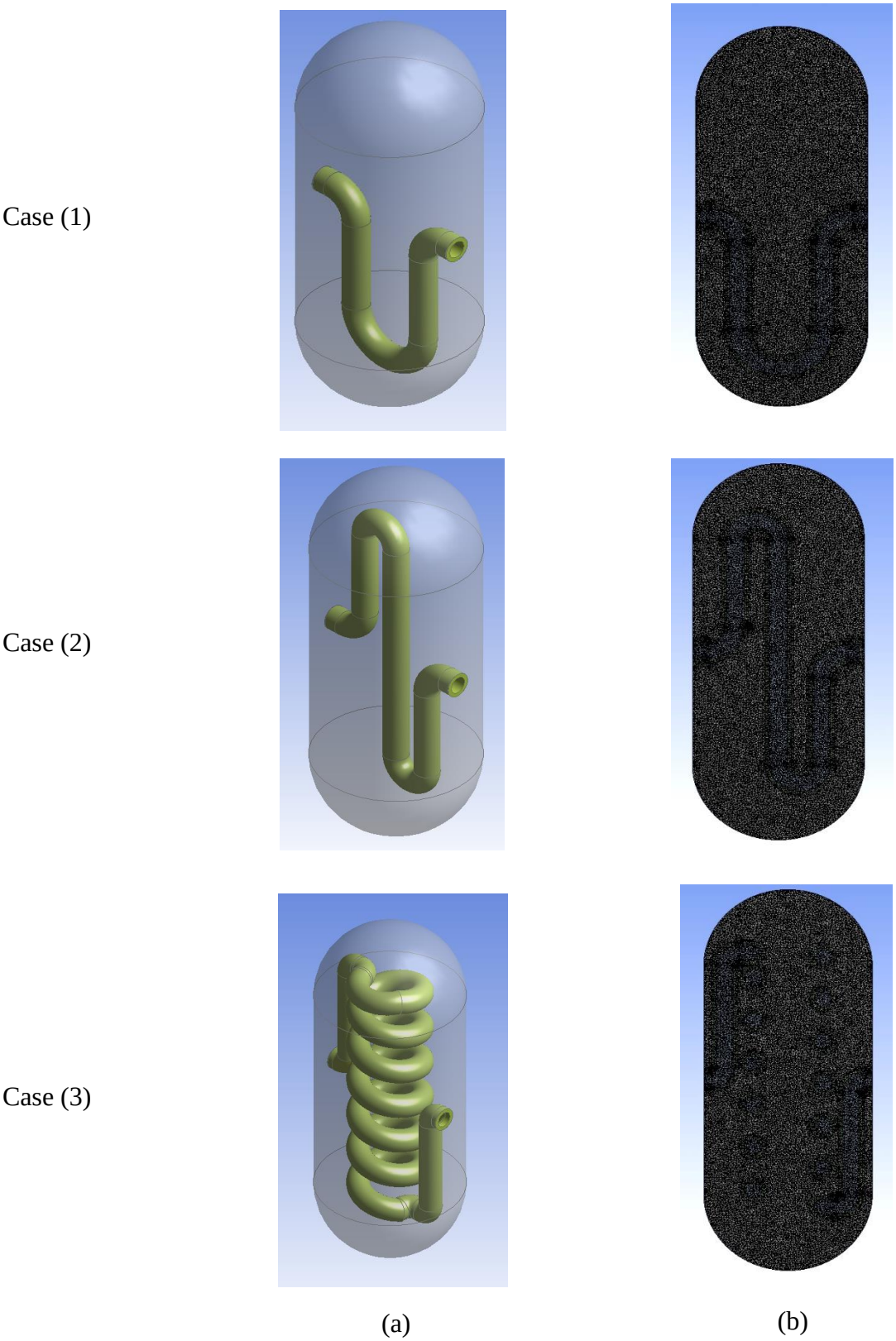

Figure 4-29: (a) Physical Domain, (b) Grid Generation.

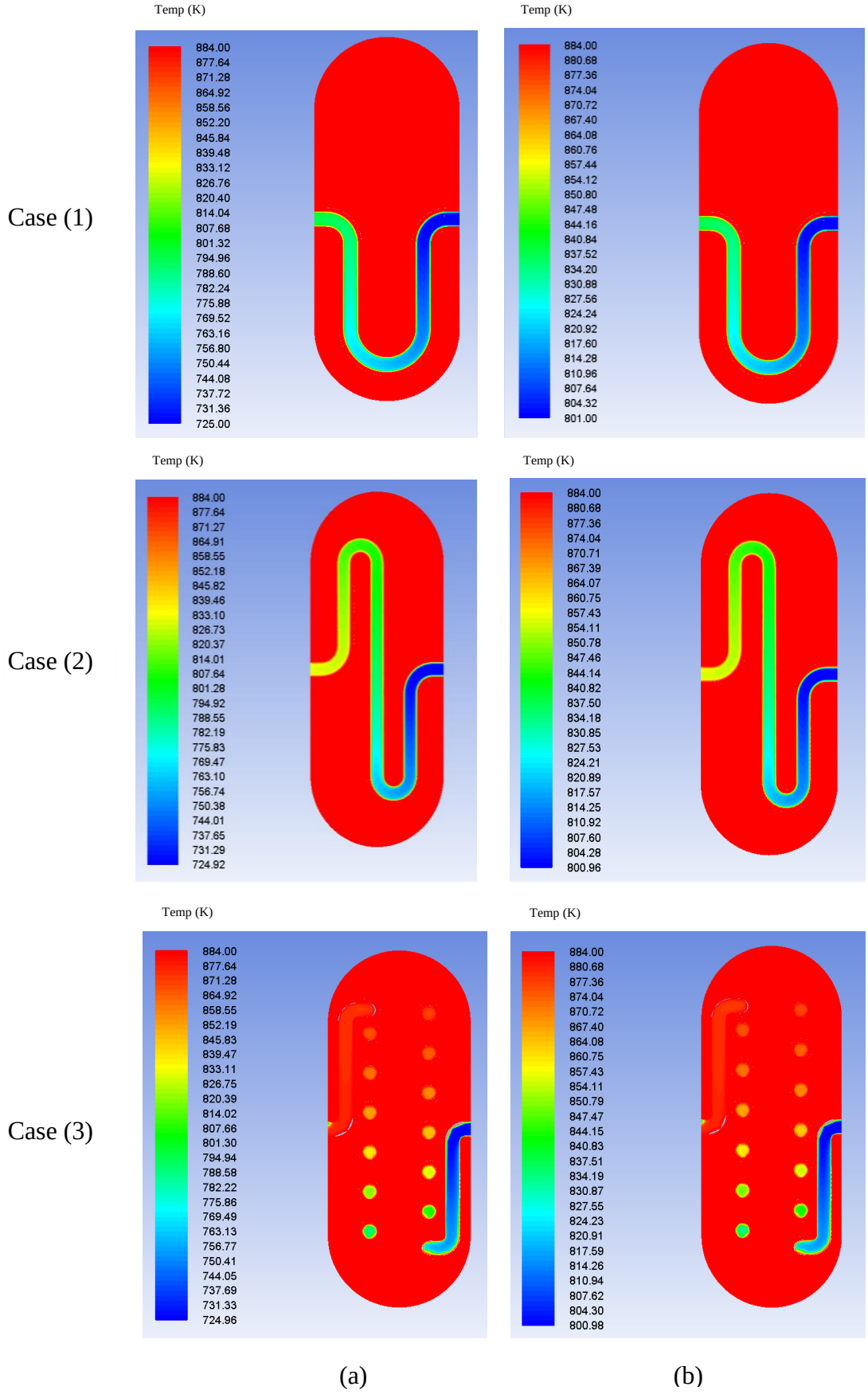

Figure 4-30: The temperature contours of the bluff body case studies when using inlet ammonia temperatures (a) 725 K and (b) 801 K.

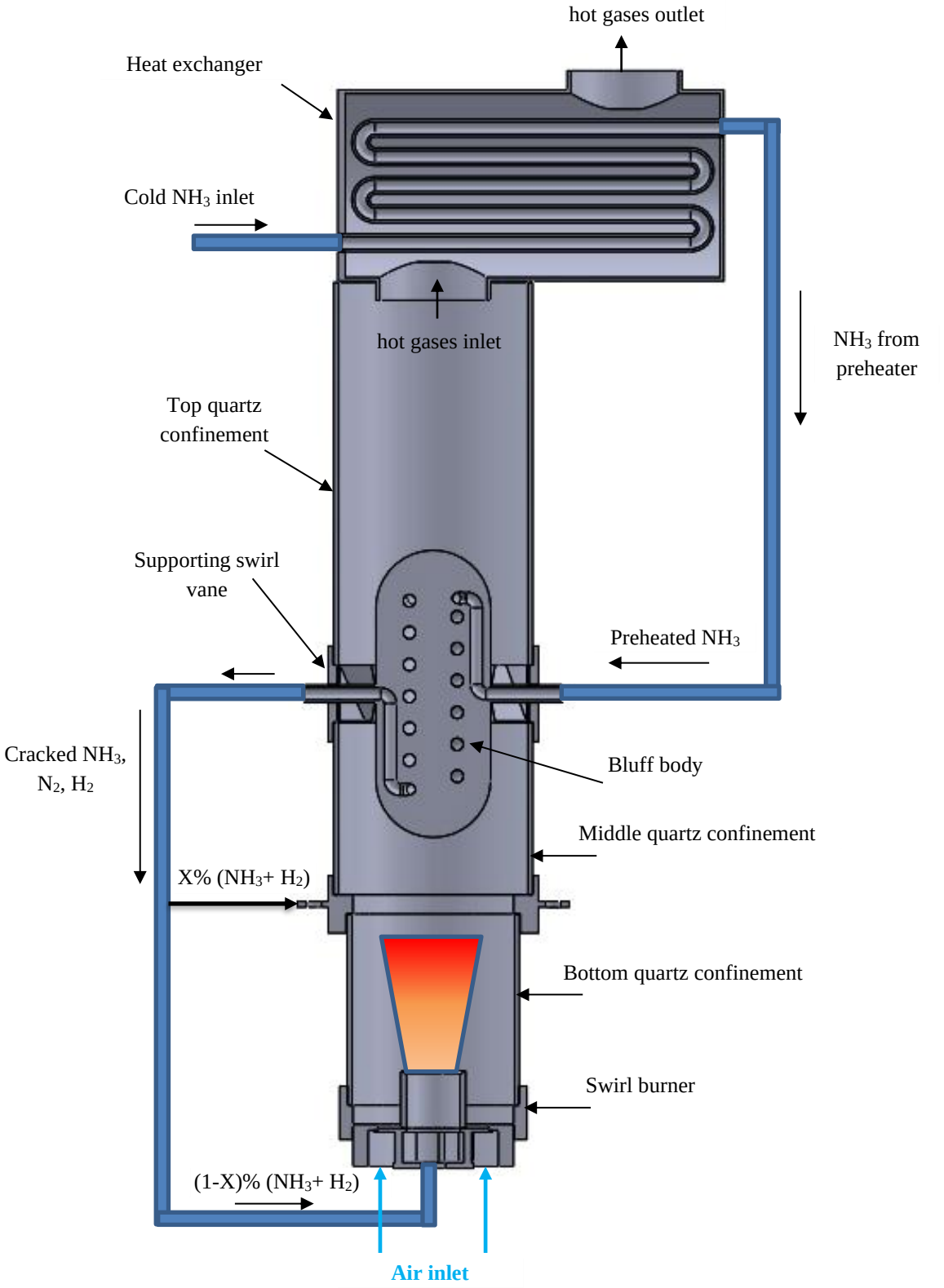

Figure 4-31: Final schematic diagram for the conceptual design of ammonia cracking system.

4.5 Effects of Presence of Cracking System on Flow Field Characteristics: Isothermal Conditions Using Swirl Burner

Isothermal conditions using a non-premixed swirl burner were simulated in order to study the effect of the presence of the bluff body on the flow field. A tetrahedron medium sized mesh; size=1.5e-3 was selected. Fuel and air were not ignited. The simulation was done at isothermal conditions at 3.1 g/s flow rate which is equivalent to ∅ =1.2 under combustion conditions.

Figure 4-32 shows an axial velocity contour that defines the effect of the cracking system on the hydrodynamic behaviour of the flow field. It can be noticed that there is a considerable change in the structure of the CRZ due to the presence of the bluff body at the middle of the combustor. Moreover, Figure 4-32 illustrates an increase of the size and strength of the CRZ using the bluff body, which is believed is a consequence of the overpressure caused by the restriction, leading to greater pressure decays which at the same time enhance the recirculation structure. Therefore, the predicted boundaries under isothermal conditions show a longer CRZ in the case of a bluff body, with a recirculation zone extending up to the combustor outlet.

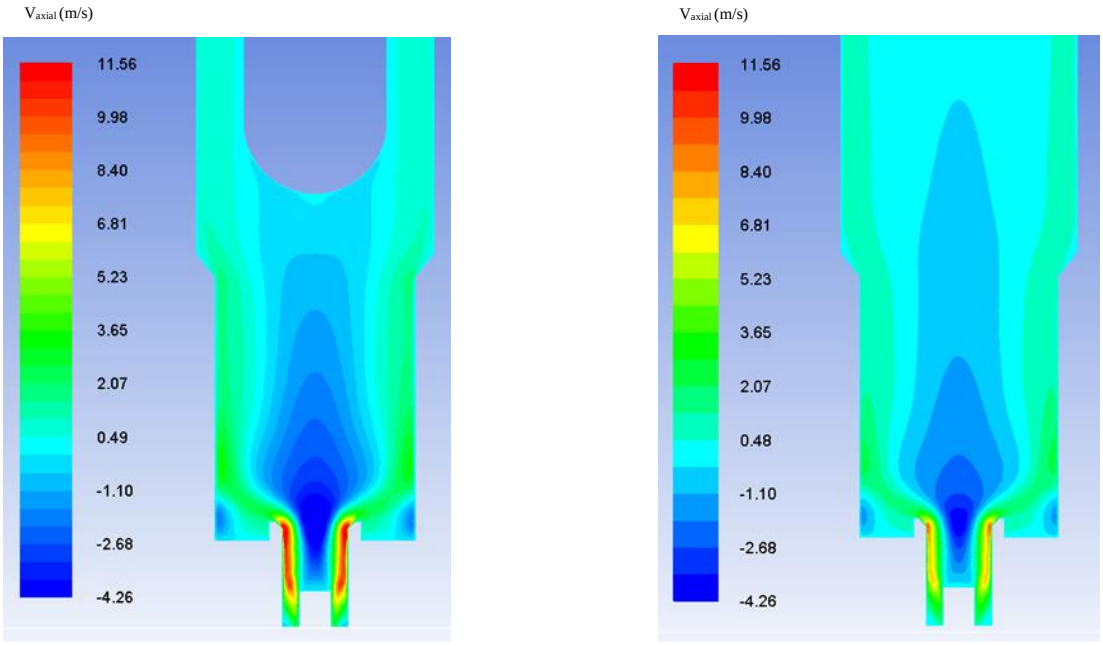

(a) With bluff body

(b) Without bluff body

Figure 4- 32: Effect of cracking system on the size of the CRZ using flowrate 3.1 g/s.

4.6 Numerical Validation

In order to validate numerical simulations and confirm accuracy with experimental tests, an analysis was performed using data produced by previous PhD students working with this rig [205]. Comparison of results, Figure 4-33, shows that the range of velocities is within those obtained using experimental analyses.

The latter were obtained using Laser Doppler Anemometry (LDA), a powerful technique that produced high statistical confidence with small deviations after 10,000 measurements per point. Further information can be found elsewhere [205]. Therefore, these results confirm that the numerical calculations would be in agreement with further experiments, allowing us to continue with the manufacturing of the cracking device for experimental tests.

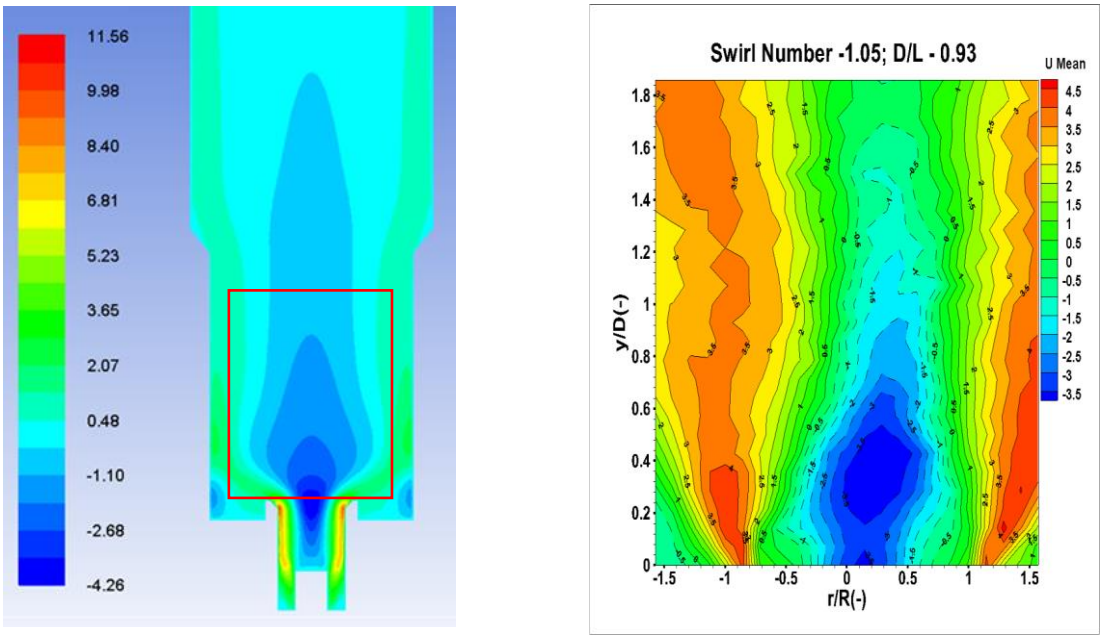

Figure 4-33: Comparison between numerical (left) and experimental (right) isothermal tests. The highlighted region in the numerical analysis is the one obtained during experiments.

CHAPTER 5

Experimental Evaluation of the Presence of the Cracking System on Combustion and Flow Characteristics

"An experiment is a question which science poses to Nature, and a Measurement is the recording of Nature's answer."

Max Planck

5.1 Introduction

Swirl combustors form well-known coherent flow structures which provide low-velocity regions that enable flame anchoring, and have a substantial effect on flame stability, combustion intensity, and the size of the flame. These effects have been demonstrated for a wide range of operating conditions on numerous occasions [22]. The interaction between swirl structures, incoming flow, swirl burner and combustor geometries are such that operational changes in any of these parameters is likely to substantially alter the stability regime downstream of the burner exit plane.

This chapter includes several sections. Section 5.2 characterises the confined flame and investigates the blowoff limit of the burner with changes in equivalence ratio and flame power (heat) output. Section 5.3 determines heat transfer rates through the bluff body to predict the efficiency of the ammonia thermal cracking system. Section 5.4 investigates behaviour of the flow field in the second recirculation zone upstream the bluff body and finally, Section 5.5 summarises the findings reported in the body of the chapter.

5.2 Effect of Cracking System on Flame Characterization

The swirl burner with swirl number S=1.05, nozzle diameter 28 mm and length 30 mm, with a bluff rod of about the same length at the centre was used to assess the flame behaviour and to determine the stability limits. The non-premixed combustion experiments performed in this study used pure methane as the baseline fuel. The flame was confined within three cylindrical quartz tube of total length 400 mm, as explained

in Section 3.8.2, to improve blowoff limits by reducing air flow interactions with the flame. The fuel and air entering the burner were kept at ambient temperature and pressure.

5.2.1 Blowoff Limit Characterization

The blowoff limits were characterised for different flow rates to determine safe operational boundaries for the burner in confined flame conditions in order to define stable combustion regimes.

The blowoff limit can be determined in two ways, either by establishing stable combustion, fixing the flow rate of the air and varying the fuel flow rate until extinction occurs; or by establishing stable combustion, keeping the fuel flow rate constant and increasing the air flow rate gradually until the point of extinction is reached [17]. In this study, the second method was chosen.

Table 5-1 gives the fuel-air mixtures for the flame at which blowoff occurred. The fuel and air flow rates were varied to give different equivalence ratios and flame power i.e., heat output. Currently, for most industrial burners the blow-off limit is in the range of 0.7 to 0.8 equivalence ratio, and most research studies are attempting to extend this limit to much lower equivalence ratios, for example, 0.5, to achieve lower NOx emissions. In Table 5-1, the presence of the new bluff body, designed as a cracker system, on the blowoff limit should be noted. All blowoff limits are for equivalence ratios < 0.52, going as low as 0.08 at the lowest flow rates. This is achieved due to the preheating of the fuel via the cracking system before it re-enters the main fuel inlet. This preheating will reduce the chemical reaction times of the reactants which will in turn influence how the equivalence ratio affects blowoff.

Table 5- 1: Blowoff limits for the flame.

Fuel (L/min)	Air (L/min)	Fuel (g/s)	Air (g/s)	Equivalence Ratio (Ø)	Power (kW)
1	126	0.011	2.52	0.08	0.6
2	156	0.022	3.12	0.12	1.1
3	180	0.033	3.60	0.16	1.7
4	193	0.044	3.86	0.20	2.2
5	220	0.056	4.40	0.22	2.8
6	226	0.067	4.52	0.25	3.3
7	230	0.078	4.60	0.30	4.0
8	235	0.089	4.70	0.33	4.5
9	240	0.100	4.80	0.36	5.0
10	256	0.111	5.12	0.37	5.6
11	270	0.122	5.40	0.39	6.1
12	276	0.134	5.52	0.42	6.7
13	280	0.145	5.60	0.44	7.2
14	290	0.156	5.80	0.46	7.8
15	300	0.167	6.00	0.48	8.4
16	310	0.178	6.20	0.49	8.9
17	319	0.189	6.38	0.51	9.5
18	325	0.200	6.50	0.53	10

5.2.2 Burner Flame Characteristic

The temperature and pressure were kept at atmospheric. The fuel and air flow rates were also varied to give the limits of the stable combustion regimes. Table 5-2 gives the fuel-air mixtures for the combustion, when the fuel was kept constant at 0.200 g/s, while the air was varied to give different equivalence ratios.

Table 5- 2: Methane-air mixture.

Fuel (L/min)	Air (L/min)	Fuel (g/s)	Air (g/s)	Equivalence Ratio (Ø)	Power (kW)
18	70	0.2	1.4	2.50	10
18	85	0.2	1.7	2.02	10
18	100	0.2	2.0	1.72	10
18	115	0.2	2.3	1.50	10
18	130	0.2	2.6	1.30	10
18	145	0.2	2.9	1.20	10
18	160	0.2	3.2	1.07	10
18	175	0.2	3.5	0.98	10
18	190	0.2	3.8	0.90	10
18	205	0.2	4.1	0.84	10
18	220	0.2	4.4	0.78	10
18	235	0.2	4.7	0.73	10
18	250	0.2	5.0	0.69	10
18	265	0.2	5.3	0.65	10
18	280	0.2	5.6	0.61	10
18	295	0.2	5.9	0.58	10

Figure 5-1 shows the changes in the flame shape with increasing air flow rate for a constant fuel rate of 0.20 g/s with power output of 10.0 kW for different equivalence ratios captured using a digital camera. It can be seen from Figure 5-1 (1, 2) with equivalence ratios of 2.50 and 2.02, respectively, that the flame is sooty, yellowish and turbulent, and propagates within the nozzle annulus. The flame moves towards the bluff body, and this yellow flame required more air to get such a stable condition.

The flame becomes gradually stabilised itself as the air flow rate increased. At an air flow rate of 2.9 g/s and the equivalence ratio of 1.20, Figure 5-1 (6), the flame retains its yellow colour, but a central recirculation zone (CRZ) appears. The CRZ becomes well developed and gradually leaves the annulus and moves downstream of the flame zone.

In the seventh picture, Figure 5-1 (7), at an equivalence ratio of 1.07, the flame becomes more stable with a blue flame and yellow bands at its centre.

With further increase in air flow rate, the yellow band at the centre of the flame disappears, and the flame becomes well-structured, stable and completely blue. Figure 5-2 (13) shows that the increased air flow rate stabilised the flame near the burner head, and indicates the existence of an intense reaction zone probably due to the higher laminar burning velocity of the flame.

The width of the flame gradually reduces and becomes detached from the nozzle annulus. The CRZ also attains its maximum width, with strong recirculation and mixing of the air and preheated fuel with the hot products of combustion, provides anchorage for the flame, and efficient combustion. This mechanism is common to most swirl flames and has been widely reported in the literature [23].

With the blue flame, combustion and heat release are mainly in the swirling and core straight jets. The influence of the bluff body and swirling jets are clearly observed in the flame.

With further increase of air flow, the flame progressively shortens. At an air mass flow rate of 280 litres/min (5.6 g/s) and an equivalence ratio of 0.61, we see in Figure 5-2 (15), that the blue flame spreads around the burner nozzle with strong oscillations and reaches its blowoff limit at an air flow rate of 295 litres/min (5.9 g/s) and equivalence ratio of 0.58. If the air/gas ratio is increased further, the flame blows off and disappears from the tube.

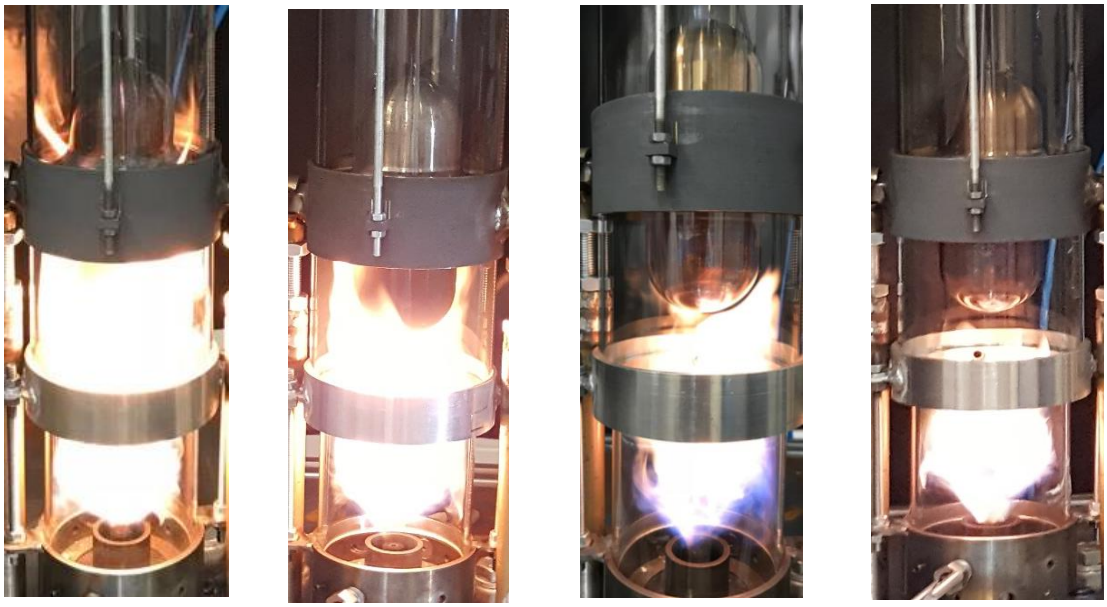

(1) Ø=2.5 (2) Ø=2.02 (3) Ø=1.72 (4) Ø=1.5

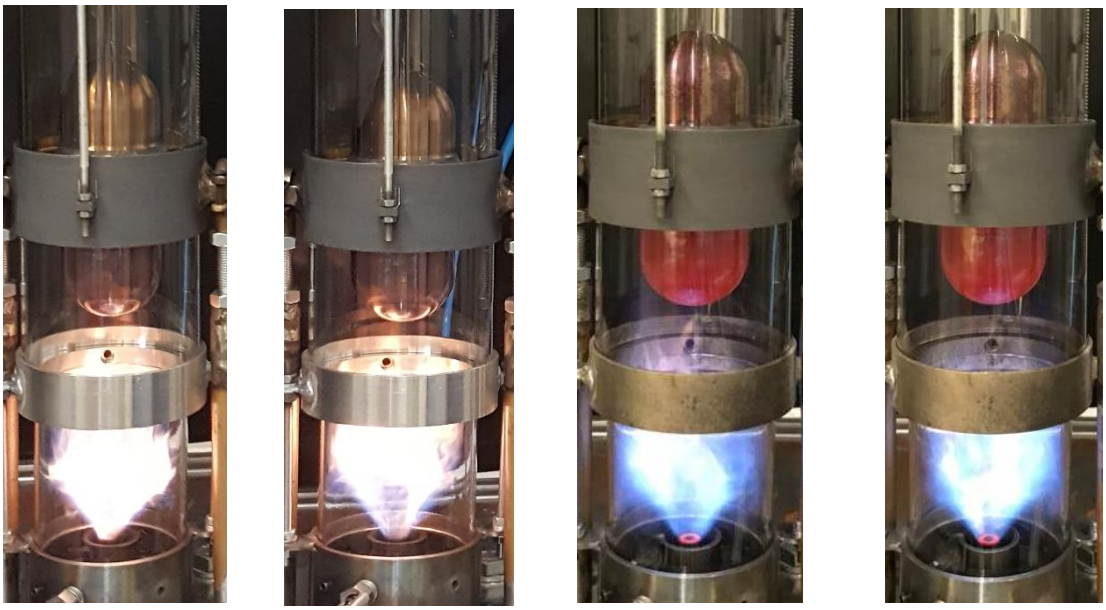

(5) Ø=1.3 (6) Ø=1.2 (7) Ø=1.07 (8) Ø=0.98

Figure 5- 1: Effect of the presence of the cracking system on flame characterization for a fuel mass flow rate of 0.2 g/s, and 0.98 < Ø < 2.5.

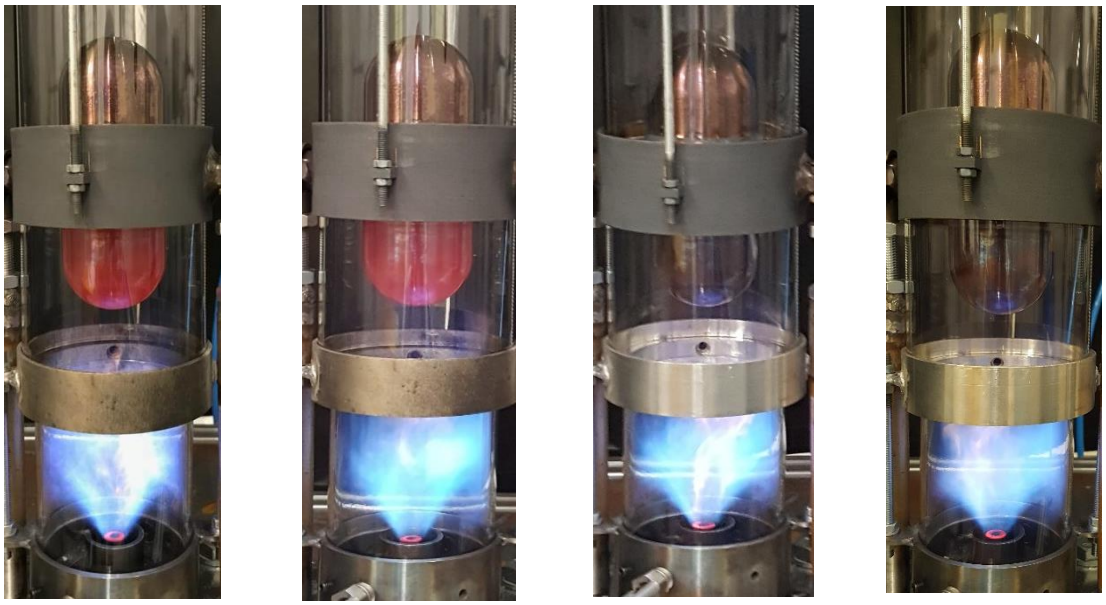

(9) Ø=0.9 (10) Ø=0.84 (11) Ø=0.78 (12) Ø=0.73

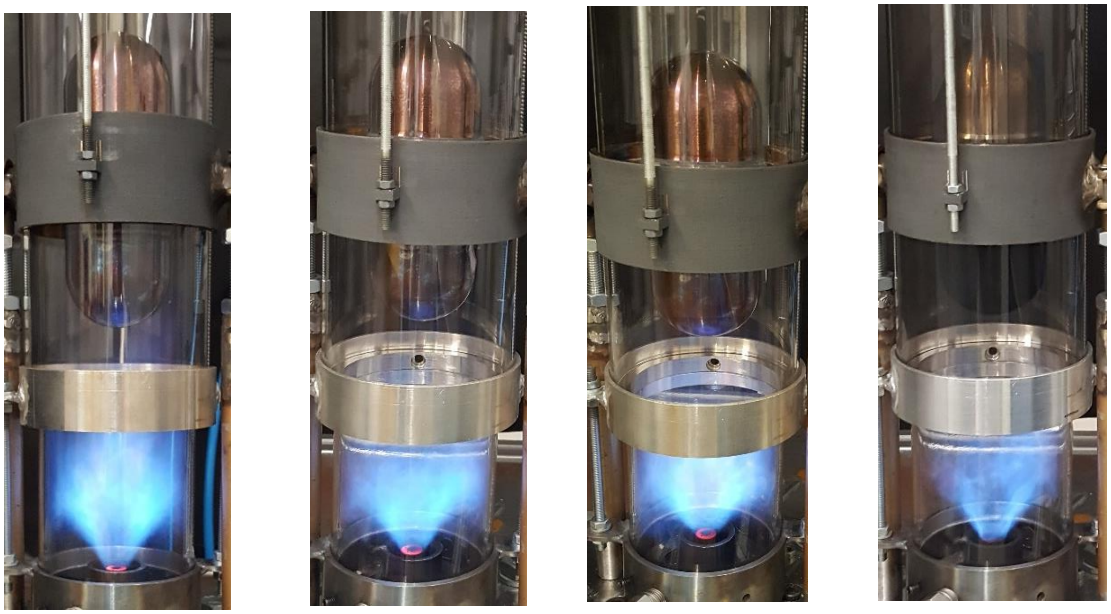

(13) Ø=0.69 (14) Ø=0.65 (15) Ø=0.61 (16) Ø=0.58

Figure 5- 2: Effect of the presence of the cracking system on flame characterization for a fuel mass flow rate of 0.2 g/s, and 0.58 < Ø < 0.9.

5.2.3 Effect of Cracking System on the Stability limit

Figure 5-3 compares the stability limits for three different values of fuel flow rate 0.134 g/s, 0.145 g/s and 0.20 g/s with Okon's results [205] obtained at a fuel flow rate 0.134 g/s. Okon's tests were for the same swirl burner, but without the new cracking system.

The variation in the combustor geometry, and addition of the new bluff body cracking system seem to have had a significant influence on the blowoff limit with equivalence ratio reduced to 0.46 as compared to 0.70 [205]. The effect is caused by geometrical changes and the pre-heating of the methane by passing it through the cracking system. It can be concluded that the presence of the bluff body cracking system affects the hydrodynamics of the swirling flow upstream of the bluff body, playing a significant role as both stabilization device and cracking method.

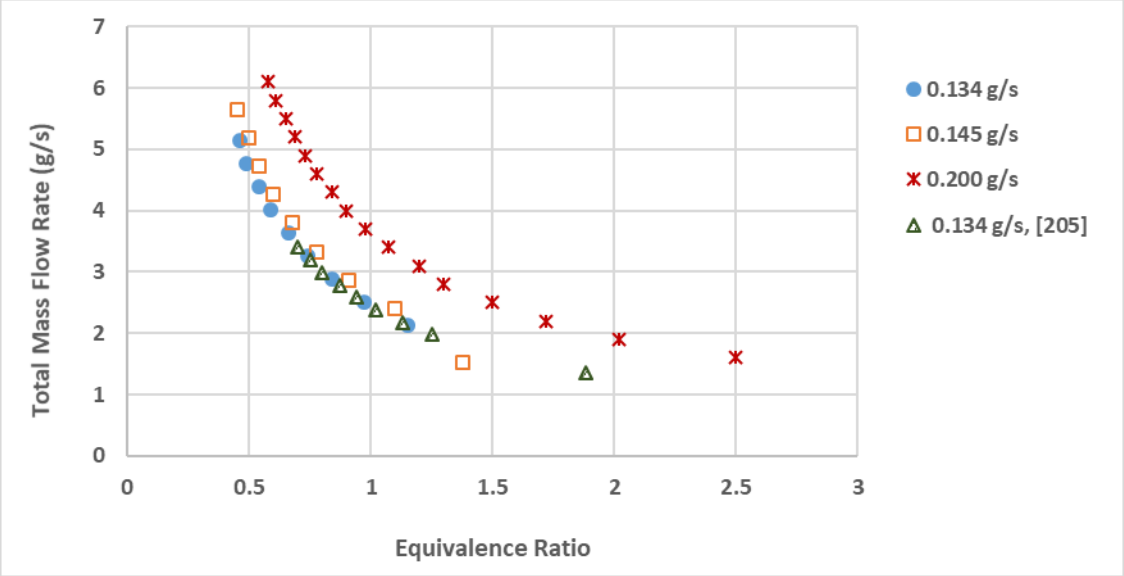

Figure 5- 3: Flame blowoff limits for different fuel flow rate.

5.3 Thermal Efficiency of the Cracking System

The bluff body, spiral heat exchanger, through which the methane passed before re-entering the swirl burner, is able to withstand the increases in temperature and flow pressure. It expanded and contracted without mechanical failure during these pressure and/or temperature increases. The methane temperature which entered the bluff body was kept constant at 300K.

Figure 5-4 shows the temperature variation of the methane outlet temperature as it leaves the bluff body for three power outputs: 3.3 kW [0.067 g/s of fuel], 6.7 kW [0.134 g/s of fuel] and 10.0 kW [0.200 g/s of fuel].

It is clear from the profiles in Figure 5-4 that the methane leaves the bluff body at a high temperature. It shows that the higher the heat energy generated by the flame the hotter the temperature of the gas leaving the heat exchanger. Also, it shows that the temperature of the methane leaving the heat exchanger increases with time after flame ignition until it reaches an equilibrium value.

It can also be seen that the temperature at the outlet of the heat exchanger, which is to be used for the cracking process, reached a stable value of 671 K after about 1400 seconds when using a power of 3.3 kW, 708 K after about 1300 seconds when using a power of 6.7 kW, and 788 K after about 1200 seconds when using a power of 10.0 kW. Thus, the cracking system appears to have the thermal characteristics needed to achieve partial cracking, with temperature differentials ranging from 370 to 488 K between inlet and outlet, reaching the temperature needed to start splitting ammonia.

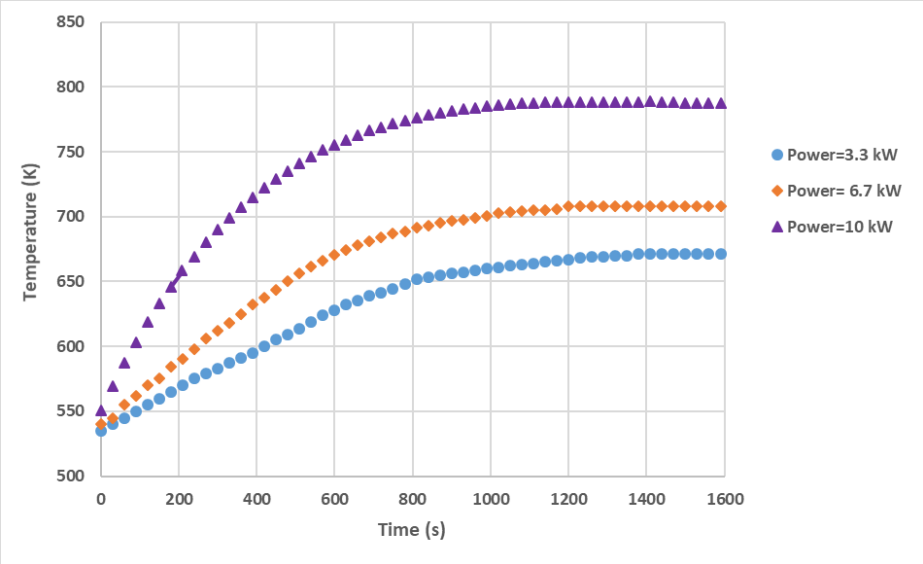

Figure 5- 4: The variation of temperature through bluff body with duration of combustion process.

The heat exchanger effectiveness is defined as the ratio of the heat transferred in the actual heat exchanger to the maximum possible heat transfer, [198]:

$$Effectiveness\ (\epsilon) = \frac{actual\ heat\ transfer}{maximum\ possible\ heat\ transfer} \tag{5.1}$$

The easiest way of calculating the actual heat transfer, the heat energy gained by the cold fluid as it passes though the bluff body is according to the first law of thermodynamics, see Equations (4.8) and (4.9). The maximum possible heat transfer for the exchanger would be calculated using the difference between the two "inlet" temperatures for the hot and cold fluids as:

$$q_{max} = (\dot{m}Cp)_{min}\left(T_{h_{inlet}} - T_{c_{inlet}}\right) \tag{5.2}$$

Where,

$\dot{m}$: is the mass flowrate of methane (kg/s) (0.067, 0.134 and 0.200 g/s)

Cp : is the specific heat of methane= 2.232 kJ/kg. K

T_{cinlet} = Temperature of the methane as it enters the bluff body (300 K)

T_{hinlet} = Temperature of the hot gases of combustion.

To assess the performance of the cracking system (i.e. effectiveness), the following assumption was made.

The temperature of the bluff body is equal to the temperature of the hot gases impinging on it which is about 884 K. This value is taken from the previous CFD simulation, as described in Section 4.4.

In a general way the effectiveness is expressed as [198]:

$$Effectiveness\ (\epsilon) = \frac{\Delta T(minimum\ fluid)}{Maximum\ temperature\ difference\ in\ heat\ exchanger} \tag{5.3}$$

Table 5-3 shows that cracking system has a calculated effectiveness of about 64% when using burner power of 3.3 kW, 70% for 6.7 kW, and reaches 84% for 10.0 kW. It can be seen that the manufactured cracking system will raise the temperature of the inlet fuel sufficiently to achieve the design cracking performance.

Table 5-3: Cracking system effectiveness for different burner power outputs.

Power (kW)	Effectiveness (%)
3.3	64
6.7	70
10.0	84

5.4 Flow Field Behaviour Upstream the Bluff Body Zone

Many studies have favoured used Laser Doppler Anemometry (LDA) and Particle Image Velocimetry (PIV) diagnostic systems to obtain detailed information about the behaviour of swirling flows [22, 222]. Unfortunately, large power laser systems could not be used in this study because of reflection from either the quartz tube or the bluff body, producing noisy, inaccurate patterns. Moreover, both techniques require the use of seeding particles, but the presence of the bluff body, unfortunately, enhances the speed of the flow around it, reducing the time available for measurements making this means of measurement impractical.

For such reasons, a LED lamp controlled by an Image Processing Stroboscope BVS-II Wotan, and a high-speed camera (Baumer-GAPI Viewer v1.6 Camera) were used to investigate the effect of the bluff body on the flow field.

The images shown in Figure 5-5 provided clear information on the effect of the bluff body on adjacent flow field characteristics. It can be seen that the circular profile of the bluff body produced a wide secondary recirculation zone upstream of the bluff body, producing vortex flows and rapid mixing which can contribute to reduce NO emissions. The size of these vortices, and the velocity of the flow (already known from the bulk values obtained from the rotameters) gave estimated recirculation times in the range 0.0005 to 0.05 seconds. These results will be used for a numerical examination using CHEMKIN- PRO of their likely effects on NOx emissions. More details can be found in the next chapter.

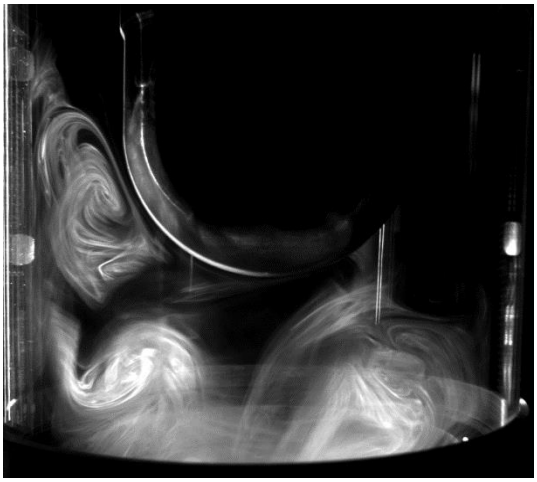

(a) Flowrate=1.6 g/s

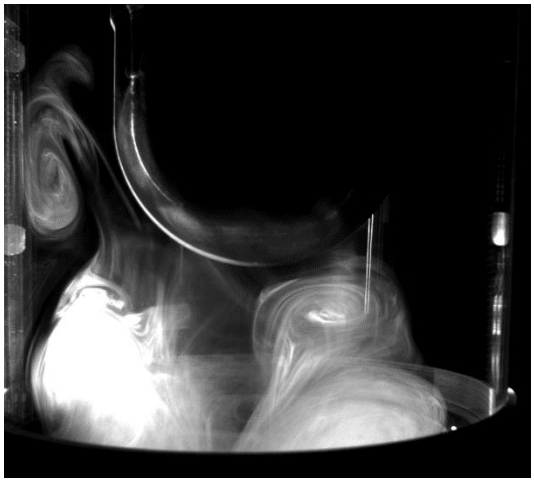

(b) Flowrate=3.1 g/s

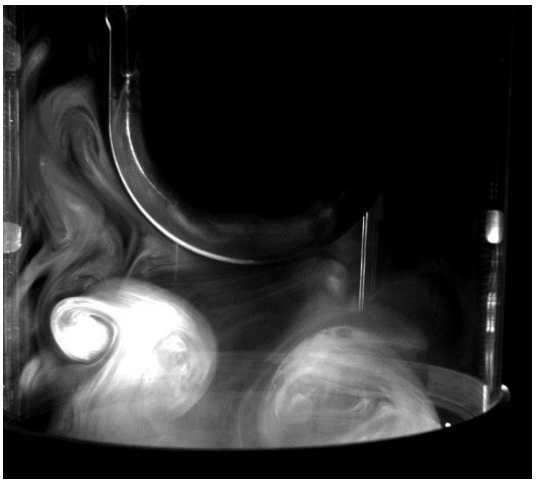

(c) Flowrate=4.6 g/s

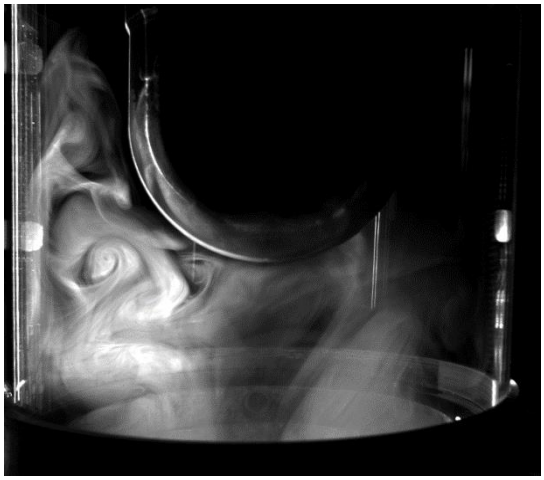

(d) Flowrate=6.1g/s

Figure 5- 5: Flow tomography at different flowrate.

CHAPTER 6

Kinetic Modelling Study of Ammonia and Hydrogen Combustion with Reduction of NO_x

"You will never do anything in this world without courage. It is the greatest quality of the mind next to honour."

Aristotle

6.1 Introduction

Ammonia is being considered for fuelling gas turbines as a new sustainable fuel source through the use of thermal cracking to produce hydrogen and unburned ammonia. Ammonia being carbon-free could assist the transition towards a hydrogen economy. However, one of the main constraints of such a technique is that although the combustion of ammonia produces no CO_2, the emissions do contain a large proportion of NO_x. In this work, cracked ammonia obtained from a modified combustion rig was used to fuel a simulated a swirl burner under preheating conditions as shown previously in Figure 3-10.

Many numerical studies and fundamental experimental investigations have explored the combustion performances of a variety of NH_3/H_2/air blends and found substantial differences between different proportions [223]. Lee et al. [173] evaluated unstretched laminar burning velocities and stretch effects for laminar, H_2/NH_3/air mixture flames in a freely propagating spherical configuration and compared results with numerical predictions. They found that hydrogen substitution enhanced NO_x and N_2O emissions in fuel-rich ammonia/air flames. Valera-Medina et al. [95] demonstrated that high hydrogen concentration leads to high NO emissions combined with a low operability range. Therefore, although hydrogen enhances important combustion parameters such as flame speed and reactivity, it is clear that further research is needed to find the right concentration in order to avoid an increase in NO.

The current research project investigated the potential of ammonia as a clean fuel, particularly the emissions from NH_3/H_2/air combustion for various blends. The performance of various blends were analysed to identify the one that produced the lowest NO with highest combustion efficiency (i.e. lowest proportion of unburned ammonia and highest combustion temperatures). Also, the effects of fuel NH_3 concentration on NO emissions were pursued. Finally, the effect of post-combustion injection of ammonia/hydrogen for different blends, with residence time also being studied in order to further reduce any remaining NO in the emissions.

To achieve this goal, the present project employed a novel reaction model based on Mathieu's mechanism [223]. This mechanism was used to improve understanding of the evolution of species using ammonia blends and to comprehensively validate the combustion properties such as NOx emissions, etc. The improved mechanism is prepared with 'sufficient' accuracy for use in CFD calculations for prediction of the turbulent reacting flow field inside a gas turbine combustor fuelled by ammonia/hydrogen mixes.

6.2 Numerical Analysis

6.2.1 Combustion characteristics at low-pressure and fuel rich conditions

The modelling of the chemical kinetics of laminar burner-stabilised flames and freely propagating flames are both widely used in steady, one-dimensional studies and is frequently used to describe the combustion of various fuels or determine mixture flammability limits [201].

The initial composition of the NH_3/H_2/air mixture is calculated using an equivalence ratio $\emptyset$=1.2, with power outputs ~10 kW, and using a great variety of blends as listed in Table 6-1. As illustrated in Table 6-1, five NH_3/H_2 blends were used for the evaluation, starting from 50% NH_3 (vol%) with the remainder hydrogen, and increasing in steps of 10% (vol%) NH_3, see Table 6-1. The overall complete chemical reaction used in the calculations is presented in Equation (6.1).

$$x\,NH_3 + y\,H_2 + a_{stoi}(O_2 + 3.76\,N_2) \rightarrow bH_2O + cN_2 \quad (6.1)$$

And

$$Moles = \frac{Mass}{M_w} \tag{6.2}$$

Where, M_w is the molecular weight of species.

Mass of air could be calculated as:

$$\dot{m}_{air})_{actual} = \dot{m}_{fuel})_{actual} * \left(\frac{A}{F}\right)_{actual} \tag{6.3}$$

Table 6- 1: Numerical matrix of initial Fuel/air mixture with Ø =1.2, power ~10 kW.

NH_3%	NH_3 (mol/s)	H2 (mol/s)	Mass of NH_3 (g/s)	Mass of H_2 (g/s)	Mass of Air (g/s)
50	0.018	0.018	0.306	0.036	2.159
60	0.021	0.014	0.357	0.028	2.602
70	0.024	0.010	0.406	0.020	2.632
80	0.027	0.007	0.452	0.013	2.660
90	0.029	0.003	0.496	0.006	2.688

In this simulation, adiabatic conditions were assumed, For laminar flame studies, a freely propagating flame rich in NH_3/ H_2/ air mixture was simulated for different amounts of the NH_3/H_2 fuel blend, where X which is expressed as a percentage of the NH_3/H_2 amount injected downstream the post flame zone. X was changed from 0% to 4% (vol%).

6.2.2 Chemical Reactor Network (CRN) Analyses

CHEMKIN-PRO is one of the most popular software packages used to simulate chemical reactions and analyse chemical kinetics. It was originally developed by Sandia National Laboratory, after which it was maintained and enhanced by Reaction Design Inc., and has recently become part of ANSYS software.

CHEMKIN- PRO calculations were used with a novel reaction model based on Mathieu's mechanism [223]. The simulation was conducted using a chemical reactor network (CRN), which uses chemical engineering models of ideal reactors, such as the perfectly stirred reactor (PSR) and the plug flow reactor (PFR), to describe the flow field as an arrangement of reactors where detailed reaction mechanisms can be applied.

The CRN model, supported by CFD codes (which provide extensive information on turbulent mixing and residence time distribution of complex reactive flows) can be used to apply mathematical models to analyse large detailed chemical reaction mechanisms easily with relatively small computational demands. Thus, allowing the application of CFD to CRN algorithms [224].

The PSR, also referred to as a continuously stirred tank reactor, is a type of zero-dimensional homogenous open system. As a result of high diffusion rates or forced turbulent mixing, the contents of a perfectly-mixed reactor are assumed spatially uniform inside the control volume and sufficiently mixed to be represented by spatially averaged or bulk properties. Thus, in a PSR the rate of conversion of reactants to products is completely controlled by chemical reaction rates not by mixing processes, and mass transport to the reactor walls is assumed to be infinitely fast [225]. In many practical applications of low-pressure processes or highly diffuse operating conditions, this assumption is valid as a result of the dominance of species diffusion renders [226].

The flow through the reactor is characterised by a residence time which can be found as the ratio of combustor volume to the bulk flow rate [227]:

$$\tau_{residence} = \frac{Volume}{Volumetric\ Flowrate} = \frac{V}{Q} = \frac{V\rho}{\dot{m}} \tag{6.4}$$

Where,

V : is the reactor volume (m^3)

Q : is the gas volumetric flow rate at combustion conditions (m^3/s)

ρ : is the density inside the reactor (kg/m^3)

$\dot{m}$: is the mass flow rate through the reactor (kg/s)

In a conventional combustor the residence time is about 7ms and for a micro-combustor 0.5ms [228].

In this work, the CRN included four clusters formed by two-hybrid PSR-PFR configurations. This type of network is commonly used to simulate mixing and flow characteristics in gas turbine combustors [178]. A schematic of the network is presented in Figure 6-1. The first cluster represents the swirling flame and CRZ. The

second cluster represents post flame zone, while the third cluster represent the injection of a small proportion (X%) of the NH_3/H_2 blend into the post-combustion flow to reduce NO levels through a second recirculation zone, finally ending in a 15 cm long. Different post-combustion recirculation zones were assessed to evaluate the impact of the bluff body configuration and the suggested injection strategy with different values of residence time (t =0.0005,0.005 and 0.05 sec).

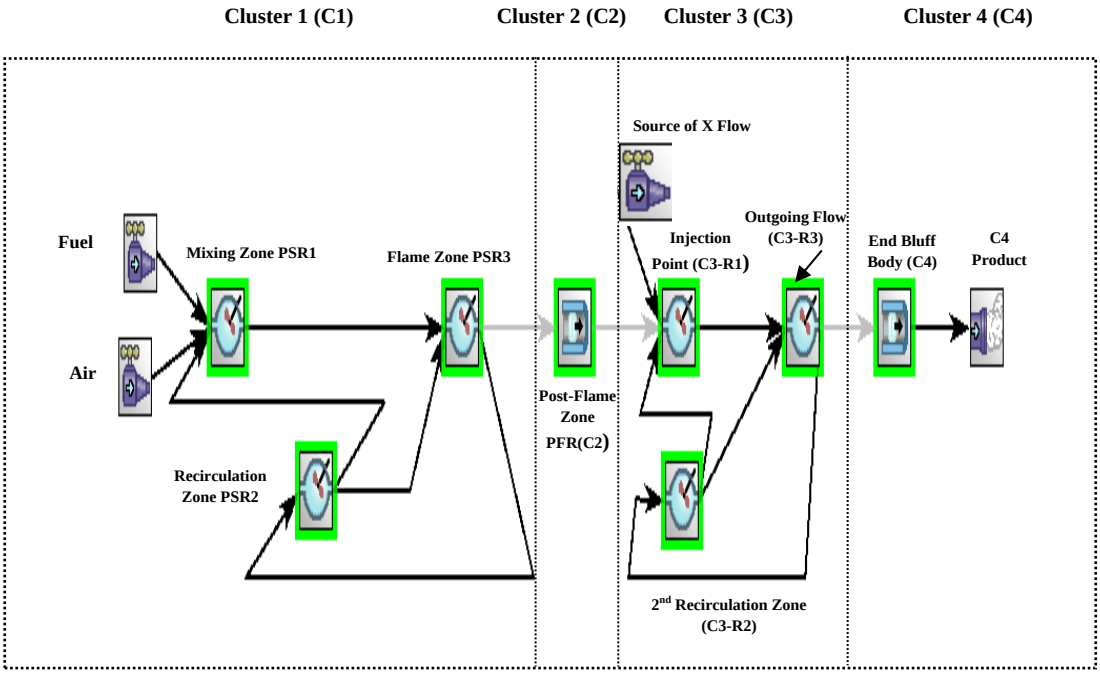

Figure 6- 1: PSR-PFR schematic for ammonia cycle.

6.3 Results

To evaluate the best ammonia and hydrogen blends for highest combustion efficiency, this study numerically simulated five NH_3/H_2 blends. Figure 6-2 shows the unburned ammonia as NH_3 mole fraction as a function of distance along the duct (C4). It was found that the lowest amount of unburned ammonia occurs at 60% NH_3-40% H_2 with highest flame temperature, Figure 6-3. Interestingly, the NH_3 mole fraction remained more or less constant with distance along the duct.

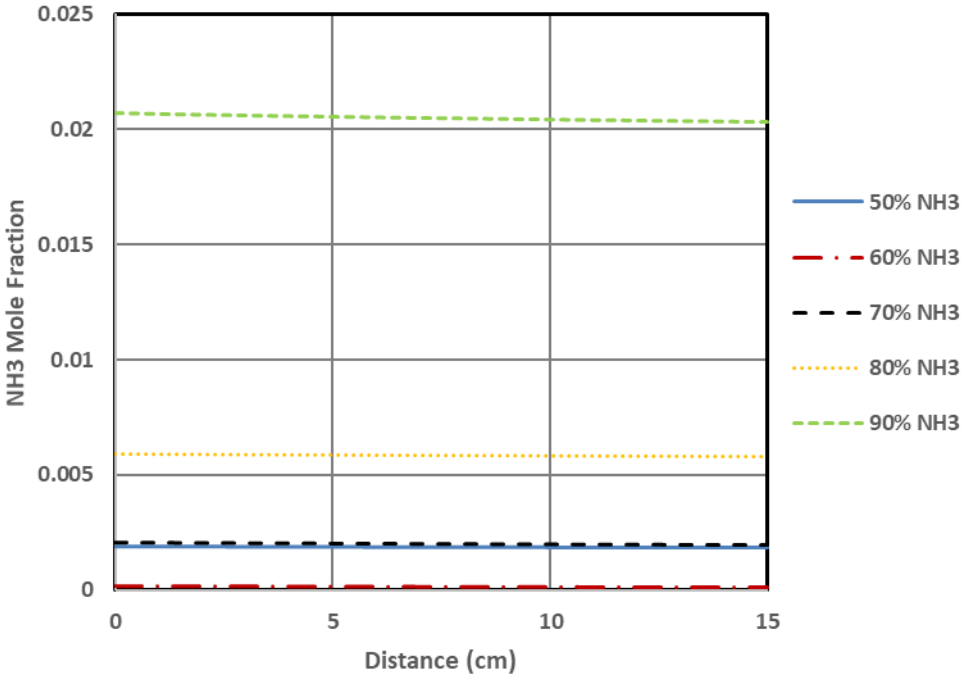

Figure 6- 2: Unburned ammonia with distance along duct (C4).

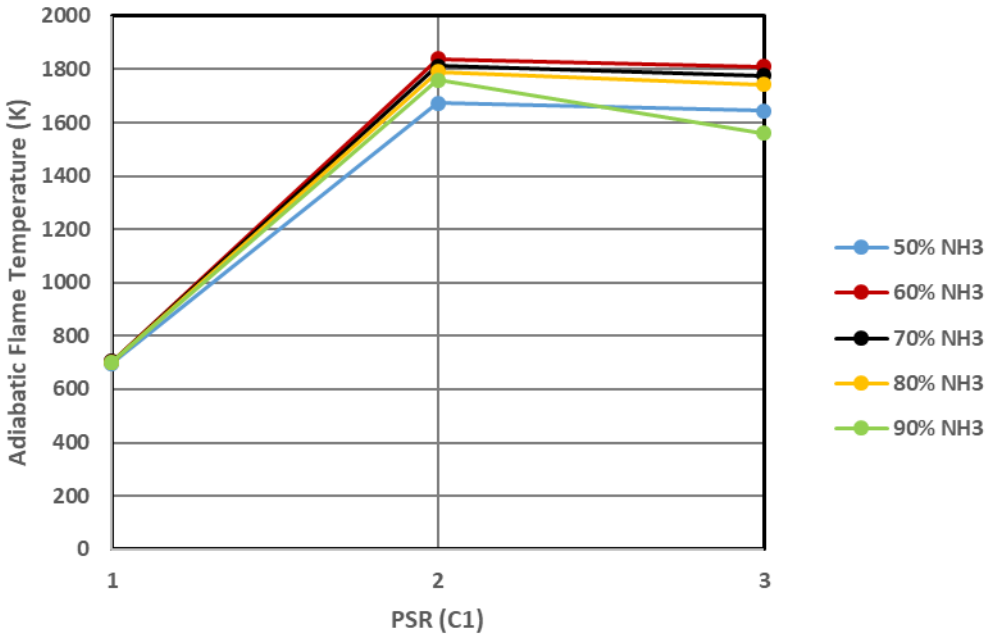

Figure 6- 3: Adiabatic flame temperature (K).

However, it can be seen from Figure 6-4 that 60% NH_3 produced at least five times the NO level of the other blends tested. It was concluded that no single blend can simultaneously give lowest level of unburned ammonia and minimum NO level.

Accordingly, in an attempt to minimise the NO formation, a small amount of the NH_3/H_2 fuel mixture - which was varied from 0% to 4% (vol%) - was injected downstream of the primary flame zone in a high circulation zone before the combustor containing the bluff body, see Figure 3-10.

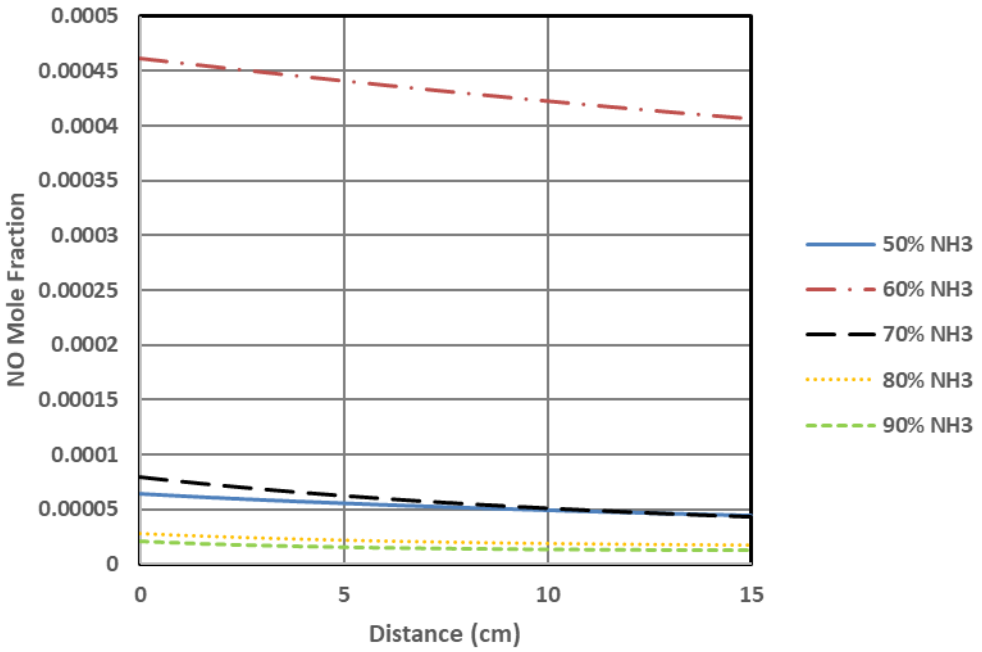

Figure 6- 4: NO emissions at different NH3/H2 mixtures with distance along duct (C4).

Figures (6-5) to (6-7) show NO emissions from a 60%-40% NH_3/H_2 fuel mixture for different amounts of the ($0 \leq X\% \leq 4$) injected downstream of the post flame zone. It can be seen that NO formation levels decreased when the X ratio was increased, due to extending the interaction between the thermal NOx and the newly injected species from the ammonia cracking process. Furthermore, it can be seen that the NO levels tend to decrease with increased residence time in the second recirculation zone in order to reduce the entrainment of reactive species [179].

It was obvious that the NO mole fraction in the exhaust gas decreased with increase in residence time. This behaviour indicates that adding NH_3/ H_2 blends as a reducing

agent plays a role in consuming NO formed in the post-combustion zone, as expected. Partially cracked NH_2 radicals obtained from the decomposition of hot, injected ammonia will lead to their recombination with NO at lower temperatures, thus following the path $NH_2 \rightarrow NH \rightarrow N_2$. The increase in NH_2 reactions will block those produced by OH emissions, i.e. the OH radical has been already depleted in the post-combustion zone while consuming NOx [223].

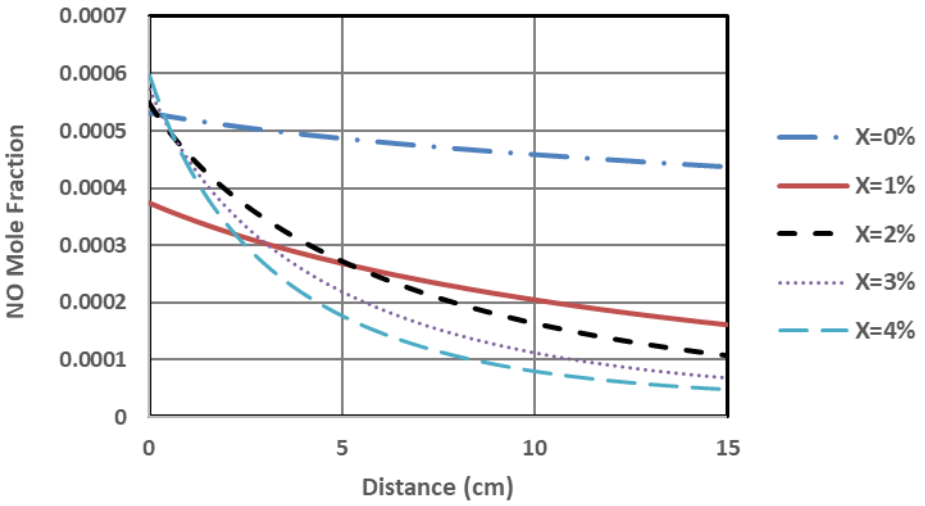

Figure 6- 5: NO emissions at 60% NH3/ for X values at residence time 0.0005s.

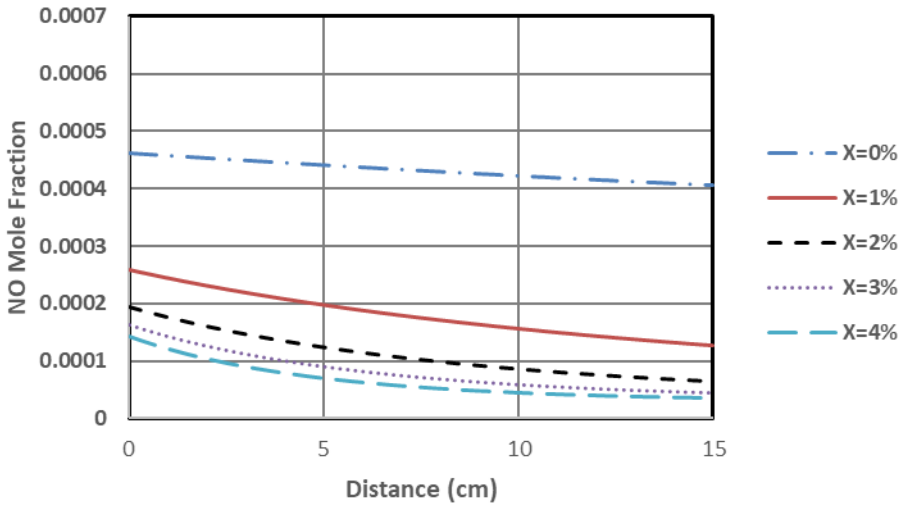

Figure 6- 6: NO emissions at 60% NH3/ for X values at residence time 0.005s.

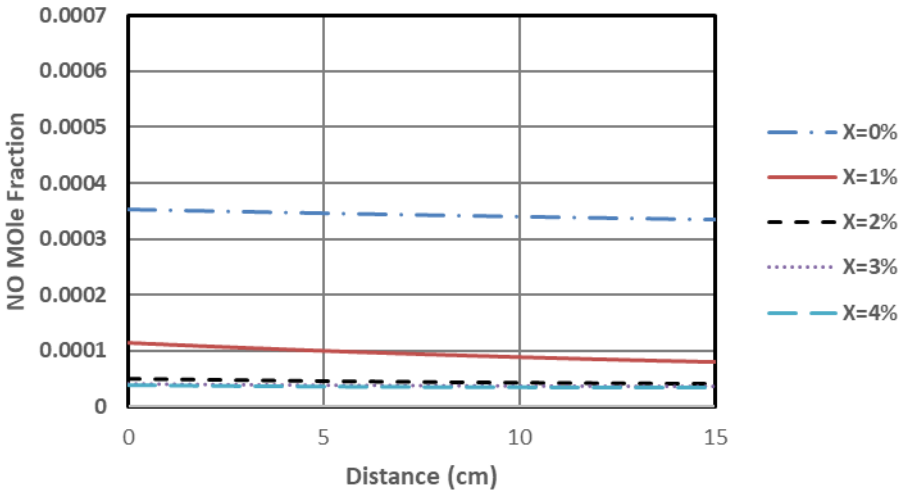

Figure 6- 7: NO emissions at 60% NH3/ for X values at residence time 0.05s.

Figures 6-8 shows the sensitivity analysis for NO, which identifies the importance of the reaction close to the flame zone. $NH_2+N \leftrightarrow N_2+2H$ is the most promising reaction for NO formation, while the reactions $N+NO \leftrightarrow N_2+O$ and $NH_2+NO \leftrightarrow N_2+H_2O$ also play essential roles for NO consumption.

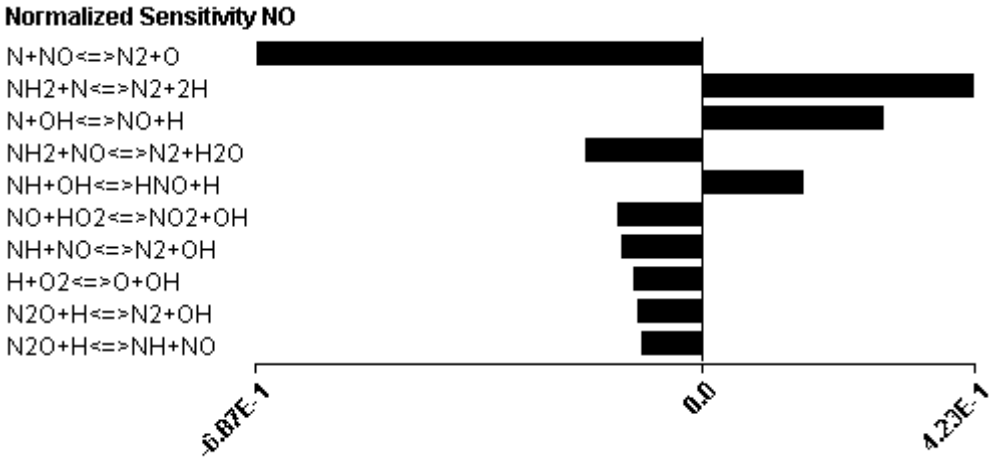

Figure 6- 8: NO sensitivity in flame zone.

Figure 6-9 shows the main reaction pathways of NO formation. The major source of NO formation comes from the oxidation of HNO and NH_2 at high temperatures. However, as previously mentioned, NH_2 at lower temperatures of reaction, i.e. similar to those found in the post-combustion injection, follow a path that leads to N_2 production.

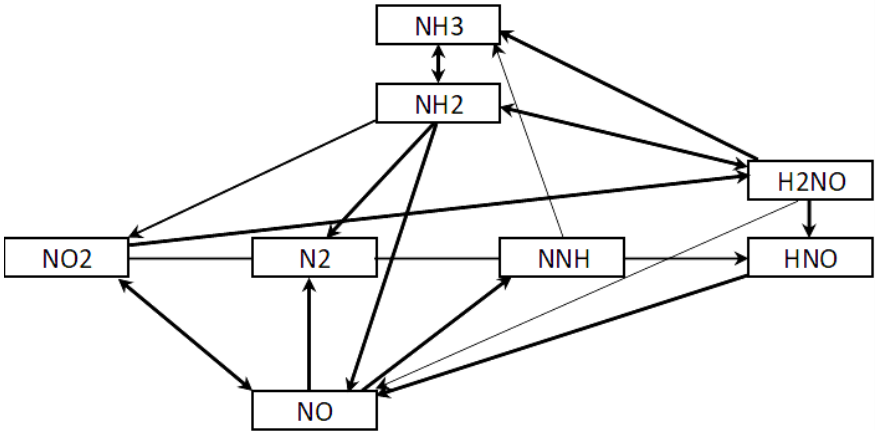

Figure 6- 9: Ammonia reaction pathway of NO formation in the flame zone.

Figure 6-10 represents a one-dimensional numerical simulation of the best case: 60% NH_3 - 40% H_2, with X=4% and residence time=0.05 sec. It shows that the gas ignition occurs in the flame zone (PSR3) with an increase of temperature in the recirculation zone (PSR2), see Figure 6-1, where NH_3 and H_2 keep reacting. The increased concentration of water vapour at the hot boundary can also be seen; this causes a corresponding increase of the flame temperature which caused increased concentration of light radicals such as H_2, O_2 and NO, in the reaction zone, where NO_2 is negligible as compared with NO.

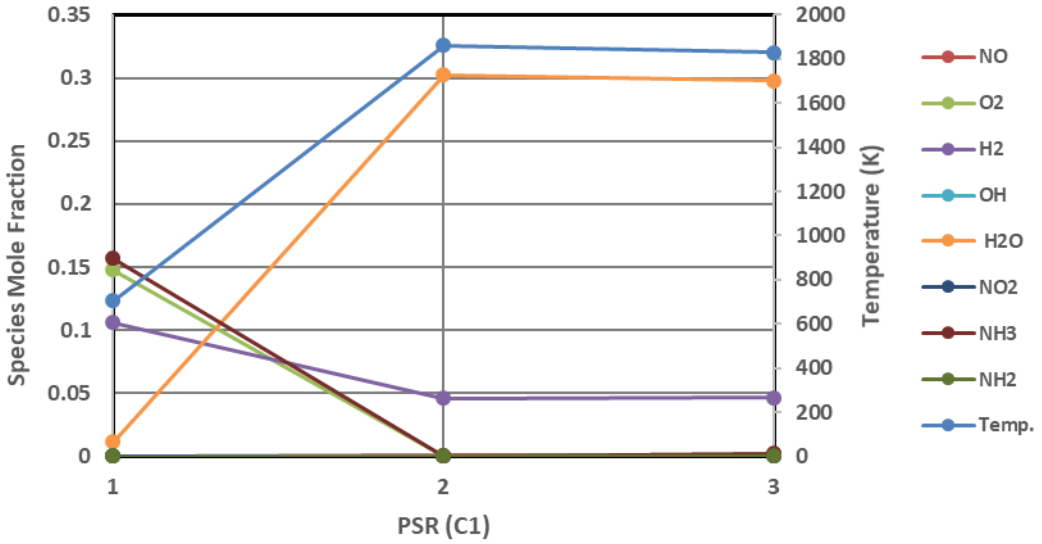

Figure 6- 10: One-dimensional simulation of the PSR (C1) reaction using a swirling network for 60% NH3, X=4% and t=0.05 sec.

Figure 6-11 indicate the rise in temperature due to the reactions of OH, NH_2, NO, and O_2 radicals that are highly active species, starting at the beginning of the post-flame reaction region with hot H_2. The effect of injecting 4% of the 60% NH_3 blend on the amount of uncracked ammonia, and NO levels in both post-combustion zone and end of the bluff body respectively, for t = 0.05 sec, can be seen in Figures 6-12 and 6-13.

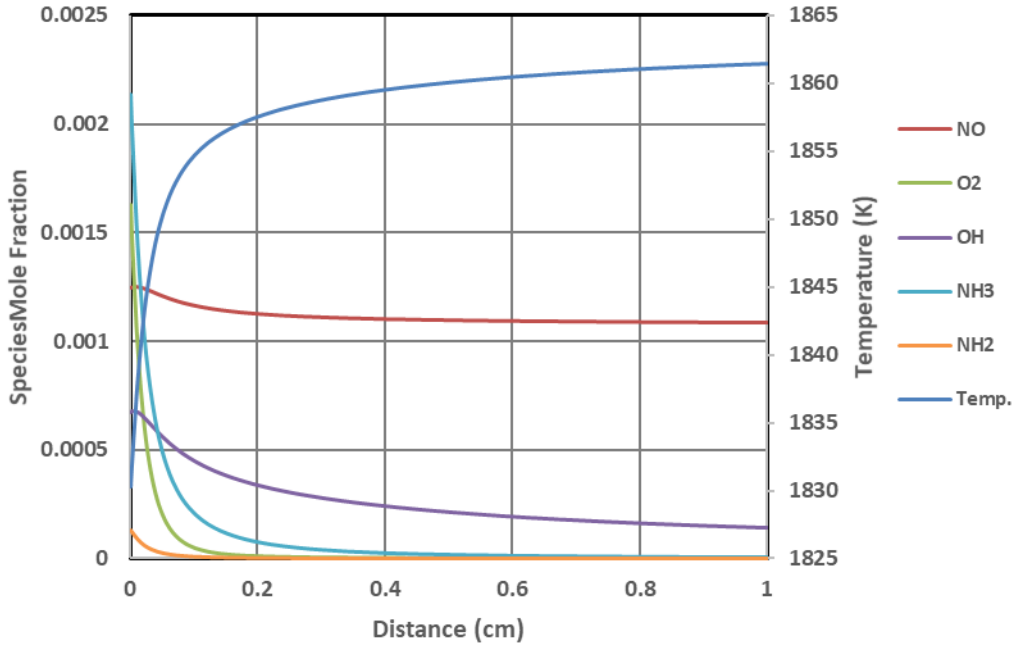

Figure 6- 11: One-dimensional simulation of the PFR (C2) reaction using a swirling network for 60% NH3, X=4% and t=0.05 sec.

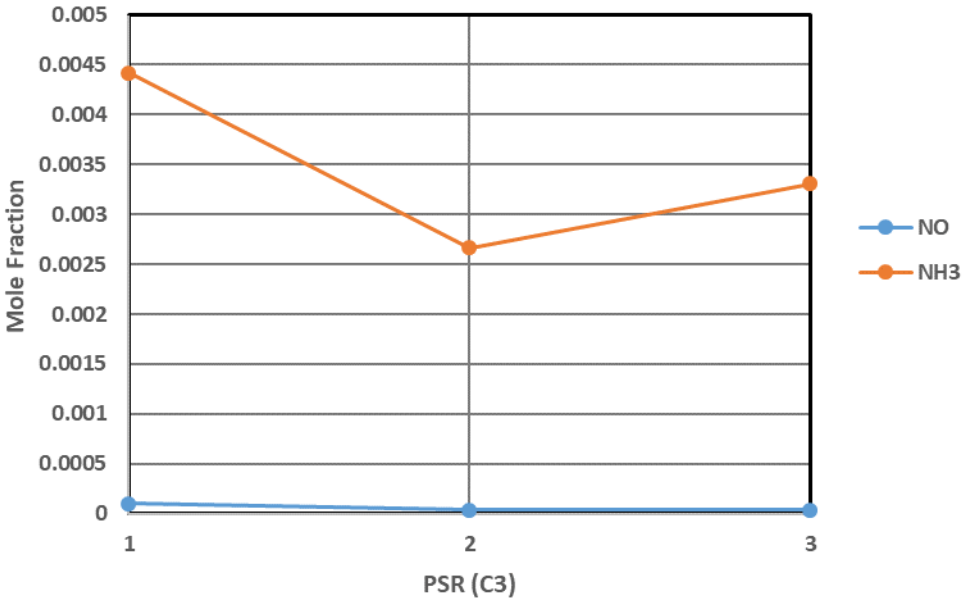

Figure 6- 12: One-dimensional simulation of the PSR (C3) reaction using a swirling network for 60% NH3, X=4% and t=0.05 sec.

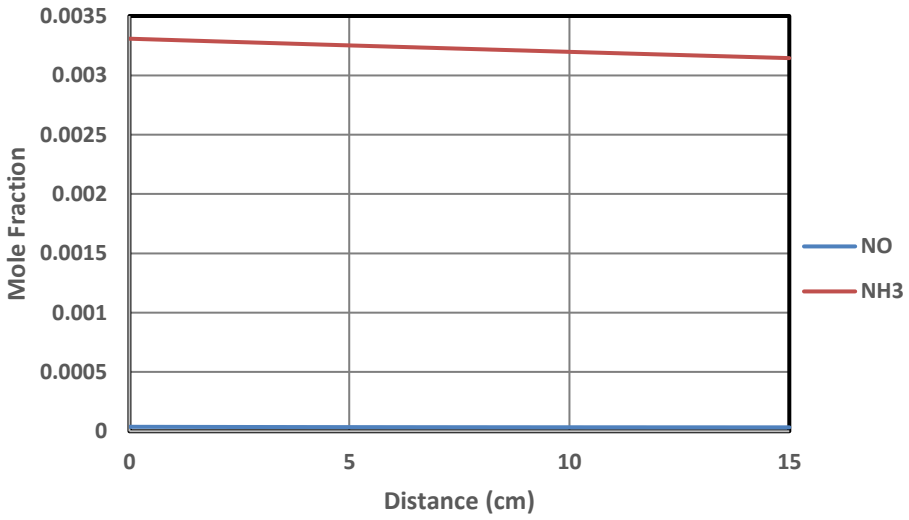

Figure 6- 13: One-dimensional simulation of the PFR (C4) reaction using a swirling network for 60% NH3, X=4% and t=0.05 sec.

CHAPTER 7

Summary of Results and Discussions

"For every fact, there is an infinity of hypotheses."

Robert Maynard Pirsig

7.1 Summary of Results and Discussions

One of the most important current scientific discussions is on the causes of acid rain, increasing air pollution and global warming due to greenhouse effects. One proposed solution is using alternatives fossil fuels, and the search for these has extended in all directions. In recent decades, ammonia has been used as a means of hydrogen storage that can be easily dissociated and used as a sustainable fuel source for transport fuel cells and power generation. Ammonia is easier to produce, handle, store and distribute than hydrogen, and with an existing, well-developed distribution infra-structure has promising commercial viability. The hydrogen density of ammonia is three times higher than demonstrated by most metal hydrides [5].

Furthermore, ammonia's cost per volume of stored energy is less expensive than hydrogen [13, 35]. Despite its toxicity, ammonia presents a significantly lower fire hazard compared to hydrogen and gasoline [16]. Additionally, ammonia has proven to be a satisfactory substitute for hydrocarbon fuels in a GT engine and showed that it was possible to attain high efficiencies with ammonia combustion [93]. Therefore, in this study, the initial, research was dedicated to understanding the fundamental characteristics of the combustion of ammonia-based fuels, and the challenge it posed when used as a fuel, especially increasing NO_x emissions.

Due to its low flame speed, ammonia is very difficult to use directly as a primary fuel. Ammonia needs to be cracked into hydrogen and nitrogen to become an efficient fuel for use in conventional internal combustion engines and GTs [95, 173]. Thus, it is of great importance to develop new devices and techniques for use with GTs that can use green ammonia for power generation. Several researchers have studied the structure

of partially cracked ammonia-air flames [44][101], leading to the development of thermal cracking processes, but the relevant literature is limited.

This study has reported the construction of a hydrogen generating system using thermal cracking of ammonia. Such a device offers the possibility of ammonia as a fuel and eliminating the problems associated with hydrogen storage and transport. Ammonia cracking is considered to provide good power loading, flame stability, low NOx emissions and increased efficiency. The thermal cracking method has been considered the best due to the efficiency of the decomposition process and the elimination of the need for a catalyst.

This chapter will describe how numerical simulations and experiments were conducted to assist in the design of an efficient thermal cracking system which could be use ammonia as a working fuel in GT applications.

7.2 Design the Proposed Cracking System

The idea behind the cracking system is to use the hot exhaust gases from a combustor using non-premixed burner, to preheat the ammonia as it passed through a heat exchanger. The ammonia was heated as it passed through internal passages inside the purpose built bluff body - heat exchanger - cracking system, which was placed along the longitudinal centre of the combustor, see Figure (4-3). The outlet temperature of the ammonia as it leaves the bluff body should be sufficient for the process of cracking the ammonia into hydrogen and ammonia should have begun. After that, the products from cracking system i.e. ammonia and hydrogen will be fed to the burner as the main fuel, see Figure (4-1).

The suggested system was developed through several CFD simulations to design a conceptual thermal cracking system suitable for use with a GT [181]. The CFD package ANSYS 16 FLUENT was used to analyse both the combustion and heat transfer regimes in order to produce a model that could be built in-house and tested experimentally.

7.2.1 Combustion Simulation

In this study, a novel device using a bluff body - heat exchanger to thermally pre-crack ammonia was evaluated. The proposed system used high-temperature exhaust gas from a GT to thermally crack ammonia to produce hydrogen and ammonia. The resulting hydrogen-ammonia mixture was used as a fuel for a modern GT. One of the design issues in a GT combustion chamber is stabilizing the flame. Non-premixed swirling flames have been used in designated aero combustors because of their advantages regarding flame stabilization [197]. However, even though swirling flows are very complicated and hard to simulate, a non-premixed, no-swirling diffusion burner was considered in this study. A 3D model of every part used in the design of the cracking system was developed using CAD software (Solid Works).

The CFD work was based on the RANS turbulent combustion flow model, using the standard k-ε model because it is considered more accurate for a wide range of wall-bounded and free shear flows. The probability density function model was used to predict the primary properties of the mixture and to illustrate the interaction between chemical reaction and turbulence [216, 217]. All the CFD analyses were conducted using non-premixed 100% methane burned completely with an output power of 10 kW at 0.2 g/s flowrate of fuel, under confined conditions with a total length of the container of 400 mm. Various bluff body geometries (shape, size and position) were examined in an attempt to enhance the heat transfer rate from the flame to the bluff body to enhance the ammonia cracking process. Twelve different geometries were investigated, with the end of the bluff body facing the burner having, in turn, a circular, triangular and parabolic profile (see Figure 4-4). Numerical modelling was used to decide the shape and dimensions of the system, which was then built and experimentally tested.

The circular profile where the bluff body was along the centre-line of the combustor was found to be the design that gave the most homogeneous flame profile and which provided sufficient heat transfer to the bluff body to raise its temperature enough to crack the ammonia passing through it. The cracked ammonia could then be a source of fuel for the burner.

7.2.1.1 Enhancement the Flow Inside the Combustor

An axial swirl vane was incorporated in the design to hold the bluff body in place within the quartz tube containing the combustion/flame (see Figure 4-14 and 4-15 a). Additionally, the axial swirl vanes generated turbulence inside the combustion chamber, around the bluff body enhancing heat transfer. High flow velocity and turbulent kinetic energy would accelerate the diffusion and mixing of the flue gases and speed the products to the exit. The use of the axial swirl vanes increased the performance of the burner and reduced emissions, due to enhanced mixing of gas products at the outlet. In addition, the dimension of the bottom of the combustor was decreased in size to increase homogeneity by further mixing of the flue gases with the secondary air.

7.2.2 Heat Exchanger Simulation

Different shell and tube heat exchangers were considered for pre-heating the ammonia. The performances of three designs of a shell and tube heat exchanger with cross flow were simulated. This procedure allowed prediction of the outlet temperature of the ammonia as it enter the bluff body for all three designs of heat exchanger. The ammonia output temperature obtained when using a three tube pass heat exchanger was 725 K; and for both heat exchangers which consisted of five tube passes and a spiral tube shape reached 801 K. These values were used as a boundary condition in the simulation of the final bluff body design.

7.2.3 Bluff Body Simulation

The design of the bluff body was based on the profile that provided a high temperature for ammonia cracking. Thus, using previous analyses (i.e. of shape, improved heat exchange, flow patterns, feasibility for manufacturing purposes, etc.), a final design was conceptualised. The ammonia temperature as it left the heat exchanger had to be low enough to cool the bluff body and, at the same time, high enough to start the cracking process, which many researchers report as 873 K [44, 124]. Both outlet temperatures of the ammonia, 725 K and 801 K obtained from the heat exchanger simulation were tested here as the input boundary condition for three different tube paths for tubes of circular cross-section, inside the bluff body. It was found that when

using a spiral path the output temperature reached 880 K, sufficient for ammonia cracking, see Figure 4-30.

7.2.4 Isothermal Simulation

Isothermal conditions using a non-premixed swirl burner as simulated in this study were validated against results previously obtained using Laser Doppler Anemometry work for a swirl burner with the same geometry [205], see Figure 4-33. The simulation also studied the effect of the presence of the bluff body - cracking system on the flow field to predict the hydrodynamic profiles of the new system.

7.3 Manufactured the Proposed Cracking System

After CFD validation of the cracking system and having chosen the best-case for the design of each part, the final cracking system was manufactured to test its efficiency. The Renishaw AM250 Laser Melting System (3D Printer) was used to build the final cracking system layer by layer directly from the digital CAD files using powder bed fusion technology with stainless-steel as the powder. Post-processing by a lathe removed sacrificial supports, which had been added to the bluff body design to enable a successful build.

7.4 Experimental Work

Some changes were made to the final system to reduce the cost of installation, for example, using a previously characterized 20 kW generic swirl burner which is available at Cardiff University [205], instead of using a diffusive non-premixed burner for the experimental programme.

7.4.1 Burner Operational Limit

The 20 kW generic swirl burner was used to investigate flame characteristics and other combustion features with different fuels (methane and/or ammonia). The system was run with methane as the test fuel and air as the oxidant, with burner swirl number of 1.05 under confined flame conditions. To achieve lower NOx emissions, most research studies are attempting to extend the blow-off limit to much lower equivalence ratios, for example, 0.5. Currently, for most industrial burners the blow-off limit the equivalence ratio is in the range of 0.7 to 0.8. The thermal cracking system proved to be advantageous in extending the stability range of the burner.

All blowoff limits obtained were for equivalence ratios < 0.52, see Table 5-1. This was achieved due to the preheating of the fuel via the cracking system before it entered the main fuel inlet. This preheating reduced the chemical reaction times of the reactants which, in turn, influenced how the equivalence ratio affected the blowoff limit. The variation in the combustor geometry and addition of the new bluff body cracking system was found to have had a significant influence on the blowoff limit with equivalence ratio reduced to 0.46 as compared to 0.70 for the same swirl burner without the new cracking system [205].

7.4.2 Thermal Cracking System Efficiency

The effectiveness and efficiency of the cracking system were determined. The results show that the temperature of the methane leaving the heat exchanger increased with time after flame ignition until it reached an equilibrium value. Also, the cracking system appeared to have the thermal characteristics needed to achieve partial cracking, with temperature differentials ranging from 370 to 488 K between inlet and outlet. This meant the manufactured system was able to raise the temperature of the inlet stream (CH_4 or NH_3) sufficiently to achieve its designed cracking performance and to start splitting the ammonia. It was found that the cracking system had a calculated effectiveness of about 64% when using burner power of 3.3 kW, 70% for 6.7 kW, and reached 84% for 10.0 kW. The cracker possessed an average efficiency of 73 % over the possible range of heat outputs; 6.7 - 10.0 kW, see Table 5-3.

7.4.3 Flow Field Dynamic

The effect of the hydrodynamic profile of the bluff body (cracker) on the flow field was also studied. It was found that the chosen geometrical profile of the cracking system led to the formation a wide secondary recirculation zone upstream of the bluff body, producing vortex flows and rapid mixing which can contribute to reducing NO_x emissions. The size of these vortices, and the velocity of the flow (already known from the bulk values obtained from the rotameters) gave estimated recirculation times in the range 0.0005 to 0.05 seconds. These results were used for a numerical examination using CHEMKIN-PRO to assess their likely effects on NOx emissions.

7.5 Chemical Kinetics Modelling

7.5.1 Ammonia/ Hydrogen Combustion

Non-premixed ammonia/hydrogen flames were simulated by using a freely propagated laminar combustion model using modified chemical mechanisms [223]. The initial compositions of the NH_3/H_2/air mixtures were calculated using an equivalence ratio ϕ=1.2, with power outputs ~10 kW, and using a great variety of blends, see Table 6-1. The combustion characteristics of NH_3/H_2/air mixtures were evaluated at low pressure and under fuel rich conditions using five NH_3/H_2 mixes, starting from 50% NH_3 (vol%) with the remainder hydrogen, and increasing in steps of 10% (vol%) NH_3. The performance of the various blends was analysed to identify the one that produced the lowest NO with highest combustion efficiency (i.e. the lowest proportion of unburned ammonia and highest combustion temperatures). It was found that the lowest amount of unburned ammonia occurs at 60% NH_3-40% H_2 a mix which also had the highest flame temperature, but this ratio produced the highest NO emissions.

7.5.2 NO Emission Reduction

To reduce NO emission, a small amount (X%) of the NH_3/H_2 mix was injected into the post-combustion flow, downstream of the primary combustion zone, but upstream of the bluff body. The X% value was changed from 0% to 4% (vol%). It was found that the NO formation levels decreased when the X ratio was increased, due to extending the interaction between the thermal NOx and the newly injected species from the ammonia cracking process. This behaviour indicated that adding NH_3/H_2 blends as a reducing agent played a role in consuming the NO formed in the post-combustion zone.

To further reduce any remaining NO in the emissions, different post-combustion recirculation zones were assessed to evaluate the impact of the bluff body configuration. The injection strategy was used with three different values of residence time (t =0.0005, 0.005 and 0.05 sec). It was found that increasing residence time for the second recirculation zone generated by the bluff-body reduced the NO level to its minimum value. Thus, this injection technique produced a useful result which is promising for further investigations and shows promise for future burner design to minimise the adverse impact of the combustion process on the environment.

7.6 Overall Discussion and Further Considerations

Future gas turbines will be expected to operate over a wide range of alternative fuels with low-cost engine modifications enabling the change from one fuel to another, according to price and availability. Consequently, many researchers are actively working to develop the burner design of GT power plants so they are capable of being powered by alternative gaseous fuels, with stable flames and low levels of unwanted emissions. At present, the vast majority of energy consumed by human societies are from non-renewable and depleting fossil fuel sources. Learning from the lessons of the past, it is seen to be necessary to develop new energy technologies to increase the efficiency and fuel flexibility of GT combustion systems [229].

The global energy sector is embarking on possibly its most significant step towards decarbonisation, to reduce greenhouse gas emissions which are widely accepted to accelerate adverse global climate change. The goals also include (i) to secure energy resources sufficient to meet perceived needs, (ii) to generate power in a way that meets the environmental standards of the day, and (iii) to ensure a reliable and affordable energy supply [230]. Using ammonia as a fuel in GTs is a step to achieving these goals. Ammonia is worth consideration as a renewable energy carrier, as it has advantages in generation, transportation and utilisation.

An important element in energy sector research is the focus on achieving fuel sustainability and avoiding supply and price fluctuations. Ammonia, as a fuel, is attracting the attention of many researchers who are attempting to overcome its drawbacks related to the its low flammability limit, high NOx emissions and flame stability issues. Due to its low flame speed, ammonia is very difficult to use directly as a primary fuel and needs either to be cracked into hydrogen, nitrogen and ammonia radicals, or mixed with enhancers (another fuel) to become an efficient fuel for GTs. This study is an attempt to contribute to this dynamic by designing a novel thermal cracking system to crack the ammonia and produce ammonia-hydrogen blends to be directly fed to the GT combustors.

The design process consisted of the following essential steps. First, CFD simulation used to design a cracking system with selection of the best profile for the cracker based on thermal, flow, and manufacturing considerations. It was found that a circular profile with spiral passages to pass ammonia inside the cracker, gave the best performance

and met the ease-of-manufacturing requirements. It was concluded that CFD simulation was critical in the design of the novel system. This CFD technique saved time and design costs. Moreover, it was demonstrated that the manufactured system performed according to the CFD predictions.

It was found that the novel cracking system had a positive effect on the combustion in the swirl burner used in the experimental campaign. It was found that the presence of the cracker produced wider blow-off limits than the original burner design (i.e., without the existence of the thermal cracking system in the combustion chamber).

Regarding the NOx emissions, this study showed that injecting a small amount of NH_3/H_2 blend as a reducing agent into the post-combustion flow played a role in consuming the NO formed in the post-combustion zone. Also, it was found that increasing residence time in the second recirculation zone generated by the cracker reduced the NO level to the minimum value obtained.

The main aim of the thesis was achieved through sequential CFD modelling and experimental steps that are described throughout the thesis. The suggested design is promising and opens new horizons of using ammonia as a fuel in real GT combustors. However, further experimental studies should be carried out investigate the effect of the cracking system on the NOx emission in addition to the CFD calculations reported in this thesis.

CHAPTER 8

Conclusions and Recommendations for Future Work

"The important thing in science is not so much to obtain new facts as to discover new ways of thinking about them."

William Lawrence Bragg

8.1 Conclusions

Specific conclusions will be given here with respect to the original objectives of the present study:

- In order to develop a new system to crack ammonia in an efficient way, both CFD and experimental methods were used to enhance the combustibility of ammonia by first cracking the ammonia to produce hydrogen, which is added to the ammonia to provide a fuel that is a mix of hydrogen-ammonia. CFD simulations have been used to design the thermal cracking system as conceived. A non-premixed combustion model under atmospheric and confined conditions with output power 10 kW was used for all the numerical work in this thesis.

- To decide the shape and dimensions of the novel device to be used as a bluff body to thermally pre-crack ammonia, numerical modelling was used to determine the final dimensions of the cracking system which was then built and experimentally tested. Simulations were performed using twelve different geometries of the bluff body with different shapes, sizes and positions in the combustion zone. The results showed that the circular-end profile to be the design that gave the most homogeneous flame profile, provided an effective temperature to heat the bluff body which in turn was used to crack the ammonia passing through it. Also, this geometrical profile provided sufficient space to pass the ammonia through a different passage to crack the ammonia. Also, some modifications were added to the bluff body, an axial swirl vane and a

reduction in the dimension at the bottom of the combustor. It can be concluded that the use of these enhancers increased the performance of a burner and reduced emissions, due to enhanced mixing of gas products at the combustor outlet.

- To help the ammonia start cracking, there needs to be a preheating process. Three different cross-flow heat exchanger designs could be used for this purpose, using the hot exhaust gases (as previously simulated) to heat the ammonia. The pre-heated ammonia then passed through the bluff body - cracker to test whether the temperature required for cracking (about 880 K) could be attained when using different passages inside the bluff-body. The results indicate that the required temperature for ammonia cracking was obtained when using a spiral passage inside the bluff-body (see Figure 4-30, case 3).

- In order to manufacture the final design chosen for the thermal cracking system, at minimum cost and time, a 3D printer was used, the Renishaw AM250 Laser Melting System with a nanocomposite material. It was found that this technique ensured high-quality build of complex geometries and is suitable for all qualified metals including stainless-steel as the powder.

- To investigate the flame characteristics, blowoff limits and other combustion features, experimental tests were carried out using a 20 kW generic swirl burner. The experimental work used methane as the test fuel and air as the oxidant, with burner swirl number of 1.05. The flame was confined within three contiguous cylindrical quartz tube of total length 400 mm. It can be concluded that the thermal cracking system extended the stability range of the burner. All blowoff limits obtained were for equivalence ratios < 0.52, due to the preheating of the fuel via the cracking system before it entered the main fuel inlet.

- The blowoff limit was reduced from 0.70 to 0.46 in the presence of the bluff body, due to reducing the chemical reaction times of the reactants as compared to using the same swirl burner without the new cracking system. It can be

concluded that the presence of the bluff body cracking system affects the hydrodynamics of the swirling flow upstream of the bluff body, playing a significant role as both stabilization device and cracking method.

- To determine the effectiveness of the cracking system when used with GT combustion systems using ammonia, the effectiveness of the bluff body was calculated for different values of output power. It was found that the cracking system is efficient in raising the temperature of the inlet fuel with either methane or ammonia to achieve its designed cracking performance. The average efficiency was predicted to reach 73 %.

- To evaluate the impact of various bluff body configurations, different post-combustion recirculation zones were assessed. It was found that the thermal cracking system led to the formation of a wide secondary recirculation zone upstream of the bluff body, this produced vortices which can contribute to reducing NO emissions. Calculations showed residence values between 0.0005 and 0.05s within these secondary recirculation zones.

- In order to identify the NH_3/H_2 blends that produced the lowest proportion of unburned ammonia and highest combustion temperatures, Non-premixed ammonia/hydrogen flames were simulated using a freely propagated laminar combustion model with modified chemical mechanisms [223] . It was found that the lowest amount of unburned ammonia and highest temperature occurred at 60% NH_3-40% H_2, but this ratio also produced the highest NO emissions.

- Injecting a small amount (X%) of the NH_3/H_2 mix into the post-combustion flow has been suggested as a means of reducing NO. This was confirmed when it was found that the NO formation levels decreased when the X% increased, indicating that adding NH_3/H_2 blends plays an important role in consuming NO formed in the post-combustion zone. Furthermore, it was found that increasing the size of second recirculation zone upstream of the bluff body, i.e. increasing the residence time caused further reduction in NO emission. This injection technique is worthy of further investigation. It can be concluded that the cracking system can affect the flame topology and hence the emission levels.

8.2 Recommendations for Future Work

The outcomes and findings of this study could open new horizons for utilising ammonia-based fuels (such as ammonia/hydrogen) for combustion applications. Furthermore, the present results suggest the needs for further research to be conducted on large combustion systems, using ammonia cracked into hydrogen and nitrogen.

Based on the present work some related future studies should be considered.

- More advanced turbulence models such as Large Eddy Simulation are needed to reveal the complex coherent structures produced by swirling flow and cracking systems. These models should provide better visualisation of the recirculation zone to give a clearer picture of the flame behaviour and aerodynamic flow motions especially in the shear layer region. Such a model could usefully provide the velocity profile at any plane even upstream of the bluff body.

- More modelling work will be needed on the chemical kinetics of ammonia/ hydrogen flames since data for ammonia as the primary fuel in the ammonia/hydrogen blends are limited. Furthermore, more verification is needed on the mechanisms of reduction for future practical simulation studies.

- To achieve high flame stability and lower emissions in ammonia/hydrogen combustion: new injection strategies are needed, different swirl numbers tested for application in GT power generation utilising ammonia fuel blends, blending of ammonia with other fuels to enhance combustion performance.

- More advanced diagnosis technologies need to be included in future experimental work to analysis the flow field characteristics of zones downstream of the nozzle and upstream of the bluff body. Bespoke considerations are required to avoid high intensity reflection that can be detrimental to measurements and equipment.

- Investigate the design of a heat exchanger to preheat the ammonia before it passed through the bluff body - cracker. To increase the effectiveness of the

cracking system by giving increased control of the temperature variation of the fuel as it passes though the bluff body.

- Use a catalyst promoter such as Pd, Pt, Rh and Ru, as an active component for further decomposition of ammonia into nitrogen and hydrogen; increasing ammonia decomposition.

- To monitor the levels of ammonia dissociated into hydrogen/nitrogen after the cracking process, an ammonia analyser will be needed to determine the relative quantities of ammonia, hydrogen and nitrogen radicals produced by the cracking system. As a result, the ratio of hydrogen and ammonia needed for efficient combustion and/or post combustion injection to reduce NO levels could be controlled.

- One of the main limiting aspects of the present work was the health and safety regulations of the university. So, to use the ammonia in this study a new cage to put the external ammonia cylinders is needed. This cage will reduce the likelihood of unauthorised personnel to access ammonia cylinders and to avoid any harm could be occurs. Digital rotameters are needed to control the flux of ammonia from a far distance as the rotameters used currently in the lab are too close to ammonia flames, thus exposure is high. New Perspex window at the front of the system was needed to create an isolated zone for extraction, with low probability of leaks and to reduce exposure to ammonia gases. Also, an extra panel was needed at the front of the extraction hood to avoid ammonia leaks. These are recommendations required for further ammonia testing at Cardiff University.

References

[1] T. Hughes, I. Wilkinson, E. Tsang, I. Mcpherson, T. Sudmeier, J. Fellowes, F. Liao, S. Wu, A. Valera-Medina, and S. Metz, "Green Ammonia." [Online]. Available: ww.slideshare.net/tswittrig/green-ammoniahughes-siemens-oxford, 2015.

[2] A. Valera-Medina, P. Beasley, T. Hughes, S. Morris, D. G. Pugh, R. Marsh, and J. Runyon, "Ammonia, Methane and Hydrogen for Gas Turbines," *Energy Procedia*, vol. 75, pp. 118–123, 2015.

[3] G. Faleschini, V. Hacker, M. Muhr, K. Kordesch, and R. R. Aronsson, "Ammonia for High Density Hydrogen Storage." [Online]. Available: www.researchgate.net/ publication/238065428, 2011.

[4] T. Kandemir, M. E. Schuster, A. Senyshyn, M. Behrens, and R. Schlçgl, "The Haber – Bosch Process Revisited : On the Real Structure and Stability of ' Ammonia Iron ' under Working Conditions," *Angew. Chemie Int. Ed.*, vol. 52, pp. 12723–12726, 2013.

[5] C. Zamfirescu and I. Dincer, "Using ammonia as a sustainable fuel," *Power Sources J.*, vol. 185, pp. 459–465, 2008.

[6] M. Appl, *Ammonia principles and industrial practice,*. Wiley-VCH Verlag GmbH, 1999.

[7] R. Lan, J. T. S. Irvine, and S. Tao, "Ammonia and related chemicals as potential indirect hydrogen storage materials," *Int. J. Hydrogen Energy*, vol. 37, no. 2, pp. 1482–1494, 2012.

[8] C. H. Christensen, T. Johannessen, R. Z. Sørensen, and J. K. Nørskov, "Towards an ammonia-mediated hydrogen economy?," *Catal. Today*, vol. 111, no. 1–2, pp. 140–144, 2006.

[9] P. J. Feibelman and R. Stumpf, "Comments on Potential Roles ofAmmonia in a Hydrogen Economy – A Study of Issues Related to the Use ofAmmonia for On-Board Vehicular Hydrogen Storage." [Online]. Available: Online www.pc.gov.au, 2006.

[10] J. O. Jensen, A. P. Vestbø, Q. Li, and N. J. Bjerrum, "The energy efficiency of onboard hydrogen storage," *J. Alloys Compd.*, vol. 446–447, pp. 723–728, 2007.

[11] G. Cinti, U. Desideri, D. Penchini, and G. Discepoli, "Experimental analysis of SOFC fuelled by ammonia," *Fuel Cells*, vol. 14, no. 2, pp. 221–230, 2014.

[12] V. Hacker and K. Kordesch, "Ammonia crackers," in *Handbook of Fuel Cells Fundamentals, Technology and Applications*, vol. 3, Wiley, pp. 121–127, 2003.

[13] F. Vitse, M. Cooper, and G. G. Botte, "On the use of ammonia electrolysis for hydrogen production," *J. Power Sources*, vol. 142, no. 1–2, pp. 18–26, 2005.

[14] A. Klerke, H. Christensen, K. Nørskov, and T. Vegge, "Ammonia for hydrogen storage : challenges and opportunities," *J. Mater. Chem.*, vol. 18, no. 20, pp. 2285–2392, 2008.

[15] N. J. Duijm, F. Markert, and J. L. Paulsen, "Safety assessment of ammonia as a transport fuel," Denmark, Forskningscenter, Risø National Laboratory, 2005.

[16] T. Brown, "Ammonia fuel risk levels a summary of the two existing studies of ammonia fuel safety," in *NH3 Fuel Conference*, 2015.

[17] A. H. Lefebvre and D. R. Ballal, *Gas Turbine Combustion Alternative Fuels and Emissions*, Third edit. Taylor & Francis Group, 2010.

[18] T. Patrick, "Components: Gas Turbine." [Online]. Available: http://cset.mnsu.edu/engagethermo/index.html, 1997.

[19] P. E. Rokke, J. E. Hustad, N. A. Rokke, and O. B. Svendsgaard, "Technology Update on Gas Turbine Dual Fuel, Dry Low Emission Combusion Combustion systems," in *Proceedings of ASME Turbo Expo, June 16–19, 2003*.

[20] T. Lieuwen, V. Mcdonell, and E. Petersen, "Fuel Flexibility Influences on Premixed Combustor Blowout, Flashback, Autoignition, and Stability," *J. Eng. Gas Turbines Power*, vol. 130, 2008.

[21] N. Syred, M. Abdulsada, A. Griffiths, T. O'Doherty, and P. Bowen, "The effect of hydrogen containing fuel blends upon flashback in swirl burners," *Appl. Energy*, vol. 89, no. 1, pp. 106–110, 2012.

[22] A. Valera-Medina, N. Syred, and P. Bowen, "Central Recirculation Zone Visualization in Confined Swirl Combustors for Terrestrial Energy," *J. Propuls. Power*, vol. 29, no. 1, pp. 195–204, 2013.

[23] N. Syred, "A review of oscillation mechanisms and the role of the precessing vortex core (PVC) in swirl combustion systems," *Prog. Energy Combust. Sci.*, vol. 32, no. 2, pp. 93–161, 2006.

[24] Y. Huang and V. Yang, "Dynamics and stability of lean-premixed swirl-stabilized combustion," *Prog. Energy Combust. Sci.*, vol. 35, no. 4, pp. 293–364, 2009.

[25] N. Beer and J. M.Chigier, *Combustion Aerodynamics*. Appl. Sci. Publ. LTD, 1972.

[26] X. Lu, S. Wang, H. G. Sung, S. Y. Hsieh, and V. Yang, "Large-eddy simulations of turbulent swirling flows injected into a dump chamber," *J. Fluid Mech.*, vol. 527, pp. 171–195, 2005.

[27] A. Coghe, G. Solero, and G. Scribano, "Recirculation phenomena in a natural gas swirl combustor," *Exp. Therm. Fluid Sci.*, vol. 28, no. 7, pp. 709–714, 2004.

[28] S. Roux, G. Lartigue, T. Poinsot, U. Meier, and C. Bérat, "Studies of mean and unsteady flow in a swirled combustor using experiments, acoustic analysis, and large eddy simulations," *Combust. Flame*, vol. 141, no. 1–2, pp. 40–54, 2005.

[29] A. Valera-Medina, N. Syred, and A. Griffiths, "Visualisation of isothermal large coherent structures in a swirl burner," *Combust. Flame*, vol. 156, no. 9, pp. 1723–1734, 2009.

[30] A. Valera-Medina, H. Xiao, M. Owen-Jones, W. I. F. David, and P. J. Bowen, "Ammonia for power," *Prog. Energy Combust. Sci.*, vol. 69, pp. 63–102, 2018.

[31] P. H. Pfromm, "Towards sustainable agriculture: Fossil-free ammonia," *J. Renew. Sustain. Energy*, vol. 9, no. 3, 2017.

[32] G. Strickland, "Ammonia as a hydrogen energy-storage medium," in *5th Annual Thermal Storage Meeting*, pp. 1–7, 1980.

[33] P. N. and J. Ross, "Characteristics of an NH3 - Air Fuel Cell System for Vehicular Applications," Lawrence Berkeley Laboratory, University of California, 1981.

[34] J. J. Mackenzie and W. H. Avery, "Ammonia fuel: the key to hydrogen-based transportation," in *Proc. 31st Intersociety Energy Conversion Engineering Conference*, pp. 1761–1766, 1996.

[35] C. Zamfirescu and I. Dincer, "Ammonia as a green fuel and hydrogen source for vehicular applications," *Fuel Process. Technol.*, vol. 90, no. 5, pp. 729–737, 2009.

[36] B. Cox and K. Treyer, "Environmental and economic assessment of a cracked ammonia fuelled alkaline fuel cell for off-grid power applications," *J. Power Sources*, vol. 275, pp. 322–335, 2015.

[37] T. Lipman and N. Shah, "Ammonia as an Alternative Energy Storage Medium for Hydrogen Fuel Cells: Scientific and Technical Review for Near-Term Stationary Power Demonstration Projects, Final Report." [Online]. Available: http://www.its.berkeley.edu/sustainabilitycenter, 2007.

[38] J. D. Holladay, J. Hu, D. L. King, and Y. Wang, "An overview of hydrogen production technologies," *Catal. Today*, vol. 139, no. 4, pp. 244–260, 2009.

[39] H. Yu, G. Qi, Q. Xiang, S. Wang, and M. Fang, "Aqueous Ammonia Based Post Combustion Capture: Results from pilot plant operation, challenges and further opportunities," *Energy Procedia*, vol. 37, pp. 6256–6264, 2013.

[40] M. E. E. Abashar, "Investigation of low temperature decomposition of ammonia using spatially patterned catalytic membrane reactors," *Appl. Catal. A Gen.*, vol. 236, no. 2, pp. 35–53, 2002.

[41] C. W. Gross and S. Kong, "Performance characteristics of a compression-ignition engine using direct-injection ammonia – DME mixtures," *Fuel*, vol. 103, pp. 1069–1079, 2013.

[42] A. Valera-Medina, R. Marsh, J. Runyon, D. Pugh, P. Beasley, T. Hughes, and P. Bowen, "Ammonia–methane combustion in tangential swirl burners for gas turbine power generation," *Appl. Energy*, vol. 185, pp. 1362–1371, 2017.

[43] M. Balestri, D. Cecchini, and V. Cinti, "Unconventional Fuels Experimental

Campaigns in Gas Turbine Combustor at ENEL Sesta Facility," *ASME Turbo Expo Power Land, Sea, Air*, pp. 121–128, 2004.

[44] A. Normand, "Method for generating a reducing atmosphere for heat-treating installations," US Patent 4069071, 1978.

[45] S. Grannell and D. E. Gillespie, "Ammonia flame cracker system, method and apparatus," US Patent US8691182B2, 2011.

[46] J. C. Ganley, F. S. Thomas, E. G. Seebauer, and R. I. Masel, "A priori catalytic activity correlations: The difficult case of hydrogen production from ammonia," *Catal. Letters*, vol. 96, no. 3–4, pp. 117–122, 2004.

[47] W. Merriam and E. Robert, "Cracking (chemistry)," 1934.

[48] R. A. Meyers, *Handbook of Petrochemicals Production Processes*. McGraw-Hill., 2005.

[49] J. G. Speight, *The Chemistry and Technology of Petroleum*, 4th editio. 2006.

[50] R. Sadeghbeigi, *Fluid Catalytic Cracking Handbook*, 2nd editio. Gulf Publishing, 2000.

[51] Y. Xu, Y. Suzuki, Z. G. Zhang, Y. Shen, A. C. Lua, T. V Choudhary, C. Sivadinarayana, and D. W. Goodman, "Catalytic ammonia decomposition: COx -free hydrogen production for fuel cell applications," *Catal. Letters*, vol. 72, no. 3, pp. 105–116, 2013.

[52] L. Li and J. A. Hurley, "Ammonia-based hydrogen source for fuel cell applications," *Int. J. Hydrogen Energy*, vol. 32, no. 1, pp. 6–10, 2007.

[53] A. Kirubakaran, S. Jain, and R. K. Nema, "A review on fuel cell technologies and power electronic interface," *Renew. Sustain. Energy Rev.*, vol. 13, no. 9, pp. 2430–2440, 2009.

[54] S. Giddey, S. P. S. Badwal, C. Munnings, and M. Dolan, "Ammonia as a Renewable Energy Transportation Media," *ACS Sustain. Chem. Eng.*, vol. 5, no. 11, pp. 10231–10239, 2017.

[55] G. M. Kimball, "Ammonia for Renewable Energy Systems," California Institute of Technology, Pasadena, 2007.

[56] A. Afif, N. Radenahmad, Q. Cheok, S. Shams, J. H. Kim, and A. K. Azad, "Ammonia-fed fuel cells: A comprehensive review," *Renew. Sustain. Energy Rev.*, vol. 60, pp. 822–835, 2016.

[57] A. Mcfarlan, N. Maffei, and L. Pelletier, "Direct Ammonia Fuel Cells for Distributed Power Generation and CHP," Argonne National Laboratories, Canada, 2005.

[58] A. Chellappa and M. R. Powell, "Ammonia-based hydrogen generation apparatus and method for using same," US Patent 7,867,300 B2, 2011.

[59] N. Sifer and K. Gardner, "An analysis of hydrogen production from ammonia hydride hydrogen generators for use in military fuel cell environments," *J.*

Power Sources, vol. 132, no. 1–2, pp. 135–138, 2004.

[60] A. Wojcik, H. Middleton, I. Damopoulos, and J. Van Herle, "Ammonia as a fuel in solid oxide fuel cells," *J. Power Sources*, vol. 118, no. 1–2, pp. 342–348, 2003.

[61] M. Ni, D. Y. C. Leung, and M. K. H. Leung, "Mathematical modeling of ammonia-fed solid oxide fuel cells with different electrolytes," *Int. J. Hydrogen Energy*, vol. 33, no. 20, pp. 5765–5772, 2008.

[62] M. Ni, D. Y. C. Leung, and M. K. H. Leung, "Thermodynamic analysis of ammonia fed solid oxide fuel cells: Comparison between proton-conducting electrolyte and oxygen ion-conducting electrolyte," *J. Power Sources*, vol. 183, no. 2, pp. 682–686, 2008.

[63] M. Ni, "Thermo-electrochemical modeling of ammonia-fueled solid oxide fuel cells considering ammonia thermal decomposition in the anode," *Int. J. Hydrogen Energy*, vol. 36, no. 4, pp. 3153–3166, 2011.

[64] G. Cinti, G. Discepoli, E. Sisani, and U. Desideri, "SOFC operating with ammonia: Stack test and system analysis," *Int. J. Hydrogen Energy*, vol. 41, no. 31, pp. 13583–13590, 2016.

[65] A. F. S. Molouk, J. Yang, T. Okanishi, H. Muroyama, T. Matsui, and K. Eguchi, "Comparative study on ammonia oxidation over Ni-based cermet anodes for solid oxide fuel cells," *J. Power Sources*, vol. 305, pp. 72–79, 2016.

[66] K. Kordesch, V. Hacker, R. Fankhauser, and G. Faleschnin, "Ammonia cracker for production of hydrogen," US Patent 0232224 A1, 2005.

[67] T. Hejze, J. O. Besenhard, K. Kordesch, M. Cifrain, and R. R. Aronsson, "Current status of combined systems using alkaline fuel cells and ammonia as a hydrogen carrier," *J. Power Sources*, vol. 176, no. 2, pp. 490–493, 2008.

[68] K. Kordesch, R. Aronsson, P. Kalal, V. Hacker, and G. Faleschini, "Hydrogen from cracked ammonia for alkaline fuel cell-rechargeable battery hybrids and ICE vehicles," in *Annual NH3 Fuel Conference*, 2007.

[69] S. Gobesfeld, "Ammonia-Fueled Electric Vehicle Preference of a direct ammonia fuel cell," *University of Delaware, NH3-Energy Conf*, 2017.

[70] S. Kong, M. Veltman, and C. Gross, "Performance of a Compression-Ignition Engine Using Direct-Injection of Liquid Ammonia / DME Mixture," *Iowa State University, NH3-Energy Conf*. 2011.

[71] T. Alessandro and B. Paolo, "Device for hydrogen enrichment of the fuel of internal combustion engine fed by ammonia, during the start-up and during the steady state," Patent WO 004344 Al, 2011.

[72] C. Boffito and J. D. Baker, "Getter materials for cracking ammonia," US Patent, 5,976,723, 1999.

[73] T. J. Pearsall and C. G. Garabedian, "Combustion of Anhydrous Ammonia in Diesel Engines," *SAE Trans.*, vol. 76, pp. 3213–3221, 1968.

[74] M.-V. Aliasghar, "Predictions and measurements of spark-ignition engine characteristics using ammonia and other fuels," PhD Thesis, University of London, 1988.

[75] T. Hollinger, "Internal combustion engines and air pollution," *Annual NH3 Fuel Conference*. [Online]. Available: https://nh3fuelassociation.org/wp-content/uploads/2012/05/hollinger05.pdf, 2005.

[76] Y. Woo, J. Y. Jang, Y. J. Lee, and J.-N. Kim, "Recent progress on the Ammonia-Gasoline and the Ammonia-Diesel dual fueled ICE in Korea," in *Des Moines, 11th NH3 Fuel Conference*, pp. 22–24, 2014.

[77] A. Reiter and S.-C. Kong, "Demonstrate Ammonia Combustion in Diesel Engines," in *4th Annual NH3 Fuel Conference on Ammonia*, 2007.

[78] A. J. Reiter and S. C. Kong, "Combustion and emissions characteristics of compression-ignition engine using dual ammonia-diesel fuel," *Fuel*, vol. 90, no. 1, pp. 87–97, 2011.

[79] C. Gross, G. Zacharakis-jutz, and S.-C. Kong, "Update on Ammonia Engine Combustion Using Direct Fuel Injection," in *9th Annual NH3 Conference*, 2012.

[80] S. Kong, "Combustion Efficiency and Exhaust Emissions of Ammonia Combustion in Diesel Engines," in *4th Annual NH3 Fuel ConferenceAnnual NH3 Fuel Conference*, 2007.

[81] K. Ryu, G. E. Zacharakis-Jutz, and S. C. Kong, "Performance characteristics of compression-ignition engine using high concentration of ammonia mixed with dimethyl ether," *Appl. Energy*, vol. 113, pp. 488–499, 2014.

[82] M. Veltman and S.-C. Kong, "Developing Fuel Injection Strategies for Using Ammonia in Direct Injection Diesel Engines," in *7th Annual NH3 Conference*, 2010.

[83] S. M. Grannell, D. N. Assanis, S. V. Bohac, and D. E. Gillespie, "The Fuel Mix Limits and Efficiency of a Stoichiometric, Ammonia, and Gasoline Dual Fueled Spark Ignition Engine," *J. Eng. Gas Turbines Power*, vol. 130, no. 4, p. 042802, 2008.

[84] S. M. Grannell, D. N. Assanis, D. E. Gillespie, and S. V Bohac, "Exhaust emissions from a stoichiometric, ammonia and gasoline dual fueled spark ignition engine," *Proc. ASME Intern. Combust. Engine Div. 2009 Spring Tech. Conf.*, pp. 1–7, 2009.

[85] S. Frigo and R. Gentili, "Analysis of the behaviour of a 4-stroke Si engine fuelled with ammonia and hydrogen," *Int. J. Hydrogen Energy*, vol. 38, no. 3, pp. 1607–1615, 2013.

[86] M. Comotti and S. Frigo, "Hydrogen generation system for ammonia-hydrogen fuelled internal combustion engines," *Int. J. Hydrogen Energy*, vol. 40, no. 33, pp. 10673–10686, 2015.

[87] F. R. Westlye, A. Ivarsson, and J. Schramm, "Experimental investigation of

nitrogen based emissions from an ammonia fueled SI-engine," *Fuel*, vol. 111, no. 2, pp. 239–247, 2013.

[88] C. S. Mørch, A. Bjerre, M. P. Gøttrup, S. C. Sorenson, and J. Schramm, "Ammonia/hydrogen mixtures in an SI-engine: Engine performance and analysis of a proposed fuel system," *Fuel*, vol. 90, no. 2, pp. 854–864, 2011.

[89] K. Ryu, G. E. Zacharakis-Jutz, and S. C. Kong, "Performance enhancement of ammonia-fueled engine by using dissociation catalyst for hydrogen generation," *Int. J. Hydrogen Energy*, vol. 39, no. 5, pp. 2390–2398, 2014.

[90] A. Karabeyoglu and B. Evans, "Selection of NH3 for Gas Turbine Use," in *Portland, 8th NH3 Conference*, 2011.

[91] J. R. Bartels, "A feasibility study of implementing an Ammonia Economy," MSc Thesis, Iowa State University, 2008.

[92] F. Belvoir, "Development of Ammonia Burning Gas Turbine Engine," U. S. Army Engineer Research and Development Laboratories, 1966.

[93] D. T. Pratt, "Performance of ammonia-fired gas-turbine combustors," University of California Department of Mechanical Engineering Thermal Systems Division, Technical Report No. 9, 1967.

[94] B. Evans, "Using Local Green Energy and Ammonia to Power Gas Turbine Generators," *Sacramento, 10th NH3 Fuel Conf., Sept.*, 2013.

[95] A. Valera-Medina, D. G. Pugh, P. Marsh, G. Bulat, and P. Bowen, "Preliminary study on lean premixed combustion of ammonia-hydrogen for swirling gas turbine combustors," *Int. J. Hydrogen Energy*, vol. 42, no. 38, pp. 24495–24503, 2017.

[96] N. Iki, O. Kurata, T. Matsunuma, T. Inoue, M. Suzuki, T. Tsujimura, and H. Furutani, "Micro Gas Turbine Operation with Kerosene and Ammonia," in *Des Moines, The 11th Annual NH3 fuel conference*, pp. 1–22, 2014.

[97] N. Iki, O. Kurata, T. Matsunuma, T. Inoue, M. Suzuki, T. Tsujimura, and H. Furutani, "Micro Gas Turbine Firing Ammonia," in *Chicago, 12th Annual NH3 Fuel Conference*, pp. 1–39, 2015.

[98] N. Iki, O. Kurata, T. Matsunuma, T. Inoue, M. Suzuki, T. Tsujimura, and H. Furutani, "Power Generation and Flame Visualization of Micro Gas Turbine Firing Ammonia or Ammonia-Methane Mixture," in *Los Angeles, 13th Annual NH3 Fuel Conference*, pp. 1–22, 2016.

[99] O. Kurata, N. Iki, T. Matsunuma, T. Inoue, T. Tsujimura, H. Furutani, H. Kobayashi, and A. Hayakawa, "Performances and emission characteristics of NH3-air and NH3-CH4-air combustion gas-turbine power generations," *Proc. Combust. Inst.*, vol. 36, no. 3, pp. 3351–3359, 2017.

[100] S. K. Ayaz, O. Altuntas, and H. Caliskan, "Effect of ammonia fuel fraction on the exergetic performance of a gas turbine," *Energy Procedia*, vol. 144, pp. 150–156, 2018.

[101] J. C. Ganley, E. G. Seebauer, and R. I. Masel, "Development of a micro reactor for the production of hydrogen from ammonia," *J. Power Sources*, vol. 137, no. 1, pp. 53–61, 2004.

[102] S. F. Yin, B. Q. Xu, X. P. Zhou, and C. T. Au, "A mini-review on ammonia decomposition catalysts for on-site generation of hydrogen for fuel cell applications," *Appl. Catal. A Gen.*, vol. 277, no. 1–2, pp. 1–9, 2004.

[103] S.-F. Yin, Q.-H. Zhang, B. Xu, W.-X. Zhu, C.-F. Ng, and C.-T. Au, "Investigation on the catalysis of COx-free hydrogen generation from ammonia," *J. Catal.*, vol. 224, pp. 384–396, 2004.

[104] S. J. Wang, S. F. Yin, L. Li, B. Q. Xu, C. F. Ng, and C. T. Au, "Investigation on modification of Ru/CNTs catalyst for the generation of COx-free hydrogen from ammonia," *Appl. Catal. B Environ.*, vol. 52, no. 4, pp. 287–299, 2004.

[105] D. C. Huang, C. H. Jiang, F. J. Liu, Y. C. Cheng, Y. C. Chen, and K. L. Hsueh, "Preparation of Ru-Cs catalyst and its application on hydrogen production by ammonia decomposition," *Int. J. Hydrogen Energy*, vol. 38, no. 8, pp. 3233–3240, 2013.

[106] C. Plana, S. Armenise, A. Monzón, and E. García-Bordejé, "Process optimisation of in situ H2 generation from ammonia using Ni on alumina coated cordierite monoliths," *Top. Catal.*, vol. 54, no. 13–15, pp. 914–921, 2011.

[107] A. Di Carlo, A. Dell'Era, and Z. Del Prete, "3D simulation of hydrogen production by ammonia decomposition in a catalytic membrane reactor," *Int. J. Hydrogen Energy*, vol. 36, no. 18, pp. 11815–11824, 2011.

[108] A. Di Carlo, L. Vecchione, and Z. Del Prete, "Ammonia decomposition over commercial Ru/Al2O3catalyst: An experimental evaluation at different operative pressures and temperatures," *Int. J. Hydrogen Energy*, vol. 39, no. 2, pp. 808–814, 2014.

[109] E. N. Gobina, J. S. Oklany, and R. Hughes, "Elimination of ammonia from coal gasification streams by using a catalytic membrane reactor," *Ind. Eng. Chem. Res.*, vol. 34, no. 11, pp. 3777–3783, 1995.

[110] M. E. E. Abashar, "Integrated catalytic membrane reactors for decomposition of ammonia," *Chem. Eng. Process.*, vol. 41, no. 5, pp. 403–412, 2002.

[111] G. Papapolymerou and V. Bontozoglou, "Decomposition of NH, on Pd and Ir Comparison with Pt and Rh," *J. Mol. Catal. A Chem.*, vol. 120, no. 1381, pp. 165–17, 1997.

[112] M. Itoh, M. Masuda, and K. Machida, "Hydrogen Generation by Ammonia Cracking with Iron Metal-Rare Earth Oxide Composite Catalyst.," *Mater. Trans.*, vol. 43, no. 11, pp. 2763–2767, 2002.

[113] W. Zheng, J. Zhang, Q. Ge, H. Xu, and W. Li, "Effects of CeO2 addition on Ni/Al2O3 catalysts for the reaction of ammonia decomposition to hydrogen," *Appl. Catal. B Environ.*, vol. 80, no. 1–2, pp. 98–105, 2008.

[114] R. Z. Sørensen, L. J. E. Nielsen, S. Jensen, O. Hansen, T. Johannessen, U.

Quaade, and C. H. Christensen, "Catalytic ammonia decomposition: Miniaturized production of COx-free hydrogen for fuel cells," *Catal. Commun.*, vol. 6, no. 3, pp. 229–232, 2005.

[115] M. Wang, J. Li, L. Chen, and Y. Lu, "Miniature NH3 cracker based on microfibrous entrapped Ni-CeO2/Al2O3 catalyst monolith for portable fuel cell power supplies," *Int. J. Hydrogen Energy*, vol. 34, no. 4, pp. 1710–1716, 2009.

[116] H.-P. Minak and G. Gross, "Method of treating vapors containing ammonia and hydrogen sulfide," US Patent 5,672,326, 1997.

[117] C. Busson and T. Nietsch, "Process for cracking ammonia present in a gas containing hydrogen sulphide," US Patent 5,853,682, 1998.

[118] X. K. Li, W. J. Ji, J. Zhao, S. J. Wang, and C. T. Au, "Ammonia decomposition over Ru and Ni catalysts supported on fumed SiO2, MCM-41, and SBA-15," *J. Catal.*, vol. 236, no. 2, pp. 181–189, 2005.

[119] W. I. F. David, J. W. Makepeace, S. K. Callear, H. M. A. Hunter, J. D. Taylor, T. J. Wood, and M. O. Jones, "Hydrogen production from ammonia using sodium amide," *J. Am. Chem. Soc.*, vol. 136, no. 38, pp. 13082–13085, 2014.

[120] J. Zhang, H. Xu, X. Jin, Q. Ge, and W. Li, "Characterizations and activities of the nano-sized Ni/Al2O3 and Ni/La-Al2O3 catalysts for NH3 decomposition," *Appl. Catal. A Gen.*, vol. 290, no. 1–2, pp. 87–96, 2005.

[121] H. Liu, H. Wang, J. Shen, Y. Sun, and Z. Liu, "Preparation, characterization and activities of the nano-sized Ni/SBA-15 catalyst for producing COx-free hydrogen from ammonia," *Appl. Catal. A Gen.*, vol. 337, no. 2, pp. 138–147, 2008.

[122] S. Hikazudani, C. Inazumi, H. Nakanishi, N. Nakamura, and H. Arikawa, "Ammonia engine system," US Patent 0283960 A1, 2011.

[123] K. Nagaoka, T. Eboshi, Y. Takeishi, R. Tasaki, K. Honda, K. Imamura, and K. Sato, "Carbon-free H2 production from ammonia triggered at room temperature with an acidic RuO2/γ-Al2O3 catalyst," *Sci. Adv.*, vol. 3, no. 4, Apr. 2017.

[124] G. W. Burke, "Apparatus for decomposing ammonia," US Patent 1915120, 1933.

[125] S. R. Graville, "Destruction of waste gas," US Patent 0018035 A1, 2001.

[126] D. A. Goetsch and S. J. Schmit, "Production of hydrogen by autothermic decomposition of ammonia," US Patent 0037244A1, 2002.

[127] L. R. Arana, S. B. Schaevitz, A. J. Franz, M. A. Schmidt, and K. F. Jensen, "A microfabricated suspended-tube chemical reactor for thermally efficient fuel processing," *J. Microelectromechanical Syst.*, vol. 12, no. 5, pp. 600–612, 2003.

[128] S. Grannell, C. Stack, and D. Gillespie, "Comparison of Combustion Promoters for Ammonia and Two Ways to Run Engines on Ammonia as the Only Fuel," in *2010 Annual NH3 Fuel Conference*, 2010.

[129] J. Engbaek, "Ammonia cracker for Hydrogen Generation for PEM Application," in *Annual NH3 Fuel Conference,* 2008.

[130] A. Page, D. Dekel, Z. Gottesfeld, and S. Gottesfeld, "Use of ammonia as source of hydrogen fuel and as a getter for air-CO2 in alkaline membrane fuel cells," US Patent 9236624B2, 2013.

[131] D. Chakraborty., P. H.Y., and T. Johannessen, "Apparatus for generating hydrogen from ammonia stored in solid materials and integration thereof into low temperature fuel cells," Patent WO 2011107279Al, 2011.

[132] J. E. Brandenburg, "Plasma reactor for cracking ammonia and hydrogen-rich gases to hydrogen," US Patent 7,037,484 B1, 2006.

[133] D. T. Pratt and E. S. Starkman, "High-temperature kinetics of ammonia-air combustion," *Symp. Combust.,* vol. 12, no. 1, pp. 891–899, 1969.

[134] C. J. Dasch and R. J. Blint, "A Mechanistic and Experimental Study of Ammonia Flames," *Combust. Sci. Technol.,* vol. 41, no. 5–6, pp. 223–244, 1984.

[135] J. F. Grcar, P. Glarborg, J. B. Bell, M. S. Day, A. Loren, and A. D. Jensen, "Effects of mixing on ammonia oxidation in combustion environments at intermediate temperatures," *Proc. Combust. Inst.,* vol. 30, no. 1, pp. 1193–1200, 2005.

[136] N. Sullivan, A. Jensen, P. Glarborg, M. S. Day, J. F. Grcar, J. B. Bell, C. J. Pope, and R. J. Kee, "Ammonia conversion and NOx formation in laminar co-flowing nonpremixed methane-air flames," *Combust. Flame,* vol. 131, no. 3, pp. 285–298, 2002.

[137] Z. Tian, Y. Li, L. Zhang, P. Glarborg, and F. Qi, "An experimental and kinetic modeling study of premixed NH3/CH4/O2/Ar flames at low pressure," *Combust. Flame*, vol. 156, no. 7, pp. 1413–1426, 2009.

[138] Ø. Skreiberg, P. Kilpinen, and P. Glarborg, "Ammonia chemistry below 1400 K under fuel-rich conditions in a flow reactor," *Combust. Flame,* vol. 136, no. 4, pp. 501–518, 2004.

[139] A. A. Konnov, "Implementation of the NCN pathway of prompt-NO formation in the detailed reaction mechanism," *Combust. Flame,* vol. 156, no. 11, pp. 2093–2105, 2009.

[140] C. Duynslaegher, H. Jeanmart, and J. Vandooren, "Ammonia combustion at elevated pressure and temperature conditions," *Fuel,* vol. 89, no. 11, pp. 3540–3545, 2010.

[141] C. Duynslaegher, H. Jeanmart, and J. Vandooren, "Kinetics in ammonia-containing premixed flames and a preliminary investigation of their use as fuel in spark ignition engines," *Combust. Sci. Technol.,* vol. 181, no. 8, pp. 1092–1106, 2009.

[142] C. Duynslaegher, F. Contino, J. Vandooren, and H. Jeanmart, "Modeling of ammonia combustion at low pressure," *Combust. Flame,* vol. 159, no. 9, pp.

2799–2805, 2012.

[143] T. Mendiara and P. Glarborg, "Ammonia chemistry in oxy-fuel combustion of methane," *Combust. Flame*, vol. 156, no. 10, pp. 1937–1949, 2009.

[144] J. Li, H. Huang, N. Kobayashi, Z. He, Y. Osaka, and T. Zeng, "Numerical study on effect of oxygen content in combustion air on ammonia combustion," *Energy*, vol. 93, pp. 2053–2068, 2015.

[145] J. Ströhle and T. Myhrvold, "An evaluation of detailed reaction mechanisms for hydrogen combustion under gas turbine conditions," *Int. J. Hydrogen Energy*, vol. 32, no. 1, pp. 125–135, 2007.

[146] R. Mével, S. Javoy, F. Lafosse, N. Chaumeix, G. Dupré, and C. E. Paillard, "Hydrogen-nitrous oxide delay times: Shock tube experimental study and kinetic modelling," *Proc. Combust. Inst.*, vol. 32 I, no. 1, pp. 359–366, 2009.

[147] J. Herzler and C. Naumann, "Shock-tube study of the ignition of methane/ethane/hydrogen mixtures with hydrogen contents from 0% to 100% at different pressures," *Proc. Combust. Inst.*, vol. 32 I, no. 1, pp. 213–220, 2009.

[148] C. Olm, I. G. Zsély, T. Varga, H. J. Curran, and T. Turányi, "Comparison of the performance of several recent syngas combustion mechanisms," *Combust. Flame*, vol. 162, no. 5, pp. 1793–1812, 2015.

[149] O. Mathieu and E. L. Petersen, "Experimental and modeling study on the high-temperature oxidation of Ammonia and related NOx chemistry," *Combust. Flame*, vol. 162, no. 3, pp. 554–570, 2015.

[150] B. Li, Y. He, Z. Li, and A. A. Konnov, "Measurements of NO concentration in NH3-doped CH4+air flames using saturated laser-induced fluorescence and probe sampling," *Combust. Flame*, vol. 160, no. 1, pp. 40–46, 2013.

[151] C. Brackmann, V. A. Alekseev, B. Zhou, E. Nordström, P. E. Bengtsson, Z. Li, M. Aldén, and A. A. Konnov, "Structure of premixed ammonia + air flames at atmospheric pressure: Laser diagnostics and kinetic modeling," *Combust. Flame*, vol. 163, pp. 370–381, 2016.

[152] "GRI-Mech V. Gas research institute, GRI Mech, Ver. 3.0.," Date posted Oct. 2018.

[153] M. Zieba, A. Brink, A. Schuster, M. Hupa, and G. Scheffknecht, "Ammonia chemistry in a flameless jet," *Combust. Flame*, vol. 156, no. 10, pp. 1950–1956, 2009.

[154] A. G. Shmakov, O. P. Korobeinichev, I. V. Rybitskaya, A. A. Chernov, D. A. Knyazkov, T. A. Bolshova, and A. A. Konnov, "Formation and consumption of NO in H2+ O2+ N2 flames doped with NO or NH3 at atmospheric pressure," *Combust. Flame*, vol. 157, no. 3, pp. 556–565, 2010.

[155] P. Kumar and T. R. Meyer, "Experimental and modeling study of chemical-kinetics mechanisms for H2-NH3-air mixtures in laminar premixed jet flames," *Fuel*, vol. 108, pp. 166–176, 2013.

[156] J. Li, H. Huang, N. Kobayashi, Z. He, and Y. Nagai, "Study on using hydrogen and ammonia as fuels: Combustion characteristics and NOx formation," *Int. J. Energy Res.*, vol. 38, no. 9, pp. 1214–1223, 2014.

[157] D. H. Um, J. M. Joo, S. Lee, and O. C. Kwon, "Combustion stability limits and NOx emissions of nonpremixed ammonia-substituted hydrogen-air flames," *Int. J. Hydrogen Energy*, vol. 38, no. 34, pp. 14854–14865, 2013.

[158] H. Nozari and A. Karabeyoğlu, "Numerical study of combustion characteristics of ammonia as a renewable fuel and establishment of reduced reaction mechanisms," *Fuel*, vol. 159, pp. 223–233, 2015.

[159] A. Hayakawa, A. Ichikawa, Y. Arakawa, T. Kudo, and H. Kobayashi, "Enhancement of Reaction and Stability of Ammonia Flames using Hydrogen Addition and Swirling Flows," in *Chicago 12th Annual NH3 Fuel Conference*, 2015.

[160] H. Xiao and A. Valera-Medina, "Chemical Kinetic Mechanism Study on Premixed Combustion of Ammonia/Hydrogen Fuels for Gas Turbine Use," *J. Eng. Gas Turbines Power*, vol. 139, no. 8, p. 081504, 2017.

[161] H. Xiao, A. Valera-Medina, and P. J. Bowen, "Modeling Combustion of Ammonia/Hydrogen Fuel Blends under Gas Turbine Conditions," *Energy and Fuels*, vol. 31, no. 8, pp. 8631–8642, 2017.

[162] H. Xiao, A. Valera-Medina, P. Bowen, and S. Dooley, "3D Simulation of Ammonia Combustion in a Lean Premixed Swirl Burner," *Energy Procedia*, vol. 142, pp. 1294–1299, 2017.

[163] H. Kobayashi, "Ammonia Combustion for Energy System," in *Japan-Norway Hydrogen Seminar*, 2017.

[164] C. Duynslaegher, "Experimental and numerical study of ammonia combustion," Doctoral Thesis, Universite Catholique de Louvain, 2011.

[165] T. Johannessen, "Method and Device for Ammonia Storage and Delivery Using in-situ Re-saturation of a Delivery Unit," US Patent US20130263927A1, 2013.

[166] J. D. Peter-Hoblyn, E. N. Balles, J. E. Hofmann, and T. J. Tarabulski, "Reducing NOx Emissions from an Engine by Temperature-Controlled Urea Injection for Selective Catalytic Reduction," US Patent 5,976,475, 1999.

[167] T. D. Elmøe, R. Z. Sørensen, U. Quaade, C. H. Christensen, J. K. Nørskov, and T. Johannessen, "A high-density ammonia storage/delivery system based on Mg(NH3)6Cl2 for SCR-DeNOx in vehicles," *Chem. Eng. Sci.*, vol. 61, no. 8, pp. 2618–2625, 2006.

[168] O. Kurata, N. Iki, T. Inoue, T. Matsunuma, T. Tsujimura, H. Furutani, H. Kobayashi, and A. Hayakawa, "Combustion Emissions from NH3 Fuel Gas Turbine Power Generation Demonstrated," in *AIChE Annual Meeting*, 2017.

[169] C. M. Nam and B. M. Gibbs, "Application of the thermal DeNOxprocess to diesel engine DeNOx: An experimental and kinetic modelling study," *Fuel*, vol. 81, no. 10, pp. 1359–1367, 2002.

[170] I. Dincer and C. Zamfirescu, "Apparatus for Using Ammonia as a Sustainable Fuel, Refrigerant and NOx Reduction Agent," US Patent 8,272,353 B2, 2012.

[171] H. Nozari, G. Karaca, O. Tuncer, and A. Karabeyoglu, "Porous medium based burner for efficient and clean combustion of ammonia–hydrogen–air systems," *Int. J. Hydrogen Energy*, vol. 42, no. 21, pp. 14775–14785, 2017.

[172] A. Ichikawa, A. Hayakawa, Y. Kitagawa, K. D. K. A. Somarathne, T. Kudo, and H. Kobayashi, "Laminar burning velocity and Markstein length of ammonia/hydrogen/air premixed flames at elevated pressures," *Int. J. Hydrogen Energy*, vol. 40, no. 30, pp. 9570–9578, 2015.

[173] J. H. Lee, J. H. Kim, J. H. Park, and O. C. Kwon, "Studies on properties of laminar premixed hydrogen-added ammonia/air flames for hydrogen production," *Int. J. Hydrogen Energy*, vol. 35, no. 3, pp. 1054–1064, 2010.

[174] J. H. Lee, S. I. Lee, and O. C. Kwon, "Effects of ammonia substitution on hydrogen/air flame propagation and emissions," *Int. J. Hydrogen Energy*, vol. 35, no. 20, pp. 11332–11341, 2010.

[175] T. Meyer, P. Kumar, M. Li, K. Redfern, and D. Diaz, "Ammonia Combustion with Near-Zero Pollutant Emissions," in *8th Annual NH3 Fuel Conference*, 2011.

[176] M. Woo, B. C. Choi, and A. F. Ghoniem, "Experimental and numerical studies on NOx emission characteristics in laminar non-premixed jet flames of ammonia-containing methane fuel with oxygen/nitrogen oxidizer," *Energy*, vol. 114, no. x, pp. 961–972, 2016.

[177] H. Xiao, A. Valera-Medina, R. Marsh, and P. J. Bowen, "Numerical study assessing various ammonia/methane reaction models for use under gas turbine conditions," *Fuel*, vol. 196, pp. 344–351, 2017.

[178] T. Rutar and P. C. Malte, "NOx Formation in High-Pressure Jet-Stirred Reactors With Significance to Lean-Premixed Combustion Turbines," *J. Eng. Gas Turbines Power*, vol. 124, no. 4, p. 776, 2002.

[179] S. Li, S. Zhang, H. Zhou, and Z. Ren, "Analysis of air-staged combustion of NH3/CH4 mixture with low NOx emission at gas turbine conditions in model combustors," *Fuel*, vol. 237, pp. 50–59, 2019.

[180] K. D. K. A. Somarathne, S. Hatakeyama, A. Hayakawa, and H. Kobayashi, "Numerical study of a low emission gas turbine like combustor for turbulent ammonia/air premixed swirl flames with a secondary air injection at high pressure," *Int. J. Hydrogen Energy*, vol. 42, no. 44, pp. 27388–27399, 2017.

[181] H. K. Versteeg and W. Malalasekera, *An Introduction to Computational Fluid Dynamits, The finite volume method*, 2nd edition. Longmans Group Ltd, 2007.

[182] ANSYS, "ANSYS® Academic Research, Release 17.2, Help System, Theory Guide, ANSYS, Inc.," vol. 15317, no. January, pp. 724–746, 2016.

[183]. F. Douglas, J. M. Gasiorek, and J. A. Swaffield, *Fluid Mechanics*, 5th ed. Pearson Education UK, 2005.

[184] D. C. Wilcox, *Turbulence Modeling for CFD*. DCW Industries, Inc. La Canada, California, 1993.

[185] A. Sayma, *Computational Fluid Dynamics*, vol. 57, no. 1. Bookboon.com, 2009.

[186] T. Fraser, "Numerical modelling of an inverted cyclone gasifier," PhD, Cardiff University, 2003.

[187] "Finite volume method." [Online]. Available: https://www.cfd-online.com/Wiki/CFD-Wiki:Copyrights. [Accessed: 08-Feb-2018].

[188] K. A. Hoffmann and S. Chiang, *Computational Fluid Dynamics,Volume II*, 4th edition. Engineering Education System, USA, 2000.

[189] R. Lohner, *Applied CFD Techniques, An introduction based on finite element methods,* 2 nd editi. West Sussex, UK: John Willey & Sons Ltd., 2008.

[190] A. W. Date, *Introduction to Computational Fluid Dynamics*. Cambridge University Press., 2005.

[191] J. H. Ferziger and M. Peric, *Computational Methods for Fluid Dynamics*, 3rd ed, Springer-Verlag Berlin Heidelberg, 2002.

[192] H. Tennekes and J. L. Lumley, *A First Course In Turbulence*. The MIT Press, 1972.

[193] D. Veynante, "Introduction to Turbulent Combustion," Laboratoire E.M2.C. CNRS - Ecole Centrale Paris, 2006.

[194] W. P. Jones and B. E. Launder, "The prediction of laminarization with a two-equation model of turbulence," *Int. J. Heat Mass Transf.*, vol. 15, no. 2, pp. 301–314, 1972.

[195] Fluent Users Services Center, "Modeling Turbulent Flows," 2006.

[196] K. K. Kuo and R. Acharya, *Fundamentals of Turbulent and Multiphase Combustion*. John Wiley & Sons, Inc., 2012.

[197] A. E. German and T. Mahmud, "Modelling of non-premixed swirl burner flows using a Reynolds-stress turbulence closure," *Fuel*, vol. 84, no. 5, pp. 583–594, 2005.

[198] J. P. Holman, *Heat Transfer*, 10th ed., McGraw-Hill, 2010.

[199] J. M. Simmie, "Detailed chemical kinetic models for the combustion of hydrocarbon fuels," *Prog. Energy Combust. Sci.*, vol. 29, no. 6, pp. 599–634, 2003.

[200] K. A. Heufer, C.-J. Sung, H. J. Curran, O. Mathieu, P. Griebel, J. Herzler, N. Donohoe, C. Naumann, A. K. Das, M. C. Krejci, E. L. Petersen, A. Kéromnès, W. J. Pitz, and W. K. Metcalfe, "An experimental and detailed chemical kinetic modeling study of hydrogen and syngas mixture oxidation at elevated pressures," *Combust. Flame*, vol. 160, no. 6, pp. 995–1011, 2013.

[201] R. J. Kee, J. F. Grcar, M. D. Smooke, J. A. Miller, and E. Meeks, "PREMIX : A Fortran Program for Modeling Steady Laminar One-Dimensional Premixed Flames," in *Sandia National Laboratories Report*, 1985.

[202] J. Li, Z. Zhao, A. Kazakov, and F. L. Dryer, "An updated comprehensive kinetic model of hydrogen combustion," *Int. J. Chem. Kinet.*, vol. 36, no. 10, pp. 566–575, 2004.

[203] Robert J. Kee, Fran M. Rupley, and E. Meeks, "Chemkin-III: A Fortran Chemical Kinetics Package for the Analysis of Gas-Phase Chemical and Plasma Kinetics," 1996.

[204] "PlusPac^{TM} for Renishaw's AM250 laser melting systems." [Online]. Available: http://resources.renishaw.com/en/download/pluspac-upgrade-for-am250--74466, 2019.

[205] O. Aniekan A., "Combustion Dynamics in a Lean Premixed Combustor with Swirl Forcing and Fuel Conditions," PhD Thesis, Cardiff University, 2017.

[206] D. Durox, J. P. Moeck, J. F. Bourgouin, P. Morenton, M. Viallon, T. Schuller, and S. Candel, "Flame dynamics of a variable swirl number system and instability control," *Combust. Flame*, vol. 160, no. 9, pp. 1729–1742, 2013.

[207] Swagelok, "Pressure Gauges Industrial and Process PGI Series." [Online]. Available: http://www.swagelok.com. [Accessed: 03-Nov-2017].

[208] Swagelok, "Proportional Relief Valves." [Online]. Available: http://www.swagelok.com. [Accessed: 03-Nov-2017].

[209] "Omega User's guide," *Omega Engineering, Inc.* [Online]. Available: http://www.omegamanual.info.

[210] U. Manual, "Image Processing Stroboscope BVS-II Wotan." [Online]. Available: https://www.polytec.com/eu/machine-vision/products/stroboscope/bvs-ii-wotan-stroboscope, 2018.

[211] "ProSound800 user instructions." [Online]. Available: https://maplindownloads.s3-eu-west-1.amazonaws.com/n89gb-4247.PDF, 2018.

[212] "Baumer-GAPI Viewer v1.6 User's Guide for Baumer-GAPI Test Tool."

[213] J. Zhang, C. R. Shaddix, and R. W. Schefer, "Design of model-friendly turbulent non-premixed jet burners for C2+ hydrocarbon fuels," *Rev. Sci. Instrum.*, vol. 82, no. 7, pp. 1–10, 2011.

[214] A. R. Masri, R. W. Dibble, and R. S. Barlow, "The structure of turbulent non premixed flame revealed by Raman Rayleigh-LIF measurements," *Prog. Energy Combust. Sci.*, vol. 22, no. 4, pp. 307–362, 1996.

[215] B. K. Gandhi, S. N. Singh, V. Seshadri, and J. Singh, "Effect of bluff body shape on vortex flow meter performance," *Indian J. Eng. Mater. Sci.*, vol. 11, no. 5, pp. 378–384, 2004.

[216] A. Fallis, *Fundamentals of fluid mechanics*, 7th editio. Wiley, 2012.

[217] B. E. Launder and D. B. Spalding, "The numerical computation of turbulent flows," *Comput. Methods Appl. Mech. Eng.*, vol. 3, no. 2, pp. 269–289, 1974.

[218] P. J. Linstrom and W. G. Mallard, "NIST chemistry WebBook," 2018.

[219] C. A. Martins, A. P. Pimenta, J. A. Carvalho Jr., M. A. Ferreira, and A. A. Caldeira-Pires, "CH and C2 radicals characterization in natural gas turbulent diffusion flames," *J. Brazilian Soc. Mech. Sci. Eng.*, vol. 27, no. 2, 2006.

[220] K. S. Ramesh and P. S. Dusan, *Fundamentals of Heat Exchanger Design*. John Wiley & Sons, Inc, 2003.

[221] J. M. Coulson and J. F. Richardson, *Chemical Engineering*, 5th Editio. Butterworth-Heinemann, 1998.

[222] A. S. Alsaegh, A. Valera-Medina, N. A. Hussein, M. A. Al-Fahham, F. A. Hatem, and C. T. Chong, "Effects of different nozzle configurations on swirl flow topology in tangential swirl burners," *Energy Procedia*, vol. 158, pp. 2317–2322, 2019.

[223] A. Valera-medina, M. Gutesa, H. Xiao, D. Pugh, A. Giles, B. Goktepe, R. Marsh, and P. Bowen, "Premixed ammonia / hydrogen swirl combustion under rich fuel conditions for gas turbines operation," *Int. J. Hydrogen Energy*, vol. 44, no. 16, pp. 8615–8626, 2019.

[224] V. Fichet, M. Kanniche, P. Plion, and O. Gicquel, "A reactor network model for predicting NOx emissions in gas turbines," *Fuel*, vol. 89, no. 9, pp. 2202–2210, 2010.

[225] P. Gray and S. K. Scott, "Autocatalytic reactions in the isothermal, continuous stirred tank reactor," *Chem. Eng. Sci.*, vol. 38, no. 1, pp. 29–43, 2002.

[226] A. R. D. T. Junior, T. C. Hayashi, and P. S. Schneider, "A reactor network model for predicting NOx emissions in an industrial burner," *14th Brazilian Congr. Therm. Sci. Eng.*, 2012.

[227] A. Abou-Taouk, "Optimization of Chemical Kinetic Mechanisms and Numerical Simulations of Industrial Gas Turbine Burners," PhD Thesis, Chalmers University of technology, 2014.

[228] J. H. Miles, "Measurement of the Post-Combustion Residence Time in a Gas Turbine Aero-Engine," *50th AIAA Aerosp. Sci. Meet.*, p. 1–37, January 2012.

[229] I. E. Agency, "World Energy Outlook: Executive Summary," *OECD/IEA*. [Online]. Available: www.iea.org/t&c, 2018.

[230] O. Wyman, "World Energy Trilemma." [Online]. Available: www.worldenergy.org, 2017.